Plasma polymerisation: study and application

Caroline Noël

Plasma Polymerisation:

Study and Application

Ph. D. Thesis

By

Caroline NOËL

Department of Chemistry

University of Durham

2009

Je dédie ces quelques pages à mes parents Martine et Jean-Claude qui ont largement contribué à ma réussite, à mon frère Bertrand qui m'a hébergé quand j'avais le mal du pays, et également à Tom, mon mari, pour son soutien et son amour.

Statement of Copyright

Declaration

The work described in this thesis was carried out in the Chemistry Department at the University of Durham between October 2003 and August 2007. It is the original work of the author, except where otherwise acknowledged, and has not been submitted previously for a degree at this or any other University.

Raman fluorescence measurements were performed by Lee Harris and Richard Garrod (University of Durham).

Acknowledgements

I would like to thank my supervisor Professor J.P.S. Badyal for his help and guidance throughout my PhD, and also for his financial support. Thanks also to everyone who worked in lab 98 during my time there, for their advice and support, and yes somehow to the 'singers' who contributed to the good ambiance in the lab.

Thanks also to Dr John Sanderson for his help with peptide chemistry as well as for letting me carrying some experiments in his lab during my first year.

A special thanks also to Kelvin and Barry, at the electrical workshop, Peter and Malcolm, the glassblowers, Jim and Neil, at the mechanical workshop, and the whole chemistry department for their help and technical support.

Abstract

Molecular interactions are often studied using immobilised organic and biological entities at the surface of a substrate. Functionalisation of such surfaces can be achieved via different technologies such as Langmuir-Blodgett films, self-assembled monolayers and spin-coated layers. The main drawback of these methods is the dependence on the substrate, limiting the scope of possible applications. Conversely, plasma polymerisation entails the deposition of thin polymeric films at the surface of a wide variety of substrates. The development of pulsed plasma has opened new paths allowing the high controllability of the functionality and the thickness of the deposited layer. This thesis describes the functionalisation of a surface with pentafluorophenyl ester in a one-step process, reaching higher immobilization yield of bio-molecules than in a multi-step process.

Also, the nature of pulsed-plasma polymers provides additional benefits such as irregular surfaces which make functionalities more accessible for subsequent reactions such as enzymatic modification as investigated in the fourth chapter.

Finally, the last two chapters of this thesis deal with the occurrence of trapped free radicals within plasma polymers and their ability to induce graft-polymerisation of polymer brushes without prior attachment of initiators at the surface of a substrate. A comparison is drawn between a 'conventional' method using an initiator immobilised on the surface and trapped radicals to induce graft polymerisation. The influence of he nature of the monomer used during plasma polymerisation along with the conditions of deposition are studied with respect to the rate of subsequent graft polymerisation of styrene and the amount of trapped free radicals.

Table of Contents

Table of Figures

Table of Schemes

Table of Tables

I

CHAPTER ONE

Introduction to plasma polymerisation

I.1. INTRODUCTION

Tailoring the surface properties of a material is of interest in many areas such as textiles[1,2], biosensors[3,4], contact lens technology[5] and microprocessors[6]. Indeed, a material can retain its bulk properties (e.g. mechanical, electrical, optical) and be functionalised on its surface with appropriate properties depending on the field of applications (e.g. corrosion resistance[7,8], low wear[9], low friction[10], biocompatibility[11,12], hydrophobicity[13, 14], protein resistance[15], genomics[16]...).

Several methods have been developed to functionalise the surface of a substrate. This can be done either by alteration of the existing chemical functions present at the surface of a material, or by depositing an extra layer upon it. Control is of great importance to restrict the alteration of the polymer surface to monolayer quantities in order to maintain the bulk properties of the polymer. This chapter presents plasma polymerisation as the method chosen in this thesis to modify surfaces of materials.

I.2. PLASMA POLYMERISATION

I.2.1. Introduction

Plasma polymerisation is a substrate-independent[17], solventless deposition technique used to modify material surfaces. Gas discharges are used to polymerise organic vapours at low temperatures to deposit thin films onto a wide variety of surfaces. Furthermore, the reaction mechanism allows the polymerisation of organic compounds that do not polymerise under conventional chemical conditions such as methane[18], tetramethylsilane[19,20] or hexafluoropropene[21].

The resulting thin films often present the following properties:

- excellent adhesion to a wide variety of substrate materials

- strong resistance to most chemicals because highly branched and cross-linked
- controllable thickness (0.01 – 100 μm) of almost or completely flawless nature
- minimal alteration to the bulk properties of the polymeric substrate (as opposed to conventional surface grafting)

In practice, deposition of a polymeric material is achieved by introducing organic vapours of a monomer in a chamber in which a discharge is ignited, generating high energy species (e.g. radicals, ions, molecules in excited electronic state). These species then interact with other species and with a substrate through elastic and inelastic collisions forming new bonds and new species. The degree of polymerisation depends on monomer flow rate, system pressure, discharge power, geometry of the system, reactivity of the monomer, frequency of the excitation signal and temperature.

A wide range of functionalities can be obtained by plasma polymerisation, such as anhydride[22] , aldehyde[23], alcohol[24,25,26], amine[27,28], amide[29], cyano[30], ester[31] , epoxide[32], carboxylic acid[33,34], thiol[16], halogen[35,36,37], perfluorocarbon[38,39], or even metal atoms[40,41].

Before a more in-depth description of the plasma polymerisation process, a brief overview of plasmas is given.

I.2.2. Definition of plasma

Langmuir described plasma as the fourth state of matter, alongside the solid, gas and liquid states[42]. Its energy level is far beyond the ones of the other three. A plasma can be described as a quasi-neutral assembly of charged and neutral particles exhibiting collective behaviour[43]. Such behaviour results from the fact that localised concentration of charged particles affect the motion of other plasma particles even at a long distance. A plasma has a well-defined potential and density, and can maintain neutrality when

slightly perturbed (Debye shielding[44]). An important parameter commonly used to describe plasmas is the Debye length, λ_D (Equation I-1). It represents the distance over which a charge imbalance will not be perceived by the rest of the ionised gas, hence maintaining the electric neutrality[45]:

Equation I-1

$$\lambda_D^2 = \frac{kT}{4\pi ne^2}$$

Where k is the Boltzman constant, T is the temperature, n the charge density and e the electron charge.

When $T=10^4$ K and $n=10^{10}$, then $\lambda_D=7x10^{-3}$ cm. In a reactor of relatively large size, an electric discharge can be assumed to be a plasma.

I.2.3. Classification of plasmas

Plasma can be broadly divided into three categories[43] depending on the relationship between the average energy of the different species presenting the plasma.

I.2.3.1. Complete thermodynamic equilibrium plasmas (CTE)

A CTE plasma is determined as a plasma where the temperatures of all species are equal. Such plasmas exist only in stars or during the short interval of a strong explosion; they do not exist in controlled laboratory conditions.

I.2.3.2. Local thermodynamic equilibrium plasmas (LTE)

This class of plasma is generated when the gas temperature equals the electron temperature. This occurs when the gas molecules are heated over 20,000 K. LTE plasmas are thermodynamically stable under small variation of the plasma conditions. However, such temperatures are undeniably unsuitable for chemical deposition as organic molecules would degrade.

I.2.3.3. Non-local thermodynamic equilibrium plasmas (Non-LTE)

Non-LTE plasmas, also referred to as 'cold' plasmas, occur at low-pressure. They can be generated at ambient temperature. In such plasmas, thermodynamic equilibrium is not achieved because electrons, ions and neural molecules have different modes of gaining and dissipating energy. Electrons do not lose energy by elastic collisions with molecules, whereas ions and molecules lose their entire energy by collisions with another ion or molecule, consequently, a significant energy difference arise between the different species. In a low pressure glow discharge, $T_{electron}$ is of the order of 10^4 K (and depends upon the electric field), T_{ion} is 300-1000 K, and $T_{molecule}$ is about 300 K.

Cold plasmas are of particular interest for chemical deposition due to the relatively low temperatures generated. In the laboratory, they are created mainly by electric discharge to maintain a continuous plasma state for a relatively long period of time.

I.2.4. Interactions occurring in a cold plasma

I.2.4.1. Homogeneous reactions

I.2.4.1.a. Reactions of electrons with heavy species

After gaining energy from the exterior electromagnetic field, electrons transfer it to the gas to excite and sustain the plasma. This process occurs mainly by inelastic collisions which lead to a variety of reactions (see Table I-1).

Table I-1 – Reactions of electrons with heavy species in a cold plasma

Type of reaction	Description	Equation
Excitation	when electrons have sufficient energy, they can promote heavy targets to excited electronic states	$e + A \rightarrow e + A^*$
Ionization	if electrons have high energy, they can produce ions with or without dissociation of the molecule	$e + AB \rightarrow AB^+ + 2e$ $e + AB \rightarrow A^+ + B^- + e$ *Dissociative ionization*
Dissociation	inelastic collision of an electron with a molecule can cause its dissociation without the formation of ions	$e + AB \rightarrow A + B + e$
Recombination	the charged particles are lost from the plasma by recombination of particles of opposite charges	$e + AB^+ \rightarrow A + B$ $e + A^+ \rightarrow A + hv$

I.2.4.1.b. Reactions between heavy species

These reactions occur between ions, radicals, atoms and molecules during collision. They can be divided in two types, those involving at least one ion and those involving a radical.

- Ion-molecule reactions:

Type of reaction	Description	Equation
Recombination of ions	ions can collide to form either a molecule in the ground state or to neutralise the ions by forming two excited atoms, both releasing energy through radiation	$A^+ + B^- \rightarrow AB + h\nu$ $A^+ + B^- \rightarrow A^* + B^* + h\nu$
Chain transfer	during collision, an electric charge can be transferred between an ion and a neutral particle. This can be accompanied or not by dissociation	$A + B^+ \rightarrow A^+ + B$ $A^+ + BC \rightarrow A + B^+ + C$
Transfer of heavy reactant	new species are created after collision	$A^+ + BC \rightarrow \begin{cases} AB^+ + C \\ AB + C^+ \end{cases}$
Associative detachment	in a collision between a negative ion and a radical, the ion can attach itself to the radical and neutralizes by releasing the electron	$A^- + BC \rightarrow ABC + e$

- Radical-molecule reactions:

Type of reaction	Description	Equation
Electron transfer	two neutral particles collide to from two ions (one molecule has to have very high kinetic energy and is therefore rare in cold plasmas)	$A + B \rightarrow A^+ + B^-$
Ionization	two neutral particles collide causing ionization of one of them	$A + B \rightarrow A^+ + B + e$
Penning ionization / dissociation	when metastable species (B^*) collide with neutral species, the excited metastables transfer their excess energy to the target, causing ionization or dissociation	$A + B^* \rightarrow A^+ + B + e$ $A_2 + B^* \rightarrow 2A + B$
Attachment of atoms	similar to associative detachment reactions of the ion-molecule type only with neutral species	$A + BC + M \rightarrow ABC + M$
Disproportionation		$A + BC \rightarrow AB + C$
Recombination of radicals	chemically active radicals collide to form stable molecules. This can be achieved by disproportionation or combination	
Chemiluminescence	when an atom or a molecule collides with another atom, it can become excited. This can occur during a chemical reaction or not The excited radical returns then from its excited state to its energetic ground level by radiative decays	$A^* + BC \rightarrow A + BC^*$ $B + CA \rightarrow A + BC^*$ $BC^* \rightarrow BC + h\nu$

I.2.4.2. Heterogeneous reactions

Heterogeneous reactions involve a solid surface exposed to the plasma and plasma species (atoms, molecules, radicals or polymers formed in the plasma).

- Adsorption: when a species come in contact with a surface, they can be adsorbed on the surface.
- Recombination or compound formation: atoms or radicals from the plasma can react with adsorbed species to form new compounds.
- Metastable relaxation: an excited metastable species from the plasma can release its energy and return to the ground state by collision with a solid surface.
- Sputtering: when positive ions arrive at the surface with sufficient energy, it can remove atoms from the surface. These atoms can either be from the surface or adsorbed on it.
- Polymerisation: radicals in the plasma can react with radicals adsorbed on the surface and form polymers. Two radicals adsorbed onto a surface can also form polymer chains.

I.2.5. Polymerisation mechanism

I.2.5.1. Polymer formation

General consideration shows that plasma process in a glow discharge can take place simultaneously through several channels (chain radical, ionic...)[46]. However, the most common polymerisation mechanism retained is that of a 4-step radical process[43]:

- *Initiation*: free radicals or atoms are produced by collision of the monomer molecules with electrons or ions. Radical formation occurs by dissociation of either gaseous molecules or adsorbed ones.

- *Propagation*: formation of a polymer chain takes place in the gas phase as well as at the substrate surface. In the gas phase, the process involves radical-molecule and ion-molecule interaction. At the surface, propagation occurs by interaction of surface free radicals with gas phase or adsorbed molecules, radicals or ions.

- *Termination*: same reactions as those involved in the propagation process resulting in the formation of the final product.

- *Reinitiation*: under impact of energetic particles or under photon absorption, polymer chains can give rise to new radicals which can in turn enter the reaction chain.

According to Yasuda[47], plasma polymerisation can be represented by the Rapid Step Growth Polymerisation (RSGP) mechanism. In Figure I-1, P_x describes a neutral species that can be the original precursor monomer or a dissociation product including atoms. The RSPG can proceed through two parallel cycles. Cycle I occurs through repeated activation of the reaction products from monofunctional activated species, and cycle II through difunctional of multiactivated species. Both cycles play equivalent roles in plasma polymerisation.

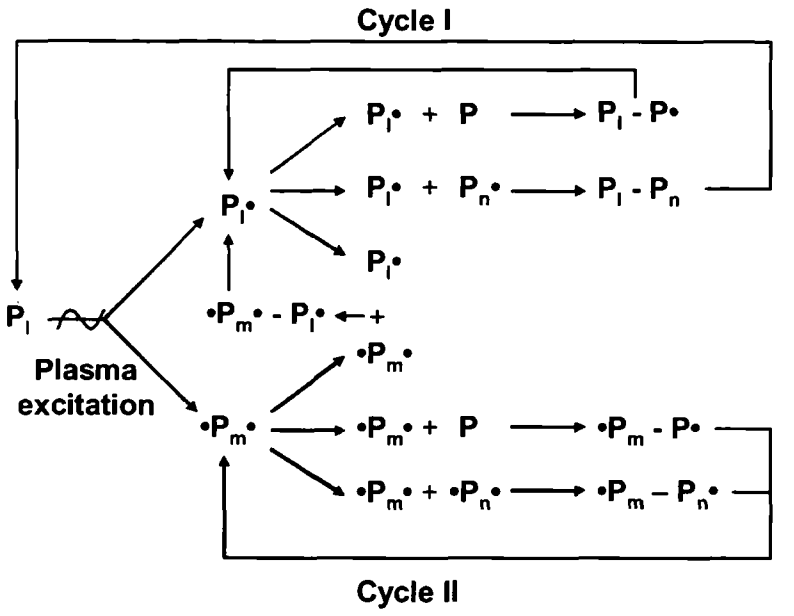

Figure I-1- Mechanisms for Rapid Step Growth Polymerisation[47]

Ionic species can also contribute to polymerisation through ion-molecule reactions or through interactions between positive and negative ions. This is especially the case in plasmas containing high concentration of negative ions (e.g. plasma of halogens and / or oxygen). However, since at pressure of around 1 torr (=133.3 Pa) the amount of free radicals is 10^5 times higher than that of ionic species, free radicals are the dominant species controlling the polymerisation by radical-molecule and radical-radical interactions. Residual free radicals involved in the RSGP mechanism may remain in the polymer as trapped free radicals, conferring a unique feature of plasma polymer films. This is the object of Chapter V and VI and will be further discussed in those chapters.

The singularity of plasma polymerisation can cause formation of products which couldn't be obtained under thermodynamic equilibrium[43]. However, due to the complexity of the plasma chemistry, it is not always possible to control the chemical pathways and predict the plasma parameters required for a certain outcome. Moreover, the state of the plasma depends on a lot of external parameters, such as electric power,

pressure, gas flow rate as well as on internal parameters, that is rate constants of reactions forming or destructing plasma species.

I.2.5.2. Ablation

The plasma process is complicated since once the plasma is ignited the gas phase is not only composed of the monomer but is a complex mixture of ionized and excited species of the monomer and of fragments of polymers. Not all of these chemical reactions lead to products formation, two opposite processes compete[47]:

- Polymer formation
- Ablation

The ablation process is mainly due to non-polymerisable species created within the plasma (e.g. H_2, HX, X_2...) interacting with the film in formation. The most extreme case occurs with perfluorocarbons where HF and F_2 etch the film away almost as rapidly as it grows.

This is called the principle of competitive ablation and polymerisation (CAP) and can be represented as followed:

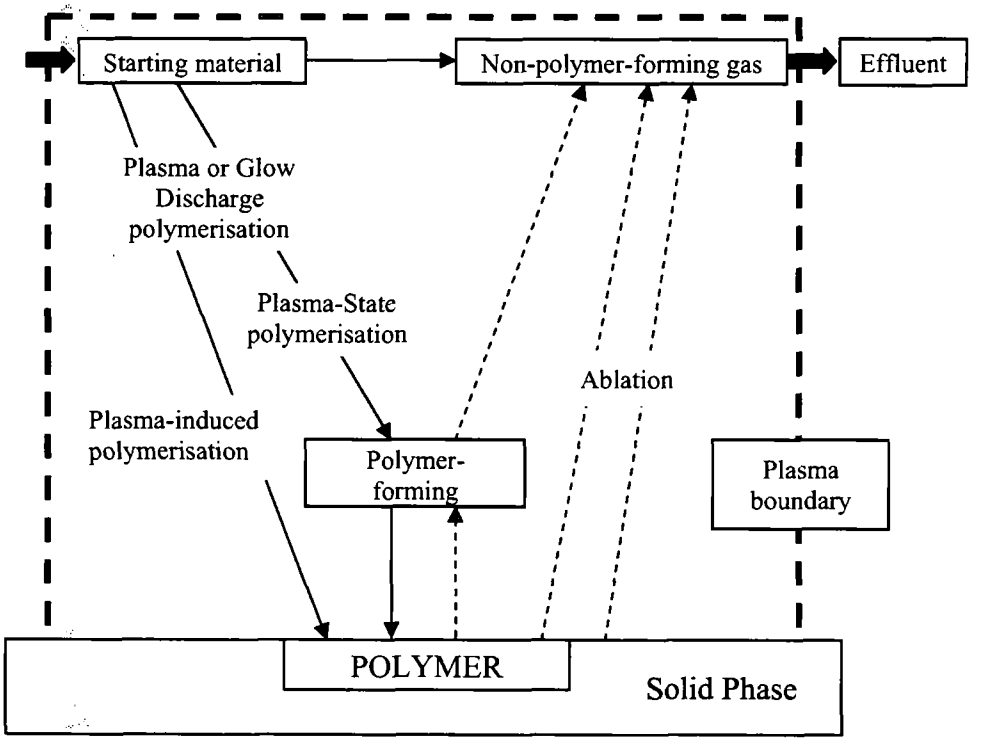

Figure I-2 - Overall mechanism of plasma polymerisation

I.3. PLASMA GENERATION

I.3.1. DC versus RF discharge

The simplest way of generating a discharge is to apply a DC electric current between two electrodes in a gas. Most of the space between the two electrodes is filled by a bright glow known as the negative glow[48]. The positive column is a conduit of current from the negative glow to the anode. This is where the definition of plasma can be applied. However, by decreasing the pressure or the reactor length, this region can be eliminated without extinguishing the glow discharge. This is because the negative glow contains a higher concentration of charged species than the positive column. Therefore, the plasma deposition will occur preferentially on the cathode[49]. If the frequency of the electric field is increased to radio frequency (RF), the negative glow region can be eliminated; in that case, the deposition of the plasma polymer occurs on the substrate place between the electrodes with the same rate as in DC glow discharge. Moreover, RF

discharge has been found to be less destructive in terms of plasma polymer properties, and it is more efficient in sustaining the glow discharge.

A frequency of 13.56 MHz is commonly used for RF discharge, but it is only a value allocated by the international communications authorities at which radiations at a certain frequency without interfering with communications are allowed[48].

I.3.2. Continuous Wave versus Pulsed plasma polymerisation

To plasma polymerise a monomer on a surface and preserve its structure, it is necessary to limit the interactions of the monomer with energetic species in the plasma. To control the cross-link density and to improve retention of the monomer, several parameters can be considered[49]:

- to limit the power input
- to work at relatively high pressure
- to limit the residence time of molecules in the plasma
- to avoid ionic bombardment

The pulsed plasma polymerisation technique has been developed 15 years ago[50] to improve monomer retention. This is achieved by pulsing the electric discharge, which increases the efficiency of the plasma polymerisation. During the ''on'' time, both ions and reactive neutral species are produced. However, since ions often have shorter lifetimes than neutrals, during the ''off'' time the ratio of neutrals to ions will increase, and thus, the competition between growth and etching reactions at the surface will be altered to favour film deposition from reactive neutrals.

The average power delivered to the system during pulsing is given by Equation I-2.

$$\textbf{Equation I-2} \quad < P >= P_p \left(\frac{t_{on}}{t_{on} + t_{off}} \right)$$

Where P_p is the power delivered by the power supply, t_{on} the time on and t_{off} the time off.

Therefore, the peak power used is considerably less than that of the continuous wave operation if a low duty cycle is used. The surface retention of some monomers was found to improve with lower duty plasmas. Film controllability is attributable to a higher degree of chemical selectivity in the 'plasma off' periods due to the fact that highly energetic species such as ions dissipate more rapidly than the less reactive neutral radicals, which are what give rise to polymerisation.

I.3.3. Reactor

Several types of reactors can be coupled with an electric field[49]. For low-frequency DC glow discharge, internal electrodes are required. With this technique, a uniform electric field can be created, but the drawbacks are contamination of the electrodes as they are situated in the reactor, and the amount of monomer actually entering the plasma and bypassing the electrodes cannot be determined. With sufficient high frequencies, the electrodes can be removed outside the reactor. They can be placed in order to create an electric field either perpendicular or parallel to the cylindrical axis of the reactor. Alternatively, an inductive coupling can be created by wrapping a copper coil around the reactor.

The latter reactor is the one used for the plasma deposition carried out in this work because it presents the advantage of not having to clean the electrodes after plasma treatment. Moreover, with the set up used (see schematic on Figure I-3) a pressure of

less than 0.2 mbar can be maintained in the reactor, and the introduction of the sample in the reactor is facilitated.

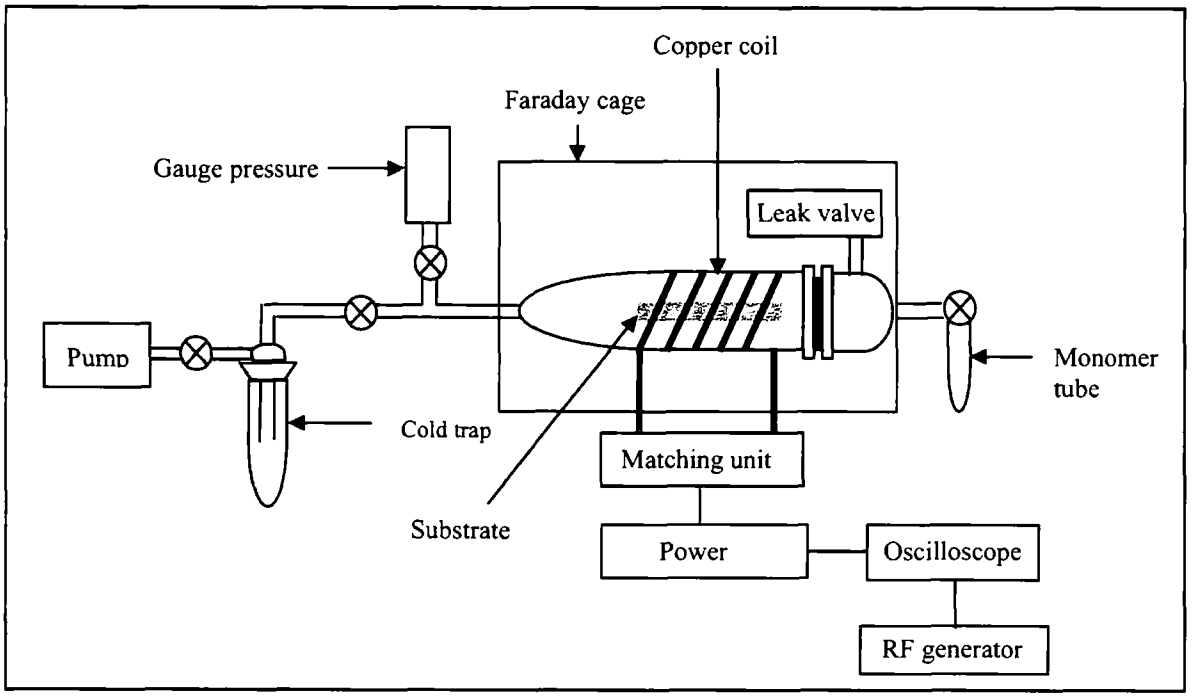

Figure I-3 – Diagram of a reactor used for the production of glow discharge

The monomer vapours flow continuously into the plasma reactor whilst the glow discharge is in progress. The monomer is wholly or partially consumed in the conversion to plasma polymer. Gaseous by-products and unconverted monomer are continuously pumped out of the reactor and condensed in the cold trap to prevent any vapour from entering the pump.

A LC (inductance – capacitor) matching unit, composed of variable capacitors, is used to reduce the Standing Wave Ratio (SWR), which represents the ratio of the reflected power (which is not used to ignite the plasma but is lost as heat) to the input power sent into the coils. The RF power supply is triggered by a signal generator. The pulse width and amplitude are monitored with an oscilloscope.

I.4. REFERENCES

1 - Janca, J.; Stahel, P.; Buchta, J.;Subedi, D.;Krcma, F.;Pryckova, J., *Plasmas Polym.*, **2001**, 6, 15-26

2 - Iriyama, Y.; Yasuda, T.; Cho, D.L.; Yasuda, H., *J. Appl. Polym. Sci.*, **1990**,39 (2), 249-264

3 - Wang, J., *Anal. Chem.*, **1995**, 67 (12), 487 – 492

4 - Nakamura, H.; Karube, I., *Anal. Bioanal. Chem.* **2003**, 377 (3), 446-468

5 - Jones, L.; Dumbleton,K., 26-32, **2002**, http://www.optometry.co.uk/files/2a85c209e250a4b2b829811247ea977d_jones20020920.pdf

6 - Datta, M., *Electrochim. Acta*, **2003**, 48 (20-22), 2975-2985

7 - Bloyce, A.; Qi, P.-Y.; Dong, H.; Bell, T., *Surf. Coat. Technol.*, **1998**, 107, 125–132

8 - Yamamoto, Y.; Nishihara, H.; Aramaki, K., *J. Electrochem. Soc.*, **1993**, 140 (2), 436-443

9 - PalDey, S.; Deevi, S.C., *Mater. Sci. Eng., A*, **2003**, 342, 58-/79

10 - Langlade, C. ; Vannes, B. ; Taillandier, M. ; Pierantoni, M., *Tribol. Int.*, **2001**, 34, 49–56

11 - Elbert, D.L.; Hubbell, J.A., *Annu. Rev. Mat. Sci.*, **1996**, 26:365-94

12 - Pan, Y.V.; Wesley, R.A.; Luginbuhl, R.; Denton, D.D.; Ratner, B.D., *Biomacromol.*, **2001**, 2, 32-36

13 - Hochart, F.; Levalois-Mitjaville, J.; De Jaeger, R.; Gengembre, L.; Grimblot, J., *Appl. Surf. Sci.*, **1999**, 142, 574–578

14 - Olde Riekerink, M. B.; Terlingen, J. G. A.; Engbers, G. H. M.; Feijen, J., *Langmuir*, **1999**, 15, 4847-4856

15 - Teare, D.O.H.; Schofield, W.C.E.; Garrod, R.P.; Badyal, J.P.S., *J. Phys. Com. B*, **2005**, 109, 20923-20928

16 - Schofield, W.C.E.; McGettrick, J.; Bradley, T.J.; Badyal, J.P.S.; Przyborski, S., *J. Am. Chem. Soc.*, **2006**, 128, 2280-2285

17 - Lintz, H. K.; Murrell, S. R.; Crawley, R. L.; Daukas, J. C. *J. Vac. Sci. Technol., A.* **1988**, 6, 1869

18 - Yasuda, T.; Yoshida, K.; Okuno, T.; Yasuda, H., *J. Polym. Sci. Part B: Polym. Phys.*, **1988**, 26 (10), 2061-2074

19 - Fonseca, J.L.C.; Apperley, D.C.; Badyal, J.P.S., *Chem. Mater.*, **1993**, 5, 1676-1682

20 - Tajima, I.; Yamamoto, M., *J. Polym. Sci. Part A: Polym. Chem.*, **1987**, 25, 1737-1744

21 - Yaganawa, Y.; Masutani, Y.; Kogoma, M.; Tanaka, K., Thin *Solid Films*, **2007**, 515, 4116–4120

22 - Jenkins, A.T.A.; Hu, J.; Wang, Y.Z.; Schiller, S.; Foerch, R.; Knoll, W., *Langmuir*, **2000**, 16, 6381-6384

23 - Leich, M.A.; Mackie, N.M.; Williams, K.L.; Fisher, E.R., *Macromol.*, **1998**, 31, 7618-7626

24 - Kurosawa, S.; Aizawa, H.; Talib, Z. A.; Atthoff, B.; Hilborn, J., *Biosens. Bioelectron.*, **2004**, 20, 1165-1176

25 - Hozumi, K., *Pure Appl. Chem.*, **1988**, 60, 697-702

26 - Tarducci, C.; Schofield, W.C.E.; Badyal, J.P.S., *Chem. Mater.*, **2002**, 14, 2541-2545

27 - van Os, M.T.; Menges, B.; Foerch, R.; Vancso, G.J.; Knoll,W., *Chem. Mater.*, **1999**, 11, 3252-3257

28 - Wu, Z.; Yan, Y.; Shen, G.; Yu, R., *Anal. Chim. Acta*, **2000**, 412, 29-35

29 - Teare, D.O.H. ; Barwick, D.C.; Schofield, W.C.E.; Garrod, R.P.; Beeby, A.; Badyal, J.P.S., *J. Phys. Chem. B*, **2005**, 109, 22407-22412

30 - Tarducci, C.; Schofield, W.C.E.; Badyal, J.P.S., *Chem. Mater.*, **2001**, 13, 1800-1803

31 - Schofield, W.C.E.; Badyal, J.P.S., *Plasma Chem. Plasma Process.*, **2006**, 26, 361-369

32 - Tarducci, C.; Kinmond, E.J.; Badyal, J.P.S., *Chem. Mater.*, **2000**, 12, 1884-1889

33 - Jafari, R.; Tatoulian, M.; Morscheidt, M.; Arefi-Khonsari, F., *React. Funct. Polym.*, **2006**, 66, 1757-1765

34 - Spanos, C.G., Badyal, J.P.S.; Goodwin, A.J.; Merlin, P.J., *Polym.*, **2005**, 46, 8908-8912

35 - Mackie, N.M.; Dalleska, N.F.; Castner, D.G.; Fisher, E.R., *Chem. Mater.*, **1997**, 9, 349-362

36 - Calderon, J.G.; Timmons, R.B., *Macromol.*, **1998**, 31, 3216-3224

37 - Teare, D.O.H.; Barwick, D.C.; Schofield, W.C.E.; Garrod, R.P.; Ward, L.J.; Badyal, J.P.S., *Langmuir*, **2005**, 21, 11425-11430

38 - Coulson, S.R.; Woodward, I.S.; Badyal, J.P.S., *Langmuir*, **2000**, 16, 6287-6293

39 - Tran, N.D.; Dutta, N.K.; Roy Choudhury, N., *Thin Solid Films*, **2005**, 123-132

40 - Chen, X.; Rajeshwar, K.; Timmons, R.B.; Chen, J.-J.; Chyan, O.M.R., *Chem. Mater.* **1996**, 8, 1067-1077

41 - Han, L.M.; Rajeshwar, K.; Timmons, R.B., *Langmuir*, **1997**, 13, 5941-5950

42 - Langmuir, I., *Phys. Rev.*, 33, **1929**, 954

43 - Grill, A., Cold Plasma in Materials Fabrication – From fundamentals to applications, IEEE Press, 1994

44 - Inagaki, N, Plasma Surface Modification and Plasma Polymerisation, Technomic, Lancaster, 1996

45 - Sturrock, P.A., Plasma Physics: An Introduction to the Theroy of Astrophysical, Geophysical & Laboratory Plasmas, Cambridge University Press, 1994

46 - Polak, L.S.; Lebedev, Y.A., Plasma chemistry, Cambridge International Science Publishing, 1998

47 - Yasuda, H., Plasma polymerisation, Academic press Inc., Orlando, Florida, 1985

48 - Chapman, B., Glow Discharge Processes, Wiley-Interscience, New York, 1980

49 - d'Agostino, R., Plasma Deposition, Treatment, and Etching of Polymers, Academic Press, London, 1990

50 - Savage, C.R.; Timmons, R. B.; Lin, J.W., *Chem. Mater.* **1991**, 3, 575-577

II

CHAPTER TWO

Surface Analysis and other Techniques

II.1. SURFACE ANALYSIS TECHNIQUES

II.1.1. X-ray Photoelectron Spectroscopy (XPS)

II.1.1.1. Basics of the XPS technique

X-ray photoelectron spectroscopy is a versatile technique used to analyse the elemental and chemical composition of surfaces.

The surface of a sample is excited by a monochromatic soft X-rays source of known energy hν, and as photoionisation of atoms in the sample occurs, core level photoelectrons of binding energy E_b (<hν) are ejected[1]. Their kinetic energy E_k is then measured in the spectrometer. The equation established by Rutherford in 1914 relating the kinetic energy to the binding energy, was subsequently modified to give the following[2] (Equation II-1):

Equation II-1 $$E_k = h\nu - E_b$$

Since each element presents a unique binding energy, measurement of the kinetic energy of the photoelectrons provides elemental analysis. The main region of interest is electron energies ranging from 100 to 1200 eV. Furthermore, XPS can give information about the chemical environment of atoms as binding energy, and hence kinetic energy, depends also on the atoms neighbouring[3].

The surface sensitivity of XPS lies in the fact that the sampling depth equals the inelastic mean free path λ of the detected electrons. Electrons at a statistical distance bigger than λ from the surface are not detected as they are more likely to have undergone inelastic collision, thus losing their energy. For the energy of interest, 100-1000 eV, the mean free path vary between 10 and 100 Å[2]. Hence the electrons are only originating from the first atomic layers. A further factor on the depth of analysis is the

angle at which electrons are detected from the surface. The greatest depth of analysis is for detection normal to the surface; here around 95% of electrons are emitted from a depth of 3 λ (the escape depth). If the take-off angle (taken from the surface of the substrate) is increased, the escape depth becomes a function of 3 $\lambda \sin \theta$.

II.1.1.2. Ultra-High Vacuum (UHV)

During experimental studies, surfaces need to be maintained in a constant sate[2] because:

- Photoelectrons need to be able to travel from the surface of the sample to the detector without striking a gas atom as this would alter its kinetic energy
- Any contamination of the surface before and during analysis must be avoided

Hence, measurements are always performed in Ultra-High Vacuum (UHV) (in the range of 10^{-8} to 10^{-9} torr).

The pressure in the main chamber is usually evaluated by an ion gauge measuring the current carried by ions formed in the gas by impact of electrons. Two types of ion gauges are available: hot cathode and cold cathode. In the experiments carried out for this thesis, a hot cathode ion gauge is used. The hot filament, usually iridium, emits electrons into the vacuum, where they collide with gas molecules to create ions. These positively charged ions are accelerated toward a collector where they create a current in a conventional ion gauge detector circuit. The amount of current formed is proportional to the gas density or pressure. Most hot-cathode sensors measure vacuum in the range of 10^{-2} to 10^{-10} torr.

II.1.1.3. The Auger effect

The analysis of XPS spectra can be made difficult due to the presence of the Auger effect[2]. When a photoelectron is ejected from the atomic core level under excitation, the hole created in the energy level can be quickly filled by an electron from a higher level

shell. The energy released by this process can either be in the form of an X-ray or, most probably, be transferred to another electron which is, in turn, ejected from the atom (Auger electron). Its energy is determined by the binding energies of the atomic energy levels of the participating atom and can therefore be used on its own for elemental analysis (Auger Electron Spectroscopy – AES)[4].

Because this effect can occur with X-ray radiations as well, XPS spectra can also exhibit Auger electron peaks which can complicate their interpretation. However, as Auger electron energies are independent of the source, Auger peaks can be easily identified by changing the source of radiation and acquiring another spectrum.

The two processes occurring under X-ray irradiations are represented in Figure II-1.

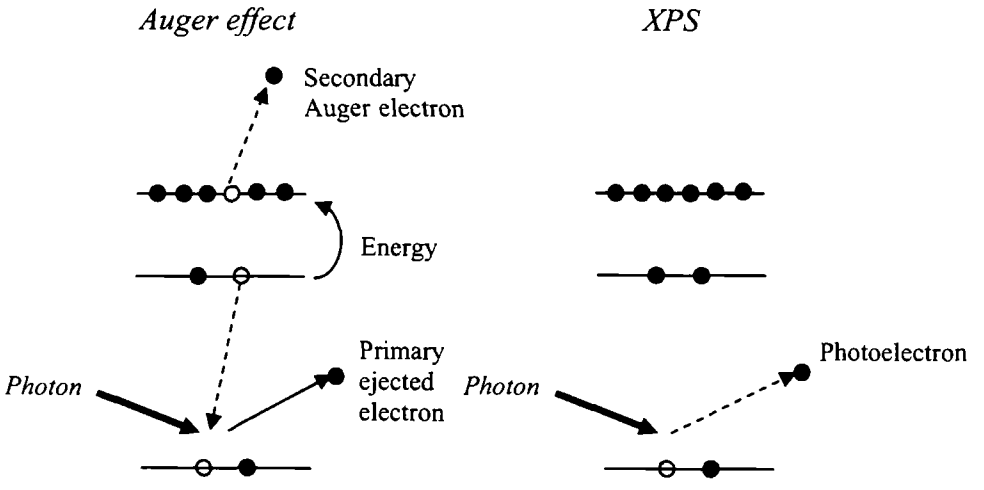

Figure II-1 – Representation of the processes involved in XPS

Both are kept constant during the acquisition of a spectrum[5].

II.1.1.4. Energy resolution requirements

To allow the identification of different chemical states of an element by XPS, the same absolute resolution needs to be applied to any photoelectron peak in the spectrum. Equation II-2 gives the resolution between absolute and relative energy resolution:

Equation II-2 $$R = \frac{\Delta E}{E_0}$$

where R: relative resolution

ΔE: absolute resolution = full width at half-maximum (FWHM) height of a chosen peak

E_0: kinetic energy of the peak position

If the natural line widths of the aluminium or magnesium X-ray sources (see Table II-1) were to be matched by the energy resolution at the maximum available energies, a resolution of about 6×10^{-4} would be required. This can be achieved relatively easily by the use of a very large analyser but not without a significant loss of sensitivity.

To overcome this problem, the kinetic energies of the photoelectrons are retarded. Two different methods are commonly used:

- Deceleration to a constant pass energy (Constant Analyser Transmission mode CAT) ⇨ equivalent to constant absolute energy resolution

- Deceleration by a constant ratio (Constant Retard Ratio mode CRR) ⇨ equivalent to constant relative energy resolution

In the CAT mode, quantification is easier; however signal-to-noise ratio becomes worse towards low kinetic energy. In the CRR it is exactly the opposite.

Retardation is usually achieved by means of lenses placed just before the aperture of the analyser.

II.1.1.5. Instrumentation

An XPS spectrometer is composed mainly of a monochromatic X-ray source, an electron analyser and a detector. It can be represented as in Figure II-2:

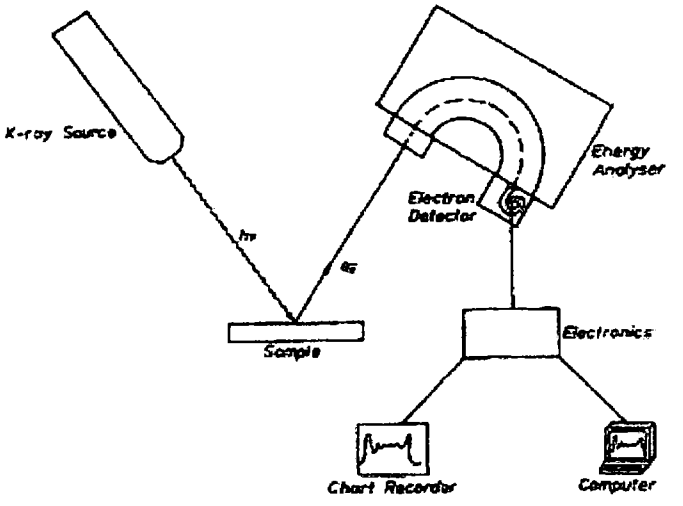

Figure II-2 - Schematic representation of an XPS[4]

II.1.1.5.a. XPS sources

X-rays are generated by heating a filament near earth potential, from which electrons are accelerated toward an anode at a high positive potential to produce a continuum of bremsstrahlung radiation with characteristic x-ray lines superimposed[3] (Figure II-3). These X-ray lines are a result of relaxation of atoms ionized during electron bombardment. During this process, electrons from an outer shell fill inner shell vacancies whilst emitting an x-ray.

A thin-aluminium window separates the sample from the source to prevent any contamination of the source and to attenuate high-energy bremsstrahlung radiation without affecting the characteristic radiation.

Since the flux irradiating the sample varies inversely as the square of the distance from the anode to the sample surface, the sample should be placed as close to the anode as possible[2].

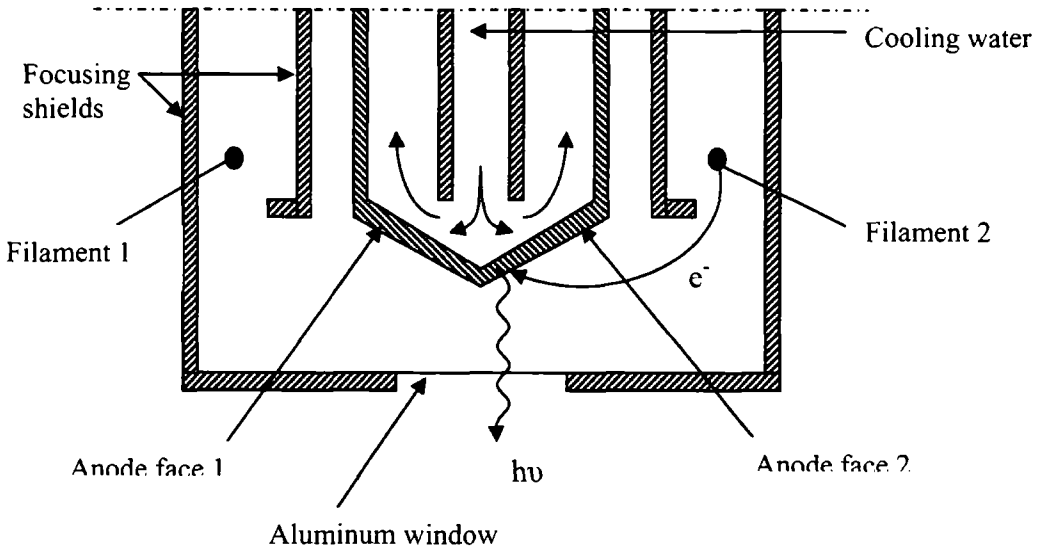

Figure II-3 – Soft X-ray source with dual anode

The choice of the anode material is governed by the following conditions:

- The X-rays need to be of sufficient energy to excite core-levels electrons of all elements (i.e. > 1 keV)
- The X-rays intensity has to be intense enough to produce a detectable electron flux
- The material has to be good conductor to sustain heat transfer (cooling system present)
- The X-ray lines need to have a narrow line width (< 1 eV) in comparison to the intrinsic core-level line widths and chemical shifts of the sample under study
- The material has to be simple to use and to maintain

The two most common nearly monochromatic sources are Mg and Al as their K_α lines are sufficiently energetic and have a relatively narrow line-width (see Table II-1). Moreover, these two materials are easy to handle and stable. The material is deposited onto a cooper block as a thick layer (10 μm) to ensure conductivity.

Table II-1 – Energies and widths of some characteristic soft X-ray lines

Material	Line	Energy (eV)	Width (eV)
Y	Mζ	132.3	0.47
Zr	Mζ	151.4	0.77
Nb	Mζ	171.4	1.21
Mo	Mζ	192.3	1.53
Ti	Lα	395.3	3
Cr	Lα	572.8	3
Ni	Lα	851.5	2.5
Cu	Lα	929.7	3.8
Mg	Kα	1253.6	0.7
Al	Kα	1486.6	0.85
Si	Kα	1739.5	1
Y	Lα	1922.6	1.5
Zr	Lα	2042.4	1.7
Ti	Kα	4510	2
Cr	Kα	5417	2.1
Cu	Kα	8048	2.6

Most XPS instruments have a dual Mg/Al anode. The main interest is that X-ray produces Auger electrons as well as photoelectrons; the energy of the first ones is independent of the source, whereas the binding energy of the second ones is. Therefore, the apparent binding energy of Auger peaks appears to change (by 233 eV) on going from Al Kα to Mg Kα radiation, whereas photoelectrons peaks do not shift. This is useful to differentiate Auger peaks from photoelectron peaks, but also to resolve peaks that may interfere with each other.

If the K_α lines are monochromatic enough in the case of aluminium and magnesium, other X-ray sources do not produce single X-ray lines, but a series of lines superimposed on the Bremsstrahlung continuum[4], which can cause peak assignment and

interpretation problems. To remove the unwanted components, monochromatisation of the source is performed by using a diffraction grating (e.g. quartz single crystal). This enhances the signal-to-noise ratio and improves energy resolution, but it greatly decreases the X-ray intensity due to dispersion.

II.1.1.5.b. Electron energy analyser

The measurement of an electron energy spectrum is performed by an electron energy analyser of electrostatic type. There are three common ones:

- The retarding field analyser (RFA)
- The cylindrical mirror analyser (CMA)
- The concentric hemispherical analyser (CHA)

II.1.1.5.b.1. The retarding field analyser

RFA is the oldest type of analyser. The incident electrons are directed towards a series of four grids concentric with a collecting screen. The inner and outer grids are at ground potential whilst the two others are connected together at the retarding potential. A small modulating voltage from a signal source is superimposed to the retarding potential as a reference.

A relative resolution of 0.5 – 1 % is generally obtained with this type of analyser, which does not provide XPS measurement with good enough absolute resolution in the energy range of interest. Moreover, all electrons with energies greater than the potential are allowed to reach the collector leading to a very poor signal-to-noise ratio.

II.1.1.5.b.2. The cylindrical mirror analyser

The CMA consists of two cylinders of different radii positioned coaxially. The inner cylinder is grounded whilst the outer is at a potential $-V$. Electrons emitted from a source at an angle α pass through an aperture in the inner cylinder and those with a

particular energy E_0 are deflected by the outer cylinder through another aperture onto a focus point.

The very high transmission of the single-pass CMA makes is really attractive for AES technique. However, unlike AES sources, XPS ones are not focused, leading to poor luminosity since the acceptance area of the analyser is smaller than the source area. Moreover, absolute resolution obtained with a single-pass CMA is too poor for XPS analysis[5].

Double-pass CMAs have been developed to overcome the luminosity problem for XPS. Two CMAs are mounted in series with pre-retarding grids before the entrance slit. This allows the selection of a fixed band-pass energy instead of a unique energy E_0, which increases resolution. However, when the pass energy is decreased to reach absolute resolution (< 1 eV), the signal intensity decreases greatly.

II.1.1.5.b.3. The concentric hemispherical analyser

CHA is currently the analyser of choice for XPS since it overcomes some problems encountered with the two other types of analyser.

A CHA consists of two metal hemispheres of radii R_1 (inner) and R_2 (outer): one hemisphere being shaped concave, and the other convex. They are arranged such that their centres of curvature are coincident (see Figure II-4). Different voltages are placed on each hemisphere to produce an electric field between the two hemispheres. The potential is applied in order to have the outer hemisphere negative and the inner one positive. In the middle, an equipotential exists, radii R_0. The voltage is swept to obtain the energy spectrum. Electrons are injected into the gap between the hemispheres. If the electrons are travelling very fast, they will impinge on the outer hemisphere. If they are travelling very slowly, they will be attracted to the inner hemisphere. Hence electrons

must possess a specific kinetic energy E_{pass} (pass energy) to be transmitted through the analyser to the detector.

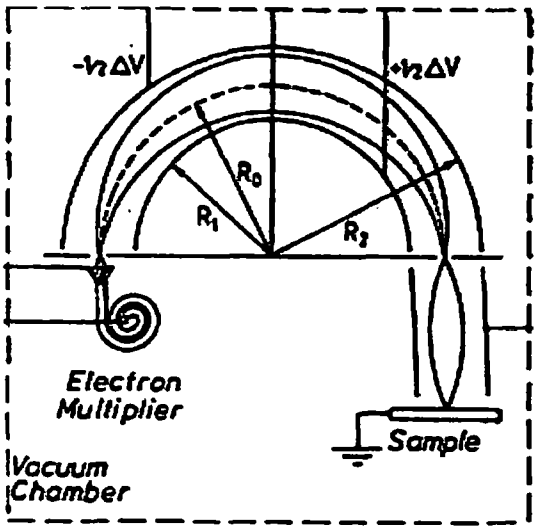

Figure II-4 – Schematic of a concentric hemispherical analyser (CHA)[4]

To improve luminosity at high-energy resolution, a system of lenses can be used. This allows the sample to be place further away form the analyser entrance slit, allowing the X-ray source to be closer to the surface to be analysed.

Another advantage of the CHA over the CMA is that the narrow acceptance angle makes it well-suited for angle-dependence measurements, whilst the CMA collects over 360°.

II.1.1.5.c. Detector - Electron multiplier

After passing through the analyser, the electrons are then focused onto a channel electron multiplier or channeltron. This device works as a detector and allows the measurement of the current generated by the electrons. After the CHA, the current is in the region of 10^{-16} to 10^{-14} A, which is really low for conventional detection instruments. The channeltron consists of a small curved lead-doped glass tube coated inside by a semiconducting material possessing a high secondary electron yield. A voltage of a few kilovolts is applied between the ends of the multiplier. The electrons entering the device

collide with its wall, generating secondary electrons, which are then accelerated until they strike the wall again, and so on. The gain is generally of the order of 10^8 A on the current, and the background count is low (< 1count per minute)[3].

II.1.2. Fourier Transform (FT-IR) spectroscopy

II.1.2.1. Basics of the IR spectroscopy

Infrared spectroscopy is one of the most common spectroscopic techniques. It is mainly used to determine the chemical structure of a compound, organic or inorganic, by measuring the absorption related to different vibrations within the molecule. The identification can be achieved because a specific functional group, or structural characteristic, has a unique vibrational frequency. The effects of all the different functional groups taken together constitute a unique molecular "fingerprint" that can be used to confirm the identity of a sample. This technique can be operated with various samples such as liquids, gases as well as solids (powder or films).

A vibrational mode is IR-active only if there is a change in the molecular dipole moment during the vibration[6]. Therefore, anti-symmetric vibrational modes and vibrations due to polar groups will absorb in the IR region. The characteristic vibrational frequency is referred as a 'group frequency', which is the vibrational band consistently produced by a certain sub molecular group of atoms in a characteristic spectral region.

In practice, a radiation from a broad band source is dispersed through a monochromator into component frequencies. It subjects molecules to excitation in selected spectral regions (the most common being 4000 – 200 cm^{-1}). A detector then collects the information about their changes in vibrational energy. The molecule is

excited to a higher vibrational state by absorbing a part of the IR radiation. Equation II-3 gives the transmittance at a given wave number:

Equation II-3 $$T = \frac{I}{I_0}$$

Where T is the transmittance, I the intensity of the transmitted light after sample absorption and I_0 the intensity of the incident light before sample absorption.

II.1.2.2. FTIR spectroscopy

Fourier transform spectrometers have recently replaced dispersive instruments for most applications extending greatly the capabilities of infrared spectroscopy. Instead of viewing each component frequency sequentially, in FTIR spectroscopy all frequencies are examined simultaneously which improved a lot the signal-to-noise ratio. This is achieved by replacing the monochromator by an interferometer[7] (described in following paragraph).

FTIR spectroscopy has three main advantages over conventional IR spectroscopy:

- Rapid signal averaging
- Greater light throughput
- Better wavelength calibration

These improved a lot speed and sensitivity of the technique. Indeed, it decreases the acquisition time down to few seconds and requires smaller sample size or concentration.

II.1.2.3. Instrumentation

Modern spectrometers are composed of three main elements: a radiation source, a Michelson interferometer and a detector.

II.1.2.3.a. Sources

IR spectrometers commonly use an inert solid material heated to incandescence by an electric current as a source. Three popular types of sources are the Nernst Glower, composed mainly of rare-earth oxides (e.g. zirconium, thorium), the Globar, which is a silicon carbide rod and the Nichrome coil. All these sources emit in the IR region and approach the energy distribution of a theoretical black body, which holds the radiation over all wavelengths. Moreover, the total radiation of such a black body is proportional to its absolute temperature; therefore increasing the temperature of the source maybe accompanied by an energy increase in the unwanted short wavelengths. Most IR sources are operated at a temperature where the energy maximum is near the short wavelength limit of the spectrum.

The same types of radiation sources are used for both dispersive and Fourier transform spectrometers. However, the source is often water-cooled in FTIR instruments to provide better power and stability.

II.1.2.3.b. Michelson Interferometer

An interferometer is used in FT-IR spectrometers as a replacement for the monochromator. It allows the analysis of a radiation by evaluating the intensity of the transmitted light for each wavelength. A schematic of the interferometer is given in Figure II-5:

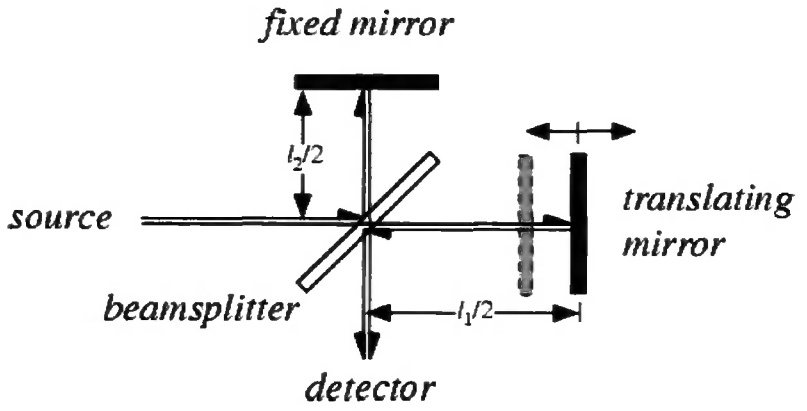

Figure II-5 – Schematic of the Michelson interferometer[8]

The Michelson interferometer contains a fixed mirror, a moving mirror and a beam-splitter. The two mirrors are positioned at a right angle to each other and orientated perpendicularly, and the beam-splitter is placed at the top of the right angle and orientated at a 45° angle relative to the two mirrors. The beam-splitter transmits half of the incident radiation to the moving mirror and reflects the other half to the fixed mirror. The two beams are reflected by the mirrors back to the beam-splitter where they recombine. When the fixed mirror and moving mirror are equidistant from the beam-splitter, the amplitudes of all frequencies are in phase and interfere constructively. As the moving mirror is moved away from the beam-splitter (retarded), an optical path difference is generated. A pattern of constructive and destructive interferences (interferogram) is generated which depends on the position of the moving mirror and on the frequency of the radiation resulting in the time-modulation of the light intensity. This source beam is then directed through the sample compartment to the broad-band detector and a fast Fourier Transform gives the signal corresponding to each frequency.

II.1.2.3.c. Detectors

Detectors used in IR spectrometers can be categorized into two classes: thermal detectors and photon detectors.

Thermal detectors measure the heating effect produced by infrared radiation. This is achieved by determining quantitatively a variety of physical properties: in pneumatic device, such as Golay detector, the expansion of a non-absorbing gas is evaluated, in thermistors, the electrical resistance is measured, and in thermocouples, voltage at junction of dissimilar metals is considered.

Photon detectors exploit the interaction of IR radiation with a semiconductor material. Non-conducting electrons are excited to a conducting state, which generates a small current or voltage.

Thermal detectors provide a linear response over a wide range of frequencies but exhibit slower response times and lower sensitivities than photon detectors.

II.1.2.4. Infra-red spectroscopy at surfaces

Increasing demand in thin film characterization brought FTIR technique forward. Indeed, unlike many surface analysis techniques, infra-red spectrometry has the great advantage of being non-destructive[9].

There are a number of ways in which the IR technique may be implemented for the study of adsorbates on surfaces:

- For samples with high surface area, transmission spectroscopy or diffuse reflectance spectroscopy are commonly used. However, only isotropic samples or those oriented in a plane can be analysed that way. Indeed, the electric field vector in both modes is parallel to the surface, which means that only molecular groups with dipolar moments parallel to the surface will adsorb IR photons.
- For studies on low surface area samples with molecular groups preferentially oriented at an angle to the surface normal, reflection-absorption spectroscopy or

multiple internal reflection spectroscopy are employed. The experiments carried out for this thesis exploited the low surface area sampling technique, thus only these will be described thereafter.

II.1.2.4.a. Reflection Adsorption Infra-Red Spectroscopy (RAIRS)

When a wave impinges on an interface between two media with different indices of refraction, it splits into two beams; a refracted and a reflected one (cf. Figure II-6).

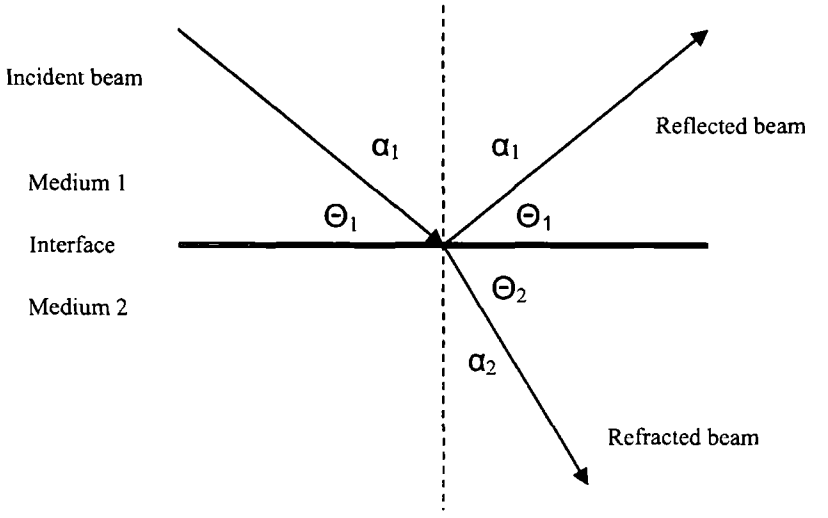

Figure II-6 – Splitting of an incident beam at an interface

Snell's law gives the relationship between angles of incidence and refraction[10] (Equation II-4):

Equation II-4 $$n_1 \sin(\alpha_1) = n_2 \sin(\alpha_2)$$

Where n_x is the refractive index in medium x, α_1 is the incident angle, and α_2 is the refracted angle.

This equation can also be rearranged under the following (Equation II-5):

Equation II-5 $$\frac{c_1}{\cos(\theta_1)} = \frac{c_2}{\cos(\theta_2)}$$

Where c_x is the speed of the wave in medium x, θ_1 the grazing angle (i.e. the angle formed by the wave with the interface in medium 1), and θ_2 the angle from the normal of the refracted wave.

When the angle θ_1 reaches a critical value, $\theta_{crit} = \cos^{-1}\left(\frac{c_1}{c_2}\right)$, the incident beam is entirely reflected. Below the critical angle, the angle of incidence is generally referred to as the grazing angle.

Greenler et al.[11] showed that when the beam reaches the surface at grazing angle, the electric field at the surface is maximised. Molecules near the interface can absorb some of this IR radiation, but only if the dipole moment for the transition is perpendicular to the plane of the surface. Radiation polarized parallel to the surface plane has a near zero electric field near the surface. Thus, an IR absorption spectrum for adsorbed species can be obtained, yielding molecular identity information.

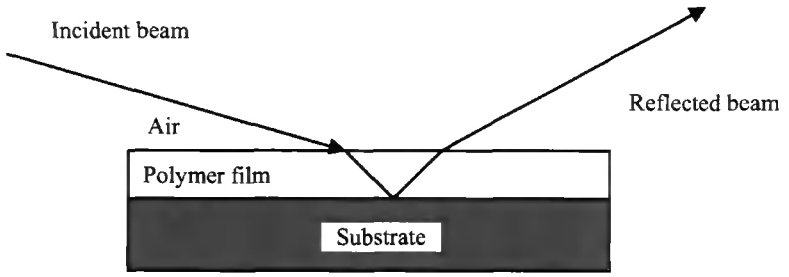

Figure II-7 – Grazing Angle Reflection

On this basis, RAIRS technique can be used to study thin film deposited at the surface of a highly-reflective sample, such as a metal single crystal surface. The IR beam arrives at the surface of a gold or silicon surface at grazing angle ($\theta_{1(Gold)}=84^\circ - \theta_{2(Silicon)}=66^\circ$). The major problem of this technique is that of sensitivity since the film is usually very thing (down to 20nm). Thanks to recent improvements with FTIR

spectroscopy, this has been greatly improved. Low frequency modes (<600cm^{-1}) are generally not observable, the region covered lies between 4000 – 700 cm^{-1}.

II.1.2.4.b. Multiple Internal Reflections Spectroscopy (MIR)

In this technique, also referred to as Attenuated Total Reflection (ATR) spectroscopy, the IR beam is guided in an IR transparent crystal (e.g. polished silica, silver chloride, germanium, diamond) by total reflection (i.e. the crystal has to have a refractive index much higher than the sample). Due to quantum mechanical properties of the IR light, the electromagnetic field extends beyond the crystal surface as a so-called evanescent field, and can be absorbed by species present on the surface of the sample. The penetration within the sample can vary between 0.1 and 1 μm depending on the wavelength of the IR source[12].

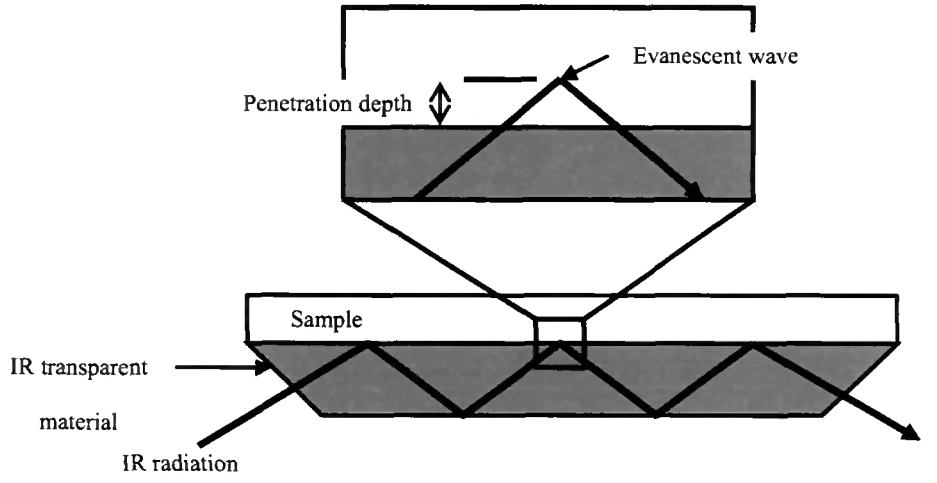

Figure II-8 - Total internal reflection at the interface of an internal reflection element. Depth of penetration of the evanescent wave is approximately 1 μm.

By placing any sample (liquid, compacted powder or film) directly onto the surface of the crystal, this evanescent wave allows the detection of its chemical nature.

II.1.3. Video contact angle measurements (VCA)

Contact angle measurement is of great importance in all solid-liquid-fluid interfacial phenomena[13].

Liquids have a specific surface tension which is the force that minimizes the surface energy of liquid droplets and causes them to adopt the shape with the lowest surface area to volume ratio (=sphere). When a droplet is brought into contact with a surface this spherical shape is perturbed, this leads to an increase in the surface energy necessitating that work be done against the surface tension. Upon deposition on a surface a liquid droplet will spread as a result of the surface energy outweighing the surface tension of the liquid.

The measurement of the angle that the liquid makes with an ideal (i.e. rigid, flat, chemically homogeneous, insoluble, and non-reactive) solid surface, termed the intrinsic contact angle θ, is a qantitative assessment of the wettability of the substrate surface towards this liquid[14] (see Figure II-9).

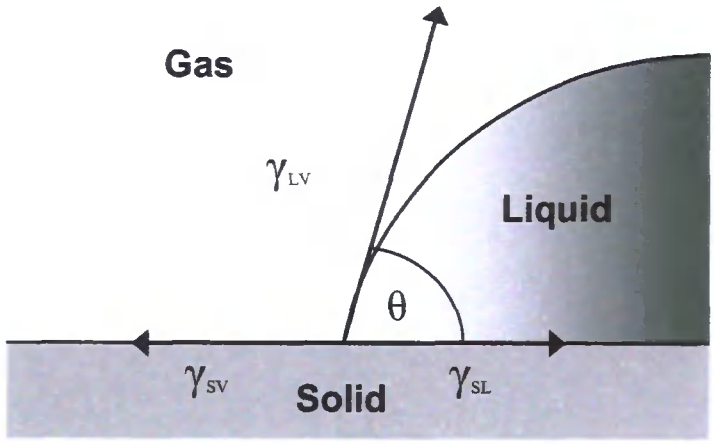

Figure II-9 – Contact angle formation on a solid surface

where indices L, S and V stand for "liquid", "solid" and "vapour" phase, and the symbol γ represents the interfacial energy between two phases.

Young[15] developed the first equation (Equation II-6) to relate the intrinsic contact angle to the surface energy components:

Equation II-6

$$Cos\theta = \frac{\gamma_{SV} - \gamma_{SL}}{\gamma_{LV}}$$

However, this simple equation was subsequently modified to account for the fact that real solid surfaces are usually rough and chemically heterogeneous. On such surfaces, the actual contact angle (defined as the angle measured from the tangent to the surface of the solid at any given point on the contact line to the tangent to the liquid-fluid interface at this point) may vary from point to point. Moreover, if the solid surface is chemically heterogeneous, the local intrinsic contact angle also varies from point to point. Therefore the intrinsic contact angle can be rather different from the measured contact angle, which makes the accurate measurement of the substrate surface energy less straightforward.

The contact angle measurement technique is very surface sensitive as it gives information about the first 5-10 Angstroms[16]of a substrate. Practically the VCA is used to deposit a measured volume of liquid onto a surface and a CCD camera captures the image of the droplet settling on the surface. A snap shot of the image (see Figure II-10) is captured and markers used to define the droplet perimeter, allowing a computer algorithm to determine the tangent to the droplet and hence contact angle the droplet makes with the surface.

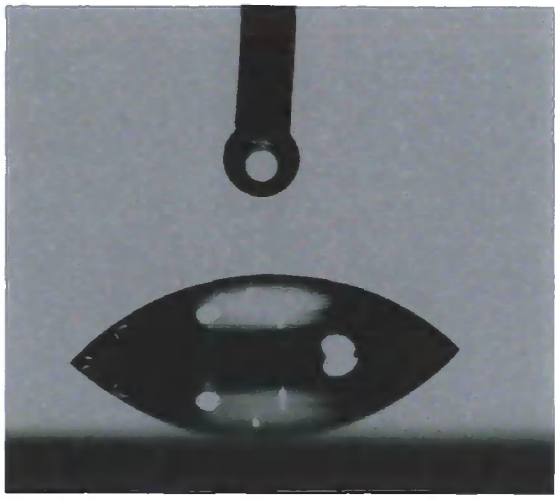

Figure II-10 - Snap shot of a droplet of water onto coated glass[17]

A contact angle of 0° indicates a completely wettable surface towards the liquid used. In contrast, a contact angle of 180° indicates completely repellent surface.

II.1.4. Reflectometry

Reflectometry is a non-destructive technique used to measure the thickness and the refracting index of a transparent thin film deposited onto a known substrate[18]. This technique is particularly effective for film thicknesses ranging from 20 nm to 5 μm and offers the advantage of not being affected by film inhomogeneity.

Reflectometry relies upon the interaction of a film with light. The determination of these optical constants depends upon the interference pattern (or fringes) resulting from partial reflection / transmission through partially reflecting surfaces, phenomenon observed by Perot and Fabry over a century ago[19] (Figure II-11).

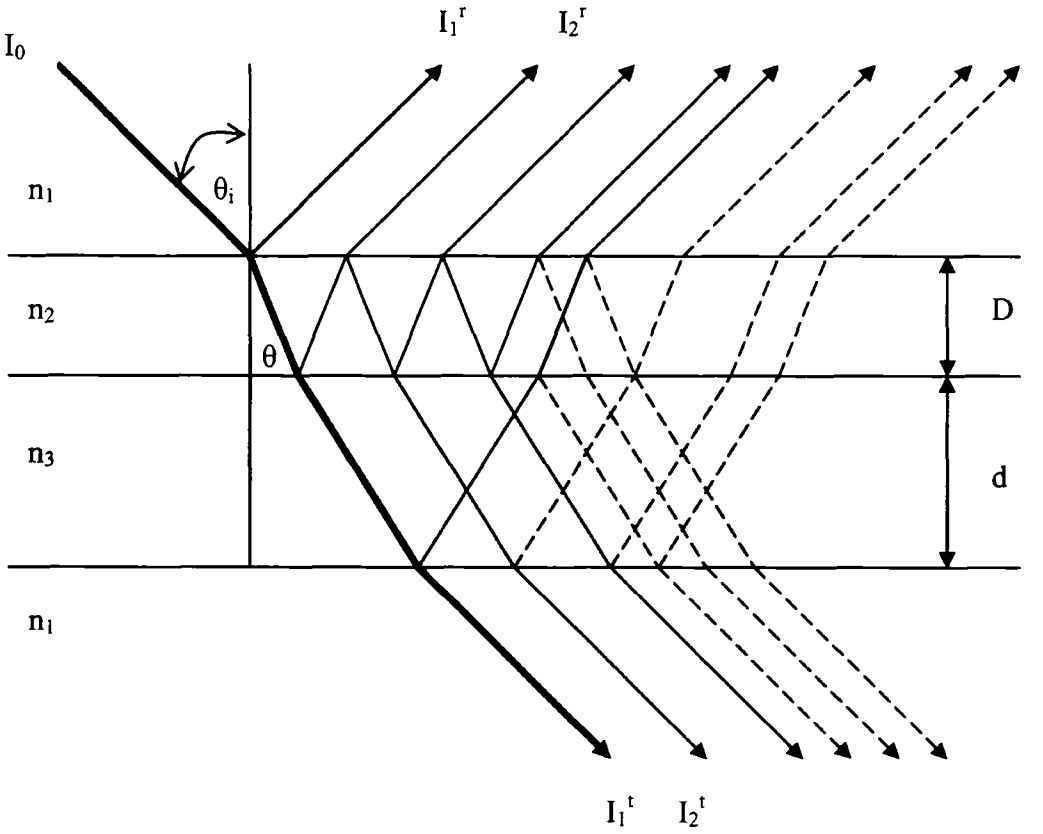

Figure II-11 – Interference caused by light travelling different paths through a thin film deposited onto a surface

When a thin film is deposited at the surface of another material, both top and bottom surfaces of the film reflect / transmit light, with the total amount reflected / transmitted being dependent upon the sum of these two reflections / transmissions. Furthermore, at a given wavelength, these two reflections / transmissions may add together constructively or destructively depending upon their phase relationship. Thus, by varying the wavelength, the fixed detectors observe a succession of minima and maxima for the intensities of the reflected / transmitted lights (see Figure II-12).

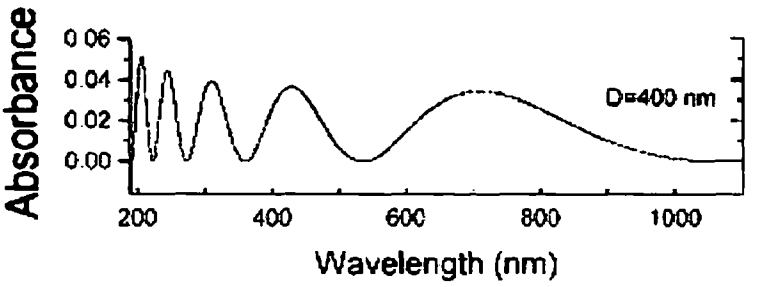

Figure II-12 – Absorbance spectra for a 400 nm - soap film[20]

The data collected by the detectors is fitted to the Cauchy model for dielectric materials[21]. In this model the refractive index, n(e), and the absorption coefficient, k(e), can be described by Equation II-7.

Equation II-7

$$n(e) = n_0 + n_1 e + n_2 e^2 + n_3 e^3 + n_4 e^4$$
$$k(e) = k_0 + k_1 e + k_2 e^2 + k_3 e^3 + k_4 e^4$$

where e is the photon energy in electron volts and n_0-n_4, k_0-k_4 are the model parameters.

The Levenberg-Marquardt method is then used as the non-linear curve-fitting algorithm to find the model parameters. The thickness of the thin film is then determined from its dependence on the relationship between the reflectance, n and k of the film, n and k of the substrate, surface roughness and angle of incidence.

Practically, the reflectance and transmittance of a sample are measured over a range of wavelengths, usually from 190 nm to 1000 nm. The light source, a quartz-tungsten halogen lamp, passes through a monochromator and is then focused onto the sample at an angle of 30° (see Figure II-13). The reflected and transmitted lights are then detected and the intensities are conveyed to a computer for further analysis.

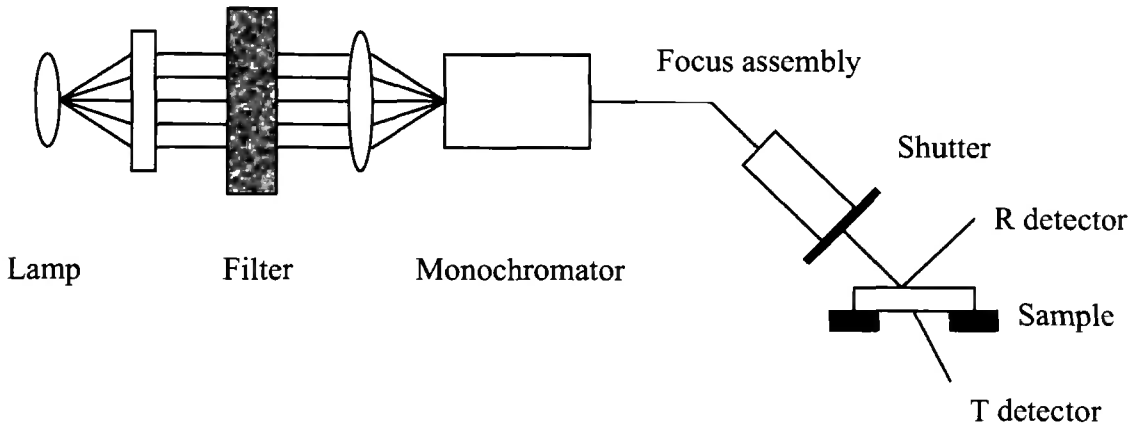

Figure II-13 – Schematic of a reflectometer

For the experiments carried out in this thesis, silicon wafer is the chosen substrate. Since it is a totally reflective material, only reflectance measurements were used.

II.2. OTHER TECHNIQUES

This part presents a brief description of the different techniques used in the experiments carried out for this thesis.

II.2.1. Reverse-phase High Performance Liquid Chromatography (RP-HPLC)

Chromatography can be described as a physical method of separation in which the components of a sample are distributed between a stationary and a mobile phase by means of physicochemical and chemical interactions. The mixture to be analysed can be of gas or liquid nature. Liquid chromatography is described in more details in this paragraph.

II.2.1.1. Basics of High-Performance Liquid Chromatography (HPLC)

Liquid chromatography is a technique used to separate and analyse the components of complex liquid mixtures that cannot be handled by Gas Chromatography (GC) because

either they are not sufficiently volatile and cannot pass through the column or they are thermally unstable and decompose under the conditions of separation. Hence, HPLC is well suited for fragile bio-molecules and has been widely used in biochemistry to understand and describe the structural basis of biological molecules as they relate to function. HPLC provides a powerful tool for the purification of such molecules without modifying their structure.

Separation is based on the attractive forces between molecules carrying charged groups of opposite signs. The different components of a sample to analyse interact to different extents with a non-polar mobile phase and a polar stationary phase (usually silica), and therefore take different times to move from the position of introduction to the position of detection.

The two classical types of liquid chromatography are:

- In *Liquid Solid chromatography* (LSC), an adsorbent (for e.g., alumina or silica) is packed into a column and is eluted with a suitable liquid. A mixture to be separated is introduced at the top of the column and washed through by the eluting liquid. If a component is weakly adsorbed onto the surface of the solid stationary phase, it will travel down faster than another one more strongly adsorbed.
- In normal *Liquid Liquid Chromatography* (LLC), the stationary phase is a liquid coated onto a finely divided inert solid support. Separation is due to differences in the partition coefficient of solutes between the polar stationary liquid and the non-polar liquid mobile phase.

In both methods described above, the column can generally be used only once.

HPLC arose from the development of the open-column methods and from the availability of smaller particle size for the stationary phase[22]. The stationary phase is

made of porous silica a few microns diameter and the separation mechanisms depend on the chemical nature of the bonded groups to the surface of the silica. Because of the very small size of the particles, when they are packed they create a strong resistance to solvent flow, therefore the mobile phase has to elute through the column under high pressure. The composition of the mobile phase can either be constant ('isocratic' elution) or it can change during the experiment to improve separation or to decrease the timescale of the experiment ('gradient' elution).

Unfortunately, HPLC is unable to provide unequivocal identification of the components of a mixture. If a reference material and an unknown one have the same retention time, they are not necessary the same compound. Therefore, the HPLC technique is often associated with mass spectrometry to allow the identification of compounds with good confidence[23].

II.2.1.2. Reverse phase HPLC

In reverse phase HPLC (RP-HPLC), compounds are separated based on their hydrophobic character instead of their hydrophilic nature. Therefore, the polarity of the stationary phase is less than the polarity of the eluent. This method is often preferentially used as it is often faster, cheaper, experimentally easier and more reproducible than other HPLC techniques. Moreover, it allows a very wide scope of samples with very different polarities to be separated.

RP-HPLC is generally achieved by using a stationary phase of silica bonded with non-polar groups (for e.g. C-8, phenyl, C-18) and a polar mobile phase. However, silica bonded with polar groups (for e.g. $-NH_2$, -CN) can also be used in some cases. The solutes are eluted by order of polarity, the most polar coming out first. The retention

times can be modified by changing the polarity of the mobile phase using a gradient of a polar and a non-polar liquid[24].

The limitation of this technique is mainly due to a constriction of pH, which needs to be between 3 and 8. Below pH 3 the possible bonded groups on the silica may be removed and above pH 8 the silica would be soluble in the mobile phase and therefore, the column would be damaged irreversibly.

II.2.1.3. Instrumentation

An HPLC instrument consists of a high pressure pump, which regulates the flow rate of the mobile phase, a supply of mobile phase in which the analytes are soluble, a column with a stationary phase described earlier, an injection system (a loop generally), a detector (usually UV spectrometer) and an instrument displaying the signal. A schematic of the instrumentation is given in Figure II-14.

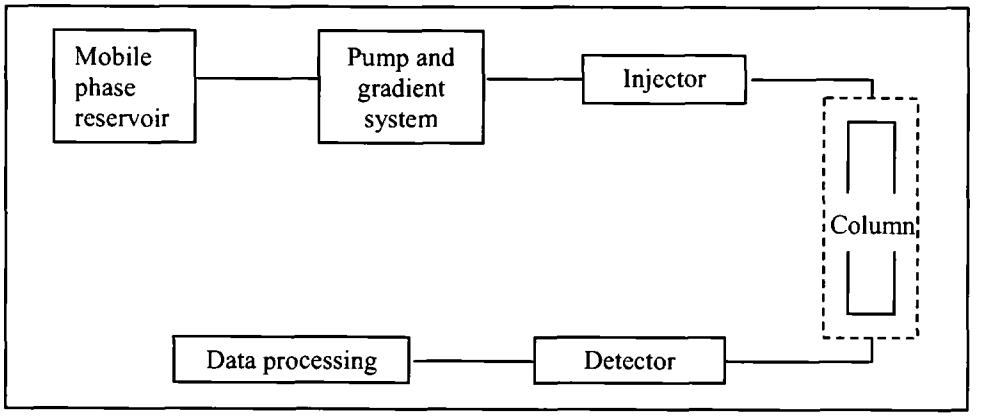

Figure II-14 - Block diagram of a typical HPLC system

The detector monitors the mobile phase emerging from the column. Its output is an electric signal proportional to some property of the mobile phase and / or of the solutes. In this work, the detector is a solute property detector and measures the adsorption of UV / visible radiation of the sample at a specific wavelength.

II.2.2. UV-vis Spectrophotometry

II.2.2.1. Basic principles

When matter interacts with an energy source (heat, sound, electricity, light, etc.) some of the energy can be absorbed, causing the particles to be elevated to different energy levels. When this process is controlled, some information can be obtained about the chemical system under investigation[25].

If a sample irradiated by a beam of light contains a substance adsorbing one of the beam's wavelengths, a plot of the amount of light absorbed versus the wavelength can be obtained (Figure II-15). The energy associated with the absorbed wavelength corresponds to the energy difference between the electronic levels involved in the excitation of the electrons in the absorber (Figure II-15-a). When the adsorbing substance is in solution, its energy levels are modified by the properties of the solvent. Thus, many different wavelengths adjacent to the main transition wavelength are also absorbed (Figure II-15-b).

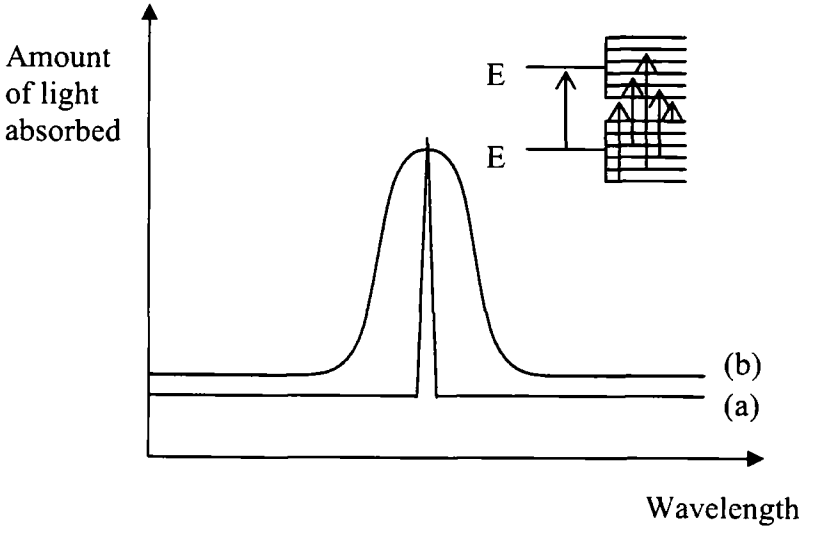

Figure II-15 – Absorption spectrum

UV-Vis spectrophotometry uses light sources with wavelengths ranging from 190 to 800 nm, corresponding to transitions of outer-shell electrons in atoms and bonding

electrons in molecules. Each chemical species has a unique set of energy levels that can absorb, but because these are too greatly modified in solution, identification is impossible through absorption measurements alone. Spectrophotometry is therefore primarily used for quantitative measurements. The amount of light absorbed by a sample is directly related to the amount of the adsorbent present in the sample (Equation II-9).

If I_0 is the intensity of the light source and I_T the intensity of the transmitted beam through the sample, the absorbance is defined as:

Equation II-8 $$A = \log\left(\frac{I_0}{I_T}\right)$$

Beer's law then gives the relationship between absorbance and concentration:

Equation II-9 $$A = \varepsilon l c$$

where ε : molar absorptivity, also called extinction coefficient

l : cell width

c : concentration of the absorbing species

II.2.2.2. Instrumentation

A spectrophotometer consists of two instruments, namely a spectrometer for producing light of any selected wavelength, and a photometer for measuring the intensity of light. A cuvette containing the sample solution is placed between the spectrometer beam and the photometer. The amount of light passing through the tube is measured by the photometer, which delivers a voltage signal to a display device, normally a galvanometer. The signal changes as the amount of light absorbed by the liquid changes.

In the visible light region, the light source is a tungsten lamp and in the UV region, a deuterium lamp. To isolate a particular wavelength, the light is reflected on a diffraction grating, which disperses each wavelength of the light beam at a different angle. By controlling the angle of deflection, each wavelength can be individually selected to pass through the sample cell into a light detector (phototube). The phototube contains a cathode coated with a substance that emits electrons when struck by photons. The electron current is measured by a meter or a digital readout (see Figure II-16).

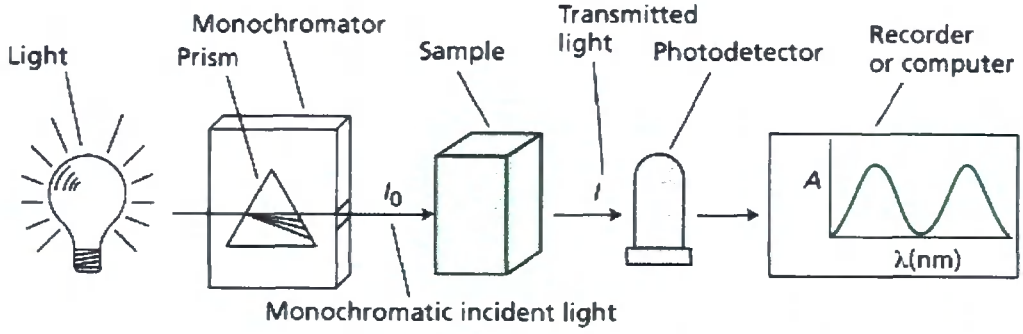

Figure II-16 – Schematic diagram of a spectrophotometer

II.2.3. Surface Plasmon Resonance (SPR)

Surface plasmon resonance is a technique used to measure refractive index changes in analytes close to the surface of a sensor. This technique is particularly well-suited to study biospecific interactions since the change in solute concentration in the surface volume resulting from these interactions is directly related to the refractive index[26].

II.2.3.1. Generalities

When a light beam propagates across an interface between two non-absorbing media from the higher refractive index medium to the lower, the light is refracted at the surface (Figure II-17 - a). When the angle of incidence reaches the critical angle and for any

value above it, all the light is reflected inside the medium of higher refractive index. This is called total internal reflection, TIR (Figure II-17 - b).

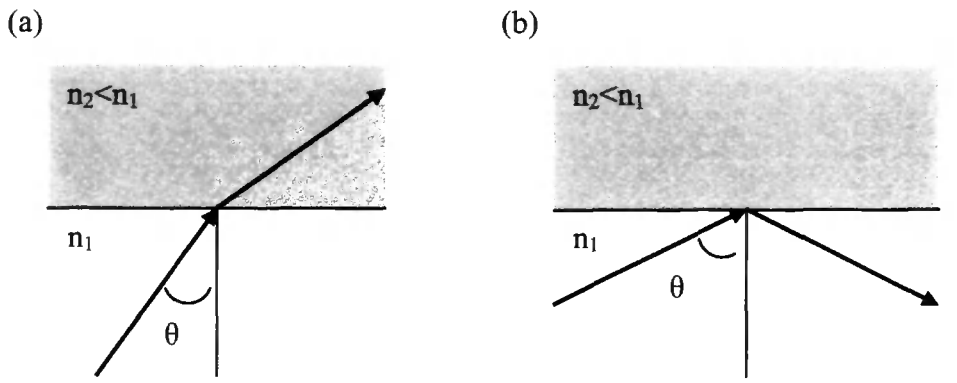

Figure II-17 - (a) Light passing from a medium of high refractive index to a medium of a lower refractive index is refracted toward the plane of the interface (b) At and above angle of incidence, total internal reflection occurs and no light passes through the second medium

Under conditions of TIR, an electric field called an evanescent field wave penetrates into the medium of lower refractive index. The wavelength of the evanescent field wave is the same of that of the incidence light. The amplitude of the wave decreases exponentially with increasing distance from the interface, decaying over a distance of one light wavelength from the surface.

If this evanescent wave is allowed to interact with a layer of conducting material, a new phenomenon is generated. The p-polarised component of the evanescent field wave (the electric field component lying in the plane of incidence) can penetrate the metal layer and excite electromagnetic waves that propagate within the metal surface at the interface with the sample solution. These are called surface plasmons.

For a non-magnetic metal like gold, the surface plasmons will also be p-polarised, and will create an enhanced wave field as they propagate on the surface of the metal

film. This enhanced wave field penetrates a short distance into the low refractive index medium.

Plasmons are generated only when the energy and momentum of the incident light vector in the plane of the metal corresponds to the energy and momentum of the surface plasmons. This is the condition of surface plasmon resonance. When this occurs, a minimum in reflected light intensity is observed.

Although the plasmons are confined to the metal layer, their propagation energy and momentum is determined in part by interaction between the evanescent wave and the medium through which it travels. The refractive index of a medium is an expression of the speed with which electromagnetic waves propagate through the medium. Thus the momentum of the surface plasmons and the condition for plasmon resonance are affected by the refractive index of the medium on the metal-coated side of the interface. Because the evanescent wave penetrates only a short distance from the interface, SPR probes the refractive index of a thin layer of medium close to the surface. Changes in the resonance angle with changes in refractive index are small: a change of 10^{-3} in the refractive index of the analyte causes a shift of 0.1° in the resonance angle. Some instruments can detect changes in refractive index as low as 10^{-6}, creating a shift in the resonance angle of $10^{-4\,\circ}$.

II.2.3.2. Instrumentation

In Biacore instrument (used in this thesis), the light source is a light emitting diode with a wavelength of 760 nm. The polarised light is focused into a wedge-shaped light beam that illuminates the sensor chip under the conditions of TIR. Under these conditions, SPR results in a reduction in the intensity of light reflected from the sensor surface at a specific angle. A plot of reflected intensity against angle shows a characteristic 'dip'.

The angle of minimum reflectance is called the resonance angle. A diode array continuously monitor the intensity of the reflected light over a range of angles, and the resonance angle is calculated to high precision by computer interpolation algorithms.

Binding between one partner immobilised on the sensor chip and another one present in sample solution leads to an increase in the mass concentration at the surface of the sensor chip, resulting in an increase in the refractive index of the solution close to the surface and a shift in the position of the resonance angle (from I to II in Figure II-18). Changes in the resonance signal over time are displayed in a graph called a sensogram. The sensogram is a direct representation of the interaction between the molecules on the sensor chip in real time.

The unit for the SPR signal is the resonance unit (RU), where 1000 RU represents a shift in resonance angle of 0.1°. A response of 1000 RU corresponds to a change in surface protein concentration of about 1 ng/mm^2. This value is almost independent of the type of the protein used. The detection limit of the technique is of the order of 10 RU (about 10 pg/mm^2).

The optical detection system uses the Kretschmann configuration, where all components are fixed and the reflected light intensity is monitored over a range of angles simultaneously. The metal film is places directly on the TIR interface, allowing maximum efficiency in plasmon generation (Figure II-18).

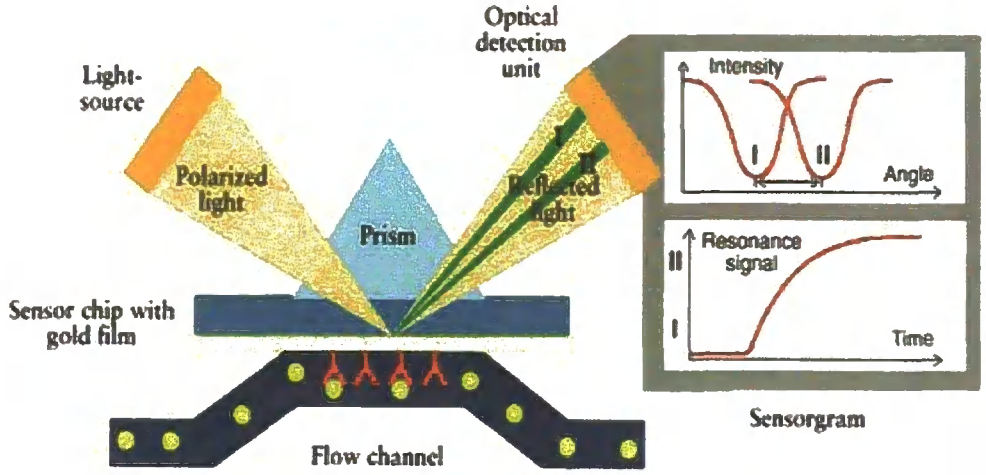

Figure II-18 – SPR detection system[26]

II.2.4. Fluorescence microscopy

Fluorescence microscopy is a technique used to image molecules which are either inherently fluorescent or stained with fluorescent tags prior to imaging. Because fluorescence is observed as luminosity on a dark background, it is possible to differentiate small features[27].

II.2.4.1. The fluorescence process

Fluorescence can be described by a three-consecutive-steps process[28]: (i) formation of one or more excited state(s) by absorption (excitation); (ii) non-radiative transitions between excited states; and (iii) energy loss accompanied by emission of radiation (Figure II-19).

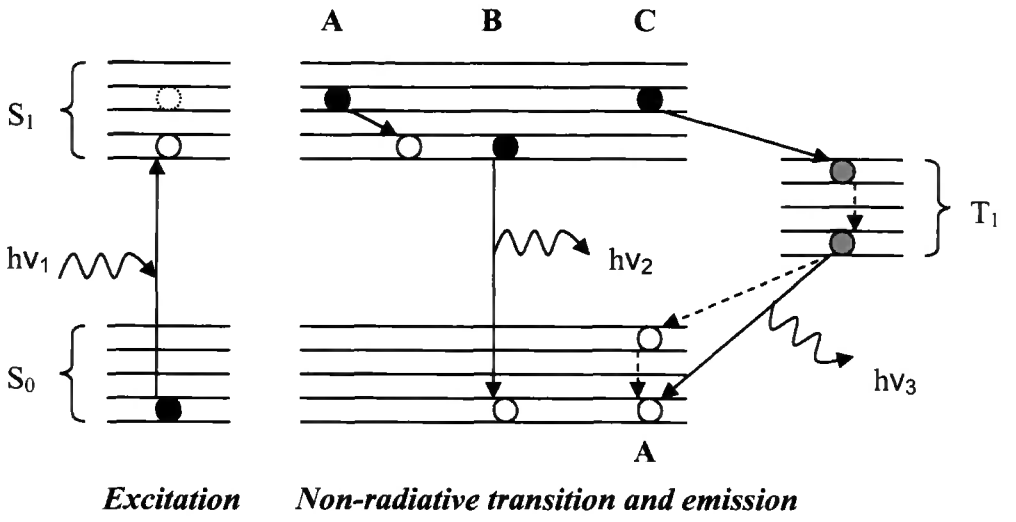

Figure II-19 – Jablonski diagram for 3-step process of photoluminescence – S_0 and S_1 ground state and excited state respectively, T_1 triplet state

When a molecule is excited by a photon of energy $h\nu_1$, electrons in the ground sate S_0 jump to sublevels of an excited state S_1. The excited electrons can then relax via three pathways. First, vibrational relaxation can bring the electrons to the lowest level of the excited state; energy is lost by external quenching reactions (A). The electrons can also undergo singlet–singlet transition from the excited state S_1 to the ground state S_0 within nanoseconds with or without emission (internal conversions) (B). This photoluminescence occurs at longer wavelength than that of excitation[29] and is known as fluorescence. Alternatively, singlet–triplet inter-system crossing can occur between the singlet excited state S_1 and the corresponding triplet excited state of slightly lower energy T_1[30,31]. Energy can be lost from the system by non-radiative pathways such as external quenching reactions of singlets or triplets and vibrational relaxation, but also by photoemission leading to phosphorescence (C).

II.2.4.2. Instrumentation

The sample is illuminated with light of a specific wavelength which is absorbed by the fluorophores, causing them to emit longer wavelengths of light.

A fluorescent microscope can be broken down into excitation source, contrast enhancement and emission detection (Figure II-20). Typical excitation sources include lamps, lasers, and light emitting diodes, whose emission is collected into a lens and passed through a filter to allow light of only the desired wavelength to be focussed onto the sample. The emitted light from the sample is collected by a nearby objective and passed through another filter to improve the signal to noise ratio by removing any light of undesired wavelength. This light is focussed onto a photo-detector which can convert the light into a spatial image of fluorescence intensity[32].

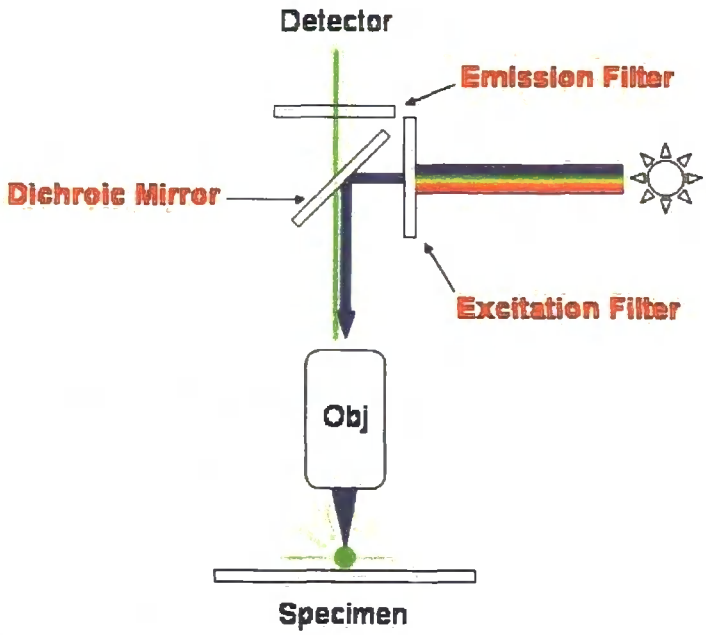

Figure II-20 – Schematic representation of a fluorescent microscope

II.3. REFERENCES

1 - Walls, J. M. In *Methods of surface analysis*, Cambridge University Press, Cambridge, 1989

2 - Briggs, D.; Seah, M. P. In *Practical Surface Analysis*, 2nd edition, Vol. 1, John Wiley & Sons, Chichester, 1990

3 - Windawi, H.; Ho, F.F.-L. In *Applied Electron Spectroscopy for Chemical Analysis*, Vol. 63, John Wiley & Sons, 1982

4 - O'Connor, D.J.; Sexton, B.A.; Smart, R.St.C. In *Surface Analysis Methods in Materials Science*, Springer-Verlag, Berlin, 1992

5 - Rivière, J. C. In *Surface Analytical Techniques*, Oxford Science Publications, 1990

6 - Colthup, N.B.; Daly, L. H.; Wiberley, S.E. In *Introduction to Infrared and Raman Spectroscopy*, 3rd Edition, Academic Press, San Diego, 1990

7 - *Handbook of Instrumental Techniques for Analytical Chemistry*, Ed. Settle, F.A., Prentice-Hall, 1997, Chapter 5

8 - http://scienceworld.wolfram.com/physics/MichelsonInterferometer.html

9 - Ferraro, J.R.; Basile, L.J. In *Fourrier Transform Infrared Spectroscopy : Applications to Chemical Systems*, Vol. 4, Academic Press, 1985

10 - http://scienceworld.wolfram.com/physics/SnellsLaw.html

11 - Greenler, R.G. *J. Chem.Phys.* **1966**, 44, 310-315

12 - C.N. Banwell In *Fundamental of Molecular Spectroscopy*, McGraw-Hill, Great Britain, 3rd Edition, 1983, Chapter 3

13 - Weiss, P. *J. Polym. Sci.: Polym. Lett. Ed.* **1979**, 17 (7), 463-464

14 - *Contact Angle, Wettability and Adhesion: Festschrift in Honor of Professor Robert J. Good Mittal – Vol. 2*, K. L. Eds, VSP International Science Publishers, 1993

15 - Wolansky, G.; Marmur, A., *Langmuir*, 14, **1998**, 5292-5297

16 - Domingue, J., *Am. Lab.*, **1990**, 22, 50-55

17 - http://en.wikipedia.org/wiki/Surface_energy

18 - Pro Optix User Manual, Version 2.0, 2000

19 - Fabry, C.; Perot, A. *Ann. Chim. Phys.* **1899**, 16, 115

20 - Huibers, P.D.T.; Shah, D.O. *Langmuir* **1997**, 13, 5995-5998

21 - Tabet, M. F.; McGraham, W. A. *Thin Solid Films* **2000**, *370,* 122

22 - Snyder, L. R.; Kirkland, J. J. In *Introduction to Modern Liquid Chromatography*, 2nd ed., John Wiley & Sons, New York, 1979

23 - Ardrey, B. In *Liquid Chromatography – Mass Spectrometry: an Introduction*, John Wiley & Sons, Chichester, 2003

24 - Lindsay, S. In *High Performance Liquid Chromatography*, 2nd ed., Analytical Chemistry by Open Learning, John Wiley & Sons: Chichester, 1992

25 - http://pharmlabs.unc.edu/spectrophotometry/text.htm

26 - *Real-Time Analysis of Biomolecular Interactions*, Nagata, K.; Handa, H.; Springer-Verlag: Tokyo, 2000

27 - Rost, F. W. D. *Fluorescence Microscopy Volume 1*; Cambridge University Press: Cambridge, 1992

28 - White, N.S.; Errington, R. *J. Adv. Drug Delivery Rev.* **2005**, 57, 17-42

29 - Atkins, P. A.; de Paula, J. *Atkins Physical Chemistry, 7th Ed*; Oxford University Press: Oxford, 2002, Chapter 17

30 - Snow, R. L.; Bills, J. L. *J. Chem. Educ.* 1974, 51, 585-586

31 - Liu, R. S. H. *J. Chem. Educ.* 2005, 82, 558-560

32 - Michalet, X.; Kapanidis, A. N.; Laurence, T.; Pinaud, F.; Doose, S.; Pfughoefft, M.; Weiss, S. *Annu. Rev. Biophys. Biomol. Struct.* **2003**, 32, 161-182

III

CHAPTER THREE

Deposition and derivatisation of reactive ester

III.1. INTRODUCTION

Direct functionalisation of surfaces is not always possible with the available methods (see Chapter I) since some molecules need to be covalently attached onto surfaces in a multiple step process to retain their functionality. Such molecules include biomolecules (DNA[1,2,3], enzymes[4,5,6], proteins[7,8], peptides[9,10], lipids[11,12], sugars[13,14] or cells[15,16]), dendrimers[17,18], fluorescent tagged molecules are particularly useful in screening and drug discovery[19] or electrochemical active molecules[20,21]. A multiple step process involves first functionalisation of the material of interest followed by derivatisation of the surface.

The high occurrence of amine functionalities in biomolecules emphasises the importance of the technologies involving covalent attachment of amine-terminated molecules onto surfaces. One of the common methods of immobilisation of amines onto surfaces by wet-chemical treatment is nucleophilic opening of epoxide ring leading to β-amino-alcohols[22,23,24,25] (see Scheme III-1 a). This reaction can be carried out in vapour-phase[23], organic solvent[26] or aqueous solution[25,27]. However, this method requires excess of amine to achieve good yields and does not work well with poor nucleophilic amines. Moreover, heating is often required for the reaction to occur, which can pose problems when sensitive epoxides are used due to the potential side reactions at high temperatures but also because biomolecules degrade under heat. This led to the development of catalytic systems to activate the epoxide ring for nucleophilic cleavage[28] but this is not always compatible with surface treatment.

Another common type of reactions for covalent attachment of amines onto surfaces is imine bond formation. This proceeds by the nucleophilic attack of a primary or secondary amine onto a carbonyl group. For example, an amine can react with an

aldehyde or a ketone (less reactive) via acidic catalysis following an addition-elimination mechanism to form an α-amino-alcohol (see Scheme III-1 b). When primary amines are used, the reaction can proceed further to yield imines[29]. When secondary amines are used, if the aldehyde or the ketone possesses a hydrogen atom on the carbon in α position of the carbonyl group, then the reaction yields enamines[29]. Covalent attachment of primary amine-terminated biomolecules is generally achieved with aldehyde derivatised surfaces[27,30,3132]. Although imines are generally stable, they can still hydrolyse under acidic conditions and necessitate further reduction to a secondary amine to improve stability. This is usually done with the highly selective, water-soluble borohydride anion[27,30,31,33] under relatively mild conditions. This procedure has not been extensively used, due to the multiple-steps involved to achieve stable covalent attachment.

Furthermore, amines can be covalently attached onto surfaces through amide bonds using carboxylic acid derivatives. The most reactive of these derivatives are acyl halides[29] (see Scheme III-1 c). Different methods have been used to introduce acyl halide groups onto surfaces. These involved either direct functionalisation of a surface[34] or activation of chemical groups already bound to a surface such as carboxylic acid[20,35] or amine[36]. Amidation can be subsequently done in vapour phase[20,34], organic solvent[35], or in aqueous media under basic conditions (Schotten-Baumann reaction)[37,38], the latter being more suitable for biomolecule attachment since some proteins have a tendency to denature in some organic solvents[39]. However, the instability of some surfaces to acylating agent such as thionyl chloride limits their use. Moreover, because of their high reactivity, acyl chloride-functionalised surfaces are unstable, when exposed to water from the atmosphere they tend to form the carboxylic acid equivalent. Recently, acyl fluorides have proven to be much more stable and do not require the use of basic pH in

aqueous medium for amidation to occur which is more compatible with most biomolecules[35].

Alternatively, a substrate can be functionalised with anhydride moieties which readily react with an amine to form an amide (see Scheme III-1 d). This reaction can take place in vapour phase[40], organic solvent[41] or in aqueous phase[42]. Anhydride groups have been introduced onto surfaces by direct grafting onto a substrate[43], by activation of carboxylic acid functions[41,44] and by plasma polymerisation[45]. However, because of their reactivity, anhydride surfaces tend to be unstable as they convert slowly to carboxylic acid when exposed for some time to moisture from the atmosphere[46]. Moreover, conditions for amide bond formation may prove difficult to establish since in aqueous solution (more suitable for biomolecules) anhydrides tend to undergo hydrolysis under basic conditions (pK_a around 3 to 5)[47] and amide bonds tend to cleave under acidic conditions[47].

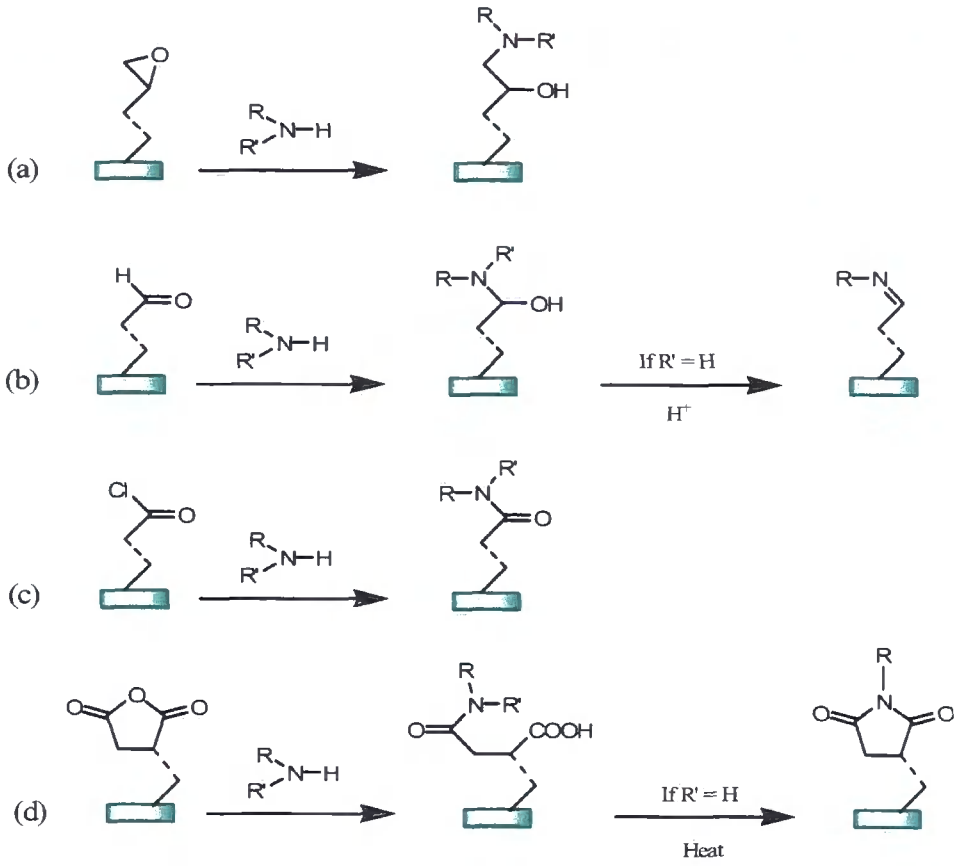

Scheme III-1– Covalent attachment of amine-terminated molecules onto functionalized surfaces

Finally amide bond formation can be generated by reaction of an amine and a carboxylic acid. However, unlike their derivatives, carboxylic acids do not possess any leaving groups, making the amidation reaction unfavourable[29]. To improve the reaction yield, Sheehan et al.[48] developed, in 1955, the first peptide bond formation using N,N'-dicyclohexylcarbodiimide (DCC) as a coupling reagent in solution. Carbodiimides are used as dehydration agents and as activating agents. The unstable product formed by the coupling readily reacts with amines or alcohols present in the reaction mixture to form respectively amides or esters (see Scheme III-2 a). Soon after, Merrifield widened the scope of application of carbodiimides as he employed the same coupling method in his solid-phase peptide synthesis[49]. However, the use of DCC encountered some redundant problems (toxicity, insoluble side products[50]), leading to the development of other carbodiimides such as N,N'-diisopropylcarbodiimide[51] (DIC) and water-soluble, 1-

ethyl-3-(3-dimethylaminopropyl) carbodiimide hydrochloride (EDC)[52,53]. Woodward et al.[54,55] developed another type of water-soluble coupling agent, 2-Ethyl-5-phenylisoxazolium-3'-sulfonate (Woodward's reagent K), which leads to the formation of a stable yet reactive ester (see Scheme III-2 b) in mild conditions. The use of Woodward's reagent K was then extended to other purposes, like spectrophotometric quantification of carboxylic acids[56] or inactivation of enzymes to elucidate their structure-function relationship[57].

One major problem when using carbodiimides and isoazoliums is that they are so reactive that they tend to induce racemisation[58]. Moreover, most of these coupling reagents give rise to unwanted reactions[59] which lower the reaction yield. To avoid these problems, reactive esters were introduced in peptide synthesis along with coupling reagents in a 2-step process. These reactive esters are relatively stable but are also very good leaving group during nucleophilic substitution, leading to amide formation in good yield (see Scheme III-2 c). In 1955, Bodanszky et al.[60] developed one of the first ester activation methods for peptide coupling using *para*-nitrophenol and later found that the *ortho* equivalent was even more efficient[61]. Later, Anderson et al.[62] introduced N-hydroxysuccinimide (NHS) coupled with carbodiimides as a much more reactive alternative to p-nitrophenol in both organic and aqueous medium. Moreover, in aqueous solution, unlike with p-nitrophenol, by-products generated by the use of NHS are soluble and hence easier to separate from the peptide formed. It is still in use today as one of the most popular method for amide bond formation[63,64] as it is compatible with most biomolecules without the need for protection. König and Geiger[65] introduced a whole new family of reactive esters to avoid loss of chirality and side product formation with 1-hydroxybenzotriazole (HOBt) either as an additive in combination with a carbodiimide or built into a variety of stand-alone reagents such as (benzotriazol-1-

yloxy)tris(dimethylamino)phosphonium hexafluorophosphate (BOP)[66] and O-benzotriazole – N, N ,N' ,N' – tetramethylene – uronium – hexafluoro - phosphate (HUBT / HBPyU)[67]. A lot of compounds of the same family were then developed to improve efficiency, such as 3,4-dihydro-3-hydroxy-4-oxo-1,2,3-benzotriazine (DHBT)[68] and more recently l-hydroxy-7-azabenzotriazole (HOAt). Carpino[69] showed that the latter was a much more efficient additive which speeds up coupling processes, reduces the loss of chiral integrity, and provides a visual indication (yellow-to colourless) of the reaction endpoint. Finally, Kovacs et al. widened the range of active esters by using pentachlorophenol (PCP)[70] and pentafluorophenol (PFP)[71] which can be used in organic solvent[72] as well as in aqueous medium[73]. PFP was shown to be very efficient and to reduce the side reactions in very mild conditions.

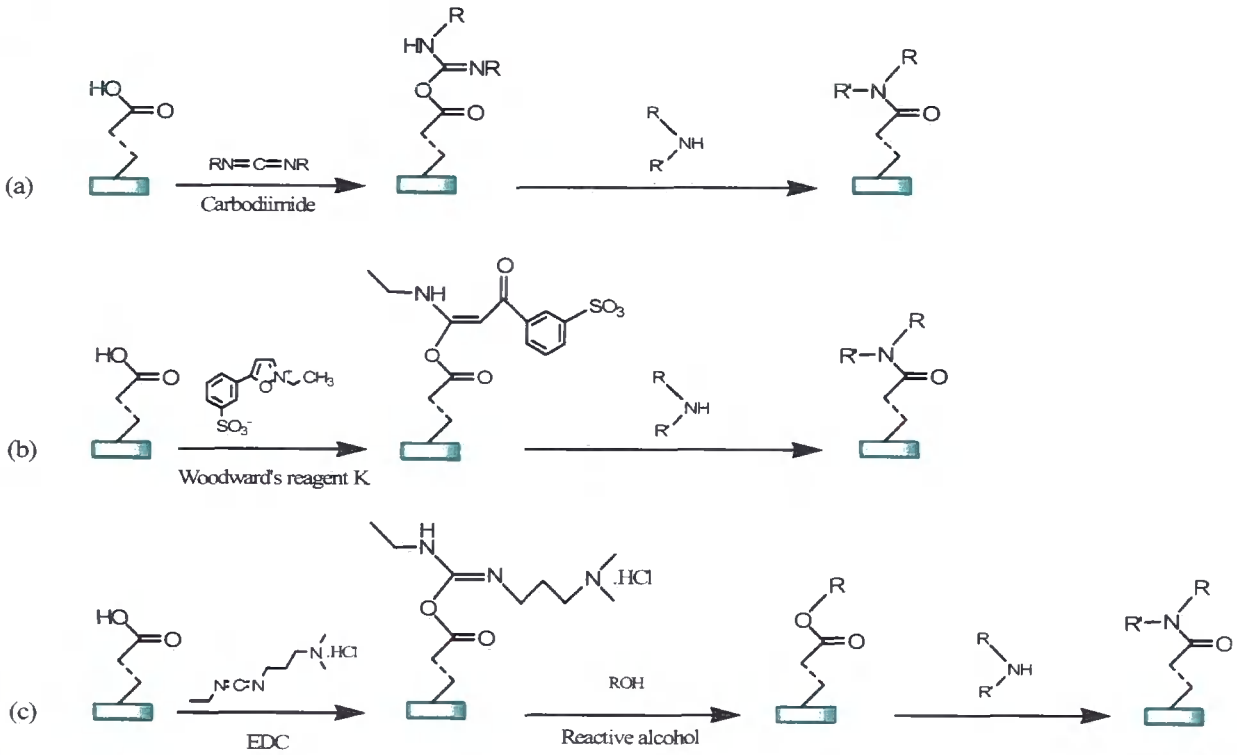

Scheme III-2 – Amide bond synthesis via coupling reagents and active esters

Amide bond formation is not limited to peptide synthesis as it is a very common reaction in organic synthesis. Therefore, to attach amine-terminated molecules in a

covalent manner to surfaces, the use of active esters became recurrent. Indeed, enzymes[74], DNA[75], proteins[76], peptides[77] and more generic molecules[78] or polymers[79] were attached onto surfaces using mainly the combination EDC/NHS (or its derivative N-hydroxy-sulfo-succinimide), but also EDC/PFP.

Usually, amide bond formation at surfaces using active esters is a multi-step process, which affects the overall yield. However, some groups directly functionalised surfaces in a single step prior to covalent attachment. For instance, Willner et al.[80] prepared a monolayer of N-hydroxysuccinimide esters chemisorbed on gold electrode. Glidle et al.[81] have electrodeposited onto gold a pyrrol derivative of pentafluorophenyl ester. Similarly, Korri-Youssoufi et al.[82] electrodeposited also onto gold a pyrrol derivative bearing the leaving group N-hydroxyphtalimide. Alternatively, whilst work for this thesis was being carried out, Francesch et al.[83] published an article in which they plasma polymerized pentafluorophenyl methacrylate onto silicon wafer for covalent attachment of biotin-ligand. The main drawback of these approaches is the necessity to first synthesise the active ester of interest containing an adequate functional group in order to create the functionalised surface, such as sulphur-sulphur bond for self-assembled monolayer formation, pyrrol group for electrodeposition and carbon-carbon double bond for plasma polymerisation. Moreover, apart from plasma polymerisation, these techniques present a limited range of substrates. Direct surface-functionalisation with active esters has not been widely covered in the literature.

In the present work, two commercially available active esters were deposited onto silicon wafer by pulsed-plasma polymerisation (whose properties and advantages are described in chapter I). The surfaces generated were subsequently derivatised by model amines and amine-terminated peptides. N-acryloxysuccinimide (NAS) (see Scheme III-3 a) and pentafluorophenyl acrylate (PFPA) (see Scheme III-3 b) were investigated

since they are both commercially available therefore there is no need for synthesis, they possess a carbon-carbon double bond and a vapour pressure ($v.p._{NAS}$ = 0.027 mbar - $v.p._{PFPA}$ = 0.149 mbar at 25°C) necessary for plasma polymerisation. Moreover, both active esters offer the advantage of being able to react in both organic and aqueous solution. Amide bond formation in aqueous media is investigated in this work.

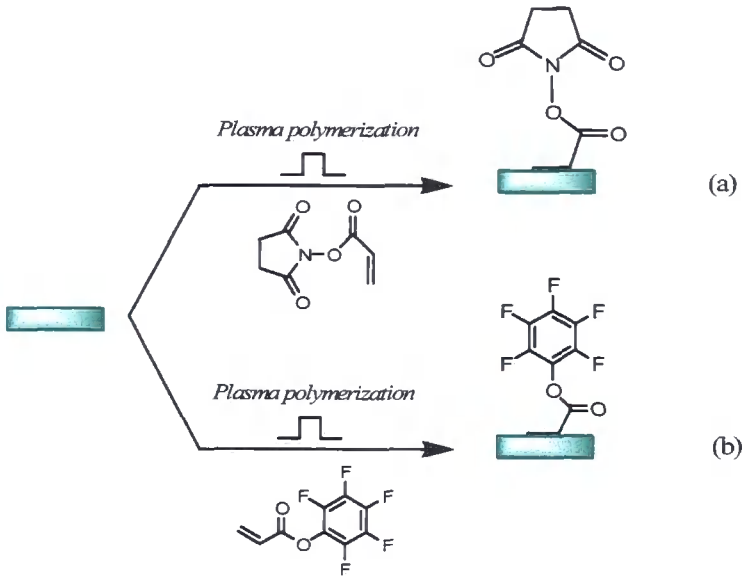

Scheme III-3 – Plasma polymerisation of reactive esters

III.2. EXPERIMENTAL

III.2.1. Plasma polymerisation of reactive esters

Monomers N-acryloxysuccinimide (99%, Acros Organics) (NAS) and Pentafluorophenyl acrylate (98%, Apollo Scienific) (PFPA) were loaded into sealable glass tubes and further purified by freeze-thaw cycles to ensure complete degassing prior to plasma polymerisation.

Pulsed plasma polymerisation of NAS was undertaken in a cylindrical glass reactor (4.5 cm diameter, 460 cm^3 volume, 3.9 x 10^{-2} mbar base pressure, 3.5 x 10^{-9} mol/s leak rate) surrounded by a copper coil (4 mm diameter, 10 turns, located 15 cm from the gas inlet) connected to a 13.56 MHz radio frequency (RF) power supply and an L-C

matching network. The plasma chamber was located inside a temperature-controlled oven and a Faraday cage. A 30 $L.min^{-1}$ rotary pump attached to a liquid nitrogen cold trap was used to evacuate the reactor, while the system pressure was monitored with a Pirani gauge. All fittings were grease-free. During pulsed plasma deposition, the RF power source was triggered by a signal generator, and the pulse shape monitored with an oscilloscope.

Prior to each deposition, the apparatus was scrubbed with detergent, rinsed in 2-propanol, and oven dried. Further cleaning entailed running a continuous wave air plasma at 0.2 mbar pressure and 40 W power lasting 30 min. Next, silicon wafers (MEMC Materials Inc) and/or gold chips were inserted into the reactor and the reactor pumped down to base pressure. At this stage, a continuous flow of NAS vapour was introduced into the chamber at a pressure of 5.8×10^{-2} mbar and 58 °C temperature for 5 min prior to plasma ignition. The duty cycle corresponded to 5 W continuous wave, bursts lasting between 10 and 100 μs (t_{on}), followed by an off-period (t_{off}) lasting between 10 and 20 ms. Upon completion of deposition, the RF generator was switched off, and the monomer allowed to continue to purge through the system for a further 5 min prior to evacuating to base pressure and venting to atmosphere.

Pulsed plasma polymerisation of PFPA was undertaken following the same procedure as NAS, but in a cylindrical glass reactor (5 cm diameter, 490 cm^3 volume, 4.8×10^{-2} mbar base pressure, 8.3×10^{-10} mol/s leak rate) surrounded by a copper coil (4 mm diameter, 8 turns, located 12 cm from the gas inlet) and enclosed in a Faraday cage at ambient temperature (21°C). The vapour pressure of the monomer was 0.25 mbar and the duty cycle corresponded to 20 W continuous wave, bursts lasting between 10 and 20 μs (t_{on}), followed by an off-period (t_{off}) fixed at 20 ms. To ensure good adhesion of the

plasma polymer, a 1 minute-continuous wave plasma was run prior to pulsing. However, for deposition rate studies, no continuous-wave was run prior to pulsing.

III.2.2. Derivatisation of reactive esters

Sodium phosphate dibasic anhydrous (99%, Aldrich) or potassium phosphate monobasic (99%, Aldrich) were used to prepare phosphate buffer solutions (PB) in water. Unless stated otherwise, buffer concentration was 0.05 M. The pH of each solution (values stated below) was adjusted by adding a few drops of either concentrated hydrochloric acid (37%, Riedel-de Haën) or sodium hydroxide (Fisher scientific). All reactions were carried out at ambient temperature (20-22°C).

Pulsed plasma NAS coated surfaces were subsequently immersed into either a solution of 2,2,2-trifluoroethylamine hydrochloride (98%, Aldrich) 30 or 100 mM in PB – 0.2 M - at pH of 9.3 or a solution of propylamine (98%, Aldrich) 60 mM in water. Samples were left to react at ambient temperature for 6 and 16 h with 2,2,2-trifluoroethylamine hydrochloride and for 1 h with propylamine. They were subsequently rinsed in deionised water several times and left to air-dry prior to analysis.

Pulsed plasma PFPA coated surfaces were immersed into the following solutions:

- deionised water or PB - pH=8.5 for 24 h, 48 h and 1 week
- diethylamine (99.5%, Aldrich) 100 mM in water and in PB - pH=8.5 for 16 h
- ethanolamine (98%, Aldrich) 100 mM in PB – 0.2 M - pH=7 for 5 h
- trifluoroethylamine hydrochloride (98%, Aldrich) 100 mM in PB - pH=8.5 for 16 h
- β-alanine (99%, Aldrich) 400 mM in PB– pH=8.5 for 24 h
- peptide Gly-Ala (Chem-Impex) 100, 200, 400 mM in PB – pH=8.5 for 24 and 48 h
- peptide Gly-Gly-His (Chem-Impex) 100 mM in PB – pH=8.5 for 24 h

All samples were rinsed several times in deionised water and left to air-dry prior to analysis.

After reaction with Gly-Gly-His, pulsed-plasma PFPA coated samples were further reacted in a solution of copper sulphate $CuSO_4$ (Aldrich) in sodium sulphate buffer (99%, Sigma-Aldrich) 0.05 M at pH=7 for 16 h, then rinsed for 1h in deionised water and left to air-dry before analysis.

Finally, pulsed plasma PFPA were reacted with DNA and protein solutions for qualitative measurements. For DNA derivatisation, amine-terminated 15 base oligonucleotide Probes I, II and III (Table III-1) were first diluted in sodium chloride / sodium citrate (SSC) buffer (3 M NaCl, 0.3 M sodium citrate dihydrate, 99%, Aldrich) pH=7 to a final concentration of 200 µM. Pulsed plasma PFPA coated surfaces were then reacted in solutions of oligonucleotide Probes I and III at a concentration of 1 µM in carbonate buffer 0.025 M pH=8.5 (99%, Aldrich) for 16h at ambient temperature. Samples were rinsed for 1h in SSC buffer and 1h30 in water before being left to dry at air.

Table III-1 – Oligonucleotides sequences (Sigma-Genosys Ltd.) employed

Oligonucleotide label	Base sequence (5' end to 3' end)	Fluorophore used	Linker
Probe I	AACGATGCACGAGCA	N/A	5'-NH_2-$(CH_2)_6$-
Probe II	TTGCTACGTGCTCGT	3'-[Cy5]	N/A
Probe III	AACGATGCACGAGCA	3'-[Cy5]	5'-NH_2-$(CH_2)_6$-

Alternatively, pulsed plasma PFPA coated surfaces were reacted in solutions of proteins I and II in PBS buffer pH=7.4 at a concentration of 20 $\mu g.mL^{-1}$ for 24h and rinsed according to process described above.

Table III-2 – Proteins used (Sigma-Aldrich)

Protein label	Protein	Fluorophore
Protein I	Goat antimouse IgG (H + L)	Alexa fluor 633
Protein II	Protein G from streptococcus sp	N/A

III.2.3. Analysis

A spectrophotometer (nkd-6000, Aquila Instruments Ltd.) was used for plasma polymer film thickness measurements. The obtained transmittance-reflectance curves (350-1000 nm wavelength range) were fitted to a Cauchy material model using a modified Levenberg-Marquardt algorithm[84].

Contact angle analysis on the pulsed plasma deposited poly-NAS and poly-PFPA films was carried out using a video capture system (ASE Products, model VCA2500XE). 2.0 µL sessile droplets of deionised water were placed onto the polymer surface and contact angle measurements taken at ambient temperature.

Chemical characterization by X-ray photoelectron spectroscopy (XPS) was undertaken using a VG Microtech electron spectrometer equipped with a non-monochromated Mg Kα X-ray source (1253.6 eV) and a concentric hemispherical analyzer (VG 100 AX) operating in the constant analyzer energy mode (CAE, pass energy = 20 eV for elemental analysis and 50 eV for wide scans). Take-off angle of 60° were used (measured from the surface of the sample). The XPS spectra for the carbon envelopes were fitted using the convention established for insulating polymers, i.e. C-C bond exhibits a photopeak at a binding energy of 285.0 eV. All the Gaussian components peaks[85] were determined using a linear background and equal full-width at-half-maximum (FWHM) on a Marquardt minimization computer software. Each Gaussian component relates to different carbon bonding, the peaks are centred on the binding energy of the bond of interest as determined by Beamson and Briggs[86]. The

peak counts have no relevance in term of values when compared with other spectra as they have been fitted to maximise the scale. Instrument sensitivity multiplication factors were taken as C(1s): O(1s): N(1s): Si(2p): F(1s) 1.00: 0.37: 0.56: 096: 0.24.

Surface Fourier transform infrared spectroscopy (FTIR) was performed on gold and silicon substrates using an FTIR spectrometer (Perkin-Elmer, model Spectrum One) equipped with a liquid nitrogen cooled MCT detector operating at 4 cm^{-1} resolution over the 700-4000 cm^{-1} range. The instrument was fitted with a reflection-absorption spectroscopy accessory (Specac) and a KRS-5 p-polarizer with the reflection angle set to 84° for gold and 66° for silicon. All spectra were averaged over 512 scans. The Y-axis in the spectra presented is chosen to maximise the visualisation of the peaks and have no relevance in terms of values.

Fluorescence quantification was achieved using a Dilor Labram microscope by irradiating a 20 mW He-Ne laser at a wavelength of 633 nm (which corresponds to the excitation frequency of the Cy5 fluorophore) and a polarization of 500:1 through the microscope objective (x10). The corresponding fluorescence signal was collected through the same objective via a backscattering configuration in combination with a cooled CCD detector. The diffraction grating was set at 1800 $lines.mm^{-1}$ with the laser filter at 10% transmission.

III.3. RESULTS

III.3.1. Deposition and reactivity of N-acryloxysuccinimide

III.3.1.1. Plasma polymerisation of N-acryloxysuccinimide

XPS analysis of the pulsed plasma deposited poly(N-acryloxysuccinimide) indicated the presence of carbon, oxygen and nitrogen. There is relatively good agreement between

the pulsed plasma deposited film and the theoretical atomic concentrations (in %) of poly(N-acryloxysuccinimide) suggesting that a high proportion of polymerisation occurred selectively at the alkene bond, and that the ester functionality remained intact during the electrical discharge process (see Table III-3).

Table III-3 – XPS analysis of N-acryloxysuccinimide plasma polymer (50 µm / 10 ms – 5 W)

Surfaces	Composition (at. %)		
	C	O	N
NAS plasma polymer - theoretical	58.3	33.3	8.3
NAS plasma polymer - experimental	65.0 ± 2.8	27.8 ± 1.9	7.2 ± 0.9

Additionally, the carbon envelope C(1s) can be fitted to five types of carbon[86] (see Figure III-1): hydrocarbon (285 eV), carbon in α-position of a carbonyl group (285.7 eV), carbon single-bonded to oxygen (286.7 eV), carbon from cyclic succinimide (288.6 eV) and carbon double-bonded to oxygen (289.7 eV). This is in good agreement with the theoretical spectra for poly-NAS. However, the presence of the carbon at 286.7 eV indicates that some of the ester functions have been lost since such carbon environment does not exist in the monomer.

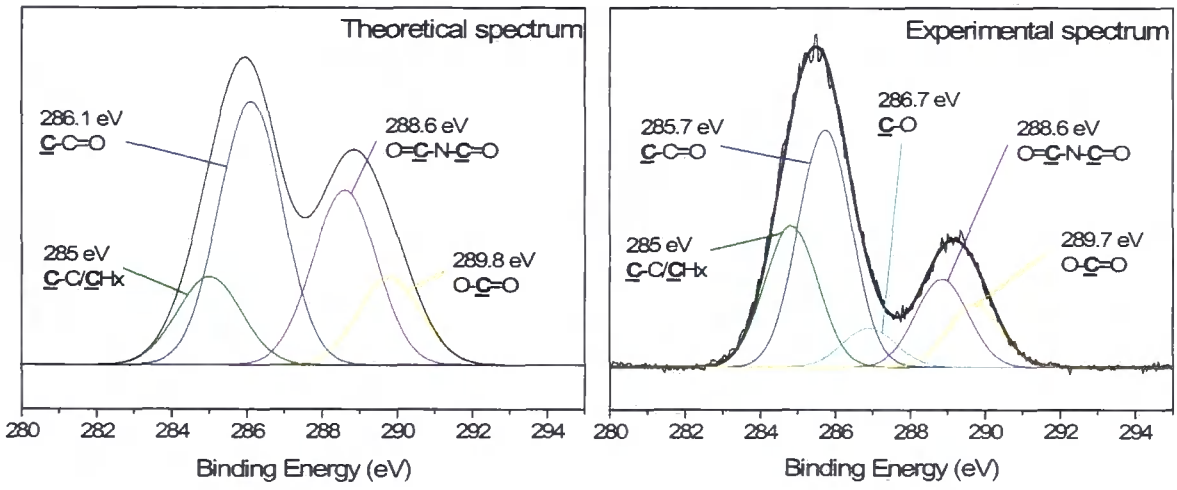

Figure III-1 - Theoretical and Experimental C(1s) XPS spectra for N-acryloxysuccinimide plasma polymer (50 µm / 10 ms – 5 W)

Infra-red spectroscopy of the film provided further evidence of functional retention in the pulsed-plasma polymerized film (see Figure III-2). The IR spectra of the monomer identified three main peaks attributable to carbonyl stretching: 1727, 1774 and 1798 cm^{-1}. Both Frey et al.[79] and Lahiri et al.[76] made the same assignment: 1727 and 1774 cm^{-1} to the imide asymmetric and symmetric stretching modes, respectively, and 1798 cm^{-1} to the ester stretching mode. The weak band at 1798 cm^{-1} is attenuated by a coupling between succinimide and the ester carbonyl group[87]. The vinyl group gives rise to the following peaks[88]: vinyl C=C stretch (1628 cm^{-1}), $=CH_2$ deformation from vinyl double bond (1405 cm^{-1}), =CH rock (1295 cm^{-1}) and $=CH_2$ rock (1049 cm^{-1}) (represented with * on Figure III-2). The band at 1425 cm^{-1} is attributed to the CH_2 bending mode, the one at 1381 cm^{-1} to the C-N-C symmetric vibration mode and the one at 1361 cm^{-1} the C-N stretching mode. The band at 1209 cm^{-1} corresponds to the C-N-C asymmetric vibration mode and the one at 1070 cm^{-1} is assigned to the ester –C(=O)-O-N- of the succinimide[87]. The negative peak observed at 1125 cm^{-1} is indicative of silicon from the substrate due to the small thickness of the plasma polymer.

The continuous-wave plasma polymerisation of NAS does not display any of the features of the monomer, indicating complete loss of functionality. However, when the plasma is pulsed, the peaks related to the succinimide ester are present. When the duty cycle of the pulse ($=\frac{t_{on}}{t_{on}+t_{off}}$) is increased, the peaks on the IR spectra are well defined, indicating good retention and higher deposition rate since the 'negative peak' due to the detection of the substrate observed with a smaller duty cycle is not visible for equal reaction time. A slight shift in frequencies is observed for the three peaks of higher wavenumbers (1798, 1774 and 1727 cm^{-1}) after polymerisation. This can be attributed

to the loss of conjugation between the vinyl double bond and the ester[88]. In the plasma polymer film, the peaks related to the C=C, $=CH_2$ and =CH bonds are not present anymore, indicating polymerisation occurred at the vinyl double bond.

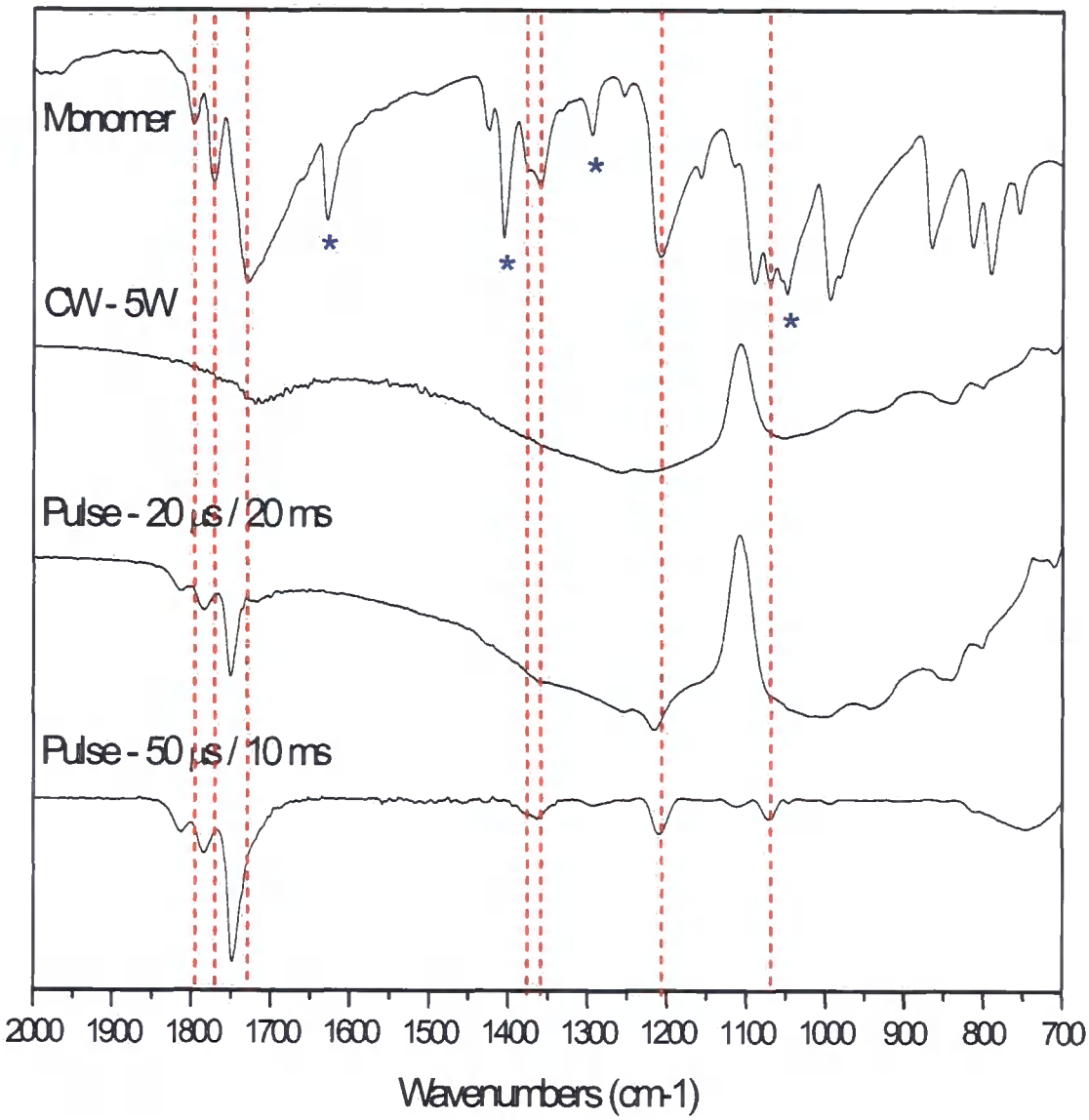

Figure III-2 – IR spectra of N-acryloxysuccinimide plasma polymer

Film deposition is also confirmed by the increase by the surface contact angle measurement indicating the surface has become less wettable after deposition (see Table III-4).

Table III-4 - Contact angle of bare silicon wafer and plasma polymer NAS film (50 µm / 10 ms – 5 W – thickness = 99 nm)

Surface	Contact angle
Bare silicon	33°
NAS plasma polymer	68 ± 3°

III.3.1.2. Derivatisation of N-acryloxysuccinimide plasma polymer

III.3.1.2.a. Reaction with trifluoroethylamine hydrochloride

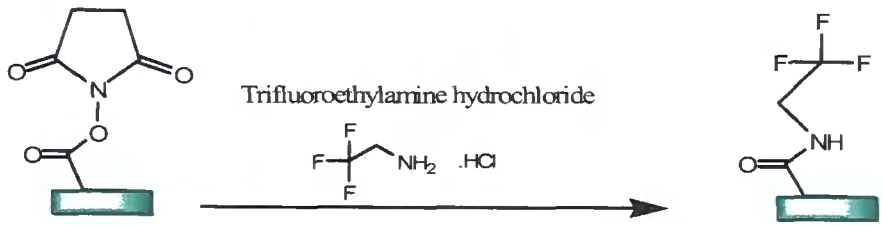

Scheme III-4 – Reaction of N-acryloxysuccinimide with trifluoroethylamine

Trifluoroethylamine hydrochloride was reacted with NAS plasma polymer film to form an amide bond. The advancement of the reaction was monitored by XPS as fluorine appears in the elemental composition of the surface. However, the difference between the theoretical atomic concentrations of a monolayer of NAS reacted with TFEA and the actual composition of the surface showed that the reaction did not go to completion (Table III-5). The reaction yield increased slightly with pH. In water almost no reaction occurred. A longer reaction time with a lower amine concentration reaches slightly higher yield.

Table III-5 – XPS analysis of N-acryloxysuccinimide (50 µm / 10 ms – 5 W) after reaction with trifluoroethylamine

Surfaces	Composition (at. %)			
	C	O	N	F
NAS plasma polymer - theoretical	58.3	33.3	8.3	
NAS plasma polymer - experimental	64.3 ± 3.1	27.8 ± 2.1	7.4 ± 1.0	
NAS + TFEA - theoretical	50	10	10	30
NAS + TFEA (100mM – pH=9.3 – 6h)	55.9	24.0	8.4	11.8
NAS + TFEA (30mM – pH=9.3 – 16h)	57.8	22.2	7.0	13.0
NAS + TFEA (30mM – pH=8.5 – 16h)	58.0	28.7	6.8	12.5
NAS + TFEA (30 mM – water – 16h)	66.6	27.1	4.66	1.64

The carbon envelope C(1s) of the surface after amidation could be fitted with the same five types of carbon environment as for the NAS plasma polymer film, with addition of three new types of carbon[86] (Figure III-3): a carbon bonded to a nitrogen and to a CF_3 group at 286.9 eV, a carbon from a linear amide at 287.4 eV and a carbon bonded to three fluorine atoms at 293 eV. These new types of carbon are the ones expected from N-trifluoroethyl propionamide. The peak related to the carbon of the amide on the succinimide group (288.7 eV) has diminished, confirming that the amidation occurs by substitution of a succinimide group with a trifluoroethyl group. The appearance of the small peak related to the carbon of the linear amide bond formed (287.7 eV) also corroborates the fact that reaction occurred. The relative proportions of the different types of carbon are given in Table III-6.

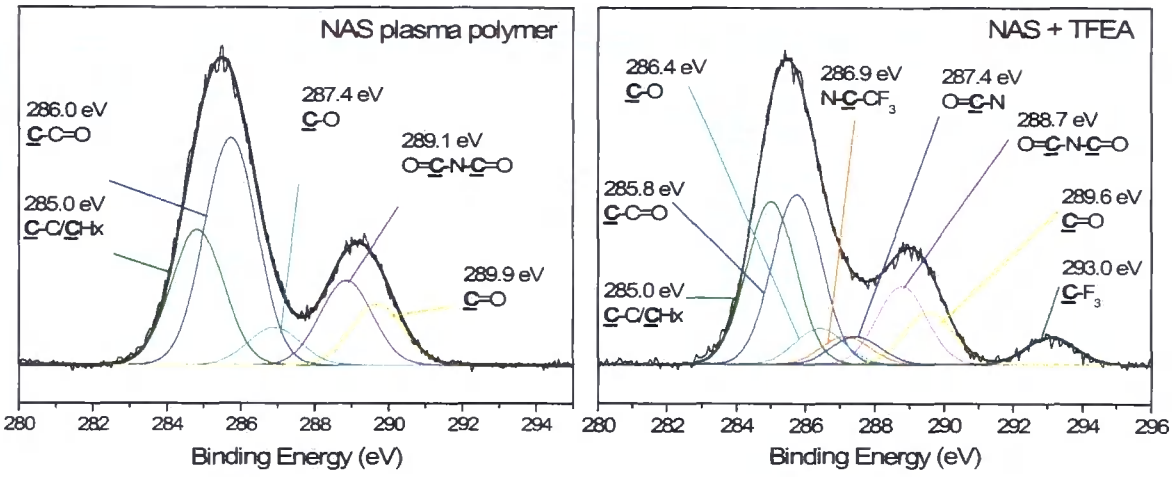

Figure III-3 – Experimental C(1s) XPS spectra of N-acryloxysuccinimide plasma polymer (50 µm / 10 ms – 5 W) before and after reaction with trifluoroethylamine

Table III-6 – Percentages of carbon environment before and after amidation of NAS with TFEA

Surfaces	Composition (%)							
	C-C/CHx	C-C=O	C-O	N-C-CF3	O=C-N	O=C-N-C=O	C=O	CF3
NAS theoretical	14.3	42.9				28.6	14.3	
NAS experimental	19.9	40.14	6.3			21.8	11.9	
NAS + TFEA theoretical	20	20		20	20			20
NAS + TFEA experimental	27.9	29.2	6.2	4.8	4.8	13.4	9.0	4.8

Contact angle measurement of the pulsed plasma (NAS) after reaction with TFEA confirmed a change. The increase in the contact angle to 84° indicates a more non-wettable surface after reaction, which correlates to the introduction of hydrophobic fluorine atoms[89] (Table III-7).

Table III-7 – Contact angle of N-acryloxysuccinimide (50 µm / 10 ms – 5 W) before and after reaction with trifluoroethylamine

Surface	Contact angle
NAS plasma polymer	70 ± 2 °
NAS + TFEA	84 ± 1 °

III.3.1.2.b. Reaction with propylamine

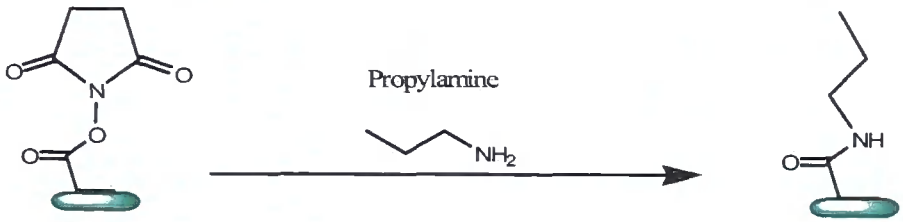

Scheme III-5 – Reaction of N-acryloxysuccinimide with propylamine

After 1h, amidation occurred as confirmed by XPS analysis (Table III-8). Indeed the carbon to oxygen ratio leapt from 2.4 to 4.5. For comparison, NAS plasma polymer was reacted without amine in water for 1h. The elemental composition of the surface was not altered, showing no hydrolysis occurred for the reaction-time considered. The variation in elemental composition can therefore be attributed exclusively to amidation.

Table III-8 - XPS analysis of N-acryloxysuccinimide (50 µm / 10 ms – 5 W) after reaction with propylamine

Surfaces	Composition (at. %)		
	C	O	N
NAS plasma polymer - theoretical	58.3	33.3	8.3
NAS plasma polymer - experimental	64.3 ± 3.1	27.8 ± 2.1	7.4 ± 1.0
NAS + PA - theoretical	75	12.5	12.5
NAS + PA (30 mM – water)	75.8 ± 1.0	17.5 ± 0.9	6.8 ± 0.0
NAS in water	66.5 ± 1.5	28.1 ± 1.2	5.5 ± 0.1

The C(1s) envelope could be fitted with the same types of carbon environment as seen with the NAS plasma polymer, with exception of the O-**C**=O initially at 289.7 eV, confirming that the reaction did not go to completion. In addition, two new types of carbon environment were generated (Figure III-4). The appearance of carbon single-bonded to nitrogen and of linear amide carbon, respectively at 286.6 and 287.5 eV, shows that reaction occurred. Moreover, the net increase in the envelope related to the hydrocarbon (285 eV) also confirms reaction since a 3-carbon-alkyl chain has replaced

a succinimide group, increasing the proportion of hydrocarbon (285 eV). Another confirmation that amidation took place is observed in the decrease of the peak for amide carbon on succinimide group (288.5 eV) (Table III-9).

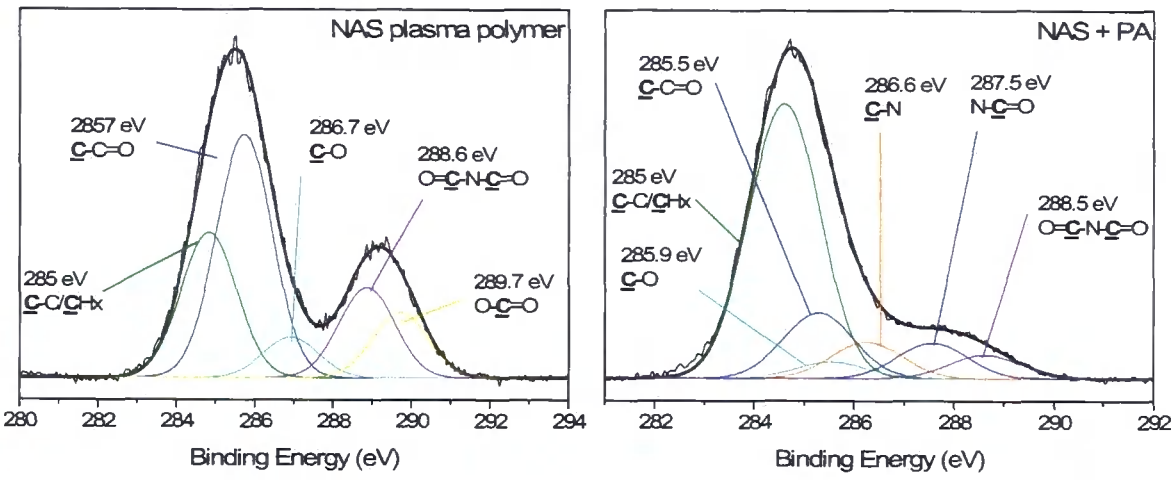

Figure III-4 – C(1s) XPS spectra of N-acryloxysuccinimide plasma polymer (50 µm / 10 ms – 5 W) before and after reaction with propylamine

Table III-9 - Percentages of carbon environment before and after amidation of NAS with PA

Surfaces	Composition (%)						
	C-C/CH$_x$	C-C=O	C-O	N-C	O=C-N	O=C-N-C=O	C=O
NAS theoretical	14.3	42.8				28.6	14.3
NAS experimental	25.3	41.2	6.9			15.4	11.1
NAS + PA theoretical	57	14		14	14		
NAS + PA experimental	60.6	14.5	3.7	8.1	7.8	5.3	

The increase in the contact angle after amidation with PA indicates that the succinimide have been replaced by a more hydrophobic alkyl chain (Table III-10).

Table III-10 – Contact angle of N-acryloxysuccinimide (50 µm / 10 ms – 5 W) before and after reaction with propylamine

Surface	Contact angle
NAS plasma polymer	68 ± 3 °
NAS + PA	78 ± 1 °

III.3.2. Deposition and reactivity of pentafluorophenyl acrylate

III.3.2.1. Plasma polymerisation of pentafluorophenyl acrylate

XPS analysis of the pulsed plasma deposited poly(pentafluorophenyl acrylate) showed there was presence of carbon, oxygen and fluorine as expected. The good agreement between the pulsed plasma deposited film and the theoretical atomic concentrations of poly(pentafluorophenyl acrylate) indicates that polymerisation occurred selectively at the alkene bond, and that the active ester functionality remains intact during the electrical discharge process (see Table III-11). The carbon envelope C(1s) can be fitted to five types of carbon[86] (see Figure III-5): hydrocarbon (285 eV), carbon in α-position of a carbonyl group (285.4 eV), carbon single-bonded to oxygen from a carboxylic ester (286.3 eV), aromatic carbon single-bonded to fluorine (287.8 eV) and carbon double-bonded to oxygen (289 eV). This is in good agreement with the theoretical spectra for poly-PFPA. In addition, the π-π^* shake-up satellite at 293.5 eV is clearly indicative of the retained aromatic structure[90].

Table III-11 – XPS analysis of pentafluorophenyl acrylate plasma polymer (10 µm / 20 ms – 20 W)

Surfaces	Composition (at. %)		
	C	O	F
PFPA plasma polymer - theoretical	56.2	12.5	31.3
PFPA plasma polymer - experimental	49.7 ± 1.8	12.0 ± 1.6	38.4 ± 2.4

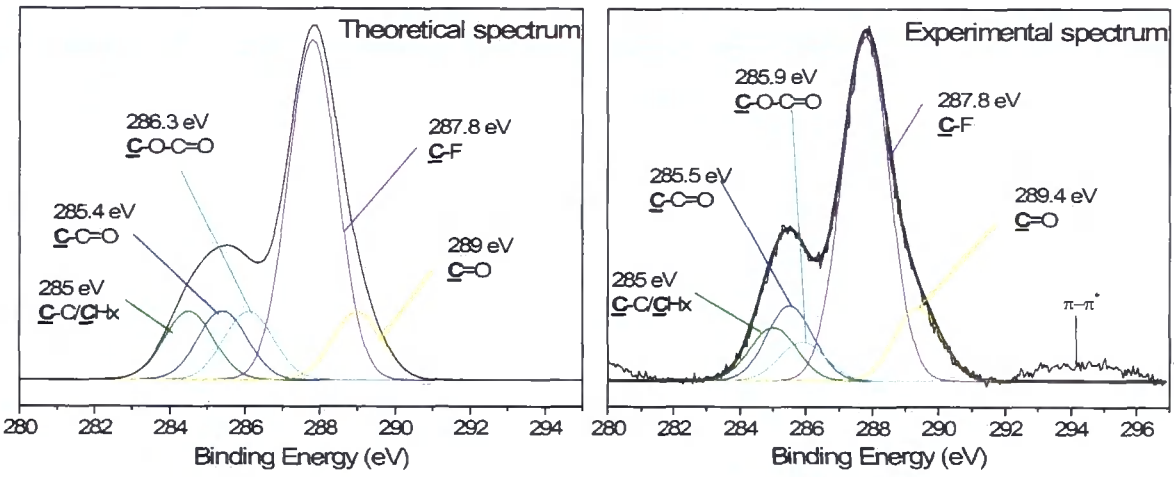

Figure III-5 - Theoretical and Experimental C(1s) XPS spectra for pentafluorophenyl acrylate plasma polymer (10 µm / 20 ms – 20 W)

Table III-12 - Percentages of carbon environment of PFPA plasma polymer theoretical / experimental

Surfaces	Composition (%)				
	C-C/CH$_x$	C-C=O	C-O-C=O	C-F	C=O
PFPA theoretical	11.1	11.1	11.1	55.6	11.1
PFPA experimental	9.8 ± 1.5	10.7 ± 1.3	8.3 ± 1.9	59.5 ± 3.4	11.7 ± 1.2

The IR spectra of the pulsed plasma poly(pentafluorophenyl acrylate) polymer confirms retention of the features of PFPA (Figure III-6). For PFPA monomer, the following assignment can be made[88] for the main peaks: an ester carbonyl stretch C=O is visible at 1770 cm^{-1}, and C-O vibration related also to the ester group is present at 1218 cm^{-1}. The four peaks indicating the presence of a vinyl C=C are situated at 1634 cm^{-1} for the C=C stretch, 1405 cm^{-1} for the =CH$_2$ deformation, 1292 cm^{-1} for the =CH rock and finally at 950 cm^{-1} for the =CH$_2$ wag. The five main peaks related to the perfluorinated aromatic ring are at 1655 cm^{-1} for the C=C stretch, 1513 cm^{-1} for the ring vibration, 1471, 1110 and 991 cm^{-1} for ring semi-circle stretch and C-F bending. The benzene ring vibration should present a peak at 1486-1500 cm^{-1}, however the

substitution of all hydrogen atoms by fluorine tends to decrease the frequency of the vibration[88].

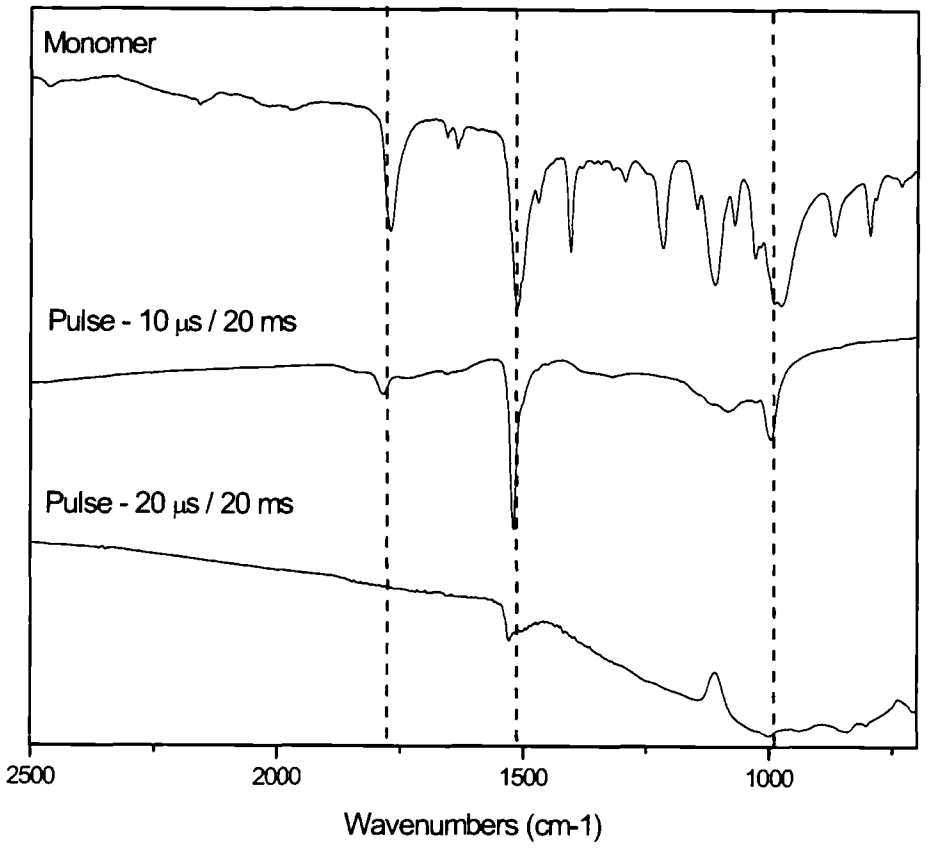

Figure III-6 – IR spectra of pentafluorophenyl acrylate plasma polymer

When PFPA is pulsed-plasma deposited, with a duty cycle of t_{on} = 20 µs / t_{off} = 20 ms, the fluorinated benzene ring is visible with its peak at 1513 cm^{-1}. However, the peak related to carbonyl group is not visible on the IR spectra. When the duty cycle varies to t_{on} = 10 µs / t_{off} = 20 ms, a better retention of functionality is observed. The carbonyl group stretch is visible at around 1780 cm^{-1} (lower frequency than in the monomer because of the loss or conjugation with the C=C double bond) and three of the bands characteristic of fluorinated benzene ring are present at 1510, 1105 and 990 cm^{-1}. The absence of the three peaks related to vinyl carbon-carbon double bond at 1630, 1400 and 1290 cm^{-1} confirms that polymerisation occurred at the alkene side of the precursor.

Contact angle measurement reflects the fact that the surface of silicon wafer has been modified with a film presenting hydrophobic functionalities (Table III-13), which is corroborates the presence of a perfluorinated benzene ring[89].

Table III-13 – Contact angle Pentafluorophenyl acrylate plasma polymer (10 µm / 20 ms – 20 W – thickness = 50 – 100 nm)

Surface	Contact angle
Silicon wafer	33°
PFPA plasma polymer	94 - 97 °

III.3.2.2. Hydrolysis studies of pentafluorophenyl acrylate

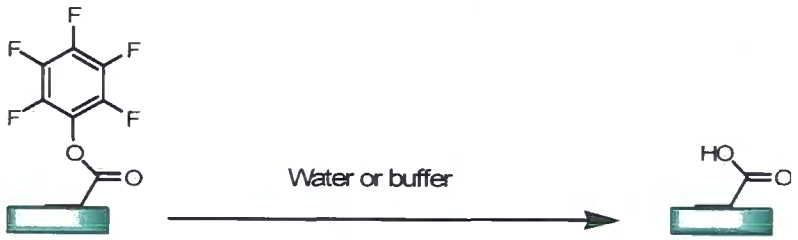

Scheme III-6 – Hydrolysis of pentafluorophenyl acrylate

To evaluate the stability of PFPA plasma polymer surfaces in aqueous media, hydrolysis studies have been undertaken in water and in buffer solution. The results presented in Table III-14 indicate that in water or in slightly basic buffer, the amount of fluorine decreases and that of oxygen increases, indicating that after 24 h some of the reactive ester functions are hydrolysed. After 48h, more esters have been hydrolysed, but the rate at which hydrolysis occurs has decreased. After a week, there seem to be almost no reactive esters left as shown by the low amount of fluorine. Some silicon probably from the substrate starts to show in the surface composition after 24h in buffer solution. This can indicate that the plasma polymer is slowly dissolving in the buffer solution. Some nitrogen has also been incorporated at the surface, probably from contamination.

After what is considered nearly full hydrolysis of the ester functionalities (1 week), the experimental elemental composition of the surface does not equal the theoretical one, indicating that hydrolysis of PFPA plasma polymer did not leave a pure carboxylic acid surface.

Table III-14 – XPS analysis of the hydrolysis of pentafluorophenyl acrylate (10 µm / 20 ms – 20 W)

Surfaces	Composition (at. %)				
	C	O	N	F	Si
PFPA plasma polymer theoretical	56.2	12.5		31.3	
PFPA plasma polymer experimental	49.7 ± 1.8	11.9 ± 1.6		38.4 ± 2.4	
PFPA after complete hydrolysis	60	40			
PFPA in water 24h	55.2 ± 3.3	15.8 ± 1.2		29.1 ± 3.4	
PFPA in buffer pH=8.5 24h	55.1 ± 0.6	16.1 ± 1.3	0.2 ± 0.1	27.7 ± 1.2	0.9 ± 0.2
PFPA in buffer pH=8.5 48h	55.9 ± 1.7	18.9 ± 2.9	0.7 ± 0.3	22.3 ± 4.3	2.2 ± 0.3
PFPA in buffer pH=8.5 1 week	61.9	26.6	5.5	2.4	3.6

The carbon envelope C(1s) of PFPA plasma polymer after hydrolysis (1 week) presents the same carbon environment as the initial surface, in addition to a small peak at 290.4 eV attributed to some CF_2 or CF_3 groups probably initially present within the bulk of the plasma polymer and exposed to the surface after hydrolysis (Figure III-7). However, the noticeable difference is that the peak related to CF bonds at 287.9 eV is far smaller than for the initial polymer, hence confirming the hydrolysis of the ester group. Moreover, the absence of the π-π^* shake-up satellite at 293.5 eV indicates removal of aromatic structure previously present at the surface. Finally, unlike what would have been expected with complete hydrolysis, the peak related to C=O did not

increase much. This means that the loss of ester functionalities was not necessarily accompanied by creation of carboxylic acid functionalities.

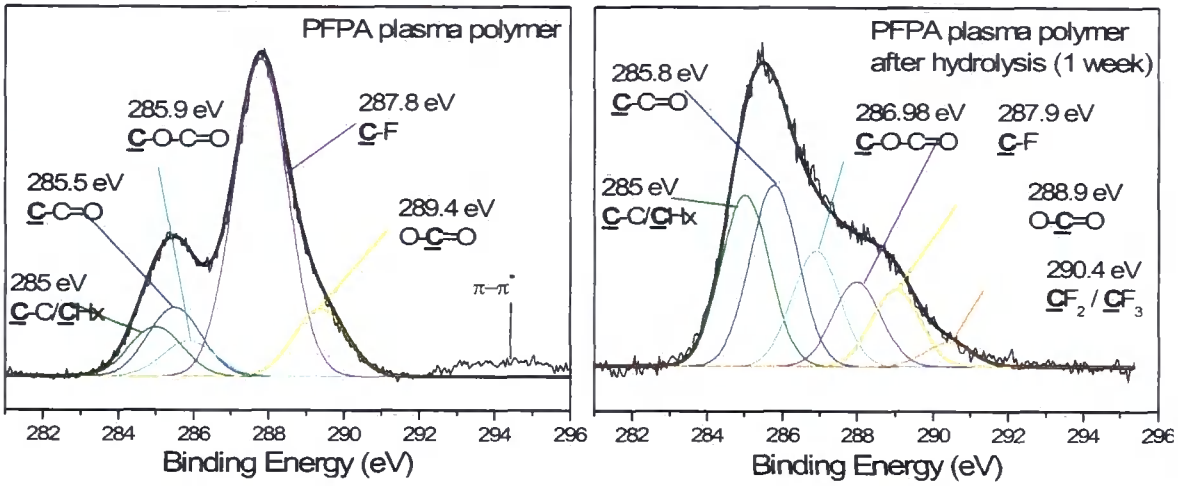

Figure III-7 – C(1s) XPS spectra of pentafluorophenyl acrylate plasma polymer (10 µm / 20 ms – 20 W) before and after hydrolysis in buffer (1 week)

With the loss of the fluorinated ring, a more hydrophilic surface is confirmed by contact angle measurement. Indeed as hydrolysis occurs, the contact angle of the PFPA plasma polymer decreases (Table III-15).

Table III-15 – Contact angle of pentafluorophenyl acrylate plasma polymer (10 µm / 20 ms – 20 W) before and after hydrolysis

Surface	Contact angle
PFPA plasma polymer	95 ±2 °
PFPA hydrolysed (24 h)	80 ±1 °
PFPA hydrolysed (48h)	67 ± 2 °
PFPA hydrolysed (1 week)	18 ± 1 °

III.3.2.3. Derivatisation of pentafluorophenyl acrylate plasma polymer

III.3.2.3.a. Reaction with diethylamine

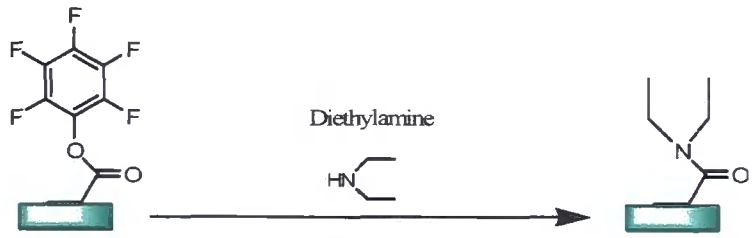

Scheme III-7 – Reaction of pentafluorophenyl acrylate with diethylamine

The nucleophilic substitution reaction of PFPA plasma polymer with the primary amine diethylamine was followed by XPS analysis. The elemental composition at the surface after reaction indicated a decrease in fluorine content accompanied by the appearance of nitrogen (Table III-16). Additionally, carbon content changes would agree with the theoretical composition of the fully reacted PFPA plasma polymer. Finally, nitrogen levels indicated nucleophilic substitution proceeded more favourably in slightly basic buffer than in water.

Table III-16 – XPS analysis of pentafluorophenyl acrylate (10 µm / 20 ms – 20 W) reacted with diethylamine

Surfaces	Composition (at. %)			
	C	O	N	F
PFPA plasma polymer theoretical	56.2	12.5		31.3
PFPA plasma polymer experimental	54.1 ± 1.4	17.2 ± 4.5		28.7 ± 5.8
PFPA + DiEA theoretical	77.8	11.11	11.11	
PFPA + DiEA - 100 mM water - 16h	58.1 ± 0.8	13.3 ± 1.0	3.1 ± 0.4	25.5 ± 2.2
PFPA + DiEA - 100 mM buffer pH=8.5 - 16h	61.9 ± 2.7	21.0 ± 1.4	5.3 ± 0.2	11.8 ± 1.5

The carbon envelope C(1s) after reaction presents seven different environments (Figure III-8): hydrocarbon (285.0 eV), carbon in α position of a carbonyl group (285.5 eV), carbon single-bonded to oxygen from an ester group (286.0 eV), a carbon single-bonded to nitrogen (286.5 eV), a carbon from an amide (287.8 eV), a carbon bonded to a single fluorine atom (288.2 eV) and a carbon from a carbonyl group (289.3 eV). All these different environments are compatible with a surface presenting active ester functions as well as amide functionalities. The fact that the peak related to the reactive ester decreased as the peak related to the amide increased provides evidence that substitution occurred. The hydrocarbon peak increased the most which is expected as two alkyl chains were introduced after reaction with the secondary amine.

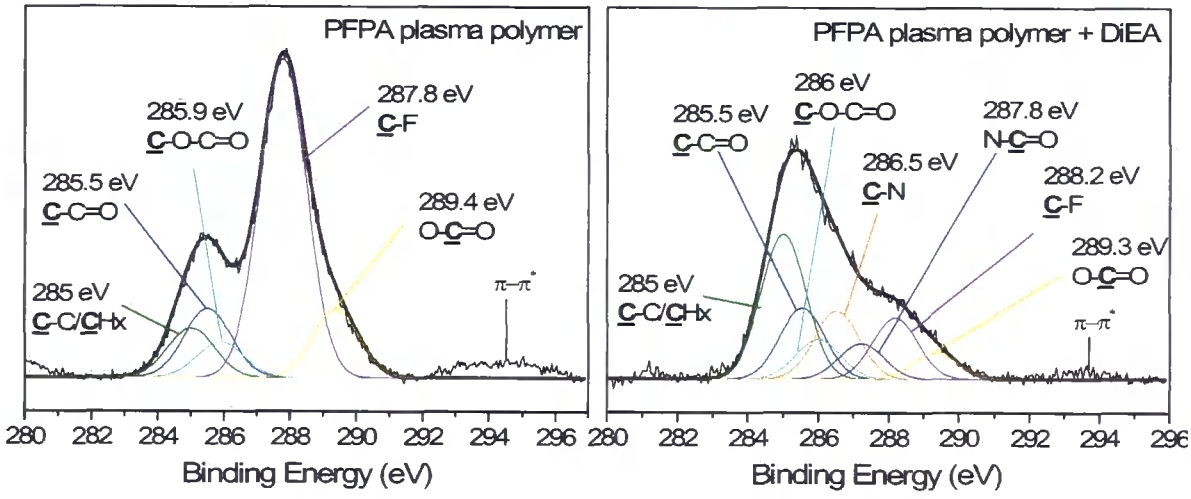

Figure III-8 – C(1s) XPS spectra of pentafluorophenyl acrylate (10 µm / 20 ms – 20 W) before and after reaction with diethylamine

The decrease in the contact angle on the derivatised surface confirms that a very hydrophobic group was substituted with another of lesser hydrophobic character (Table III-17).

Table III-17 - Contact angle of pentafluorophenyl acrylate (10 µm / 20 ms – 20 W) before and after reaction with diethylamine

Surface	Contact angle
PFPA plasma polymer	94 ± 2 °
PFPA + DiEA	80 ± 3 °

III.3.2.3.b. Reaction with ethanolamine

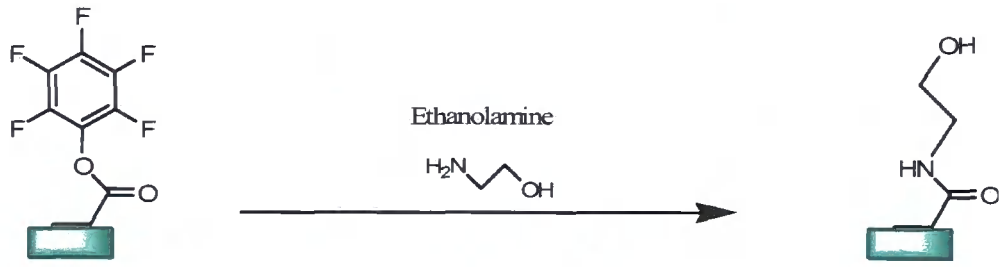

Scheme III-8 – reaction of pentafluorophenyl acrylate with ethanolamine

The covalent attachment of ethanolamine (EA) onto PFPA plasma polymer was followed by XPS. As the reaction proceeds, nitrogen appears at the surface at the same time as fluorine disappears (Table III-18). The increase in the atomic concentrations of carbon and oxygen also confirm changes in the surface composition. The remaining fluorine provides evidence that the reaction did not go to completion.

Table III-18 – XPS analysis of pentafluorophenyl acrylate (10 µm / 20 ms – 20 W) reacted with ethanolamine

Surfaces	Composition (at. %)			
	C	O	N	F
PFPA plasma polymer theoretical	56.25	12.5		31.25
PFPA plasma polymer experimental	49.7 ± 1.8	11.9 ± 1.6		38.4 ± 2.4
PFPA + EA theoretical	62.5	25	12.5	
PFPA + EA - 100 mM pH=7 - 5h	63.3 ± 0.5	25.26 ± 1.1	3.48 ± 0.3	8.01 ± 1.3

The carbon envelope C(1s) of PFPA after reaction with EA (Figure III-9) shows the five types of carbon reported previously for PFPA plasma polymer, confirming that some reactive esters functions remain at the surface. Three more environments are present, carbon single-bonded to nitrogen and carbon single-bonded to OH group, both showing at 286.9 eV, carbon from amide function at 287.8 eV, and a fluorinated carbon CF_2/CF_3 probably introduced during plasma polymerisation and exposed after reaction with ethanolamine.

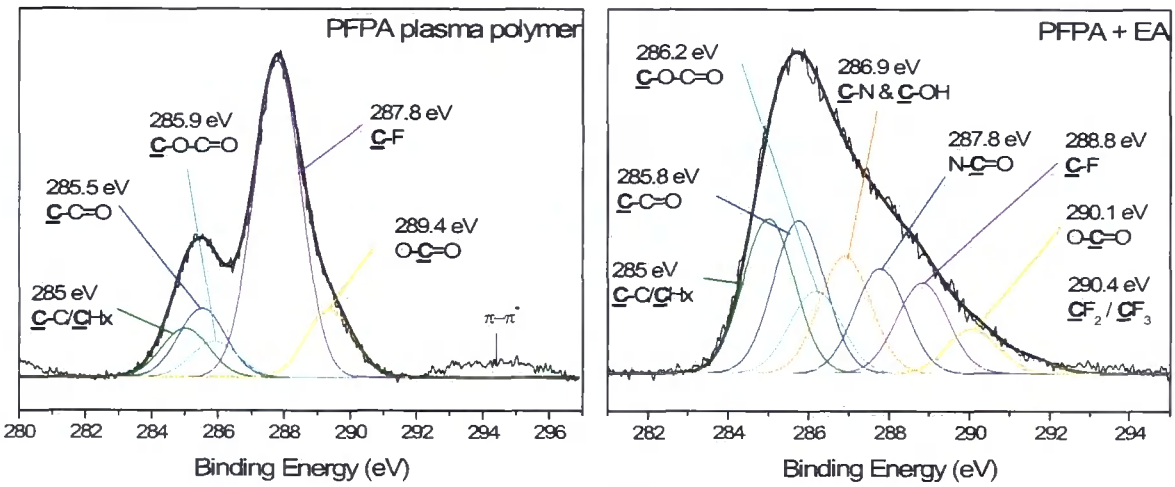

Figure III-9 – C(1s) XPS spectra of pentafluorophenyl acrylate (10 µm / 20 ms – 20 W) before and after reaction with ethanolamine

The decrease in contact angle measurement provides further evidence that hydrophobic ester groups were replaced with more hydrophilic groups. The decrease is greater after reaction with ethanolamine than for pure hydrolysis (compare Table III-15 and Table III-19) for comparable reaction time, therefore confirming hydrophilic alcohol groups were introduced at the surface, and at a faster rate than hydrolysis occurs.

Table III-19 - Contact angle of pentafluorophenyl acrylate (10 µm / 20 ms – 20 W) before and after reaction with ethanolamine

Surface	Contact angle
PFPA plasma polymer	91 ± 1 °
PFPA + EA	60 ± 2 °

III.3.2.3.c. Reaction with trifluoroethylamine

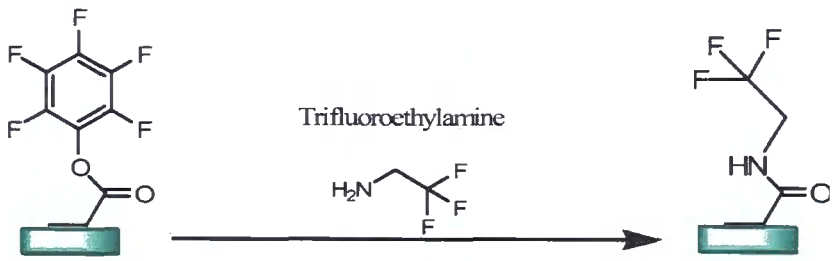

Scheme III-9 – Reaction of pentafluorophenyl acrylate with trifluoroethylamine

XPS analysis of the surface after reaction shows that very little nitrogen was introduced at the surface (Table III-20), suggesting that amidation did not occur to a great extent. The amount of oxygen at the surface increased significantly to the same level as for hydrolysis of the ester functions (see Table III-14).

Table III-20 - XPS analysis of pentafluorophenyl acrylate (10 µm / 20 ms – 20 W) reacted with trifluoroethylamine

Surfaces	Composition (at. %)			
	C	O	N	F
PFPA plasma polymer theoretical	56.2	12.5		31.3
PFPA plasma polymer experimental	49.7 ± 1.8	11.9 ± 1.6		38.4 ± 2.4
PFPA + TFEA theoretical	50	10	10	30
PFPA + TFEA - 100 mM pH=8.5 - 16h	53.6 ± 0.5	23.8 ± 0.8	1.8 ± 0.3	20.9 ± 1.6

The carbon envelope C(1s) presents the same carbon environments as PFPA plasma polymer, with addition of three other in small proportions: carbon bonded to a nitrogen and to a CF_3 group (286.7 eV), carbon from an amide group (288.3 eV) and carbon bonded to three fluorine (293.2 eV). As the elemental composition suggested, the peak related to **C**-F from the reactive ester at 288.3 eV is still large, confirming that little reactive ester have been substituted by TFEA. This is also shown by the very small peak related to **C**F_3 at 293.2 eV.

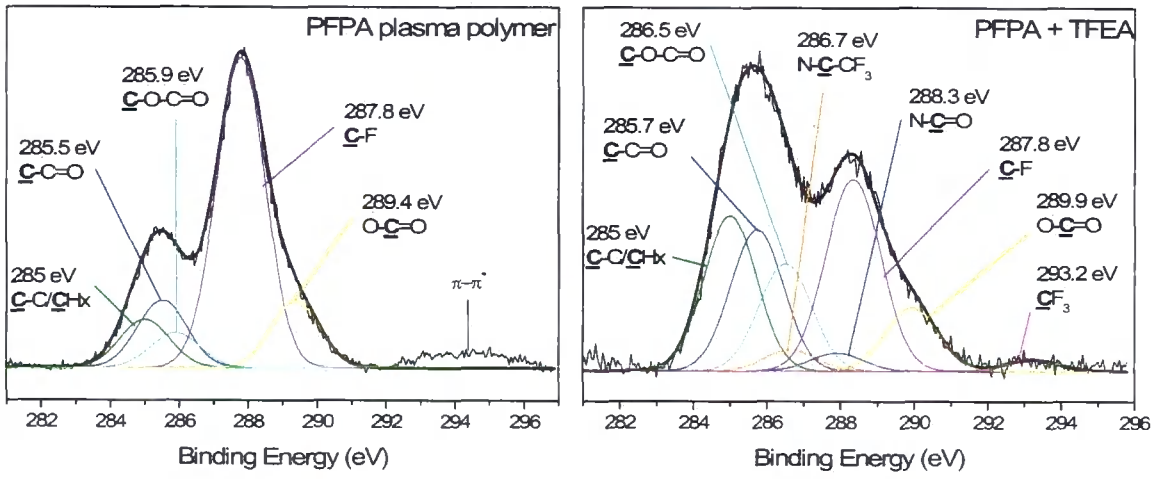

Figure III-10 – C(1s) XPS spectra of pentafluorophenyl acrylate (10 µm / 20 ms – 20 W) before and after reaction with trifluoroethylamine

Contact angle measurements show that the surface is nearly equivalent as a hydrolysed surface (p:108), with a lower contact angle as the unreacted PPFA plasma polymer surface. The introduction of TFEA should have maintained a high contact angle.

Table III-21 - Contact angle of pentafluorophenyl acrylate (10 µm / 20 ms – 20 W) before and after reaction with trifluoroethylamine

Surface	Contact angle
PFPA plasma polymer	92 ± 1 °
PFPA + TFEA	67 ± 2 °

III.3.2.4. Peptide attachment onto pentafluorophenyl acrylate plasma polymer

III.3.2.4.a. Attachment of β-alanine

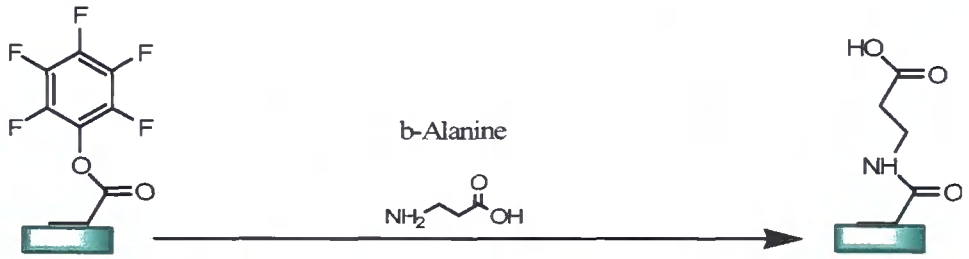

Scheme III-10 – Reaction of pentafluorophenyl acrylate with β-alanine

The attachment of the synthetic amino-acid β-alanine onto PFPA plasma polymer was followed by XPS. The introduction of nitrogen at the plasma polymer surface along with the decrease in fluorine content is consistent with successful attachment of β-alanine. Carbon and oxygen percentages also increased as expected after amidation reaction (see Table III-22).

Table III-22 – XPS analysis of the attachment of β-alanine onto pentafluorophenyl acrylate plasma polymer (10 µm / 20 ms – 20 W)

Surfaces	Composition (at. %)			
	C	O	N	F
PFPA plasma polymer theoretical	56.2	12.5		31.3
PFPA plasma polymer experimental	53.6 ± 0.9	13.8 ± 4.5		32.6 ± 5.3
PFPA + β-alanine theoretical	60	30	10	
PFPA + β-alanine 400 mM – pH=8.5 – 24h	56.8 ± 3.6	21.3 ± 2.7	3.2 ± 0.2	18.7 ± 5.7

The carbon envelope C(1s) of PFPA plasma polymer after amidation with β-alanine presents the same six carbon environment present in the original plasma polymer, with addition of two new ones (see Figure III-11): a peak at 287.0 eV accounts for carbon

bonded to nitrogen and also carbon bonded to a COOH group, and a peak at 287.6 eV characteristic of a carbon from an amide group. These two new peaks, which could demonstrate that amidation occurs, are however relatively small compared to the other environments, indicating a rather low reaction yield. The peak related to the **C**-F of the active ester is still of significant intensity, providing further evidence of the low yield of the reaction.

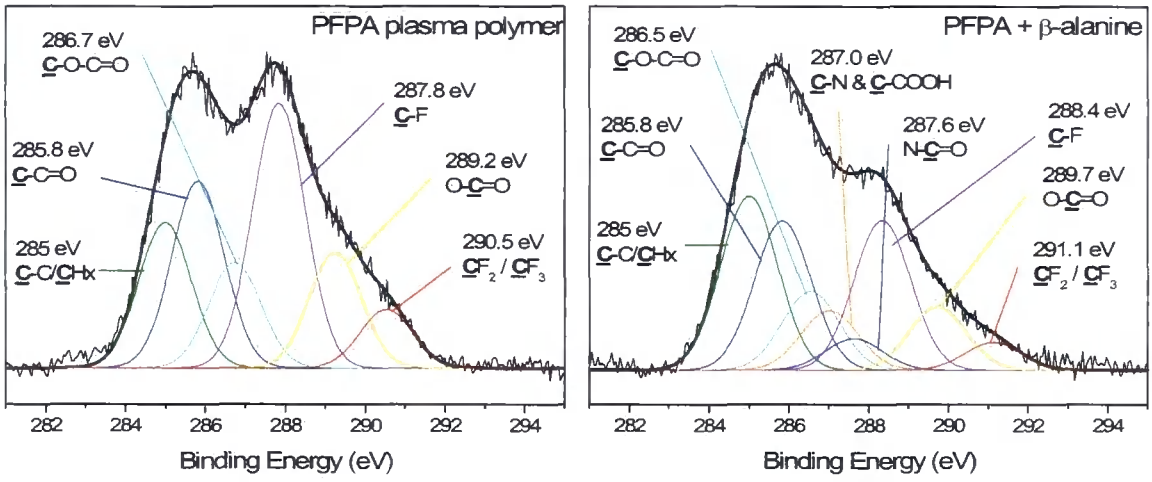

Figure III-11 – C(1s) XPS spectra of pentafluorophenyl acrylate (10 µm / 20 ms – 20 W) before and after reaction with β-alanine

The decrease in contact angle shows that some reactive ester has been substituted by a more hydrophilic group, such as carboxylic acid in the case of amidation with β-alanine.

Table III-23 - Contact angle of pentafluorophenyl acrylate (10 µm / 20 ms – 20 W) before and after reaction with β-alanine

Surface	Contact angle
PFPA plasma polymer	84 ± 2 °
PFPA + β-alanine	58 ± 2 °

III.3.2.4.b. Attachment of the di-peptide Gly-Ala

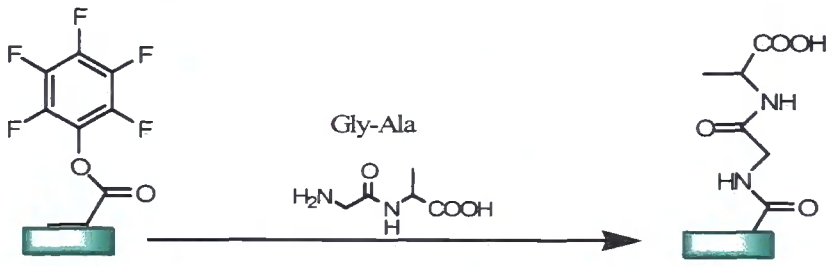

Scheme III-11 – Reaction of pentafluorophenyl acrylate with peptide gly-ala

The attachment of peptide Gly-Ala was monitored by XPS as nitrogen appeared in the surface elemental composition (Table III-24). The content in carbon, oxygen and nitrogen increased as expected after amidation reaction, and fluorine content decreased as reactive ester functions are substituted.

Table III-24 – XPS analysis of the attachment of gly-ala onto pentafluorophenyl acrylate plasma polymer (10 µm / 20 ms – 20 W)

Surfaces	Composition (at. %)			
	C	O	N	F
PFPA plasma polymer theoretical	56.2	12.5		31.3
PFPA plasma polymer experimental	51.0 ± 0.7	13.8 ± 2.0		35.3 ± 2.7
PFPA + gly-ala theoretical	57.1	28.6	14.3	
PFPA + gly-ala – 400 mM pH=8.5 – 48h	54.8 ± 0.3	22.1 ± 0.5	4.4 ± 0.1	18.8 ± 0.1

The carbon envelope C(1s) confirms the results of the elemental analysis. The surface after reaction presents the same five carbon environments as the PFPA plasma polymer, with addition of three new ones. Two of them are directly related to the amidation reaction: carbon single-bonded to nitrogen showing at 287.2 eV, and carbon from an amide at 287.6 eV. Another small peak appeared at 291.3 eV, related to $\underline{C}F_2/\underline{C}F_3$ which comes from dissociation of the monomer during plasma polymerisation

of pentafluorophenyl acrylate. The remaining peak for carbon single-bonded to fluorine provides evidence that reaction did not go to completion.

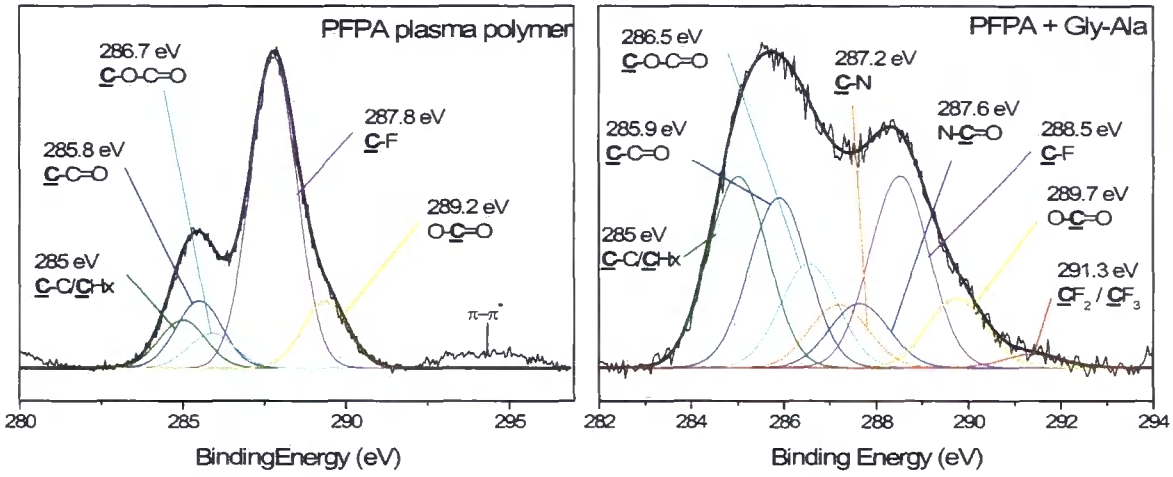

Figure III-12 – C(1s) XPS spectra of pentafluorophenyl acrylate (10 µm / 20 ms – 20 W) before and after attachment of gly-ala

The decrease in the contact angle characterises the fact that hydrophobic reactive esters have been replace by a more hydrophilic group such as carboxylic acid.

Table III-25 - Contact angle of pentafluorophenyl acrylate (10 µm / 20 ms – 20 W) before and after attachment of gly-ala

Surface	Contact angle
PFPA plasma polymer	93 ± 1°
PFPA + gly-ala – 400mM	68 ± 2 °

Figure III-13 shows the percentage of pentafluorophenyl groups which underwent reaction as a function of the peptide concentration for two reaction times (see Equation III-7 in Discussion paragraph). After 24 h reaction, the yield increases as peptide concentration increases and presents a plateau when peptide reaction is over 200 mM. After 48 h, the reaction yield is higher that after 24 h for the same peptide concentration, and the reaction yield also seems to reach a plateau.

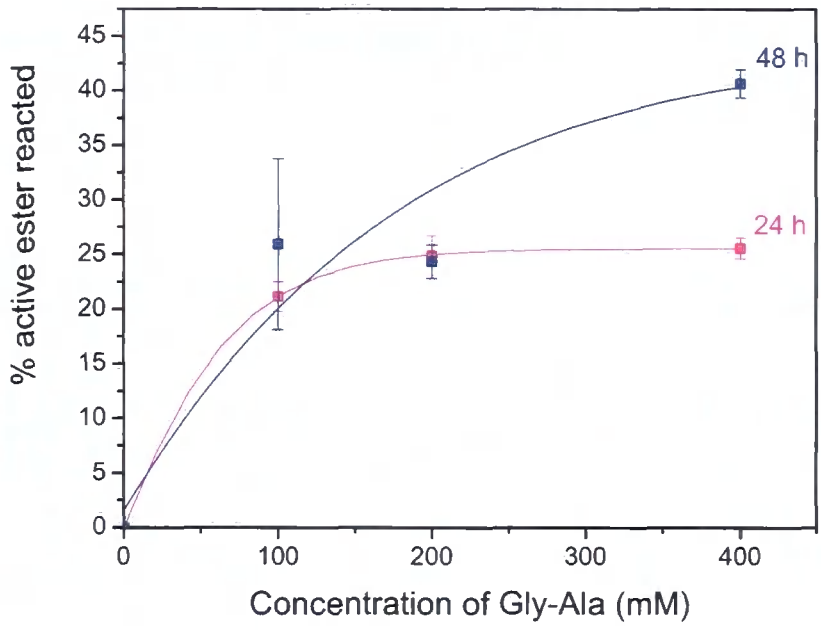

Figure III-13 – Reaction yield of Gly-Ala attached onto pentafluorophenyl acrylate plasma polymer (10 µm / 20 ms – 20 W)

III.3.2.4.c. Attachment of the tri-peptide Gly-Gly-His

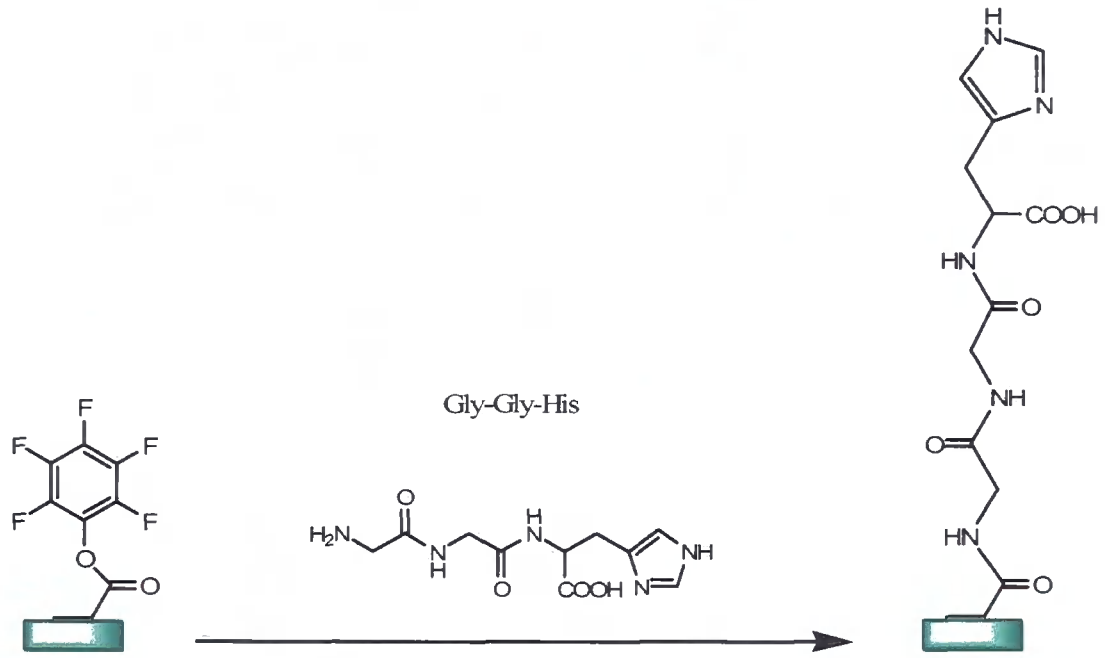

Scheme III-12 – Attachment of peptide gly-gly-his onto pentafluorophenyl acrylate plasma polymer

XPS analysis of the reacted surface indicated the presence of nitrogen (Table III-26). Carbon and oxygen content increases and a fluorine decrease, all of which are consistent with the substitution of reactive esters by peptide Gly-Gly-His.

Table III-26 – XPS analysis of the attachment of gly-gly-his onto pentafluorophenyl acrylate plasma polymer (10 µm / 20 ms – 20 W)

Surfaces	Composition (at. %)			
	C	O	N	F
PFPA plasma polymer theoretical	56.2	12.5		31.3
PFPA plasma polymer experimental	50.4 ± 0.1	14.2 ± 2.6		35.4 ± 2.6
PFPA + gly-gly-his theoretical	54.5	22.7	22.7	
PFPA + gly-gly-his 400 mM - pH=8.5 – 24h	58.7 ± 2.4	26.2 ± 1.2	6.3 ± 0.7	8.8 ± 1.9

The carbon envelope C(1s) presents the same five carbon environments as for PFPA plasma polymer along with two new ones: carbon single-bonded and double-bonded to nitrogen (286.9 eV) and carbon from an amide (287.8 eV). These two new peaks are compatible with the ones related to the tri-peptide. A peak remaining for C-F from the reactive ester confirms the observations made from the elemental composition, that is reaction did not go to 100% yield.

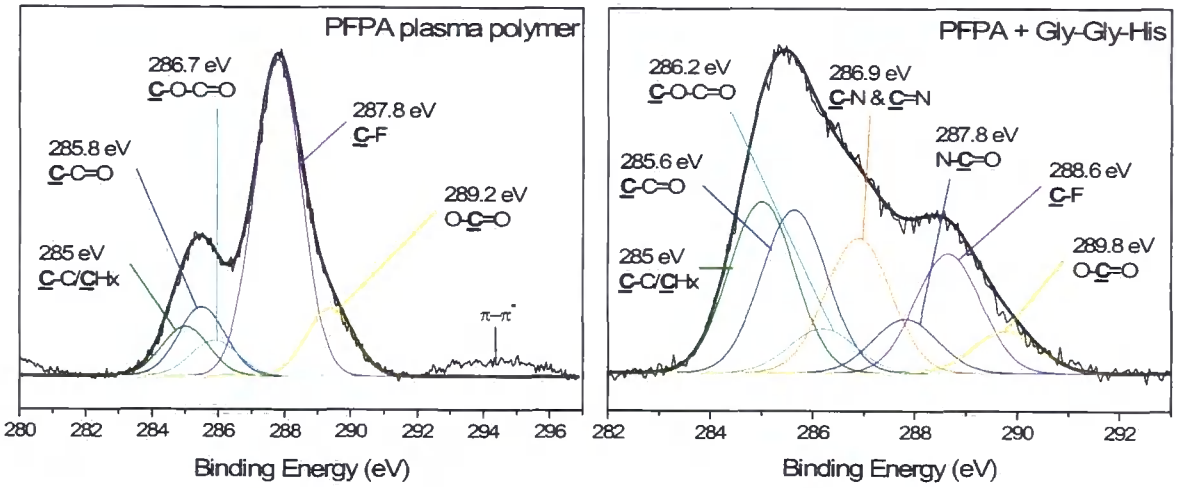

Figure III-14 – C(1s) XPS spectra of pentafluorophenyl acrylate plasma polymer (10 µm / 20 ms – 20 W) before and after attachment of gly-gly-his

To further demonstrate the availability of the peptide Gly-Gly-His, the peptide-derivatised surface was reacted with a solution containing copper ions[91,92], and the copper complexed with the peptide (as shown on Scheme III-13) was detected by XPS.

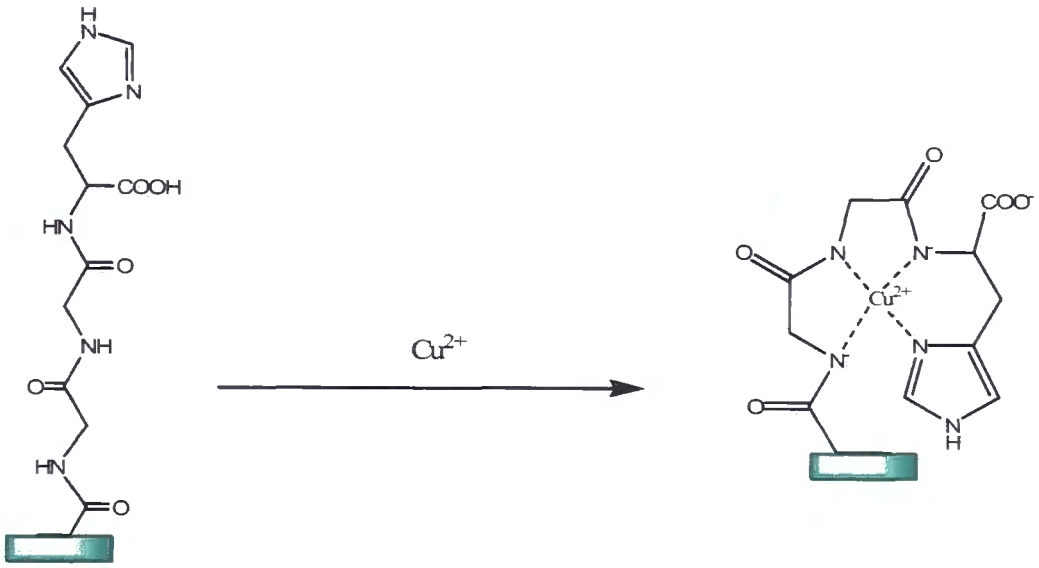

Scheme III-13 – Complexation of copper ion by the peptide gly-gly-his immobilized onto pentafluorophenyl acrylate plasma polymer

XPS wide scan analysis shows the different elements present at the surface a function of their binding energy. Carbon, nitrogen, oxygen and fluorine are present as established previously after the tri-peptide attachment. Moreover, small peaks related to

the silicon substrate[86] (binding energy = 102 and 152 eV) can be observed. Complexation of the peptide with copper ion was confirmed by the presence of the peak at a binding energy of 936 eV2 (Figure III-15).

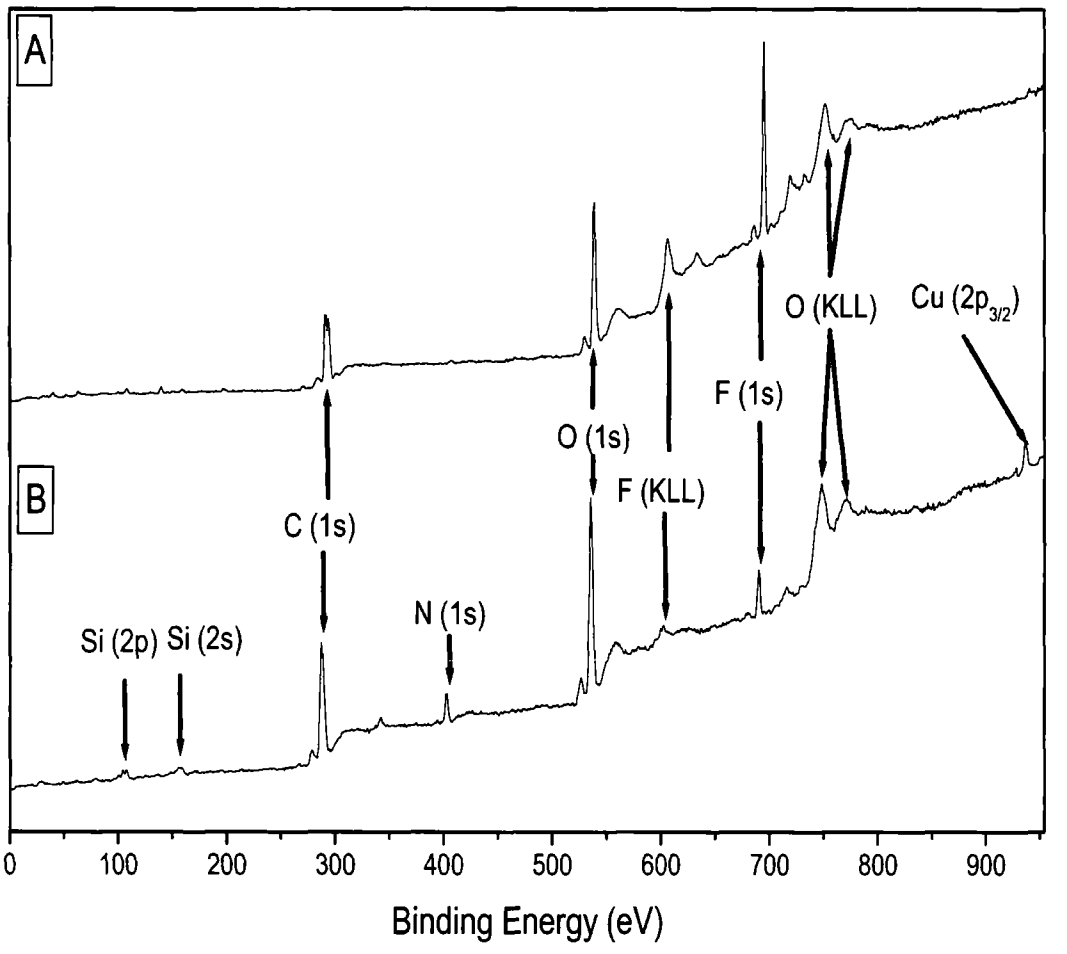

Figure III-15 – Wide scan XPS spectra of [A] PFPA plasma polymer (10 µm / 20 ms – 20 W) after reaction with copper ion solution and [B] gly-gly-his attached onto PFPA plasma polymer (10 µm / 20 ms – 20 W) complexed with copper ion

III.3.2.4.d. Immobilisation of tagged DNA and tagged protein onto PFPA plasma polymer

Qualitative assessment of DNA strand and protein immobilisation onto PFPA plasma polymer was achieved by fluorescence detection of the tagged the biomolecules. Results are presented in Table III-27.

Table III-27 – Fluorescence counts of PFPA plasma polymer before and after immobilization of tagged biomolecules

Surfaces	Fluorescence counts (10% laser)
PFPA plasma polymer	116
PFPA plasma polymer + tagged DNA	4766
PFPA plasma polymer + Protein I	96675
PFPA plasma polymer + Protein II	102
PFPA plasma polymer + Protein II after reaction with complementary Protein I	23000

PFPA plasma polymer presents low level of fluorescence. After reaction with tagged DNA strand, the fluorescence level of the surface increases confirming immobilisation. Reaction with tagged protein also yields a surface with high level of fluorescence. Furthermore, post-reaction of immobilised protein II was also confirmed by an increase in fluorescence after reaction with the complementary protein I.

III.4. DISCUSSION

III.4.1. Deposition and reactivity of N-acryloxysuccinimide

III.4.1.1. Plasma polymerisation of reactive esters N-acryloxysuccinimide and pentafluorophenyl acrylate

Pulsed plasma polymerisation is versatile technique used to functionalise surfaces in a single-step fashion with good retention of the structure of the precursor[93]. This method has been applied to a wide variety of monomers to introduce groups at the surface of a substrate such as anhydride[45], carboxylic acid[94], cyano[95], epoxide[23], hydroxyl[96], amine[97], furfuryl[98], perfluoroalkyl[99,100], halogen[101,102] and pyridine[103].

In a similar fashion, N-acryloxysuccinimide was deposited onto silicon wafer with good retention of function. Retention of succinimide groups were calculated according to Equation III-1:

Equation III-1 $$\text{Retention} = \frac{\%\text{ of carbon bearing amide groups in plasma polymer}}{\%\text{ of carbon bearing amide groups in theoretical spectra}}$$

XPS analysis (Table III-6) showed that the amount of carbon bearing succinimide groups equalled 21.8%. According to the theoretical spectra, the concentration of carbon bearing amide group should equal 28.6% for 100% retention. Therefore, retention of up to 76% of the succinimide groups was achieved with NAS. The error margin observed for the elemental composition can be accounted for the fact that the molecule has been fragmented during the discharge and lost some of the ester functionalities[104].

Similarly, pentafluorophenyl acrylate has been successfully plasma polymerised with good retention of the fluorinated ester functions. FTIR investigations indicated that decreased on-time during plasma polymerisation lead to better structural retention of the structure of the monomer[105]. Based on the carbon envelope of the PFPA plasma polymer (see Table III-12), the amount of CF_3 groups present at the surface compared to the theoretical value suggests a retention of function over 100%. However, the error margins are within experimental errors. Pulsed plasma deposited pentafluorophenyl methacrylate previously studied has led to very poor retention of the reactive ester functions and very low deposition rate[83].

III.4.1.2. Derivatisation of reactive ester plasma polymers with amines

Both ester-derivatised surfaces were reacted with a poor nucleophilic amine trifluoroethylamine hydrochloride (pK_a=7.8) in aqueous buffer. If we assume that all elements are homogeneously distributed within the XPS sampling depth both before

and after the derivatisation, the relationship between the conversion factor and the surface atomic concentrations of fluorine and nitrogen can be derived as follows. The proportion of succinimide groups which were substituted can be calculated from the concentration of fluorine [F] (in atomic %) introduced (Equation III-2) [106]. Indeed, if we look at the reaction scheme for this derivatisation (Scheme III-4), 2 atoms of carbon bearing an amide group are replaced by 3 atoms of fluorine in the composition of the surface. Therefore the amount of fluorine (in %) seen at the surface after reaction equals 3/2 of the amount of carbon from succinimide groups which have reacted (x[succinimide]$_0$) divided by the surface composition after reaction. The latter is calculated based upon the amount of atoms disappearing after reaction, the surface bears 2 atoms less than the initial surface which equals the number of carbon atoms bearing amide groups (x[succinimide]$_0$) hence the term in the divisor.

In a similar fashion, the proportions of pentafluorophenyl groups which underwent the same reaction can be calculated from the concentration of nitrogen [N] (in atomic %) introduced (Equation III-3). Looking at the reaction scheme for this derivatisation (Scheme III-9), 5 atoms of fluorine from the phenyl group are replaced by 1 atom of nitrogen in the surface composition. Therefore, the amount of nitrogen (in %) seen at the surface after reaction equals 1/5 of the amount of carbon bearing fluorine groups which have reacted (x[pentafluorophenyl]$_0$)divided by the surface composition after reaction. The latter is calculated based upon the amount of atoms disappearing after reaction, the surface bears 6 atoms less than the initial surface which equals 1/5 of the number of carbon atoms bearing fluorine groups (x[pentafluorophenyl]$_0$) hence the term in the divisor:

Equation III-2

$$[F] = \frac{3/2x[succinimide]_0}{[C]_0 + [O]_0 + [N]_0 - x[succinimide]_0} \times 100$$

Equation III-3

$$[N] = \frac{1/5x[pentafluorophenyl]_0}{[C]_0 + [O]_0 + [F]_0 - 6/5x[pentafluorophenyl]_0} \times 100$$

Where $[C]_0$, $[O]_0$, $[N]_0$ and $[F]_0$ are the initial concentrations of each element in the reactive ester plasma polymer, x is the advancement of the reaction (x=0 when no reaction occurred and x=1 when all reactive ester have reacted) and $[succinimide]_0$ and $[pentafluorophenyl]_0$ are the initial percentages of carbon bearing each reactive group in the plasma polymer (O=**C**-N-**C**=O for NAS and **C**-F for PFPA).

For NAS plasma polymer, the amount of succinimide groups which have reacted is 56% after 16h at pH=8.5 for an amine concentration of 30 mM. For PFPA plasma polymer, the amount of pentafluorophenyl groups which have undergone reaction is 33% when the amine concentration equals 100 mM. Despite the smaller amount of amine used with NAS, the yield is higher than with PFPA, therefore NAS seem to react better with poor nucleophiles. These observations seem to be in contradiction with results previously reported where PFPA was found to be more reactive than NAS[107,108]. However, the amount of succinimide having reacted with trifluoroethyl amine may be an overestimation since some succinimide have possibly undergone hydrolysis as well. Based on the percentage of CF_3 groups introduced at the surface (see Table III-6) and a retention of 76% of the succinimide groups during plasma polymerisation, only 32% of the succinimide groups reacted with the amine. Moreover, the amine concentration used with PFPA plasma polymer is much higher than with NAS, and since the amine and PFPA are bulky because of the fluorine groups, there could have been steric hindrance reducing therefore the yield with the fluorinated active ester.

With NAS plasma polymer, reaction of TFEA was also carried out in water, and the yield was calculated to be very low (10%). This is due to the pH of the aqueous media.

The pH of TFEA 30 mM in water was measured to equal 2.9, and at this pH the amine is mainly protonated as NH_3^+, making it impossible to react as a nucleophile. When the pH is increased, the amine becomes free again and is able to react with the active ester. Because, pK_a of TFEA is low (7.8), increasing the pH from 8.5 to 9.3 did not show any rise of the yield since most amine groups are already free at pH=8.5.

NAS plasma polymer was also reacted with a good nucleophilic amine, propylamine (pK_a=10.59). The advancement of the reaction can be calculated as follows:

Equation III-4

$$[O] = \frac{1/2x[succinimide]_0}{[C]_0 + [O]_0 + [N]_0 - 8x[succinimide]_0} \times 100$$

After 1h with n-propylamine 30 mM, the yield was calculated to be 88%. This result confirms that active esters react very quickly with good nucleophiles even at low concentration of the amine.

PFPA plasma polymer was reacted in turn with a nucleophilic primary amine, ethanolamine (pK_a=9.44) and a very good nucleophilic secondary amine, diethylamine (pK_a=10.98). The amount of active esters reacted with the amines can be calculated respectively by as follows:

Equation III-5

$$[N] = \frac{1/5x[penafluorophenyl]_0}{[C]_0 + [O]_0 + [F]_0 - 8/5x[pentafluorophenyl]_0} \times 100$$

Equation III-6

$$[N] = \frac{1/5x[pentafluorophenyl]_0}{[C]_0 + [O]_0 + [F]_0 - 7/5x[pentafluorophenyl]_0} \times 100$$

With these equations, 66 % of fluorinated esters were substituted with ethanolamine, and 120% were substituted by diethylamine. These calculations are valid only if the elemental composition of the surface equals the theoretical one. This is not the case in

these amidation reactions, hence the overestimation calculated. However, one can compare these two results between them as they were calculated the same way, therefore, the results show that PFPA plasma polymer react to a greater extent with better nucleophiles.

III.4.1.3. Reaction of PFPA plasma polymer with amino-acid and peptides

To evaluate the reactivity of PFPA plasma polymer towards biomolecules, the surface was reacted with an amino-acid and two short peptides. The amount of active esters which underwent reaction with β-alanine cannot be calculated via the equations previously established since the surface is not close enough to the theoretical one. However, it is possible to calculate these values for the two peptides with Equation III-7 for Gly-Ala and Equation III-8 for Gly-Gly-His as follows[106]:

Equation III-7
$$[N] = \frac{2/5x[pentafluorophenyl]_0}{[C]_0 + [O]_0 + [F]_0 - 2/5x[pentafluorophenyl]_0} \times 100$$

Equation III-8
$$[N] = \frac{x[pentafluorophenyl]_0}{[C]_0 + [O]_0 + [F]_0 + 6/5x[pentafluorophenyl]_0} \times 100$$

The calculations for a concentration of 100 mM after 48h indicate that 26% of the ester reacted with Gly-Ala and 58% with Gly-Gly-His. Up to 40% reaction was obtained with Gly-Ala by increasing the concentration. The plateau observed on Figure III-13 indicates that for a 24h-reaction, concentration is the limiting factor up to 200 mM, afterwards, the reaction is diffusion-controlled. This is further emphasized with the higher percentages of reacted esters when reaction time is doubled.

The tri-peptide Gly-Gly-His contains several amines (primary and secondary) which could potentially react with the active ester. However, the amines present in the backbone of the peptide or on the imidazole ring are more sterically hindered than the

primary amine at its end. Moreover, on a general basis primary amines are more nucleophilic that secondary amines, therefore the attachment is thought to have occurred at the primary amine end of the tri-peptide. The availability of the attached peptide was demonstrated by complexation with copper ions.

III.5. CONCLUSIONS

Two reactive esters N-acryloxysuccinimide and pentafluorophenyl acrylate have been successfully deposited by pulsed plasma polymerisation with good retention of functionalities. This one-step process allows rapid and efficient generation of reactive surfaces suitable for immobilisation of many biomolecules in a simple fashion under mild conditions.

These reactive surfaces successfully attached primary and secondary amines without the necessity of freeing them from the hydrochloride salt when this applies. The reaction yield was depending on the nucleophilicity of the amines (Table III-28 and Table III-29). Moreover, since the reactive ester is immobilised onto a surface, steric hindrance will play an important role in the reaction yield. Therefore, a less bulky ester like NAS will reach better yields that the bulky fluorinated ester PFPA, even though the latter is more reactive towards amines in solution.

Table III-28 - Reaction yield of amidation reaction onto N-acryloxysuccinimide plasma polymer (50 µm / 10 ms – 5 W)

Amine	Reaction yield (%)
Trifluoroethylamine	56
Propylamine	88

Table III-29 – Reaction yield of amidation reaction onto pentafluorophenyl acrylate plasma polymer (10 µm / 20 ms – 20 W)

Amine	Reaction yield (%)
Trifluoroethylamine	33
Ethanolamine	66
Diethylamine	120
Gly-Ala	26
Gly-Gly-His	58

The reactions were achieved in aqueous media of relatively mild pH (8.5), suitable for biomolecules. Peptides have also been immobilised onto surfaces via this method, with retention of their functions. Preliminary studies have also been carried out with amine-terminated tagged DNA, and fluorescence was observed after attachment. Enzymes and proteins can also be attached onto surfaces using reactive esters which could prove a useful tool to generate biochips on a wide variety of surfaces.

III.6. REFERENCES

1 - Strother, T.; Cai, W.; Zhao, X.; Hamers, R.J.; Smith, L.M. *J. Am. Chem. Soc.* **2000**, 122, 1205-1209

2 - Smith, E.A.; Wanat, M.J.; Cheng, Y.; Barreira, S.V.P.; Frutos, A.G.; Corn, R.M. *Langmuir* **2001**, 17, 2502-2507

3 - Schofield, W.C.E.; McGettrick, J.; Bradley, T.J.; Badyal, J.P.S., Przyborski, S. *J. Am. Chem. Soc.* **2006**, 128, 2280-2285

4 - Iannlello, R.M.; Yacynych, A.M. *Anal. Chem.* **1981**, 53, 2090-2095

5 - Guiomar, A.J.; Guthrie, J.T.; Evans, S.D. *Langmuir* **1999**, 15, 1198-1207

6 - Ganapathy, R.; Manolache, S.; Sarmadi, M.; Simonsick Jr, W.J.; Denes, F. *J. Appl. Polym. Sci.* **2000**, 78, 1783-1796

7 - Camarero, J. A.; Kwon, Y.; Coleman, M. A. *J. Am. Chem. Soc* **2004**, 126, 14730-14731

8 - Peluso, P.; Wilson, D.S.; Do, D.; Tran, H.; Venkatasubbaiah, M.; Quincy, D.; Heidecker, B.; Poindexter, K.; Tolani, N.; Phelan, M; Witte, K.; Jung, L.S.; Wagner, P.; Nock, S. *Anal. Biochem.* **2003**, 312, 113-124

9 - Xiao, S.-J.; Textor, M.; Spencer, N.D. *Langmuir* **1998**, 14, 5507-5516

10 - Min, D.-H.; Mrksich, M. *Curr. Opin. Chem. Biol.* **2004**, 8, 554-558

11 - Heyse, S.; Vogel, H.; Sanger, M.; Sigrist, H. *Protein Sci.* **1995**, 4, 2532-2544

12 - Lee, D.-C.; Chang, B.-J.; Yu, L.; Frey, S.L.; Lee, K.Y.C.; Patchipulusu, S.; Hall, C. *Langmuir* **2004**, 20, 11297-11300

13 - Love, K.R.; Seeberger, P.H. *Angew. Chem. Int. Ed.* **2002**, 41, 3583-3586

14 - Houseman, B.T.; Mrksich, M. *Chem. Biol.* **2002**, 9, 443–454

15 - Roberts, C.; Chen, C.S.; Mrksich, M.; Martichonok, V.; Ingber, D.E.; Whitesides, G.M. *J. Am. Chem. Soc.* **1998**, 120, 6548-6555

16 - Yousaf, M.N.; Houseman, B.T.; Mrksich, M. *Appl. Biol. Sci.* **2001**, 98, 5992-5996

17 - Tully, D.C.; Fréchet, J.M.J. *Chem. Comm.* **2001**, 1229 - 1239

18 - Wells, M.; Crooks, R.M. *J. Am. Chem. Soc.* **1996**, 118, 3988-3989

19 - Korbel, G.A.; Lalic, G.; Shair, M.D. *J. Am. Chem. Soc.* **2001**, 123, 361-362

20 - Duevel, R.V.; Corn, R.M. *Anal. Chem.* **1992**, 64, 337-342

21 - Doron, A.; Katz, E.; Willner, I. *Langmuir* **1995**, 11, 1313-1317

22 - Allcock, H. R.; Nelson, C. J.; Coggio, W. D. *Chem. Mater.* **1994**, 6, 516-524

23 - Tarducci, C.; Kinmond, E.J.; Badyal, J.P.S. *Chem. Mater.* **2000**, 12, 1884-1889

24 - Lee, W.; Furusaki, S.; Saito, K.; Sugo, T. *J. Colloid Interface Sci.* **1998**, 200, 66

25 - Lee, M.-R.; Shin, I. *Angew. Chem. Int. Ed.* **2005**, 44, 2881 –2884

26 - Ollevier, T.; Lavie-Compin, G. *Tetrahedron Lett.* **2002**, 43, 7891–7893

27 - Ritchie, S. M. C.; Bachas, L.G.; Olin, T.; Sikdar, S.K.; Bhattacharyya, D. *Langmuir* **1999**, 15, 6346-6357

28 - Chakraborti, A.K.; Rudrawar, S.; Kondaskar, A. *Eur. J. Org. Chem.* **2004**, 3597-3600

29 - McMurry, J. In *Organic Chemistry, 3rd ed.*; Brooks/Cole Publishing Company: Pacific Grove, CA, 1992; Chapter 24

30 - Arenkov, P.; Kukhtin, A.; Gemmell, A.; Voloshchuk, S.; Chupeeva, V.; Mirzabekov, A. *Anal. Biochem.* **2000**, 278, 123-131

31 - Zammatteo, N.; Jeanmart, L.; Hamels, S.; Courtois, S.; Louette, P. ; Hevesi, L. ; Remacle, J. *Anal. Biochem.* **2000**, 280, 143-150

32 - McLean, K.M.; Johnson, G.; Chatelier, R.C.; Beumer, G.J.; Steele, G.J.; Griesser, H.J. *Colloids Surf., B* **2000,** 18, 221-234

33 - Gribble, G.W. *Chem. Soc. Rev.* **1998**, 6, 395-404

34 - Calderon, J.G.; Timmons, R.B., *Macromol.* **1998**, 31, 3216-3224

35 - Niemz, A; Jeoung, E.; Boal, A.K.; Deans, R.; Rotello, V.M. *Langmuir* **2000**, 16, 1460-1462

36 - Tsubokawaa, N.; Kobayashib, M.; Ogasawara, T., *Prog. Org. Coat.* **1999**, 36, 39-44

37 - Sonntag, N.O.V., *Chem. Rev.*, **1953**, 52, 237-416

38 - Harte, A.J.; Gunnlaugsson, T., *Tetrahedron Lett.*, **2006**, 6321-6324

39 - Khmelnitsky, Y.L.; Mozhaev, V.V.; Belova, A.B.; Sergeeva, M.V.; Martinek, M. *Eur. J. Biochem.* **1991**, 198, 31-41

40 - Evenson, S.A.; Fail, C.A.; Badyal, J.P.S. *Chem. Mater.* **2000**, 12, 3038-3043

41 - Yan, L.; Marzolin, C.; Terfort, A.; Whitesides, G.M. *Langmuir* **1997**, 13, 6704-6712

42 - Lavadière, C. ; Delair, T. ; Domard, A. ; Pichot, C. ; Mandrand, B. *J. Appl. Polym. Sci.* **1999**, 72, 1565–1572

43 - Sathe, S.N; Srinivasa Rao, G.S.; Devi, S. *J. Appl. Polym. Sci.* **1994**, 53, 239-245

44 - Zhou, Y.; Bruening, M.L.; Bergbreiter, D.E.; Crooks, R.M.; Wells, M. *J. Am. Chem. Soc.* **1996**, 118, 3773-3774

45 - Ryan, M.E.; Hynes, A.M.; Badyal, J.P.S. *Chem. Mater.*, **1996**, 8, 37-42

46 - DuBois, D.A. U.S. Patent 5,218,053, 1993

47 - Yurkanis Bruice, P. In *Organic Chemistry, 4th ed.*; Pearson Education Inc.: Upper Saddle River, NJ; 2004

48 - Sheehan, J.C.; Hess, G.P. *J. Am. Chem. Soc.* **1955**, 77, 1067-1068

49 - Merrifield, R.B. *J. Am. Chem. Soc.* **1963**, 85, 2149-2154

50 - Bodanszky, M.; Funk, K.W., *J. Org. Chem.*, **1973**, 38, 1296-1300

51 - Siwruk, G.A.; Eynon, J.S. U.S. Patent 5,516,891, 1996

52 - Sheehan, J.C.; Cruickshank, P.A.; Boshart, G.L. J. Org. Chem. 1961, 26, 2525-2528

53 - Nakajima, N.; Ikada, Y., *Bioconjugate Chem.*, **1995**, 6, 123-130

54 - Woodward, R.B.; Olofson, R.A.; Mayer, H. *J. Am. Chem. Soc.* **1961**, 83, 1007-1009

55 - Woodward, R.B.; Olofson, R.A.; Mayer, H. *J. Am. Chem. Soc.* **1961**, 83, 1010-1012

56 - Sinha, U.; Brewer, J.M. *Anal. Biochem.* **1985**, 151, 327-333

57 - Pétra, P.H. *Biochem.* **1971**, 10, 3163-3170

58 - Izumiya, N. ; Muraoka, M., *J. Am. Chem. Soc.*, **1969**, 91, 2391-2392

59 - Bodansky, M. *Pept. Res.* **1992**, 5, 134-139

60 - Bodanszky, M. *Nature*, **1955**, 175, 685

61 - Bodanszky, M.; Fink, M.L.; Funk, K.W.; Kondo, M.; Lin, C.Y.; Bodanszky, A. *J. Am. Chem. Soc.* **1974**, 96, 2234-2240

62 - Anderson, G.W.; Zimmerman, J.E.; Callahan, F.M. *J. Am. Chem. Soc.* **1963**, 85, 3039

63 - Chinchilla, R.; Dodsworth, D.J.; Nájera, C.; Soriano, J.M., *Tetrahedron Lett.*, 42, **2001**, 4487–4489

64 - Voue, M.; Goormaghtigh, E.; Homble, F.; Marchand-Brynaert, J.; Conti, J.; Devouge, S.; De Coninck, J., *Langmuir*, **2007**, 23, 949-955

65 - König, W.; Geiger, R. *Chem. Ber.* **1970**, 103, 788–798

66 - Castro, B.; Dormoy, J.R.; Evin G.; Selve, C. *Tetrahedron Lett.* **1975**, 14, 1219-1222

67 - Dourtoglou, V.; Ziegler, J.-C.; Gross, B., Tetrahedron Lett., **1978**, 19, 1269-1272

68 - Cameron, L.R.; Holder, J.L.; Meldal, M.; Sheppard, R.C., *J. Chem. Soc., Perkin Trans. 1*, **1988**, 2895 - 2901

69 - Carpino, L.A. *J. Am. Chem. Soc.* **1993**, 115, 4397-4398

70 - Kovacs, J.; Kapoor, A. *J. Am. Chem. Soc.* **1965**, 87, 118-119

71 - Kovacs, J.; Kisfaludy, L.; Ceprini, M.Q. *J. Am. Chem. Soc.* **1967**, 89, 183-184

72 - Kisfaludy, J.; Roberts, E.; Hall Johnson, R.; Mayers, G.L.; Kovacs, J., *J . Org. Chem.*, 35, **1970**, 3563-3565

73 - Corbett, A.D.; Gleason, J.L., *Tetrahedron Lett.*, **2002**, 43 1369–1372

74 - Lin, Y.; Lu, F.; Tu, Y.; Ren, Z. *Nano Lett.* **2004**, 4, 191-195

75 - Jung, D.-H.; Kim, B.H.; Ko, Y.K.; Jung, M.S.; Jung, S.; Lee, A.Y.; Jung, H.-T. *Langmuir* **2004**, 20, 8886-8891

76 - Lahiri, J.; Isaacs, L.; Tien, J.; Whitesides, G.M. *Anal. Chem.* **1999**, 71, 777-790

77 - Yang, W.; Jaramillo, D.; Gooding, J. J.; Hibbert, D. B.; Zhang, R.; Willett, G. D.; Fisher, K. J. *Chem. Comm.* **2001**, 1982-1983

78 - Hyun, J.; Zhu, Y.; Liebmann-Vinson, A.; Beebe, Jr., T.P.; Chilkoti, A. *Langmuir* **2001**, 17, 6358-6367

79 - Frey, B.L.; Corn, R.M. *Anal. Chem.* **1996**, 68, 3187-3193

80 - Willner, I.; Katz, E.; Riklin, A.; Kasher, R. *J. Am. Chem. Soc.* **1992**, 114, 10965-10966

81 - Glidle, A.; Bailey, L.; Hadyoon, C.S.; Hillman, A.R.; Jackson, A.; Ryder, K.S.; Saville, P.M.; Swann, M.J.; Webster, J.R.P.; Wilson, R.W.; Cooper, J.M. *Anal. Chem.* **2001**, 73, 5596 - 5606

82 - Korri-Youssoufi, H.; Garnier, F.; Srivastava, P.; Godillot, P.; Yassar, A. *J. Am. Chem. Soc.* **1997**, 119, 7388 - 7389

83 - Francesch, L.; Garreta, E.; Balcells, M.; Edelman, E.R.; Borrós, S. *Plasma Processes Poly.* **2005**, 605-611

84 - Tabet, F. M.; McGahan, W. A. *Thin Solid Films* **2000**, 370, 122-127

85 - Evans, J.F.; Gibson, J.H.; Moulder, J.F.; Hammond, J.S.; Goretzki, H. *Fresenius' J. Anal. Chem.* **1984**, 319, 841-844

86 - Beamson, G.; Briggs, D. In *High-Resolution XPS of Organic Polymers: The Scienta ESCA300 Database*; John Wiley & Sons: New York, 1992

87 - Xiao, S.-J.; Brunner, S.; Wieland, M. *J. Phys. Chem. B* **2004**, 108, 16508-16517

88 - Lin-Vien, D.; Colthyp, N.B.; Fateley, W.G.; Grasselli, J.G. In *The Handbook of Infrared and Raman Characteristic Frequencies of Organic Molecules*; Academic Press: New York, 1991

89 - Wen, C.-H.; Chuang, M.-J.; Hsiue, G.-H., *Thin Solid Films*, **2006**, 503, 103-109

90 - Clark, D.T.; Dilks, A. *J. Polym. Sci. A* **1977**, 15, 15

91 - Wong, L.F.; Cooper, J.C.; Margerum, D.W. *J. Am. Chem. Soc.* **1976**, 98, 7268-7274

92 - Chow, E.; Wong, E.L.S.; Böcking, T.; Nguyen, Q.T.; Hibbert, D.B.; Gooding, J.J. *Sens. Actuators, B* **2005**, 111–112, 540–548

93 - Savage, C.R.; Timmons, R. B.; Lin, J.W., *Chem. Mater.* **1991**, 3, 575-577

94 - Fraser, S.; Short, R.D.; Barton, D.; Bradley, J.W. *J. Phys. Chem. B* **2002**, 106, 5596 -5603

95 - Tarducci, C.; Schofield, W.C.E.; Brewer, S.A.; Willis, C.; Badyal, J.P.S. *Chem. Mater.* **2001**, 13, 1800-1803

96 - Rinsch, C.L.; Chen, X.L.; Panchalingam, V.; Eberhart, R.C.; Wang, J.H.; Timmons, R.B. *Langmuir* **1996**, 12, 2995-3002

97 - Calderon, J.G.; Harsch, A.; Gross, G.W.; Timmons, R.B. *J. Biomed. Mater. Res.* **1998**, 42, 597-603

98 - Tarducci, C.; Badyal, J.P.S.; Brewer, S.A.; Willis, C. *Chem. Comm.* **2005**, 3, 406-408

99 - Hynes, A.M.; Shenton, M.J.; Badyal, J.P.S. *Macromolecules* **1996**, 29, 4220 - 4225

100 - Coulson, S.R.; Woodward, I.S.; Badyal, J.P.S.; Brewer, S.A.; Willis, C. *Chem. Mater.* **2000**, 12 2031-2038

101 - Teare, D. O. H.; Barwick, D.C.; Schofield, W.C.E.; Garrod, R.P.; Ward, L.J.; Badyal, J.P.S. *Langmuir* **2005**, 21, 11425-11430

102 - Wang, J.-H.; Chen, X.; Chen, J.-J.; Calderon,2 J.G.; Timmons, R.B. *Plasmas Polym.* **1997**, 2, 245-260

103 - Bradley, T.J.; Schofield, W.C.E.; Garrod, R.P.; Badyal, J.P.S. *Langmuir* **2006**, 22, 7552-7555

104 - Evans, J.F.; Prohaska, G.W., *Thin Solid Films*, **1984**, 118, 171-180

105 - Han, L.M.; Timmons, R.B. *J. Polym. Sci. A* **1998**, 36, 3121–3129

106 - Sutherland, I.; Sheng, E.-S.; Brewis, D.M.; Heath, R.J. *J. Mater. Chem.* **1994**, 4, 683-687

107 - Kovacs, J.; Mayers, G.L.; Johnson, R.H.; Cover, R.E.; Ghatak, U.R. *J. Org. Chem.* **1970**, 35, 1810-1815

108 - Adamczyk, M.; Fishpaugh, J. R.; Mattingly, P. G. *Tetrahedron Lett.* **1995**, 36, 8345-8346

IV

CHAPTER FOUR

Enzymatic hydrolysis

IV.1. INTRODUCTION

Surface modification has been shown to be very important in the manufacture of novel materials combining traditional bulk properties with tailored surface properties (see Chapter I: Introduction). Amongst the different methods available, enzymes demonstrated their ability as a powerful tool in the selective surface modification.

Enzymes can catalyse a wide variety of organic reactions such as hydrolysis and synthesis of esters[1], peptides[2], nucleotides[3,4], oligosaccharides[5], lactones[6] and lactams[7], oxidation-reductions of alkenes[8], alcohols[9], sulfides[10] and sulfoxides[11], addition-elimination of water[12], ammonia[13], halogenation-dehalogenation[14], polymerisation[15,16], acyloin[17] and aldol[18] condensation and Diels-Alder[19] reactions.

The class of enzymes known as esterases[20] or hydrolase enzymes, catalyses the hydrolysis of esters with water to form two products, a carboxylic acid and an alcohol. These enzymes are important as they are involved in a wide range of reactions within the human body: breaking down of fats and lipids into fatty acid and glycerol[20,21]; inactivation of the neurotransmitter acetylcholine[22]; removal of phosphate groups from molecules such as peptides and nucleotides[23,24]; and cleavage of RNA[25].

This class is further divided into several groups depending on their substrate specificity, their protein structure, and their biological function (see Table IV-1)[26].

Table IV-1 – Classification of esterases according to EC (European commission) numbers

EC number	Enzyme name
EC 3.1.1	Carboxylic ester hydrolases
EC 3.1.2	Thiolester hydrolases
EC 3.1.3	Phosphoric monoester hydrolases
EC 3.1.4	Phosphoric diester hydrolases
EC 3.1.5	Triphosphoric monoester hydrolases
EC 3.1.6	Sulfuric ester hydrolases
EC 3.1.7	Diphosphoric monoester hydrolases
EC 3.1.8	Phosphoric triester hydrolases
EC 3.1.11	Exodeoxyribonucleases producing 5'-phosphomonoesters
EC 3.1.13	Exoribonucleases producing 5'-phosphomonoesters
EC 3.1.14	Exoribonucleases producing 3'-phosphomonoesters
EC 3.1.15	Exonucleases active with either ribo- or deoxyribonucleic acid
EC 3.1.16	Exonucleases active with either ribo- or deoxyribonucleic acid
EC 3.1.21	Endodeoxyribonucleases producing 5'-phosphomonoesters
EC 3.1.22	Endodeoxyribonucleases producing other than 5'-phosphomonoesters
EC 3.1.23	(not defined)
EC 3.1.24	(not defined)
EC 3.1.25	Site-specific endodeoxyribonucleases specific for altered bases
EC 3.1.26	Endoribonucleases producing 5'-phosphomonoesters
EC 3.1.27	Endoribonucleases producing other than 5'-phosphomonoesters
EC 3.1.30	Endoribonucleases active with either ribo- or deoxyribonucleic
EC 3.1.31	Endoribonucleases active with either ribo- or deoxyribonucleic

The carboxylic ester hydrolase group is itself divided into 80 sub-groups[27] depending on their substrates, particularly on the alcohol formed after hydrolysis. The first sub-group of enzymes, referred to as carboxylesterases, are not substrate specific and therefore can hydrolyse a wide range of substrates according to the following reaction:

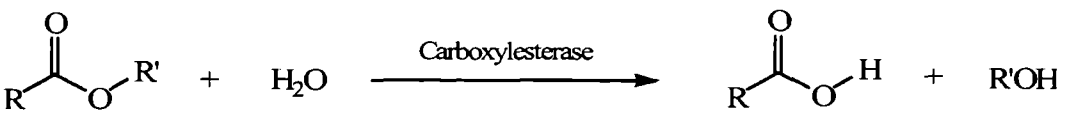

Scheme IV-1 – Reaction catalysed by carboxylesterase enzymes

This reaction constitutes the basis of this investigation. A model substrate is formed through the covalent attachment of a test molecule to a plasma polymer. The test molecule studied must possess a carboxylic acid ester group to be enzymatically hydrolysed, a functional group to allow covalent attachment onto the plasma polymer and preferably be commercially available. The amino-acid ester β-alanine ethyl ester hydrochloride combines all the conditions mentioned above. It can be covalently attached via its amine group onto pentafluorophenyl ester plasma polymer surfaces synthesised previously (see Chapter III), leaving an available carboxylic acid ester group.

Pig / Porcine Liver Esterase (PLE), a serine hydrolase enzyme, has been selected for this study due to several advantages: stability, commercially availability, low cost and the ability to hydrolyse a wide range of substrates with high stereoselectivity without the need of a co-enzyme[28]. Hydrolysis of simple esters with short alcohol chain using PLE in aqueous solution has been studied previously[29], making β-alanine ethyl ester a potential substrate for PLE.

Serine hydrolase has been shown to react via three amino-acids, aspartic acid (Asp), histidine (His) and serine (Ser) referred to as the 'catalytic triad'[30]. Asp and His assist Ser by increasing its nucleophilicity. Ser then attacks the carbonyl group of the ester creating an acyl-enzyme intermediate (AEI) and liberating the alcohol. Next, water acts as a nucleophile on the AEI and the acid is freed from the triad (see Scheme IV-2).

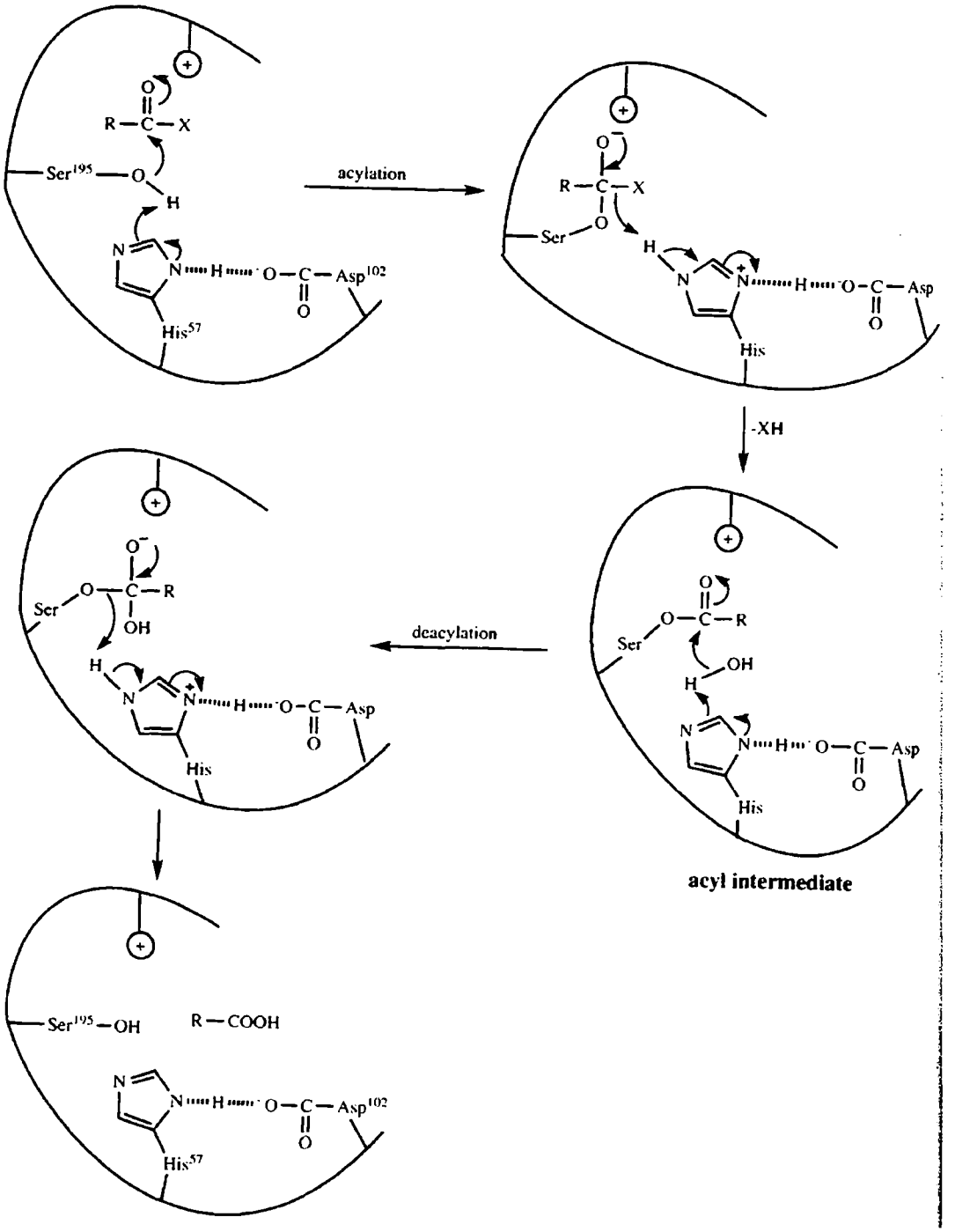

Scheme IV-2 – Mechanism of serine hydrolases[31]

To this date, PLE has not been used to modify surface-bound molecules. The challenge of this work is to demonstrate the ability of the substrate to enter the 'pocket' of the enzyme in which the 'catalytic triad' lies, ready to catalyse the hydrolysis.

IV.2. EXPERIMENTAL

IV.2.1. Enzymatic hydrolysis of β-alanine ethyl ester hydrochloride

Pentafluorophenyl acrylate plasma polymer surfaces were generated as described in Chapter III.

Enzymatic hydrolysis of β-alanine ethyl ester in solution was carried out in phosphate buffer (PB, 0.2 M (sodium phosphate monobasic (99%, Aldrich)) pH=8). β-alanine ethyl ester hydrochloride (98%, Aldrich, 0.03 M) was introduced in PB along with approximately 150 units of esterase from porcine liver (PLE)[32] (~150 units/mg, 10 mg/ml suspension, Sigma). The reaction was left to run at room temperature for increasing time intervals under continuous stirring, and HPLC analysis was done immediately after a sample was taken. A control sample was run by reacting the ester in the same conditions without the enzyme.

Reverse-phase HPLC was carried out on a Perkin-Elmer Series 200 ic pump equipped with a Supelco C8 column (250 x 4.6 mm, diameter 5 μm). The column oven was a Shimadzu CTO-SA. The absorbance was measured on a Waters 486 tunable absorbance detector. The data was then treated with National Instrument LabView 6i software. The wavelength was set at 220 nm with an AUFS (Absorbance at Full Scale Unit) varying between 0.5 and 2 for better visualisation of the peaks. The temperature was maintained at 31°C ± 1°C. The solvents used for elution were water (HPLC grade, Fisher Scientific), acetonitrile (MeCN) (HPLC grade, Fischer Scientific), both were pre-mixed with 0.10 % trifluoroacetic acid (TFAA) (spectrophotometric grade, 99+%, Aldrich) to maintain the acidity of the column and act as ion-pairing agent[33]. The flow rate was set at 1 mL/min. The solvents gradient used for experiments was:

- 6 + 5 min at 100 % of H_2O / TFA

- 4 min gradually reaching 80 % of H2O / TFA and 20 % of MeCN / TFA

- 2 min gradually reaching 100 % of MeCN / TFA

- 2 min at 100 % of MeCN / TFA

- 8 min gradually reaching 100 % of MeCN / TFA

- 2 min at 100 % of H_2O / TFA

A blank run was carried out to clean the column after each sample and to establish the baseline. Then 200 µL of the reaction mixture was introduced via a manual loop into the column and the absorbance spectra of the eluted products recorded.

Absorbance measurements of ethanol (98%, Aldrich), β-alanine (99%, Aldrich), β-alanine ethyl ester hydrochloride (98%, Aldrich), esterase from porcine liver (~150 units/mg, 10 mg/ml suspension, Sigma) and phosphate buffer (0.02M, pH=8) were taken on a Varian Carry 4000 UV-VIS-NIR spectrometer at a wavelength of 220 µm.

Attachment of β-alanine ethyl ester onto PFPA plasma polymer was carried out in phosphate buffer (0.05 M, pH=8.5) at concentrations ranging from 50 to 800 mM and for reaction times of 16 and 48h. Samples were then rinsed for 1h in deionised water and left to air-dry at room temperature.

Enzymatic hydrolysis of ester attached onto plasma polymer surfaces, were carried out using the same procedure as for enzymatic hydrolysis in solution, substituting β-alanine ethyl ester hydrochloride by the silicon wafer bearing PFPA plasma polymer + β-alanine ethyl ester. Samples were then rinsed for 3 h in sodium dodecyl sulphate (SDS)[34] (10% solution, Sigma) diluted to 1% in PB (0.2 M, pH=8) then for 1 h in PB (0.2 M, pH=8) and finally for 1 h in deionised water. Samples were left to dry in air. Control samples of ester-derivatised surfaces were reacted using the same procedure in the absence of enzyme.

Surface plasmon resonance (SPR) enzyme adsorption studies entailed plasma deposition of 18-20 nm thick poly(pentafluorophenyl acrylate) films onto a gold sensor chip (Biacore). The amino-acid ester was subsequently attached according to method described above. Enzyme absorption was monitored using a biosensor SPR system (Biacore 1000 upgrade). Enzymatic ester hydrolysis was followed by SPR in the same way as described in previous paragraph. The flow rate for all SPR experiments was set at 5 $\mu L.min^{-1}$. In all cases, the buffer (PB 0.1 M – pH=8.5) was degassed and filtered using a 200 nm cellulose nitrate filter (Whatman) prior to use. Response values were taken after samples were flushed with the buffer for 10 min.

IV.2.2. Analysis

A spectrophotometer (nkd-6000, Aquila Instruments Ltd.) was used for plasma polymer film thickness measurements. The obtained transmittance-reflectance curves (350-1000 nm wavelength range) were fitted to a Cauchy material model using a modified Levenberg-Marquardt algorithm[35].

Contact angle analysis on the pulsed plasma deposited poly-NAS and poly-PFPA films was carried out using a video capture system (ASE Products, model VCA2500XE). 2.0 µL sessile droplets of deionised water were placed onto the polymer surface and contact angle measurements taken at ambient temperature.

Chemical characterization by X-ray photoelectron spectroscopy (XPS) was undertaken using a VG Microtech electron spectrometer equipped with a non-monochromated Mg Kα X-ray source (1253.6 eV) and a concentric hemispherical analyzer (VG 100 AX) operating in the constant analyzer energy mode (CAE, pass energy = 20 eV for elemental analysis and 50 eV for wide scans). The XPS spectra for the carbon envelopes were fitted using the convention established for insulating

polymers, i.e. C-C bond exhibits a photopeak at a binding energy of 285.0 eV. All the Gaussian components peaks[36] were determined using a linear background and equal full-width at-half-maximum (FWHM) on a Marquardt minimization computer software. Each Gaussian component relates to different carbon bonding, the peaks are centred on the binding energy of the bond of interest as determined by Beamson and Briggs[37]. Instrument sensitivity multiplication factors were taken as C(1s): O(1s): N(1s): Si(2p): F(1s) 1.00: 0.37: 0.56: 096: 0.24.

Surface Fourier transform infrared spectroscopy (FTIR) was performed on gold substrates using an FTIR spectrometer (Perkin-Elmer, model Spectrum One) equipped with a liquid nitrogen cooled MCT detector operating at 4 cm^{-1} resolution over the 700-4000 cm^{-1} range. The instrument was fitted with a reflection-absorption spectroscopy accessory (Specac) and a KRS-5 p-polarizer with the reflection angle set to 84°. All spectra were averaged over 512 scans.

IV.3. RESULTS

IV.3.1. Enzymatic hydrolysis of β-alanine ethyl ester hydrochloride in solution

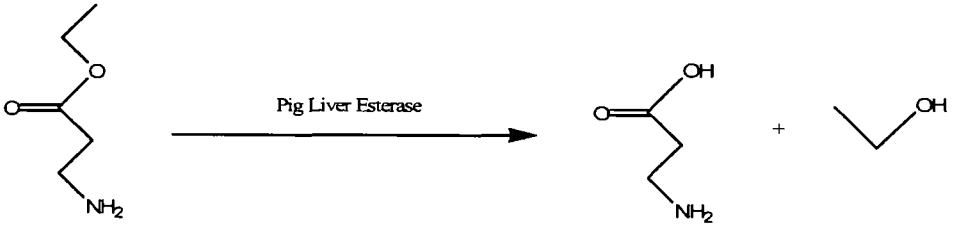

Scheme IV-3 – Enzymatic hydrolysis of β-alanine ethyl ester with Pig Liver Esterase

Chemicals detectable via HPLC analysis at the specified detection wavelength (220 nm) have been determined (Table IV-2). PLE, β-alanine and β-alanine ethyl ester absorb sufficiently at this wavelength.

Table IV-2 – Absorbance of various chemicals at a wavelength of 220 nm

Samples	Absorbance
PB	0.1899
Ethanol	0.0972
PLE	1.4955
β-alanine	1.2210
β-alanine ethyl ester hydrochloride	1.8243

The HPLC chromatograms (Figure IV-1) positively confirmed the presence of β-alanine ethyl ester at t=0 and at t=22h of reaction without enzyme. However, after 22h of reaction with the enzyme the ester had virtually disappeared, indicating the necessity of the enzyme presence for cleavage reaction to occur.

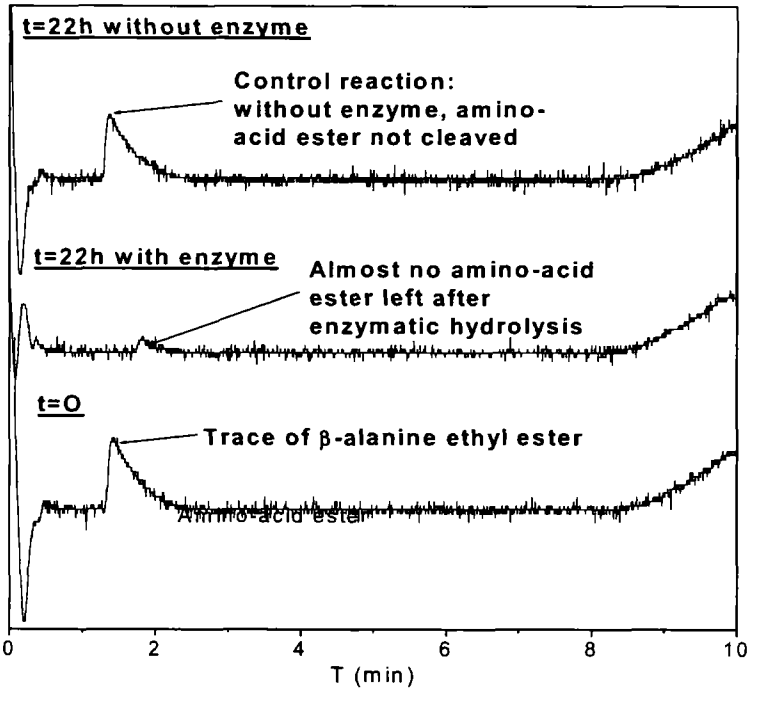

Figure IV-1 – HPLC chromatograms of the enzymatic hydrolysis of β-alanine ethyl ester by Pig Liver Esterase

IV.3.2. Attachment of β-alanine ethyl ester onto a plasma polymer surface

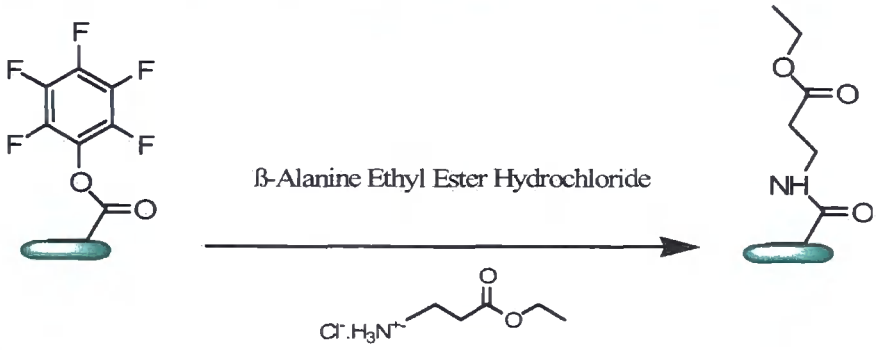

Scheme IV-4 – Attachment of β-alanine ethyl ester onto pentafluorophenyl acrylate plasma polymer

Attachment of β-alanine ethyl ester was followed by XPS analysis. The introduction of nitrogen at the surface, along with an increase in the amounts of carbon and oxygen and a decrease in the amount of fluorine, are consistent with the theoretical surface elemental composition for PFPA plasma polymer after reaction with β-alanine ethyl ester.

Table IV-3 – XPS analysis of β-alanine ethyl ester after attachment onto pentafluorophenyl acrylate plasma polymer

Surfaces	Composition (at. %)			
	C	O	N	F
PFPA plasma polymer Theoretical	56.2	12.5		31.3
PFPA plasma polymer experimental	49.7 ± 2.8	11.9 ± 2.3		38.4 ± 3.2
PFPA + β-AEE theoretical	66.7	25	8.3	
PFPA + β-AEE 800 mM – 16h	60.4 ± 3.1	19.7 ± 1.1	4.4 ± 0.4	15.5 ± 4.1

The carbon envelope C(1s) of the surface after reaction shows the same five peaks related to PFPA plasma polymer (Figure IV-2): hydrocarbon **C**-C/**C**-H_x (285 eV), carbon in α-position of a carbonyl group **C**-C=O (285.6 eV), carbon single-bonded to an

oxygen from an ester function C-O-C=O (286.2 eV), carbon bonded to one fluorine atom C-F (288.3 eV) and carbon from a carbonyl group C=O (289.4 eV). Moreover, the carbon envelope presents two new environments characteristic of an amide: carbon single-bonded to nitrogen C-N (286.8 eV) and carbon double-bonded to oxygen and single bonded to nitrogen N-C=O (287.6 eV).

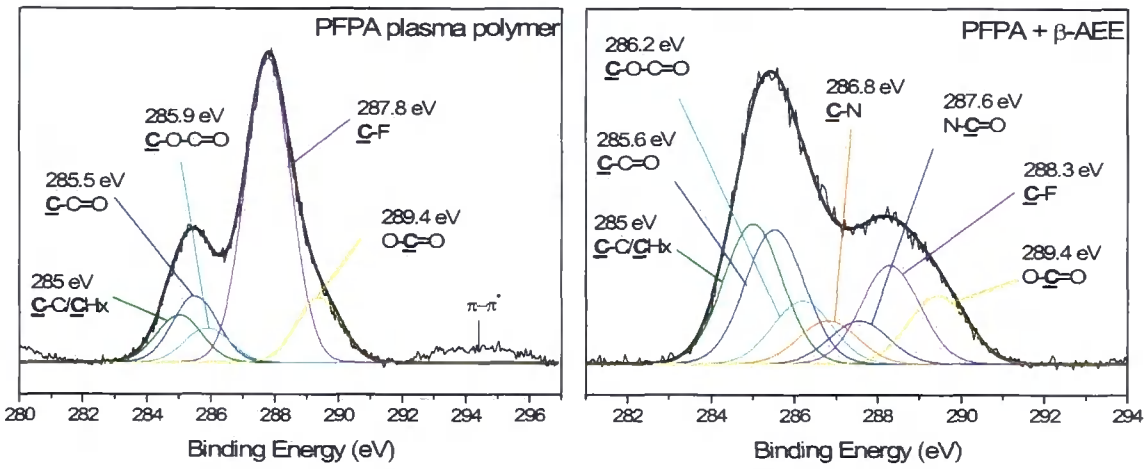

Figure IV-2 – C(1s) XPS spectra of pentafluorophenyl acrylate before and after amino-acid ester attachment

Table IV-4 gives the percentages of each carbon envelope to compare with the theoretical values of PFPA plasma polymer reacted with the amino-acid ester.

Table IV-4 – Carbon envelope C (1s) composition of surface before and after reaction between PFPA plasma polymer and β-alanine ethyl ester

Surfaces	Composition (%)						
	C-C/CH$_x$	C-C=O	C-O	N-C	O=C-N	C-F	C=O
PFPA theoretical	11.1	11.1	11.1			55.6	11.1
PFPA experimental	11.5	11.7	8.2			55.8	12.69
PFPA + β-AEE theoretical	25	25	12.5	12.5	12.5		12.5
PFPA + β-AEE 800 mM – 16h	23.7	22.8	10.6	7.3	7.3	16.7	11.6

The IR spectra of PFPA plasma polymer before and after reaction with the amino-acid ester are presented in Figure IV-3, along with the spectra of β-alanine ethyl ester hydrochloride. The amino-acid ester presents the following main peaks[38]: C=O stretching (1721 cm^{-1}), NH_3^+ bending and scissoring (1572-1609-1653 cm^{-1}), O-CH_2 deformation (1497 cm^{-1}), CH_3 asymmetric deformation (1460 cm^{-1}), O-CH_2 wag (1410 cm^{-1}), symmetric CH_3 deformation (1366 cm^{-1}), C-O stretching (1204 cm^{-1}), C-N stretch from amine (1146 cm^{-1}), CH_3 rock from ethyl ester, O-CH_2-CH_3 asymmetric stretching (1016 cm^{-1}), and NH_3^+ wagging (966 cm^{-1}). The surface of PFPA plasma polymer after amidation with the amino-acid ester presents three peaks related to PFPA plasma polymer: C=O stretch (1786 cm^{-1}), aromatic ring vibration (1525 cm^{-1}) and aromatic ring stretch (1002 cm^{-1}). These peaks are however less intense than prior to reaction indicating that there was a significant reduction in PFPA chemistry available at the surface. Furthermore, the surface presents five peaks related to the amino-acid ester: C=O from ester (1732 cm^{-1}), O-CH_2 deformation (1502 cm^{-1}), CH_3 deformation (1312 cm^{-1}), C-O stretch (1200 cm^{-1}) and O-CH_2-CH_3 symmetric stretching (1020 cm^{-1}). Additionally, two new peaks are observable: C=O stretch from amide (1656 cm^{-1}) and C-N stretch from amide (1377 cm^{-1}). Both peaks are indicative of the formation of an amide bond.

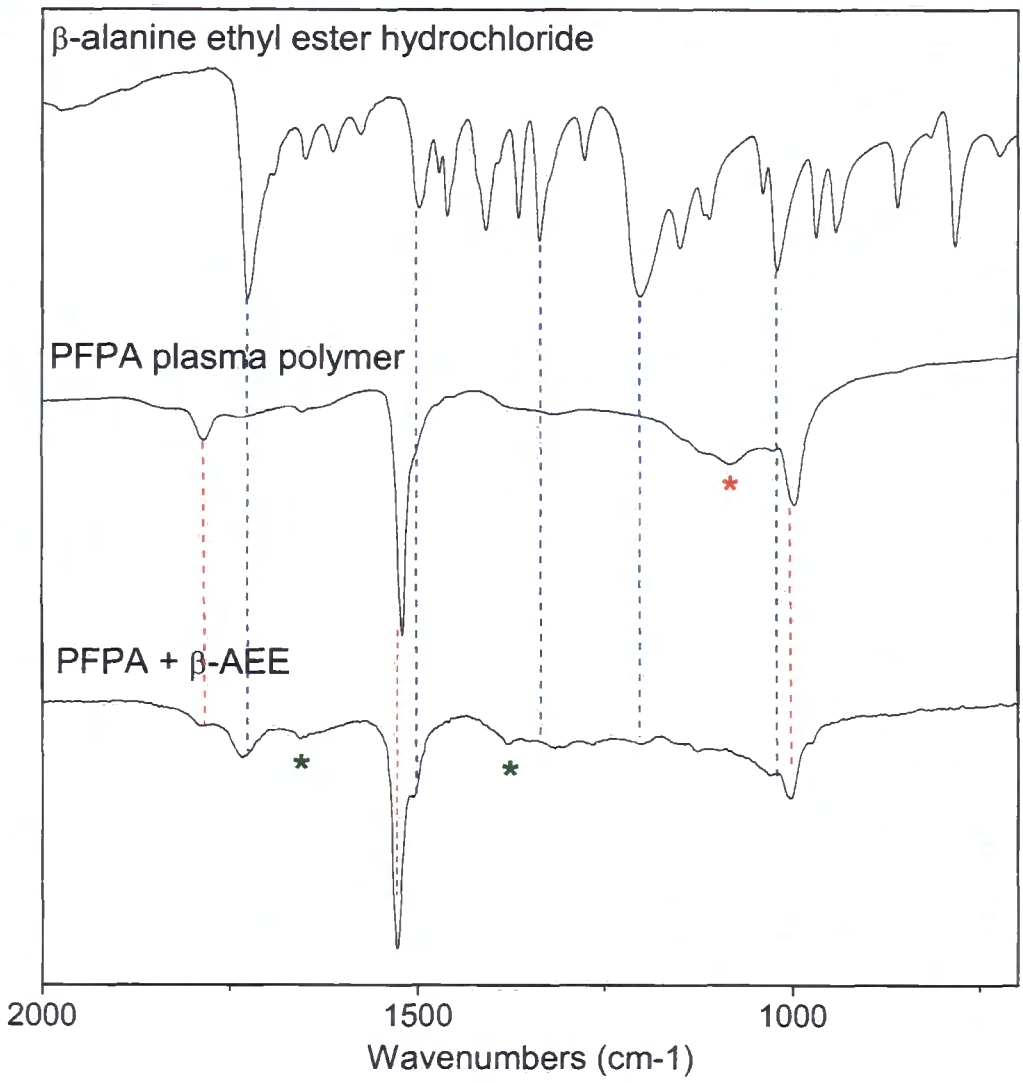

Figure IV-3 – Infra-red spectra of β-alanine ethyl ester attached onto pentafluorophenyl acrylate

A decrease in the contact angle of water onto the surface before and after attachment of β-alanine ethyl ester shows that after reaction the surface is slightly more hydrophilic. This is in agreement with the fact that a very hydrophobic perfluorinated aromatic ring has been replaced by an alkyl chain.

Table IV-5 – Contact angle of pentafluorophenyl acrylate plasma polymer before and after attachment of β-alanine ethyl ester

Surface	Contact angle
PFPA plasma polymer	94-97°
PFPA + β-AEE	80-84°

IV.3.3. Optimization of the attachment reaction of β-alanine ethyl ester onto pentafluorophenyl acrylate plasma polymer surface

The concentration of the amino-acid ester in the reaction solution is an important factor in determining the reaction yield with PFPA plasma polymer. After initial increase in reaction yield, a plateau for concentrations above 400 mM is observed (Figure IV-4). Reaction yields were calculated by using the elemental analysis of the surface after attachment of β-alanine ethyl ester hydrochloride as measured by XPS and Equation IV-1 (see Discussion paragraph).

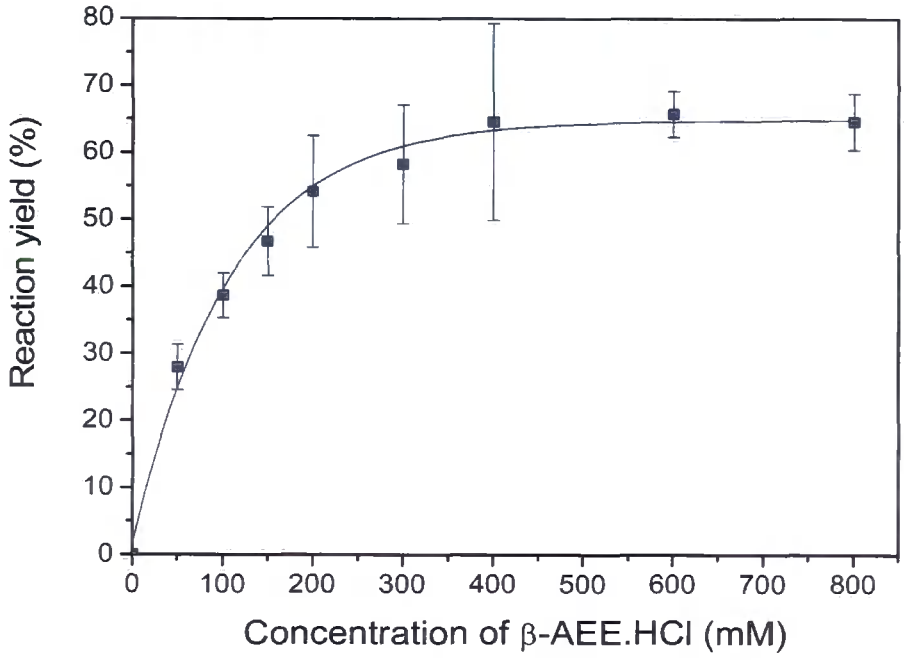

Figure IV-4 – Influence of the concentration of β-alanine ethyl ester hydrochloride on the yield of the attachment reaction after 16h based on XPS analysis

When the surface is left to react with the amino acid solution for longer, the same plateau value is reached at lower amino-acid concentration. Indeed, after 48h, the reaction yield equals the plateau value of 65% with a concentration of only 150 mM, whilst after 16h this value is reached with concentrations over 400 mM (Figure IV-5 a).

pH was also found to have an influence. After 16h, the plateau value is reached with amino-acid concentrations over 200 mM at pH=9.5, whilst for a lower pH of 8.5, the same yield required concentrations over 400 mM (Figure IV-5 b).

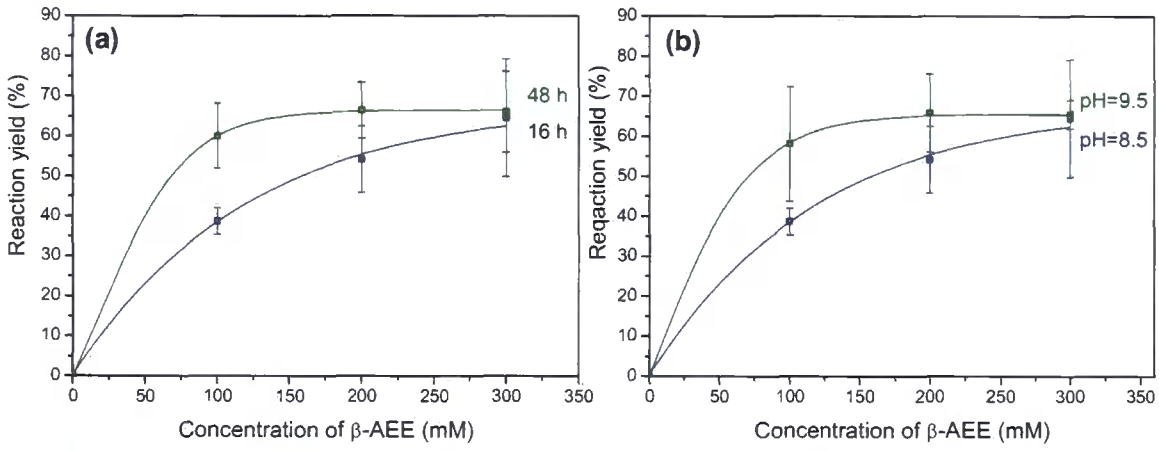

Figure IV-5 – Influence of reaction time and pH over the yield of the attachment reaction of β-alanine ethyl ester hydrochloride onto pentafluorophenyl acrylate based on XPS analysis

IV.3.4. Enzymatic hydrolysis of β-alanine ethyl ester attached onto pentafluorophenyl acrylate plasma polymer

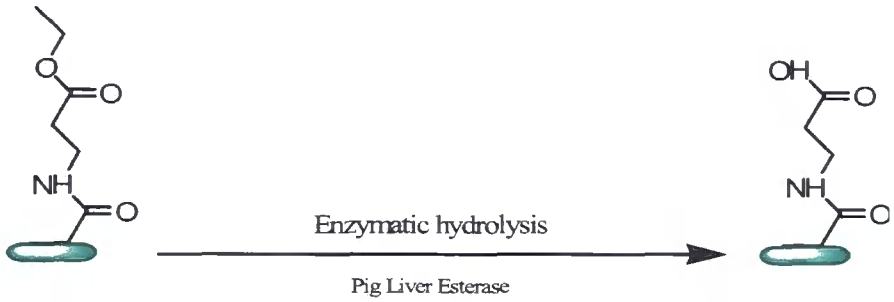

Scheme IV-5 – Enzymatic hydrolysis of the ester bond of β-alanine ethyl ester attached onto pentafluorophenyl acrylate plasma polymer with enzyme Pig Liver Esterase

Enzymatic hydrolysis of β-alanine ethyl ester attached onto pentafluorophenyl acrylate plasma polymer was followed by XPS analysis (Table IV-6). The theoretical amount of nitrogen at the surface of the amino-acid ester prior to reaction is lower than that of the corresponding amino-acid β-alanine (β –A). Indeed, after enzymatic hydrolysis of the

ester group by the esterase, the amount of nitrogen at the surface increased as expected. In a control sample, the same amino-acid ester surface was reacted in buffer without enzyme: the amount of nitrogen did not increase. The surface remained the same with a slight increase in oxygen and a decrease in fluorine which indicates partial hydrolysis of the remaining fluorinated esters.

Table IV-6 – XPS analysis of β-alanine ethyl ester attached onto pentafluorophenyl acrylate plasma polymer before and after enzymatic hydrolysis

Surfaces	Composition (at. %)			
	C	O	N	F
PFPA plasma polymer theoretical	56.2	12.5		31.3
PFPA plasma polymer experimental	49.7 ± 2.8	11.9 ± 2.3		38.4 ± 3.2
PFPA + β-AEE theoretical	66.7	25.0	8.3	
PFPA + β-AEE 400 mM – 16h	60.2 ± 2.9	18.9 ± 2.1	3.6 ± 0.1	17.3 ± 5.0
PFPA + β-Alanine theoretical	60	30	10	
PFPA + β-AEE after hydrolysis	61.8 ± 1.2	22.2 ± 0.2	6.6 ± 1.1	9.3 ± 1.4
PFPA + β-AEE in buffer (no PLE)	60.1 ± 0.9	22.4 ± 2.1	3.3 ± 1.6	14.2 ± 3.1

Residual enzyme adsorbed onto the surfaces was investigated by SPR measurements. The following table gives the SPR response after each step involved in enzymatic hydrolysis.

Table IV-7 – SPR response during enzymatic hydrolysis of β-alanine ethyl ester attached onto pentafluorophenyl acrylate plasma polymer

Step	Variation in response / initial surface (RU)*
PFPA + β-AEE	0
PFPA + β-AEE + PLE - 24h	5542 ± 125
PFPA + β-AEE after hydrolysis & rinsing	(-) 958 ± 269
PFPA + β-AEE without PLE – 24h	(-) 327 ± 161
PFPA + β-AEE without PLE & rinsing	(-) 862 ± 406

* Value for gold chip + PFPA plasma polymer + β-AEE subtracted

During enzymatic hydrolysis, the SPR response increases by 5542 RU due to enzyme adsorption at the surface of PFPA plasma polymer + β-AEE. After rinsing with SDS and water to desorb the enzyme, the response drops below the starting value by 958 RU. When the same experiment is done without the enzyme, the response decreases by 327 RU and after rinsing decreases by 862 RU as compared with the initial value.

IV.4. DISCUSSION

IV.4.1. Enzymatic hydrolysis of β-alanine ethyl ester hydrochloride in solution

The absorbance measurements showed that only the enzyme, the amino-acid ester and the corresponding amino-acid absorbed at the detection wavelength used for HPLC (220 nm). Therefore only these substances are expected to show on the spectra. However, only one trace is observed, that of the amino-acid ester. The hydrophilicity of the corresponding amino-acid is higher than that of the amino-acid ester. Since the elution solvent used at the beginning is polar (water) and the column hydrophobic, the more hydrophilic substrate is expected to elute faster. Hence, β-alanine elutes at the very beginning, along with all the salts from the buffer, showing no distinguishable

trace with the solvent gradient used. The enzyme PLE is more hydrophobic than the amino-acid ester and has therefore a higher retention time. It seems that the retention time is higher than 10 min with the conditions used in this experiment, and therefore does not show any trace on the absorbance spectra for the conditions used.

After 22h the hydrolysis reaction appears to be almost complete, β-alanine ethyl ester has proven to be a good substrate for the enzyme pig liver esterase.

IV.4.2. Attachment of β-alanine ethyl ester onto a plasma polymer surface

For the amidation reaction between the reactive ester surface PFPA plasma polymer and β-alanine ethyl ester, the reaction yield can be calculated as follow[39]:

Equation IV-1

$$[N] = \frac{1/5x[pentafluorophenyl]_0}{[C]_0 + [O]_0 + [F]_0 - 4/5x[pentafluorophenyl]_0} \times 100$$

Where $[C]_0$, $[O]_0$, $[N]_0$ and $[F]_0$ are the initial atomic percentages of each element in the reactive ester plasma polymer, x is the advancement of the reaction (x=0 when no reaction occurred and x=1 when all reactive ester have reacted) and $[pentafluorophenyl]_0$ is the initial percentages of carbon bearing the reactive group in the plasma polymer (**C**-F).

Both XPS and IR confirmed attachment with the creation of a new amide bond. The weak bands observed on the IR spectra highlight the fact that the layer of amino-acid ester is very thin, indeed XPS analysis showed that the surface contained not only β-alanine ethyl ester but also some remaining active ester groups.

The attachment yield was found to be dependent upon the initial amino-acid ester concentration. When pH of the buffer in which the reaction is carried out is increased, the plateau value is reached for lower amino-acid ester concentration. This is due to the

fact that at higher pH, more amine groups are present as NH_2 instead of NH_3^+, thus increasing the concentration of nucleophiles in the reaction mixture and displacing the equilibrium of the reaction towards the products. When time is increased, the plateau value is also reached for lower amino-acid concentration (130 mM). This indicates that the reaction is limited by diffusion of the reactant at the surface. When bulky pentafluorophenyl acrylate groups are replaced by less bulky amino-acid ester groups, the surface becomes less hindered, facilitating the arrival of more amino-acid ester groups.

IV.4.3. Enzymatic hydrolysis of β-alanine ethyl ester attached onto pentafluorophenyl acrylate plasma polymer

The increase in nitrogen amount at the surface is indicative of cleavage of the amino-acid ester by the enzyme PLE to leave behind carboxylic acid groups. This was also reinforced by the fact that the surface was unchanged after exposure to solutions without enzyme. However, the change in elemental composition at the surface was not accompanied by an expected increase in oxygen amount. These observations suggest that the enzyme was adsorbed onto the surface or immobilised at the active ester surface via its free amine groups. The decrease in the amount of fluorine seems to corroborate the second hypothesis. However, it could also indicate that active ester has been hydrolysed by the buffer. Moreover, the bulky enzyme may have needed more time to immobilise efficiently. The rinsing process has been evaluated with the enzyme PLE on PET films to establish the time the surface needs to be rinsed with SDS to remove all adsorbed enzyme (results not presented). After 3h, no nitrogen was detectable after XPS analysis of PET, indicating that all enzymes had been removed. However, the surface being different from PET, some enzyme could be irreversibly adsorbed onto it[40].

To see whether the nitrogen increase at the surface of the substrate is due to hydrolysis or to some enzyme either adsorbed or immobilised, the reaction was followed by SPR. When the enzyme solution is passed onto the amino-acid ester immobilised onto PFPA surfaces, the SPR response increases by a large amount, confirming presence of adsorbed enzyme. When the solution containing no enzyme is run, a slight decrease in the response is seen. After the rinsing procedures, the response of the surface after exposure to the enzyme solution and that of the one that has not been in contact with the enzyme are the same, indicating that no enzyme remains adsorbed onto the surface. Therefore, the increase in the amount of nitrogen at the surface after enzymatic hydrolysis, as observed by XPS, can be accounted for by enzymatic hydrolysis only and not by the presence of irreversibly adsorbed enzyme.

IV.5. CONCLUSIONS

An amino-acid ester (β-alanine ethyl ester hydrochloride) has been successfully covalently attached onto a plasma polymerized active ester (pentafluorophenyl ester). The bond created between the reactive ester and the terminal amine did not require freeing the amino-acid ester from its hydrochloride salt, and reached reaction yields up to 65%. Subsequently, the ester bond of the molecule was selectively cleaved with an enzyme (porcine liver esterase) to leave carboxylic acid groups at the surface, thus illustrating how enzyme can selectively modify chemical functions at the surface of plasma polymers. These carboxylic groups could in turn be used for further derivatisation. Therefore, enzymes are potentially a powerful tool to create chemical functions at a surface in a relatively mild fashion. Moreover, due to their specificity, spatially-controlled surface modification using enzyme is feasible, offering a promising instrument for small-scale patterning.

IV.6. REFERENCES

1 - Boland, W.; Frößl, C.; Lorenz, M. *Synthesis* **1991**, 1049-1072

2 - Homandberg, G.A.; Mattis, J.A.; Laskowski, Jr., M. *Biochem.* **1979**, 17, 5220-5227

3 - Kornberg, A. *J. Biol. Chem.* **1950**, 182, -779-793

4 - Deutscher, M.P.; Hornberg, A. *J. Biol. Chem.* **1969**, 244, 3019-3028

5 - Monsan, P.; Paul, F. *FEMS Microbiol. Rev.* **1995**, 16, 187-192

6 - Gutman, A.L.; Zuobi, K.; Guibé-Jampel, E. *Tetrahedron Lett.* **1990**, 131, 2037-2038

7 - Taylor, S.J.C.; Sutherland, A.G.; Lee, C.; Wisdom, R.; Thomas, S.; Roberts, S.M.; Evans, C. *J. Chem. Soc., Chem. Commun.* **1990**, 1120-1121

8 - Geigert, J.; Neidleman, S.L.; Dalietos, D.J.; Dewitt, S.K. *Appl. Environ. Microbiol.* **1983**, 45, 366-374

9 - Lemière, G.L.; Lepoivre, J.A.; Alderweireldt, F.C. *Tetrahedron Lett.* **1985**, 26, 4527-4528

10 - Ejiri, S.-I.; Weissbach, H.; Brot, N. *J. Bacteriol.* **1979**, 139, 161-164

11 - Black, S.; Harte, E.M.; Hudson, B.; Wartofsky, L. *J. Biol. Chem.* **1960**, 235, 2910-2916

12 - Findeis, M.A.; Whitesides, G.M. *J. Org. Chem.* **1987**, 52, 2838-2848

13 - Akhtar, M.; Botting, N.P.; Cohen, M.A.; Gani, D. *Tetrahedron* **1987**, 43, 5899-5908

14 - Itoh, N.; Izumi, Y.; Yamada, H. *Biochem.* **1987**, 26, 282-289

15 - Grunberg-Manago, M.; Ochoa, S. *J. Am. Chem. Soc.* **1955**, 77, 3165 - 3166

16 - Kalra, B.; Gross, R.A. *Biomacromol.* **2000**, 1, 501-505

17 - Wilcocks, R.; Ward, O.P.; Collins, S.; Dewdney, N.J.; Hong, Y.; Prosen, E. *Appl. Environ. Microbiol.* **1992**, 58, 1699-1704

18 - Toone, E.J.; Simon, E.S.; Bednarski, E.D.; Whitesides, G.M. *Tetrahedron* **1989**, 45, 5365-5422

19 - Oikawa, H.; Kobayashi, T.; Katayama, K.; Suzuki, Y.; Ichihara, A. *J. Org. Chem.* **1998**, 63, 8748-8756

20 - Desnuelle, P. In *The Enzymes*; P. Boyer; 3rd Ed.; Academic Press, NY, 1972. Vol.7, Chapter 19

21 - Sobotka, H.; Glick, D., *J. Biol. Chem.* **1934**, 105, 199-219

22 - Nachmansohn, D.; Rothenberg, M.A., *J. Biol. Chem.* **1945**, 158, 653-666

23 - Stec, B.; Holtz, K.M.; Kantrowitz, E.R. *J. Mol. Biol.* **2000**, 299, 1303-1311

24 - Cameron, V.; Uhlenbeck, O.C., *Biochem.* **1977**, 16, 5120- 5126

25 - Donis-Keller, H., *Nucleic Acids Res.* **1979**, 7, 179-192

26 - http://www.ebi.ac.uk/thornton-srv/databases/cgi-bin/enzymes/GetPage.pl?ec_number=3.1.-.-

27 - http://www.ebi.ac.uk/thornton-srv/databases/cgi-bin/enzymes/GetPage.pl?ec_number=3.1.1.-

28 - Tamm, C., *Pure & Appl. Chem.* **1992**, 64, 1187-1191

29 - Adler, A.J.; Kistiakowsky, G.B., *J. Am. Chem. Soc.* **1962**, 84, 695-703

30 - Faber K. *Biotransformations in Organic Chemistry;* 4th Ed.; Springer: Berlin; 2000

31 - Silverman, R. B. *The Organic Chemistry of Enzyme-Catalysed Reactions*; Revised Ed.; Academic Press: San Diego; CA; 2002

32 - *Preparative biotransformations: whole cell and isolated enzymes in organic synthesis*, Roberts, S.M.; associate editors, Wiggins, K., Casy, G.; John Wiley: Chichester, 1992

33 - Pearson, J.D.; McCroskey, M.C. *J. Chromatogr. A* **1996**, 746, 277-281

34 - Shiman, R.; Gray, D.W.; Pater, A. *J. Biol. Chem.* **1979**, 254, 11300-11306

35 - Tabet, F. M.; McGahan, W. A. *Thin Solid Films* **2000**, 370, 122-127

36 - Evans, J.F.; Gibson, J.H.; Moulder, J.F.; Hammond, J.S.; Goretzki, H. *Fresenius' J. Anal. Chem.* **1984**, 319, 841-844

37 - Beamson, G.; Briggs, D. In *High-Resolution XPS of Organic Polymers: The Scienta ESCA300 Database*; John Wiley & Sons: New York, 1992

38 - Lin-Vien, D.; Colthyp, N.B.; Fateley, W.G.; Grasselli, J.G. In *The Handbook of Infrared and Raman Characteristic Frequencies of Organic Molecules*; Academic Press: New York, 1991

39 - Sutherland, I.; Sheng, E.-S.; Brewis, D.M.; Heath, R.J. *J. Mater. Chem.* **1994**, 4, 683-687

40 - Soderquist, M.E.; Walton, A.G., *J. Colloid Interface Sci.* **1980**, 75, 386-397

V

CHAPTER FIVE

Free radicals polymerisation on plasma polymer surfaces

V.1. INTRODUCTION

The grafting of thin polymer films onto a surface is commonly used to tailor the surface properties of a material without changing its bulk. The advantage of polymer brushes over other surface modification methods (e.g. self-assembled monolayers) is their mechanical and chemical robustness, along with a wide range of possible functional groups[12]. There is also an increasing interest of using functional or diblock copolymer brushes for stimuli-responsive surfaces[3], which can change a physical property (hydrophilicity, biocompatibility) upon an external trigger, such as heat[4], pH[5], or salt concentration[6].

This formation of polymer brushes can be achieved via two methods: "grafting to" and "grafting from". The "grafting to" method consists either in the physisorption of block copolymers[7,8,9] or in the covalent attachment of a polymer chain bearing a terminal functional group onto a suitable surface moiety[10,11]. The main disadvantages of these two techniques are, in the first case, desorption of grafted entities and in the second case, limitation of graft density due to steric hindrance[12,13]. These problems are addressed when using the "grafting from" method in which polymer brushes are initiated directly from the surface. The polymerisation can be of anionic[14,15], cationic[16,17], ring-opening[18,19] and of free-radical[20,21,22,23] nature.

Free radical polymerisation occurs typically in three steps[24] (see Scheme V-1):

- *Initiation*: formation of free radicals (R•) using initiators (I) such as peroxides[25], azo compounds[26], photosentitive molecules[27] or redox-systems[28] followed by transfer or the radical to the monomer (M).

- *Propagation*: rapid reaction of this radicalised monomer molecule with another monomer, and the subsequent repetition to create the repeating chain.

- *Termination*: generally occurs by recombination where two radicals react with each other to from a single molecule, preventing further propagation. However, it can also occur by chain disproportionation where two radicals react by exchanging a proton, which gives two terminated chains, one saturated and the other with a terminal double bond.

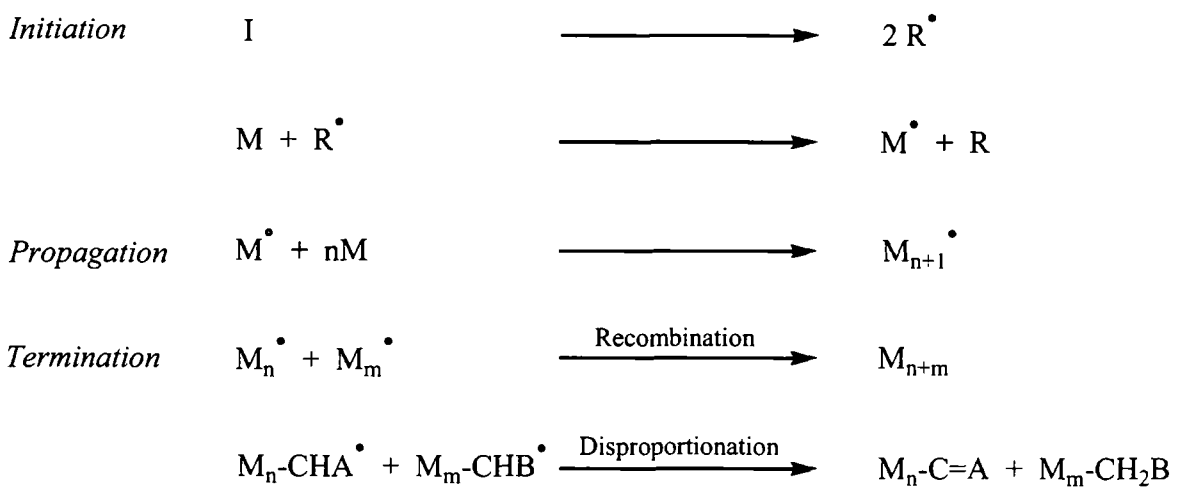

Scheme V-1 - Schematic representation of free radical polymerisation

The major advantage of free radical polymerisation is that it can be carried out under undemanding conditions and exhibits a tolerance to trace impurities. It is a simple process that can be undertaken with a wide range of monomers in organic media[29] as well as in aqueous media[30] and its mechanism is well known[31]. The disadvantages are that the reaction is highly non-selective and control over the products is non-trivial.

Amongst free-radical initiators, peroxides[25,32] and azo compounds[26,33] have been extensively used to polymerise a wide range of vinyl monomers such as styrene[34,35], ethylene[36] and various acrylates[37,38]. Azo initiators such as azobisisobutyronitrile have been widely used because they readily decompose into free radicals at relatively low temperatures (60-70°C)[39] and they also limit chain transfer processes which tend to lower the molecular weight of the final polymer product. Azoalkanes can be either

symmetrical[39] or asymmetrical[40] but are generally tertiary with functionalities such as cyano groups to stabilize the radical[41,42].

Azo free radical initiators have been successfully used to initiate polymerisation on surfaces. Azo groups were introduced onto surfaces by covalent attachment via a variety of methods such as amide bond formation on surfaces functionalised with activated carboxylic acid groups with amine-terminated azo compounds like 2,2'-azobis-(2-amidinopropane) dihydrochloride[22,43,44]. In a similar fashion surfaces presenting primary amine groups were reacted with 4,4'-azobis(4-cyanopentanoic acid)[40] or its chloroanhydride derivative[45]. Other methods include isocyanate groups immobilized onto surfaces to react with carboxylic acid or alcohol derivatives of azo groups[21,46] and synthesised azoalkanes with silane or siloxane terminal groups for self-assembled monolayers on silica particles[20,47] or silicon wafers[13,40].

Alternatively, initiation sites can be directly generated at a polymer surface after exposure to high-energy γ-radiations[48,49,50] or plasma discharges[51,52,53]. Subsequently, these initiation sites, believed to be peroxides groups introduced onto surfaces, are 'activated' when the surface is heated[54] and free radical polymerisation can occur when the treated surface is put into contact with a polymerisable monomer. In addition, Yasuda showed that in the case of plasma-deposited polymer films, trapped free radicals were formed within the polymer film and could initiate polymerisation[55]. However, graft polymerisation on such plasma polymers has scarcely been studied and most studies were done with vinyl monomer on continuous wave plasma polymers[56,57,58,59,60]. More recently, Teare et al.[61] showed that graft polymerisation on maleic anhydride plasma polymer was more effective on pulsed-plasma polymers than on continuous wave ones due to the better retention of the maleic groups. He proposed a free radical polymerisation mechanism using stabilised initiating radicals situated at the

surface. The thickness and patterning of the grafted polymer is found to be easily controllable.

This work aims at extending our knowledge of graft polymerisation initiated by trapped free radicals onto pulsed plasma polymers and comparing it to graft polymerisation using more conventional initiators. Graft polymerisation of styrene onto pentafluorophenyl acrylate plasma polymer is investigated via two initiating methods: azo groups introduced at the surface of the plasma polymer (Scheme V-2) and trapped free radicals generated within the pulsed plasma polymer.

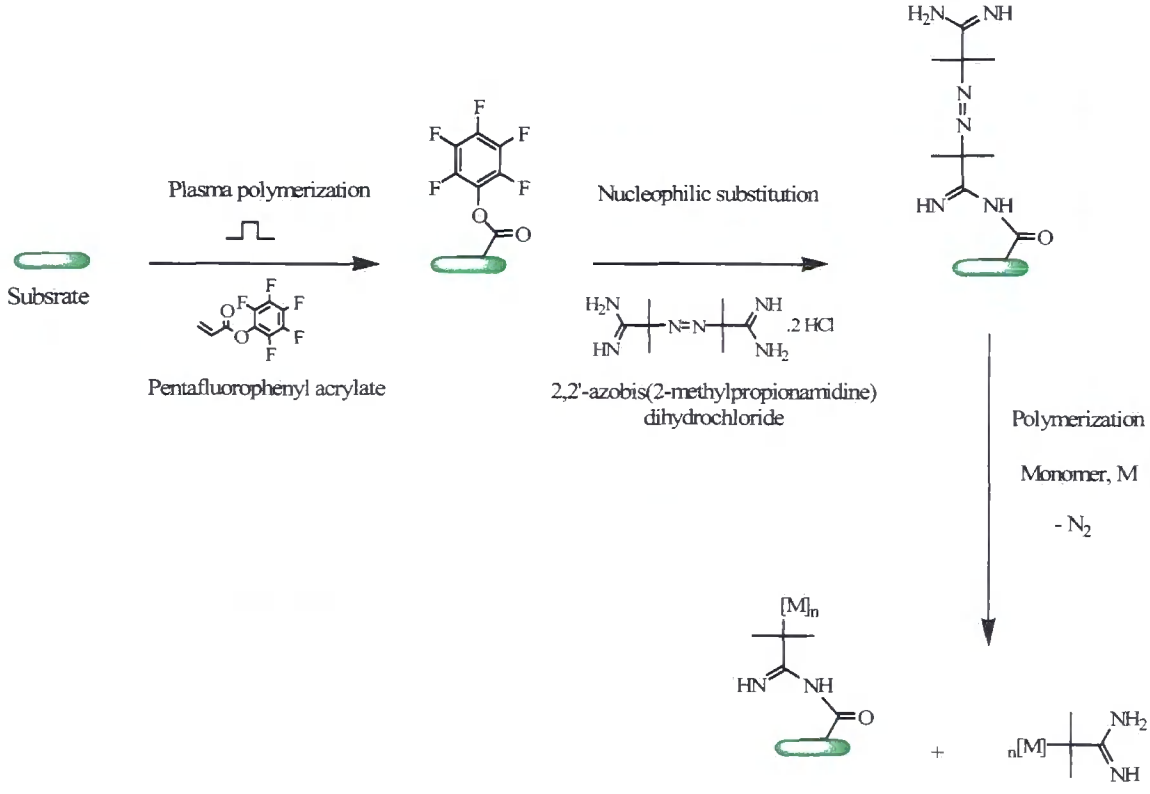

Scheme V-2- Reaction scheme of polymerisation of a monomer with 2,2'-azobis(2-methylpropionamidine) attached onto pentafluorophenyl acrylate plasma polymer

V.2. EXPERIMENTAL

V.2.1. Deposition of plasma polymer

Pentafluorophenyl acrylate plasma polymer surfaces were generated as described in Chapter III. Surfaces of 100 nm thickness were generated for subsequent reaction.

V.2.2. Attachment of 2,2'-azobis-(2-amidinopropane) dihydrochloride

Pentafluorophenyl acrylate (PFPA) pulsed plasma coated surfaces were reacted with 2,2'-azobis-(2-amidinopropane) dihydrochloride (azobis) (97%, Aldrich) 200 mM in phosphate buffer 0.05 M pH=8.5 for 48h, then rinsed 1h in water and left to dry.

These conditions were chosen after preliminary experiments (no repetition done) (see Table V-1) of attachment of 2,2'-azobis(2-methylpropionamidine) onto pentafluorophenyl acrylate plasma polymer (10 μm / 20 ms – 20 W). After 16h of reaction, the amount of nitrogen (directly related to the amount of azobis compound attached onto the surface) reaches 6 %. After 48h, this amount almost double to 10%. After 72h, the amount of nitrogen did not increase much compared to that after 48h. This seems to suggest that reaction reached a plateau value and that leaving the reaction to carry on for longer might not improve the yield further. Therefore, for the attachment of 2,2'-azobis(2-methylpropionamidine) onto pentafluorophenyl acrylate plasma polymer, a reaction time of 48h is chosen.

Table V-1 – Preliminary experiments of attachment of 2,2'-azobis(2-methylpropionamidine) onto pentafluorophenyl acrylate plasma polymer (10 µm / 20 ms – 20 W) – Experiments at 16h and 72h only done once

Surfaces	Composition (at. %)			
	C (1s)	O (1s)	N(1s)	F(1s)
PFPA plasma polymer theoretical	56.2	12.5		31.3
PFPA plasma polymer experimental	50.5 ± 0.2	13.9 ± 3.0		35.6 ± 2.8
Azobis theoretical	61.1	5.6	33.3	
PFPA + Azobis 0.2 M - pH=8.5 - 16h	61.0	15.72	5.9	17.37
PFPA + Azobis 0.2 M - pH=8.5 - 48h	60.9	17.3	9.9	12
PFPA + Azobis 0.2 M - pH=8.5 - 72h	57.4	18.3	10.7	13.7

V.2.3. Graft polymerisation of styrene

PFPA plasma polymer coated surfaces and PFPA plasma polymer + azobis coated surfaces were introduced in a sealed glass tube containing styrene (99%, Aldrich) dissolved in toluene (99%, Fisher Scientific) at a concentration of 4 M. Dissolved oxygen and other gases were removed by several freeze-pump-thaw cycles. Next, the tube was placed into an oil bath at different set temperatures ranging from 60 to 120°C for different reaction time to facilitate thermal polymerisation. Subsequently, any loosely bound polystyrene attached to the substrate surface was removed by soxhlet extraction in tetrahydrofuran (>99%, Fisher Scientific) for 16 h. Corresponding control experiments with uncoated substrates were also undertaken.

V.2.4. Quantification and quenching of trapped free radicals

Initiator quenching studies employed diphenylpicrylhydrazyl[38,62] (DPPH, 95%, Aldrich) as a free radical scavenger. This entailed immersion of each plasma polymer coated substrate into a 5 mL solution of DPPH 1.5 x 10^{-4} M in toluene. The reaction tube was sealed, and any dissolved gases were removed by multiple freeze-pump-thaw cycles. The DPPH solution was then heated in an oil bath at 80 °C for 3 h, followed by removal of the substrate and rinsing in clean toluene. The final step entailed placing DPPH treated plasma polymer films into styrene and exposing them to the previously described styrene polymerisation conditions.

For quantification studies, the adsorption of the DPPH solutions before and after reaction with the plasma polymer coated surfaces were measured on a UV-vis spectrophotometer at a wavelength of 520 nm for which DPPH exhibits maximum absorption.

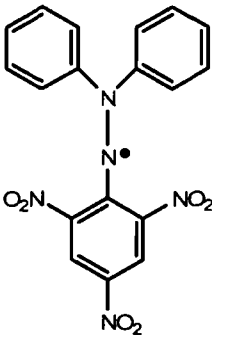

Figure V-1 - 2,2'-diphenyl-1-picrylhydrazyl radical

V.2.5. Analysis

A spectrophotometer (nkd-6000, Aquila Instruments Ltd.) was used for plasma polymer film thickness measurements. The obtained transmittance-reflectance curves (350-1000 nm wavelength range) were fitted to a Cauchy material model using a modified Levenberg-Marquardt algorithm[63].

Contact angle analysis on the pulsed plasma deposited films was carried out using a video capture system (ASE Products, model VCA2500XE). 2.0 μL sessile droplets of deionised water were placed onto the polymer surface and contact angle measurements taken at 20 °C.

Chemical characterization by X-ray photoelectron spectroscopy (XPS) was undertaken using a VG Microtech electron spectrometer equipped with a non-monochromated Mg Kα X-ray source (1253.6 eV) and a concentric hemispherical analyzer (VG 100 AX) operating in the constant analyzer energy mode (CAE, pass energy = 20 eV for elemental analysis and 50 eV for wide scans). The XPS spectra for the carbon envelopes were fitted using the convention established for insulating polymers, i.e. C-C bond exhibits a photopeak at a binding energy of 285.0 eV. All the Gaussian components peaks[64] were determined using a linear background and equal full-width at-half-maximum (FWHM) on a Marquardt minimization computer software. Since each Gaussian component relates to a specific carbon bonding, the peaks are centred on the binding energy of the bond of interest as determined by Beamson and Briggs[65]. Instrument sensitivity multiplication factors were taken as C(1s): O(1s): N(1s): Si(2p): F(1s) 1.00: 0.37: 0.56: 096: 0.24.

Surface Fourier transform infrared spectroscopy (FTIR) was performed on gold substrates using an FTIR spectrometer (Perkin-Elmer, model Spectrum One) equipped with a liquid nitrogen cooled MCT detector operating at 4 cm^{-1} resolution over the 700-4000 cm^{-1} range. The instrument was fitted with a reflection-absorption spectroscopy accessory (Specac) and a KRS-5 p-polarizer with the reflection angle set to 84°. All spectra were averaged over 512 scans.

Absorbance measurements were carried out on a Perkin Elmer Lambda 900 UV/VIS/NIR spectrometer. A first, a run was done on the DPPH solution 1.5 x 10^{-4} M in toluene between 480 and 560 nm to establish the wavelength for maximum absorbance. The wavelength was found to be 520 nm.

V.3. RESULTS

V.3.1. Polymerisation of styrene onto pentafluorophenyl acrylate plasma polymer via 2,2'-azobis(2-methylpropionamidine) dihydrochloride

V.3.1.1. Attachment of 2,2'-azobis(2-methylpropionamidine) dihydrochloride onto pentafluorophenyl acrylate plasma polymer

The covalent attachment of azobis onto PFPA plasma polymer is followed by XPS analysis. After reaction a peak related to nitrogen appears at the surface confirming amidation. The elemental composition of the surface allows the quantification of the amount of azobis groups introduced on the surface (see Table V-2). However, some fluorine remains at the surface of the plasma polymer after reaction, indicating not all pentafluorophenyl acrylate molecules present at the surface underwent reaction.

Table V-2– XPS analysis of 2,2'-azobis(2-methylpropionamidine) attachment onto pentafluorophenyl acrylate plasma polymer (10 µm / 20 ms – 20 W)

Surfaces	Composition (at. %)			
	C (1s)	O (1s)	N(1s)	F(1s)
PFPA plasma polymer theoretical	56.2	12.5		31.3
PFPA plasma polymer experimental	50.5 ± 0.2	13.9 ± 3.0		35.6 ± 2.8
Azobis theoretical	61.1	5.6	33.3	
PFPA + Azobis 0.2 M - pH=8.5 - 48h	60.9 ± 1.9	17.3 ± 0.2	9.9 ± 1.4	12 ± 3.5

The carbon envelope C(1s) after reaction presents seven different environments (Figure V-2): hydrocarbon (285.0 eV), carbon in α position of a carbonyl group (285.2 eV), carbon single-bonded to oxygen from an ester group (285.8 eV), a carbon bonded to nitrogen (286.2eV), a carbon from an amide (287.2eV), a carbon bonded to a single fluorine atom (288.4eV) and a carbon from a carbonyl group (289.7eV). All these different environments are compatible with a surface presenting active ester functions as well as amide functionalities. The fact that the peak related to the reactive ester decreased as the peak related to the amide increased provides evidence that substitution occurred. The hydrocarbon peak increased the most which is expected as four CH_3 groups were added to the surface after reaction with the azo compound.

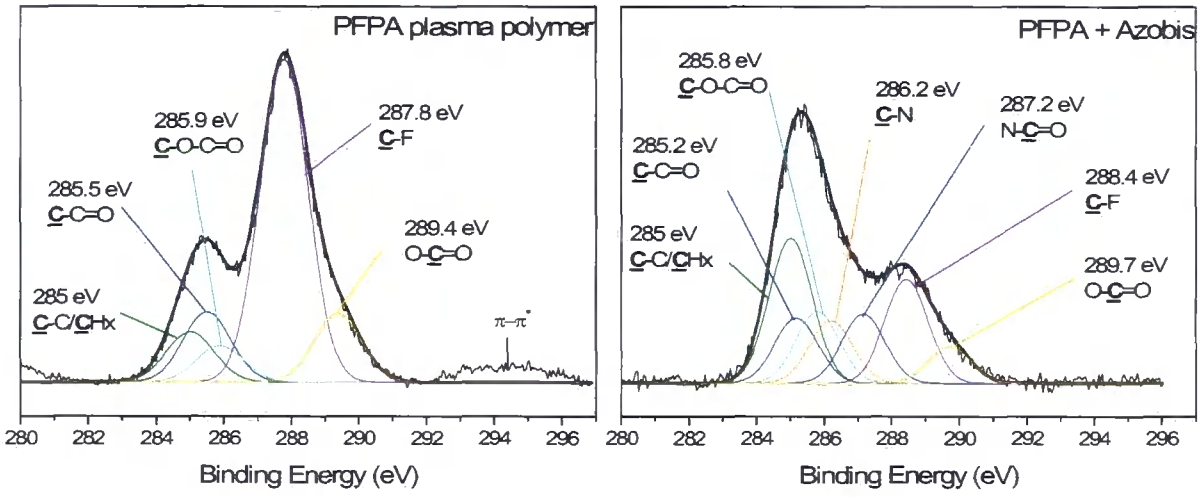

Figure V-2 - C(1s) XPS spectra of pentafluorophenyl acrylate plasma polymer (10 µm / 20 ms – 20 W) before and after reaction with 2,2'-azobis(2-methylpropionamidine)

Infra-red spectroscopy provides further evidence of the attachment of the azobis compound at the surface of PFPA plasma polymer (see Figure V-3). The following assignment can be made for the main infra-red peaks observed for 2,2'-azobis(2-methylpropionamidine)[66]: C=N / C-N stretch at 1676 cm^{-1}, NH_3^+ asymmetric deformation at 1625 cm^{-1}, NH_3^+ symmetric deformation at 1512 cm^{-1}, $C(CH_3)_2$

deformation at 1363 cm^{-1} and at 1385 cm^{-1}, C-N stretch of an amine at 1213 cm^{-1}, and a combination of C-C stretch and CH_3 rock at 1066 cm^{-1}.

The PFPA plasma polymer presents the following peaks as observed with the monomer: a carbonyl group stretch is visible at around 1780 cm^{-1} and three of the bands characteristic of fluorinated benzene ring are present at 1510, 1105 and 990 cm^{-1}.

After reaction of PFPA plasma polymer with the azobis compound, two peaks related to the PFPA plasma polymer are still present at 1526 and 999 cm^{-1} (*). The carbonyl deformation at 1780 cm^{-1} is not clearly visible as the signal is small and probably shadowed by the neighbouring peaks. Five peaks related to the azobis compound can be identified (*): C-N stretch of an amine at 1697 cm^{-1}, symmetric NH_2 deformation at 1624 cm^{-1}, symmetric NH_2 deformation at 1507 cm^{-1}, (combined with a band characteristic of the fluorinated benzene ring from the active ester), $C(CH_3)_2$ deformation at 1370 cm^{-1} and C-N stretch of an amine at 1215 cm^{-1}. Two peaks related to an amide formation can be distinguished (*): C=O stretch at 1656 cm^{-1} and C-N stretch at 1377 cm^{-1}. The signal of these peaks is weak since it was established by the XPS results that low reaction yield has been achieved.

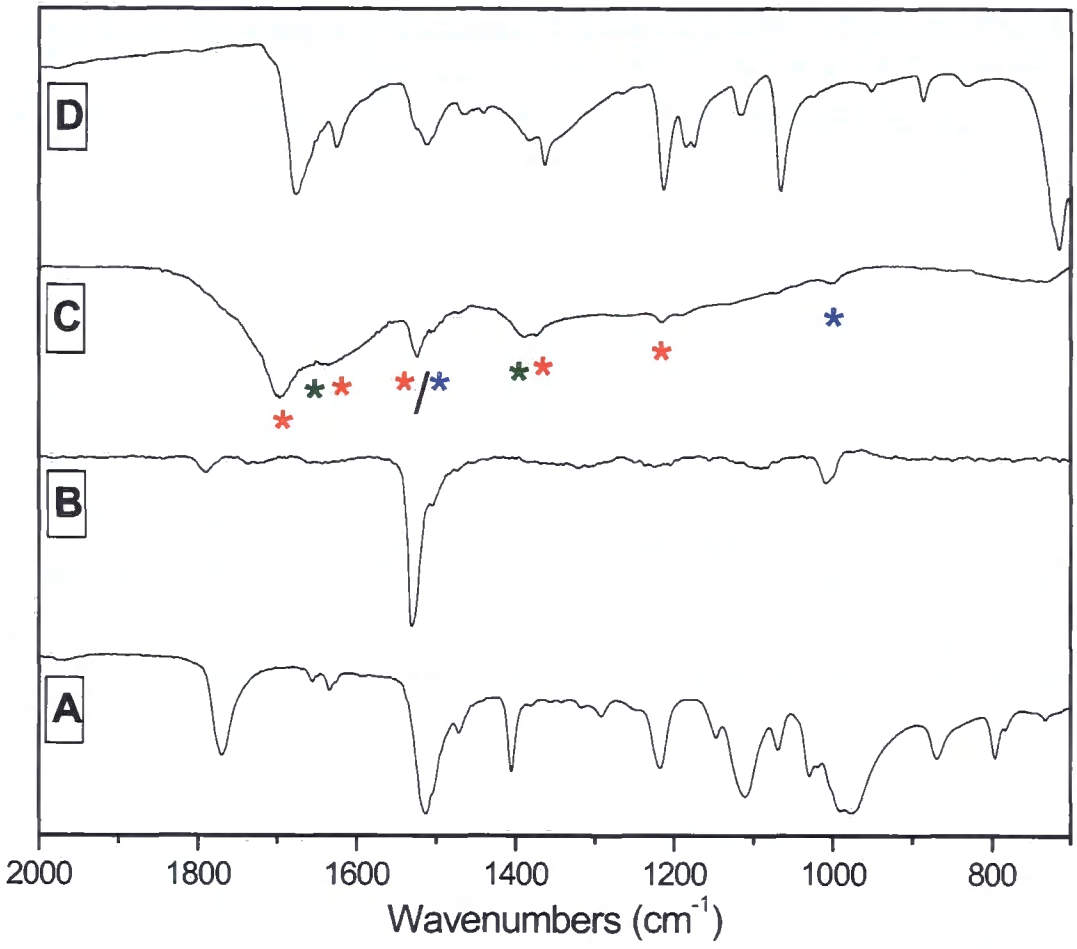

Figure V-3 – RAIRS of: (A) pentafluorophenyl acrylate monomer

(B) pentafluorophenyl acrylate plasma polymer(10 µm / 20 ms – 20 W)

(C) azobis attached onto PFPA plasma polymer (10 µm / 20 ms – 20 W)

(D) 2,2'-azobis(2-methylpropionamidine) dihydrochloride

V.3.1.2. Polymerisation of styrene onto pentafluorophenyl acrylate plasma polymer via 2,2'-azobis(2-methylpropionamidine)

Each step leading to polymerisation of styrene onto PFPA plasma polymer could be followed by XPS (see Figure V-4). PFPA plasma polymer presents three peaks related to carbon, nitrogen and fluorine. After reaction with the initiator azobis a peak attributed to nitrogen appears on the wide scan. The remaining fluorine peak at this stage indicates that reaction did not go to completion. After polymerisation, the surface is mainly composed of carbon, which is compatible with polystyrene, with some oxygen

impurities. No more nitrogen and fluorine can be detected, indicated that more than a 5-10 nm layer of polystyrene is present[67].

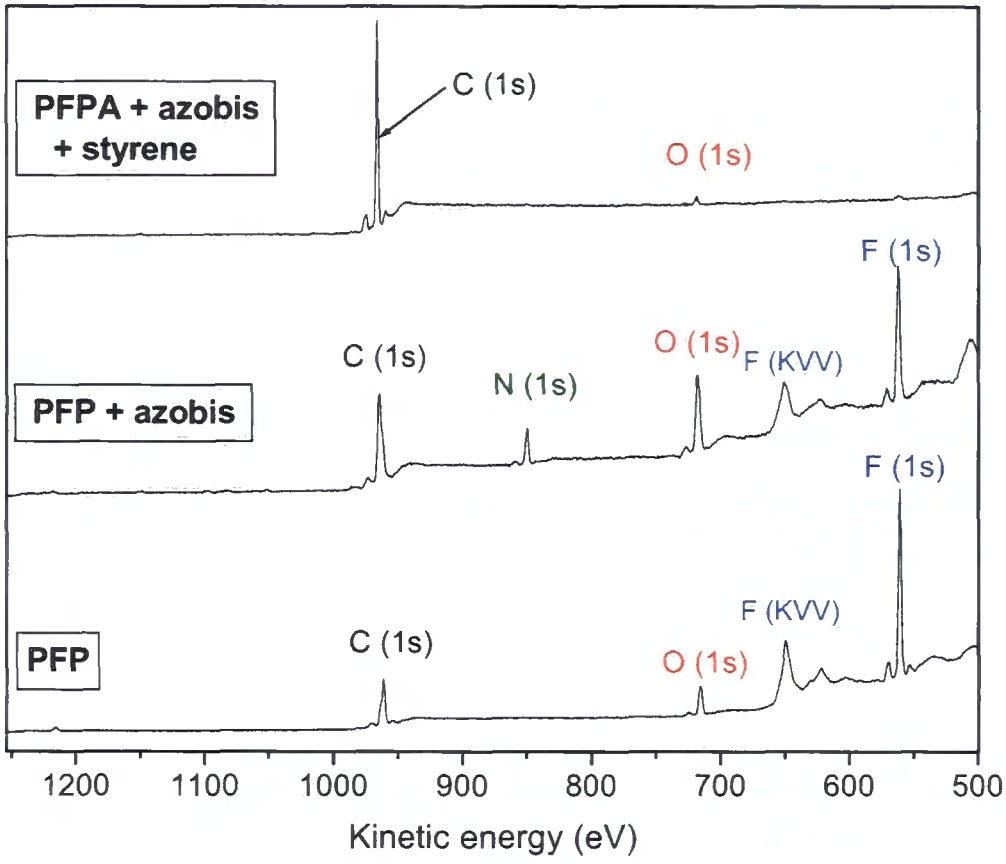

Figure V-4 - Wide scan of pentafluorophenyl acrylate plasma polymer (10 µm / 20 ms – 20 W), PFPA after attachment of 2,2'-azobis(2-methylpropionamidine) and PFPA + azobis after polymerisation of styrene

The elemental composition of the surface after each step confirms the observations made previously (see Table V-3). The longer the polymerisation is left to occur, the higher the amount of carbon at the surface. However, there seems to be always some oxygen impurities within the polystyrene layer.

Table V-3 – XPS analysis of PFPA plasma polymer (10 µm / 20 ms – 20 W) + azobis + styrene

Surfaces	Composition (at. %)			
	C (1s)	O (1s)	N (1s)	F (1s)
PFPA plasma polymer	50.5 ± 0.2	13.9 ± 3.0		35.6 ± 2.8
PFPA + Azobis	60.9 ± 1.9	17.3 ± 0.2	9.9 ± 1.4	12 ± 3.5
PFPA + Azobis + Styrene 3 h – 90°C	94.1 ± 4.0	3.8 ± 2.2	0.9 ± 0.9	1.1 ± 0.5
PFPA + Azobis + Styrene 6 h – 90°C	96.6 ± 2.0	2.7 ± 1.0		0.71 ± 0.7
PFPA + Azobis + Styrene 24 h – 90°C	97.5 ± 2.0	2.5 ± 1.2		

The carbon envelope C(1s) of PFPA plasma polymer + azobis after polymerisation of styrene only contains one type of carbon, hydrocarbon CH_x, confirming the presence of polystyrene at the surface (see Figure V-5). The presence of the π-π* shake-up satellite at 291.7 eV clearly indicates the retained aromatic structure of polystyrene[68].

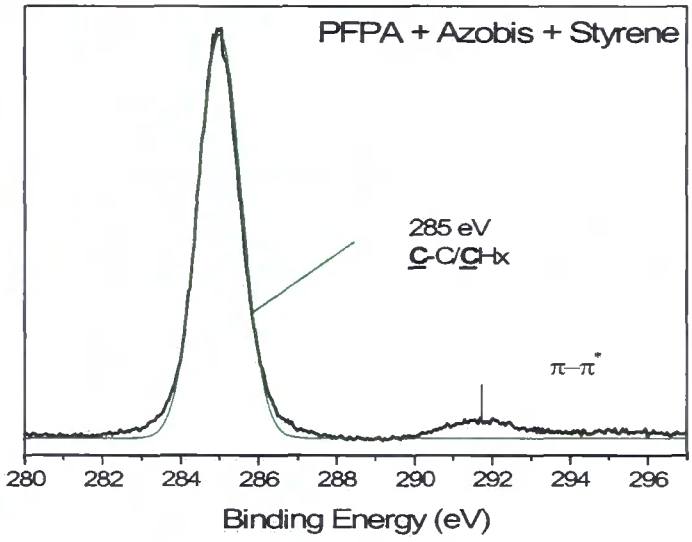

Figure V-5 - C(1s) XPS spectra of pentafluorophenyl acrylate plasma polymer (10 µm / 20 ms – 20 W) + 2,2'-azobis(2-methylpropionamidine) after polymerisation of styrene

The thickness of the polystyrene layer as a function of time at a temperature of 90°C is given in Table V-4. The thickness of the layer increases with time. After 24h, the

thickness of the polystyrene layer has increased by over 5-folds compared to the thickness after 3h.

Table V-4 – Thickness of polystyrene layer onto PFPA (10 µm / 20 ms – 20 W) + azobis after reaction at 90°C – Comparison with polymerisation of styrene onto bare silicon wafer

Time (h)	Thickness (nm)	
	PFPA + azobis	Silicon wafer
3 h	15 ± 1	2 ± 0
6 h	40 ± 1	9 ± 1
24 h	78 ± 6	11 ± 1

V.3.2. Polymerisation of styrene onto silicon wafer

As a control reaction, polymerisation of styrene was carried out on bare silicon wafer at different temperatures without any initiator to evaluate the thickness of the polystyrene irreversibly bound to the surface and not initiated by azobis compound or by free radicals trapped in the plasma polymer. (Table V-5).

After 20h about 12 nm on average of polystyrene remains to the surface, whatever the temperature. After 40h, the same amount remains for temperatures up to 105°C, but reaches 28 nm at 120°C.

Table V-5 – Thickness of polystyrene adsorbed onto silicon wafer at different reaction time and temperature

Temperature (°C)	Time (h)	Thickness (nm)
60	20	11 ± 1
	40	Too thin
75	20	8 ± 1
	40	6 ± 2
90	20	11 ± 1
	40	17 ± 2
105	20	10 ± 1
	40	11 ± 1
120	20	15 ± 2
	40	28 ± 3

V.3.3. Polymerisation of styrene onto pentafluorophenyl acrylate plasma polymer via free radicals

V.3.3.1. Quantification of free radicals

The quantification of trapped free radicals within pentafluorophenyl acrylate plasma polymer was achieved by the 2,2'-diphenyl-1-picrylhydrazyl radical (DPPH) method[35,62]. XPS analysis was performed on the plasma polymer surface after reaction with DPPH to provide evidence of the covalent attachment of the radical scavenger onto the surface (Table V-6). After 3h reaction with DPPH, 1.6% nitrogen appears at the surface, indicating that attachment occurred. After 18h, the same amount of nitrogen is present at the surface, indicating that after 3h all trapped free radicals available have reacted with DPPH.

Table V-6– XPS analysis of 2,2-diphenyl-1-picrylhydrazyl onto PFPA plasma polymer (10 µm / 20 ms – 20 W)

Surfaces	Composition (at. %)			
	C (1s)	O (1s)	N (1s)	F (1s)
PFPA plasma polymer	51.6 ± 1.7	14.5 ± 2.2		33.9 ± 0.4
PFPA + DPPH – 3 h – 80°C	57.2 ± 2.5	19.6 ± 4.7	1.6 ± 0.3	21.6 ± 7.5
PFPA + DPPH – 18 h – 80°C	57.4 ± 1.1	18.3 ± 1.3	1.5 ± 0.0	22.8 ± 2.5

The amount of DPPH which has reacted can be monitored by UV-vis spectrophotometry. Subsequently, the amount of trapped free radicals at the surface of the PFPA plasma polymer can be assessed.

Beer-Lambert law (see Equation V-1) gives the relationship between concentration and absorbance.

Equation V-1 $$A = \varepsilon l c$$

where ε : extinction coefficient

l : cell width

c : concentration of the absorbing species.

The extinction coefficient for DPPH was measured to equal 10527 $L.mol^{-1}.cm^{-1}$, which is similar to values previously obtained[69,70].

Absorbance of solutions of DPPH in toluene, DPPH in toluene heated without substrate (control experiment) and DPPH in toluene heated with the PFPA plasma polymer are then measured at 520 nm wavelength. From these values, the surface density of trapped free radicals in PFPA plasma polymer can be calculated using Equation V-2.

Equation V-2

$$d = \frac{[DPPH]_{Blank} - [DPPH]_{Substrate}}{V \times S}$$

where d : surface density of free radicals ($mol.cm^{-2}$)

$[DPPH]_{Blank}$: concentration of DPPH remaining after heating without substrate ($mol.L^{-1}$)

$[DPPH]_{Substrate}$: concentration of DPPH remaining after heating with substrate ($mol.L^{-1}$)

V : volume of DPPH solution (L)

S : surface of the substrate (cm^{-2})

The density of free radicals in pentafluorophenyl acrylate plasma polymer was measured to be $11 \pm 3 \times 10^{-9}$ $mol.cm^{-2}$.

V.3.3.2. Polymerisation of styrene onto pentafluorophenyl acrylate

Polymerisation of styrene onto PFPA plasma polymer using the trapped free radicals as initiators was followed by XPS analysis. The elemental composition of the surface before and after polymerisation at different temperature and for different reaction time is given in Table V-7. After polymerisation of styrene, the amounts of fluorine and oxygen at the surface decreased, whereas that of carbon increased. Over 90°C, the elemental composition of the surface does not seem to vary, indicating that the polystyrene layer always contain oxygen impurities no matter its thickness.

Table V-7 – XPS analysis of pentafluorophenyl acrylate plasma polymer (10 µm / 20 ms – 20 W) before and after graft polymerisation of styrene

Surfaces	Composition (at. %)		
	C (1s)	O (1s)	F (1s)
PFPA plasma polymer - theoretical	56.2	12.5	31.3
PFPA plasma polymer - experimental	51.6 ± 1.7	14.5 ± 2.2	33.9 ± 0.4
Styrene - theoretical	100		
PFPA + Styrene - 75°C - 3h	87.2 ± 5.5	9.3 ± 4.6	3.5 ± 1.0
PFPA + Styrene - 75°C - 6h	77.6 ± 26.8	10.5 ± 10.9	11.9 ± 15.9
PFPA + Styrene - 90°C - 3h	94.3 ± 0.5	4.2 ± 1.7	1.6 ± 1.2
PFPA + Styrene - 90°C - 6h	95.6 ± 2.9	3.9 ± 2.6	0.5 ± 0.3
PFPA + Styrene - 105°C - 3h	97.2 ± 0.0	2.5 ± 0.1	0.4 ± 0.1
PFPA + Styrene - 105°C - 6h	96.5 ± 0.7	3.0 ± 0.7	0.5 ± 0.1
PFPA + Styrene - 120°C - 3h	96.8 ± 2.4	3.3 ± 2.4	0 ± 0
PFPA + Styrene - 120°C - 6h	95.0 ± 0.7	3.4 ± 1.3	1.7 ± 2.0

The carbon envelope C(1s) of PFPA plasma polymer before polymerisation of styrene presents five different types of carbon environments (see Chapter III). After polymerisation of styrene (12h – 105°C), the surface presents only one type of carbon, hydrocarbon CH_x, confirming the presence of polystyrene at the surface (see Figure V-6). The presence of the π-π* shake-up satellite at 291.7 eV is indicative of the aromatic structure of polystyrene[68].

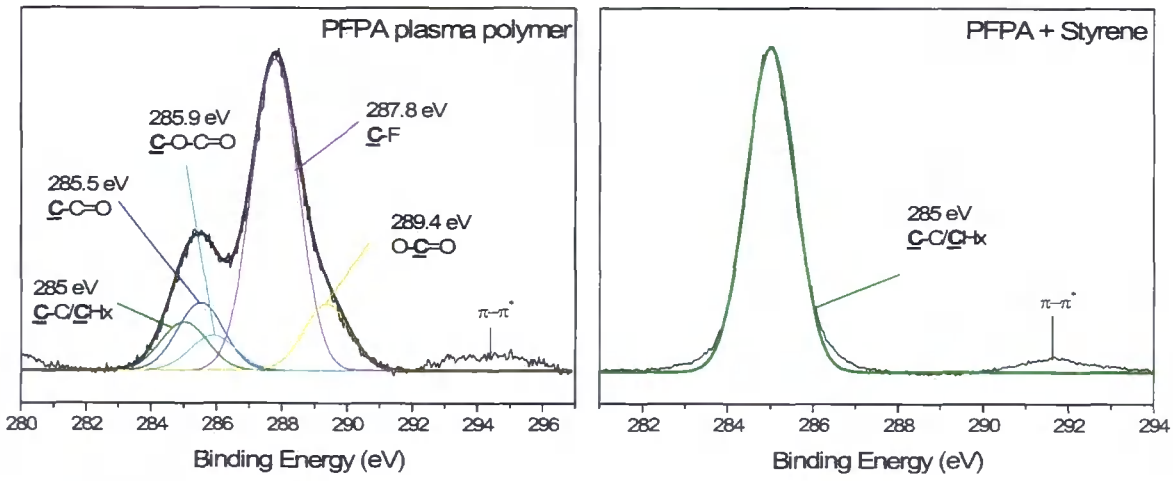

Figure V-6 - C(1s) XPS spectra of pentafluorophenyl acrylate plasma polymer (10 µm / 20 ms – 20 W) before and after polymerisation of styrene (6h – 120°C)

Infra-red spectroscopy of the film provided further evidence that polymerisation of styrene occurred at the surface of PFPA plasma polymer. Polystyrene film (ICI Melinex) presents the following main peaks[66]: CH stretch from phenyl ring (3100-3000 cm^{-1}), CH stretch from hydrocarbon CH_x groups (3000-2900 cm^{-1}), phenyl ring stretch (1600, 1492 and 1456 cm^{-1}) and phenyl ring deformation (760, 700 cm^{-1}). PFPA plasma polymer with grafted polystyrene presents the same main characteristic peaks as the Melinex polystyrene film, confirming presence of the polystyrene grafted chains (Figure V-7).

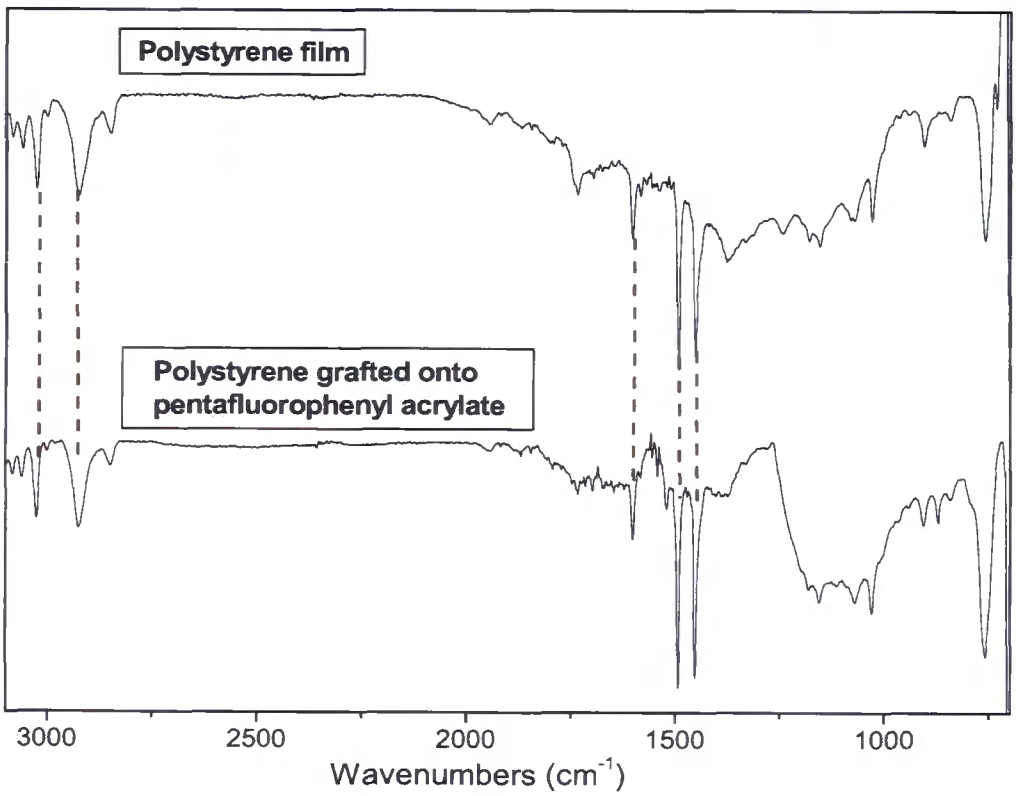

Figure V-7 – RAIRS of styrene polymerized onto PFPA plasma polymer (10 µm / 20 ms – 20 W) for 12h at 105°C and styrene film (ICI Melinex)

As reaction time and temperature are increased, the thickness of the polystyrene layer above the plasma polymer also increases (see Table V-8). After 3h, the thickness remains the same at 75 or 90°C, but this value doubles when the temperature is brought

to 105°C. This value is further increased when the temperature is raised up to 120°C. After 6h at 75°C, the thickness of the polystyrene layer is the same as that after 3h. However, when the temperature is increased to 90°C, and then 105°C, the thickness doubles each time. At 120°C, no more increase seems to be observed (Table V-8).

Table V-8 – Thickness (in nm) of polystyrene grafted onto pentafluorophenyl acrylate plasma polymer (10 µm / 20 ms – 20 W)

Temperature	Time	
	3h	6h
75°C	16 ± 1	16 ± 8
90°C (*)	7 ± 8	35 ± 5
105°C	31 ± 1	61 ± 6
120°C	44 ± 16	62 ± 23

(*) For direct comparison between the azobis method and the trapped free radicals, the grafting of styrene onto pentafluorophenyl acrylate plasma polymer was also carried out at 90°C for 24h. The thickness of the grafted polystyrene yielded 62 ± 8 nm.

Polymerisation of styrene onto PFPA plasma polymer was further investigated for different reaction times. Reaction temperature was set at 105°C since it was observed that increasing the temperature beyond that value did not have significant influence over the thickness of the grafted polymer. Moreover, blank test on bare silicon wafer showed that absorbed styrene polymer was far less significant when the temperature was 105°C when compared to a temperature of 120°C.

When the polymerisation is left to run for several hours at 105°C, a plateau value of about 100 nm seems to be reached with regards to the thickness of the polystyrene layer (Figure V-8). Beyond this value, obtained after about 20h, increasing the reaction time does not lead to an increase in the thickness of the polystyrene layer.

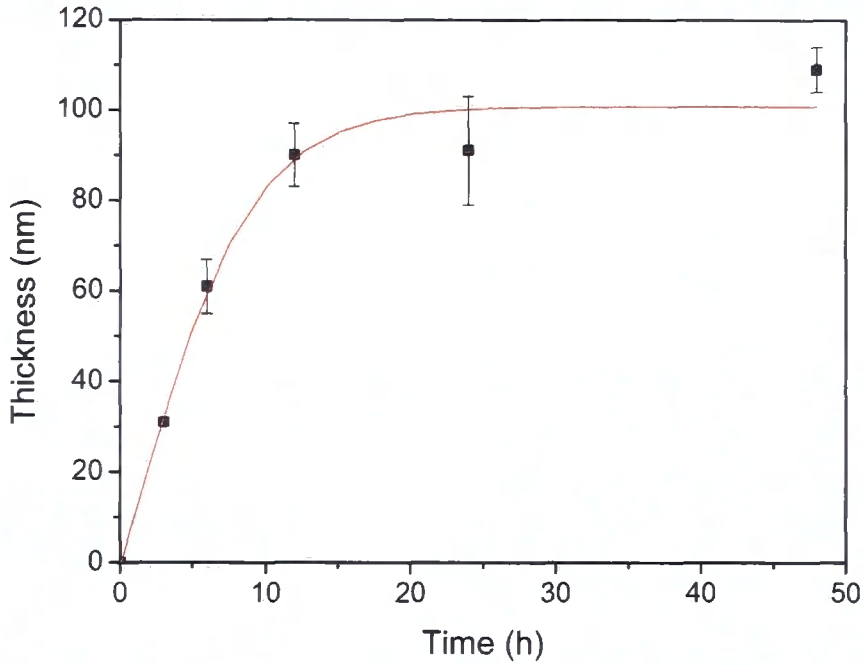

Figure V-8 – Thickness of grafted polystyrene onto pentafluorophenyl acrylate plasma polymer (10 µm / 20 ms – 20 W) at 105°C as a function of reaction time

When polymerisation of styrene is performed on PFPA plasma polymer after the surface has been reacted with DPPH, the thickness of polystyrene only reaches 15 nm compared to the 61 nm obtained with PFPA plasma polymer.

Table V-9 – Comparison of styrene polymerisation onto pentafluorophenyl acrylate plasma polymer (10 µm / 20 ms – 20 W) before and after trapping of free radicals (6 h – 105°C)

Surface	Thickness of PS (nm)
PFPA	61 ± 6
PFPA + DPPH	15 ± 1

V.4. DISCUSSION

V.4.1. Polymerisation of styrene onto pentafluorophenyl acrylate plasma polymer via 2,2'-azobis(2-methylpropionamidine) dihydrochloride

2,2'-azobis(2-methylpropionamidine) was successfully attached via amidation onto pentafluorophenyl acrylate plasma polymer. The attachment proceeded between the reactive ester and one of the primary amines on the azobis compound, imine groups being very poor nucleophile[71].

The proportions of pentafluorophenyl groups which underwent reaction with 2,2'-azobis(2-methylpropionamidine) can be calculated from the amount of nitrogen [N] (in atomic %) introduced (Equation V-3)[72]:

Equation V-3
$$[N] = \frac{6/5x[penafluorophenyl]_0}{[C]_0 + [O]_0 + [F]_0 + 2/5x[pentafluorophenyl]_0} \times 100$$

Where $[C]_0$, $[O]_0$ and $[F]_0$ are the initial atomic percentages of each element in the reactive ester plasma polymer, x is the advancement of the reaction (x=0 when no reaction occurred and x=1 when all reactive ester have reacted) and $[pentafluorophenyl]_0$ is the initial percentages of carbon bearing the reactive group in the plasma polymer (**C**-F for PFPA).

The percentage of carbon bearing the reactive group in the PFPA plasma polymer before reaction is 45 %. Therefore, the amount of pentafluorophenyl groups which have undergone reaction with azobis 0.2 M equals 18%. The bulkiness of the azobis compound along with that of pentafluorophenyl groups can account for the relatively low reaction yield. Moreover, assuming the reaction occurred only at the surface because of steric hindrance, and since the depth probed by XPS is a few monolayers, we can reasonably stipulate that the conversion rate is an underestimation.

Both the XPS and the IR spectra are compatible with the assumption that 2,2'-azobis(2-methylpropionamidine) is covalently attached onto PFPA plasma polymer. However retention of the nitrogen-nitrogen double bond could not be assessed via these analytic methods. Indeed, a bond is visible on infra-red spectra if it is polarisable[66], and the N=N being symmetrical will not show. With XPS, the carbon envelope of PFPA plasma polymer after amidation with the azobis compound presents all the expected peaks, but the nitrogen envelope could not be fitted to all nitrogen environments because the sensitivity of the machine used is too low. The presence of the nitrogen-nitrogen double bond is confirmed by the fact that polymerisation of styrene occurs at the surface of the derivatised plasma polymer, which means that thermal initiators were present at the surface.

After polymerisation of styrene, no more fluorine of nitrogen can be detected at the surface, indicating complete coverage with polystyrene.

After 24h, the polystyrene layer reaches a thickness of 78 nm. When the same reaction is carried out on bare silicon wafer, the thickness of the adsorbed layer of polystyrene only reaches 17nm. Therefore, grafting is initiated by radical polymerisation using immobilised initiators. After 3 and 6h the thickness of the polystyrene layer is low and within the limitations of the instrument used. Therefore, the polymerisation rate cannot be evaluated. If one considers the thickness after 24h, the polymerisation rate is measured to be 3.25 ± 0.25 $nm.h^{-1}$. This result shows an improvement compared to the one obtained by Hyun et al. on self-assembled monolayer (SAM) onto gold using similar pathways. They achieved grafted polystyrene layers up to 20 nm after 24h[22], which corresponds to a rate of 0.83 $nm.h^{-1}$. The roughness of plasma polymer surfaces[73] can account for this improvement since functionalities present on these surfaces are more available than on a highly ordered surface such as

self-assembled monolayers. However, the temperature used is lower (see Table V-10). Prucker[74] showed that if the temperature is lowered, the probability of deactivation of polymer radicals by recombination or disproportionation is greatly reduced, but much longer reaction times are required to achieve similar thicknesses. When preliminary reactions were carried out for his thesis, lower temperatures were investigated but none gave satisfying results. 90°C was found to be the most suitable temperature for grafting to occur after 24h. If we compare the work carried out on SAMs by Huang et al.[40], Hyun et al.[22] and Prucker et al.[20], where grafting is carried out at 60°C, the thickness of the grafted polystyrene is limited to 80 nm after 25h. This correlates to the fact that at this temperature, the half-life of the azobis initiator equals 20h[20]. When temperature is further lowered, much thicker layers are obtained but very long reaction time is required.

A summary of the results obtained in this thesis are presented in Table V-10 along with those of other groups mentioned above.

Table V-10 - Comparison of different conditions used for graft polymerisation of styrene onto a surface using immobilized azobis initiators

Surfaces	Conditions	Maximum thickness obtained of grafted PS (nm)	Rate ($nm.h^{-1}$)	Reference
PFPA plasma polymer	90°C – 24h	78	3.25	Chapter V
SAM on silica gels	60°C – 14h	40	2.86	Prucker et al.[20]
SAM on gold	65°C – 24h	20	0.83	Hyun et al.[22]
SAM on aluminium oxide	60°C – 12h	40	3.33	Huang et al.[40]
SAM on poly-siloxane	60°C – 24h	80	3.33	
SAM on silicone oxide	60°C – 12h	60	5	Prucker et al.[74]
	50°C – 96h	200	2.08	

From these results, it can be seen that after 24h, whichever the substrate, grafted layers of polystyrene can only reach 80 nm in thickness. To obtain thicker films, longer reaction times are required. However, the advantage of using plasma polymer + azobis as the substrate appears to be the most straight forward method as SAMs appear to need special treatment to ensure they are inert to subsequent grafting.

V.4.2. Polymerisation of styrene onto pentafluorophenyl acrylate plasma polymer via free radicals

One of the characteristics of plasma irradiation is the effective energy transfer to a solid surface to create stable free radicals on a variety of polymer surface[75]. Plasma-induced surface radicals thus formed permit reactions for surface modifications in several different ways such as crosslinking by activated species of inert gas, surface graft and/or block copolymerisation, and incorporation of functional groups.

The presence of trapped free radicals in pulsed plasma polymerised pentafluorophenyl acrylate film is enhanced by resonance stabilization (Scheme V-3).

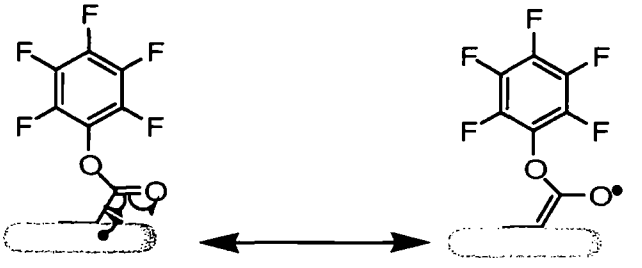

Scheme V-3 – Example of resonance stabilization of poly(pentafluorophenyl acrylate) radical

The diphenylpicrylhydrazyl method (DPPH, a free radical scavenger) was used to quantify the amount of free radicals present in the plasma polymer film. The surface density of free radicals in pentafluorophenyl acrylate plasma polymer was found to be $13 \pm 1 \times 10^{-9}$ mol.cm^{-2}. This value cannot be directly compared to any other from the

literature as the amount of free radicals present in a plasma polymer depends upon many factors[55] such as monomer, flow rate, duty cycle, etc... However, the value found for PFPA plasma polymer is of the same order of magnitude as the value found by Teare et al.[76] for maleic anhydride plasma polymer. Indeed, the surface density of free radicals on maleic anhydride plasma polymer was evaluated according to the same method and found to be $1 \pm 1 \times 10^{-9}$ mol.cm^{-2}. XPS measurements showed the introduction of nitrogen on the plasma polymer surface, thus confirming covalent attachment of DPPH at the surface after reaction with trapped free radicals. Extending the reaction time from 3 to 18 h did not show any increase in nitrogen surface concentration, indicating that all free radicals available were quenched after the 3 h - reaction time chosen.

The graft polymerisation of styrene is likely to be concentrated at radical sites located at or near the surface, where resonance and polar effects will help to stabilize the intermediate radical[24] (Scheme V-4). The resultant pentafluorophenyl acrylate - styryl radical intermediate can then participate in conventional styrene graft polymerisation from the surface until eventually termination occurs by either radical recombination or disproportionation reaction pathways[24].

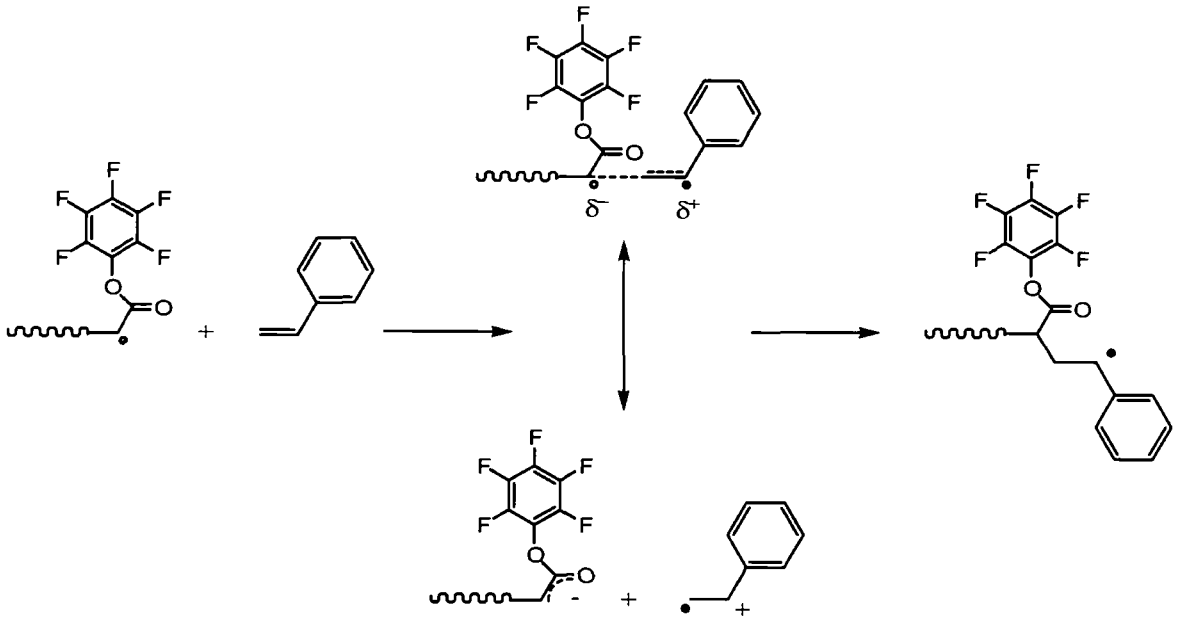

Scheme V-4 - Resonance Stabilization of Reaction Intermediate between Pentafluorphenyl acrylate radical and Styrene

Graft polymerisation of styrene onto pulsed plasma polymerised pentafluorophenyl acrylate is found to be more efficient as temperature is increase (from 75°C to 120°C). Indeed, XPS analysis of the grafted surface shows that over 90°C, after 3h, very little fluorine is detectable (Table V-7). However, some oxygen impurities seem to remain in the film even when temperature or reaction time is increased. This can be attributed to air coming in contact with the reaction mixture. The carbon envelope confirms the formation of a polystyrene layer, since only one type of carbon is present at the surface of the plasma polymer film (Figure V-6). Infra-red spectrum of the surface also corroborates the results observed by XPS (Figure V-7).

The polystyrene films grown on PFPA plasma polymer surfaces are homogeneous, and of controllable thickness. At temperatures below 90°C, polymerisation seems to be very slow since no change in thickness is observed after 3 or 6h. When temperature is set at 90°C, polymerisation is faster and a significant increase in thickness is observed

when reaction time is doubled. When temperature is further increased, the polymerisation rate also increased. A plateau seems to be reached at 105°C, since no noticeable difference is observed in the thickness of the polystyrene layer when temperature is brought up to 120°C. However, for all the temperatures used in these experiments, the thickness of the grafted polymer doubled as the reaction time varied from 3 to 6h.

When temperature is set at 105°C, the thickness of the polystyrene layer increased nearly linearly with time up to 10h (polymerisation rate of 10 $nm.h^{-1}$). Then it reaches slowly a plateau value of 100 nm for reaction time over 15 h. Thicker polymer brushes could not be generated by free-radical polymerisation since termination reaction occurs rather rapidly. These values for grafted polystyrene thicknesses are very similar to that obtained by Prucker et al.[20,74], Hyun et al.[22] and Huang et al.[40] who used free radical polymerisation with azobis as initiators to graft polystyrene onto SAMs.

In direct contrast to free radical polymerisation, 'living', also called controlled, free radical polymerisation have been used to aim at better control over the thickness of polymer brushes. Teare et al.[76] and Husseman et al.[77] employed nitroxide-mediated polymerisation to achieve grafted polystyrene layers up to 611 nm in 16 h for the first group and up to 120 nm in 24 h for the second. The main drawback of this method is the high temperature required and maintained over long period of time which might present a problem for sensitive surfaces. Baum et al.[78] showed that using RAFT (Reversible addition–fragmentation chain transfer) polymerisation, using temperature similar to that employed with azobis initiators (i.e. 60°C), polystyrene and polymethylmethacrylate brushes could be obtained after 24-48h for the first monomer and 12-24h for the second with thicknesses ranging from 11 to 28nm. The main drawback of the RAFT method is

that the thickness of the polymer brushes are limited by the rate of fragmentation of the initiator and of the polymer adducts.

The method which attracted most interest recently is the ATRP (Atom Transfer Radical Polymerisation) with which a wide range of thicknesses has been achieved for grafted polymers. In organic media, Teare et al.[79] grew thicker brushes (170 nm in 8h) using a temperature of 90°C. In aqueous media, where ATRP is known to be more rapid[79], a wider range of thicknesses have been obtained at room temperature. Yu et al. achieved polyglycidyl methylmethacrylate brushes of 28 nm after 6h[80], Brown et al. formed oligo(ethylene glycol) methacrylates brushes of 100 nm after 5h[81], Teare et al. reached poly-N-isopropylacrylamide brushes of 380 nm after 90h[79] and Moya et al. developed polyelectrolyte brushes with [2-(methacryloyloxy)ethyl]trimethylammonium of up to 27 nm in 5h[82]. Although ATRP produces highly controllable molecular weight and narrow polydispersity, and can be carried out at relatively low temperature and in aqueous media, there are still some monomers which will not polymerise under these conditions, such as acrylamide. Moreover, the initiators and the catalysts required may be quite expensive.

In numerous applications (adhesives[83,84], gas separation membranes[85], stimuli-responsive surfaces[3], biocompatible surfaces[86]...), small thicknesses are sufficient to endow a material with attractive surface properties. The method using trapped free radicals in plasma polymer offers the great advantage over the aforementioned methods of not needing any extra chemical compounds to grow polymer brushes.

The free radical nature of the graft polymerisation of styrene onto PFPA plasma polymer is verified using DPPH. Indeed, heating the pentafluorophenyl acrylate pulsed plasma polymer surface in the presence of DPPH gave rise to the capping of trapped

radical sites at the surface, thereby inhibiting styrene graft polymerisation. Thus, after 6 h at 105°C, the thickness of the polystyrene layer onto PFPA plasma polymer is four times bigger than that onto PFPA after reaction with DPPH (Table V-9). The polystyrene layer at the surface of PFPA + DPPH can be attributed to two causes. The first one is the irreversible absorption of polystyrene which could not be removed by soxhlet extraction, as observed on bare silicon wafer (see Table V-5). The second is to be attributable to subsurface trapped radicals migrating to the surface via thermal rearrangement of the plasma polymer[76].

V.4.3. Comparison between the two method of initiation

When azobis is used to initiate graft polymerisation of styrene on plasma polymers, trapped free radicals still remain within the bulk of the plasma polymer. Both can then initiate graft polymerisation. If we compare the thickness of the grafted styrene for both methods at the same temperature (Table V-11) after 3, 6 and 24 h, we do not observe any major difference. This seems to indicate that trapped free radicals are the major source of initiators and that the presence of azobis molecules at the surface of the plasma polymer has little influence over the grafting rate of styrene.

Table V-11 - Thickness (in nm) of polystyrene grafted onto pentafluorophenyl acrylate plasma polymer (10 µm / 20 ms – 20 W) with and without attachment of 2,2'-azobis(2-methylpropionamidine) dihydrochloride, polymerisation carried out at 90°C.

Surface	Time		
	3 h	6 h	24 h
PFPA	7 ± 8	35 ± 5	62 ± 8
PFPA + Azobis	15 ± 1	40 ± 1	78 ± 6

V.5. CONCLUSIONS

The synthesis of polymer brushes onto pentafluorophenyl acrylate plasma polymer was investigated via two methods. The first method entailed the introduction of azo initiators by nucleophilic substitution onto the surface followed by thermal polymerisation of styrene. Despite the low reaction yield (17.5%) of the attachment of the azobis compound, uniform polystyrene films could be produced. With this method, films with a thickness up to 78 nm were obtained. The second method used trapped free radicals within the plasma polymer film as initiators. Uniform polystyrene brushes were obtained with slightly higher oxygen impurities that with the first method.

However, at the same reaction temperature, no difference was observed between the two methods with regards to the polymerisation rate of styrene. Trapped free radicals present in the plasma polymer film are the major source of initiators and the use of azobis does not appear to have any effect.

When no azobis was used, films up to 100 nm were obtained but for a higher temperature than when azo initiators were used. However, the second method offers the great advantage to be a one-step process and provides a higher polymerisation rate.

When films up to 100 nm are desirable and if monomer allows, polymer brushes synthesised using trapped free radicals in plasma polymer films is the method of choice as it is a substrate independent method which does not require any additional reagent as opposed to controlled polymerisation conditions.

V.6. REFERENCES

1 - Edmondson, S.; Osborne, V.L.; Huck, W.T.S., *Chem. Soc. Rev.* **2004**, 33, 14–22

2 - Zhao, B.; Brittain, W.J., *Prog. Polym. Sci.* **2000**, 25, 677–710

3 - Jeong, B.; Gutowska, A., *Trends Biotechnol.* **2002**, 20, 305-311

4 - Rackaitis, M.; Strawhecker, K.; Manias, E., *J. Polym. Sci., Part B: Polym. Phys.* **2002**, 40, 2339-2342

5 - Kim, S.Y.; Cho, S.M.; Lee, Y.M.; Kim, S.J., *J. Appl. Polym. Sci.* **2000**, 78, 1381–1391

6 - Rühe, J.; Ballauff, M.; Biesalski, M.; Dziezok, P.; Gröhn, F.; Johannsmann, D.; Houbenov, N.; Hugenberg, N.; Konradi, R.; Minko, S.; Motornov, M.; Netz, R.R.; Schmidt, M.; Seidel, C.; Stamm, M.; Stephan, T.; Usov, D.; Zhang, H., *Adv. Polym. Sci.* **2004**, 165, 79-150

7 - Hadziionnou, G.; Patel, S.; Granick, S.; Tirrel, M., *J. Am. Chem. Soc.* **1986**, 108, 2869-2876

8 - Belder, G.F.; Ten Brinke, G.; Hadziioannou, G., *Langmuir* **1997**, 13, 4102-4105

9 - Balastre, M.; Li, F.; Schorr, P.; Yang, J.; Mays, J. W.; Tirrel, M. V., *Macromol.* **2002**, 35, 9480-9486

10 - Jordan, R.; Graf, K.; Riegler, H., *Chem. Commun.* **1996**, 9, 1025-1026

11 - Zhao, W.; Krausch, G.; Rafailovich, H.; Sokolov, J., *Macromol.* **1994**, 27, 2933-2935

12 - Fleer, G.J.; Cohen Stuart, M. A.; Scheutjens, J. M. H.; Cosgrove, T.; Vincent, B., *Polymers at interfaces*, Chapman & Hall, London, 1993

13 - Biesalski, M.; Rühe, J., *Macromol.* **2003**, 36, 1222-1227

14 - Jordan, R.; Ulman, A.; Kang, J.G.; Rafailovich, M.H.; Sokolov, J., *J. Am. Chem. Soc.* **1999**, 121, 1016-1022

15 - Zhou, Q.; Wang, S.; Fan, X.; Advincula, R.; Mays, J., *Langmuir* **2002**, 18, 3324-3331

16 - Jordan, R.; Ulman, A., *J. Am. Chem. Soc.* **1998**, 120, 243-247

17 - Zhao, B.; Brittain, W. J., *Macromol.* **2000**, 33, 342-348

18 - Weck, M.; Jackiw, J. J.; Rossi, R R.; Weiss, P. S.; Grubbs, R. H., J. *Am. Chem. Soc.* **1999**, 121, 4088-4089

19 - Juang, A.; Scherman, O. A.; Grubbs, R. H.; Lewis, N.S., *Langmuir* **2001**, 17, 1321-1323

20 - Prucker, O.; Rühe, J., *Macromol.* **1998**, 31, 592-601

21 - Fujiki, K.; Sakamoto, M.; Yoshida, A.; Maruyama, H., J. *Polym. Sci., Part A: Poly. Chem.* **1999**, 37, 2121-2128

22 - Hyun, J.; Chilkoti, A., *Macromol.* **2001**, 34, 5644-5652

23 - Hu, S.; Brittain, W.J., *Macromol.* **2005**, 38, 6592-6597.

24 - Stevens, M.P. *Polymer chemistry: an introduction*; 3rd Ed.; Oxford University Press: New York, 1999

25 - Bartlett, P.D.; Nozaki, K., *J. Am. Chem. Soc.* **1946**, 68, 1495-1504

26 - Hunt, M. U.S. Patent 2,471,959, 1948

27 - Cokbaglan, L.; Arsu, N.; Yagci, Y.; Jockusch, S.; Turro, N.J., *Macromol.* **2003**, 36, 2649-2653

28 - Sarac, A.S., *Prog. Polym. Sci.* **1999**, 24, 1149-1204

29 - Heuts, J.P.A.; Forster, D.J.; Davis, T.P., *Macromol. Rapid Commun.* **1999**, 20, 299-302

30 - Glöckner, P.; Ritter, H., *Macromol. Chem. Phys.* **2000**, 201, 2455–2457

31 - Moad, G.; Solomon, D.H., *The chemistry of free radical polymerisation*, Pergamon: Oxford, 1995

32 - Elvira, C.; Levenfeld, B.; Vázquez, B.; San Román, J., *J. Polym. Sci., Part A: Polym. Chem.* **1996**, 34, 2783-2789

33 - Brenner, A.R. ; Voit, B.I., *Macromol. Chem. Phys.* **1996**, 197, 2673 - 2689

34 - Mayo, F.R.; Gregg, R.A.; Matheson, M.S., *J. Am. Chem. Soc.* **1951**, 73, 1691-1700

35 - Matheson, M.S.; Auer, E.E.; Bevilacqua, E.B.; Hart, E.J., *J. Am. Chem. Soc.* **1951**, 73, 1700-1706

36 - Kodama, S.; Matsushima, Y.; Ueyoshi, A.; Shimidzu, T.; Kagiya, T.; Yuasa, S.; Fukui, K., *J. Polym. Sci.* **1959**, 41, 83-95

37 - Madruga, E.L.; San Roman, J.; Lavia, M.A.; Fernandez Monreal, C., *Macromol.* **1984**, 17, 989-992

38 - Matheson, M.S.; Auer, E.E.; Bevilacqua, E.B.; Hart, E.J., *J. Am. Chem. Soc.* **1951**, 73, 5395-5400

39 - Engel, P.S., *Chem. Rev.* **1980**, 80, 99-150

40 - Huang, W.; Skanth, G.; Baker, G.L.; Bruening, M.L., *Langmuir* **2001**, 17, 1731-1736

41 - Krstina J.; Moad G.; Willing R.I.; Danek S.K.; Kelly D.P.; Jones S.L.; Solomon D.H., *Eur. Polym. J.* **1993**, 29, 379-388

42 - Talât-Erben, M.; Bywater, S., *J. Am. Chem. Soc.* **1955**, 77, 3712-3714

43 - Roux, S.; Duwez, A.-S.; Demoustier-Chamagne, S., *Langmuir* **2003**, 19, 306-313

44 - Ista, L.K.; Mendez, S.; Pérez-Luna, V.H.; López, G.P., *Langmuir* **2001**, 17, 2552-2555

45 - Motornov, M.; Minko, S.; Eichhorn, K.-J.; Nitschke, M.; Simon, F.; Stamm, M., *Langmuir* **2003**, 19, 8077-8085

46 - Tsubokawa, N.; Kobayashi, M.; Ogasawara, T., Prog. Org. Coat. **1999**, 36, 39-44

47 - Prucker, O.; Habicht, J.; Park, I.-J.; Rühe, J., *Mater. Sci. Eng., C* **1999**, 8-9, 291-297

48 - Magat, M. US Patent 3,201,336, 1965

49 - Bhattacharya, A., *Prog. Polym. Sci.* **2000**, 25, 371–401

50 - Nho, Y.C.; Jin, J.-H., *J. Appl. Polym. Sci.* **1997**, 63, 1101-1106

51 - Bamford, C.H.; Jenkins, A.D.; Ward, J.C., *Nature* **1960**, 186, 712 – 713

52 - Osada, Y.; Iriyama, Y., *Thin Solid Films* **1984**, 118, 197-202

53 - Inagaki, N.; Tasaka, S.; Masumoto, M., *Macromol.* **1996**, 29, 1642-1648

54 - Suzuki, M.; Kishida, A.; Iwata, H.; Ikada, Y., *Macromol.* **1986**, 19, 1804-1808

55 - Yasuda, H. *Plasma Polymerization*; Academic Press: London, 1985

56 - Kuzuya, M.; Kawaguchi, T.; Mizutani, S.; Okuda, T., *J. Polym. Sci., olym. Lett.* **1985**, 23, 69-72

57 - Kuzuya, M.; Kawaguchi, T.; Nakanishi, M.; Okuda, T., *J. Chem. Soc., Faraday Trans. I* **1986**, 82, 1441-1448

58 - Kuzuya, M.; Kawaguchi, T.; Yanagihara, Y.; Nakai, S.; Okuda, T., *J. Polym. Sci., Polym. Chem.* **1986**, 24, 707-713

59 - Ji, G.; Fang, J. ; Cai, S. ; Xue, G., *Appl. Surf. Sci.* **1994**, 81, 63-68

60 - Yang, M.-R.; Chen, K.-S., *Mater. Chem. Phys.* **1997**, 50, 11-14

61 - Teare, D.O.H.; Schofield, W.C.E.; Roucoules, V.; Badyal, J.P.S., *Langmuir* **2003**, 19, 2398-2403

62 - Johnson, D.R.; Osada, Y.; Bell, A.T.; Shen, M., *Macromol.* **1981**, 14, 118-124

63 - Tabet, F. M.; McGahan, W. A. *Thin Solid Films* **2000**, 370, 122-127

64 - Hesse, R.; Chassé, T.; Szargan, R. *Fresenius' J. Anal. Chem.* **1999**, 365, 48-54

65 - Beamson, G.; Briggs, D. In *High-Resolution XPS of Organic Polymers: The Scienta ESCA300 Database*; John Wiley & Sons: New York, 1992

66 - Lin-Vien, D.; Colthyp, N.B.; Fateley, W.G.; Grasselli, J.G. In *The Handbook of Infrared and Raman Characteristic Frequencies of Organic Molecules*; Academic Press: New York, 1991

67 - Briggs, D.; Seah, M. P. In *Practical Surface Analysis*, 2nd edition, Vol. 1, John Wiley & Sons, Chichester, 1990

68 - Clark, D.T.; Dilks, A. *J. Polym. Sci. A* **1977**, 15, 15

69 - Molyneux, P. *Songklanakarin J. Sci. Technol.* **2004**, 26, 211-219

70 - Ayscough, P.B.; Brice, M.C. *J. Chem. Soc. B* **1971**, 491-498

71 - Yurkanis Bruice, P. In *Organic Chemistry, 4th ed.*; Pearson Education Inc.: Upper Saddle River, NJ; 2004

72 - Sutherland, I.; Sheng, E.-S.; Brewis, D.M.; Heath, R.J. *J. Mater. Chem.* **1994**, 4, 683-687

73 - Biederman, H. In *Plasma Polymer Films*, Imperial College Press: London, 2004

74 - Prucker, O.; Rühe, J. *Langmuir* **1998**, 14, 6893-6898

75 - Hudis, M. In *Techniques and Applications of Plasma Chemistry*, Hollahan, J. R., Bell, A. T., Eds.; Wiley: New York, 1974

76 - Teare, D.O.H.; Schofield, W.C.E.; Garrod, R.P.; Badyal, J.P.S., *Langmuir* **2005**, 21, 10818-10824

77 - Husseman, M.; Malmström, E.M.; McNamara, M.; Mate, M.; Mecerreyes, D.; Benoit, D.G.; Hedrick, J.L.; Mansky, P.; Huang, E.; Russell, T.P.; Hawker, C.J. *Macromol.* **1999**, 32, 1424-1431

78 - Baum, M.; Brittain, W.J., *Macromolecules* **2002**, 35, 610-615

79 - Teare, D.O.H.; Barwick, D.C.; Schofield, W.C.E.; Garrod, R.P.; Ward, L.J.; Badyal, J.P.S, *Langmuir* **2005**, 21, 11425-11430

80 - Yu, W.H.; Kang, E.T.; Neoh, K.G., *Langmuir* **2004**, 20, 8294-8300

81 - Brown, A.A.; Khan, N.S.; Steinbock, L.; Huck, W.T.S., *Eur. Polym. J.* **2005**, 41, 1757–1765

82 - Moya, S.E.; Brown, A.A.; Azzaroni, O.; Huck, W.T.S., *Macromol. Rapid Commun.* **2005**, 26, 1117–1121

83 - Raphael, E. ; de Gennes, P.G., *J. Phys. Chem.* **1992**, 96, 4002-4007

84 - Retsos, H.; Gorodyska, G.; Kiriy, A.; Stamm, M.; Creton, C., *Langmuir* **2005**, 21, 7722-7725

85 - Balachandra, A.M.; Baker, G.L.; Bruening, M.L., *J. Membr. Sci.* **2003**, 227, 1-14

86 - Andruzzi, L.; Senaratne, W.; Hexemer, A.; Sheets, E.D.; Kramer, E.J.; Baird, B.; Ober, C.K., *Langmuir* **2005**, 21, 2495-2504

VI

CHAPTER SIX

Plasma polymerisation and free radicals generation

VI.1. INTRODUCTION

During plasma polymerisation, the constant ion bombardment of the growing film gives rise to the formation of free radicals in the plasma polymer film[1]. The trapping of these radicals results from the imbalance between production rate and consumption rate of these radicals during the polymerisation process[2]. Yasuda showed that such radicals could induce graft polymerisation when put in the presence of a monomer at elevated temperature[3]. However, graft polymerisation on such plasma polymers has scarcely been studied and most studies concentrated on grafting of vinyl monomer onto continuous wave plasma polymers[4,5,6,7,8]. Teare et al.[9] showed that graft polymerisation on maleic anhydride plasma polymer was more effective on pulsed-plasma polymers than on continuous wave ones due to the better retention of the maleic groups[10]. They proposed a free radical polymerisation mechanism using stabilised initiating radicals situated at the surface. The thickness and patterning of the grafted polymer is found to be easily controllable.

Yasuda states that the amount of trapped free radicals varies with the type of monomer and conditions of glow discharge[3]. However, the influence of the chemical nature of the monomer along with that of the duty cycle and the flow rate over the density of trapped free radicals generated has not yet been studied in detail. This work aims at understanding this process of free radicals generation and how this affects the subsequent grafting of styrene on such plasma polymers.

VI.2. EXPERIMENTAL

VI.2.1. Plasma polymerisation

Monomers (see Table VI-1) were loaded into sealable glass tubes and further purified by freeze-thaw cycles to ensure complete degassing prior to plasma polymerisation.

Table VI-1 – List of monomers used for plasma polymerisation

Monomer	Abbreviation	Supplier	Purity (%)
Glycidyl methacrylate[11]	GMA	Aldrich	97
Maleic anhydride[12]	MA	Aldrich	95
N-acryloylsarcosine methyl ester[13]	NASME	Aldrich	97
Pentafluorophenyl acrylate*	PFPA	Apollo Scientific	98
Styrene[14]	S	Aldrich	99
4-vinyl aniline[15]	4-VA	Aldrich	97
4-vinyl benzyl chloride[16]	4-VBC	Aldrich	97

* Plasma polymerisation of PFPA is original work of this thesis and has been fully characterised in chapter III. It has been included in this chapter to widen the range of plasma polymers studied. Conditions for other monomers may vary from the literature as better retention was observed for the chosen conditions.

Pulsed plasma polymerisation of each monomer was undertaken in a cylindrical glass reactor (4.5 cm diameter, 460 cm^3 volume, 3.5×10^{-4} mbar base pressure, $< 3 \times 10^{-9}$ mol/s leak rate) surrounded by a copper coil (4 mm diameter, 10 turns, located 15 cm from the gas inlet) connected to a 13.56 MHz radio frequency (RF) power supply and an L-C matching network. The plasma chamber was located inside a Faraday cage and for NASME and 4-VA also in a temperature-controlled oven set respectively at 50 and 45°C. A 30 $L.min^{-1}$ rotary pump attached to a liquid nitrogen cold trap was used to evacuate the reactor, while the system pressure was monitored with a Pirani gauge. All fittings were grease-free. During pulsed plasma deposition, the RF power source was triggered by a signal generator, and the pulse shape monitored with an oscilloscope.

Prior to each deposition, the apparatus was scrubbed with detergent, rinsed in 2-propanol, and oven dried. Further cleaning entailed running a continuous wave air plasma at 0.2 mbar pressure and 40 W power lasting 30 min. Next, silicon wafers (MEMC Materials Inc) and/or gold chips were inserted into the reactor and the reactor pumped down to base pressure. At this stage, a continuous flow of monomer vapour

was introduced into the chamber for 5 min prior to plasma ignition. The duty cycle corresponded to continuous wave bursts during the on-time (t_{on}), followed by an off-period (t_{off}). Upon completion of deposition, the RF generator was switched off, and the monomer allowed to purge through the system for a further 5 min prior to evacuating to base pressure and venting to atmosphere. The plasma polymerisation conditions for each monomer are reported in Table VI-2.

Table VI-2 – Plasma polymerisation conditions for each monomer

Monomer	Pressure (mbar)	Power (W)	t_{on} (μs)	t_{off} (ms)	Deposition time (min)
Glycidyl methacrylate	0.2	40	20	20	20
Maleic anhydride	0.2	4	10	1.2	30
N-acryloylsarcosine methyl ester	0.1	30	20	5	15
Pentafluorophenyl acrylate	0.2	20	10	20	30
Styrene	0.2	40	100	4	1
4-vinyl aniline	0.15	20	100	4	10
4-vinyl benzyl chloride	0.2	16	20	1.2	2

VI.2.2. Free radicals quantification

Free radicals quenching and quantification studies employed diphenylpicrylhydrazyl[17,18] (DPPH, 95%, Aldrich) as a free radical scavenger. This entailed immersion of each plasma polymer coated substrate (1.5 x 1.5 cm^2) into a 5 mL solution of DPPH 1.5 x 10^{-4} M in toluene (99%, Fisher Scientific). The reaction tube was sealed, and any dissolved gases were removed by multiple freeze-pump-thaw cycles. The DPPH solution was then heated in an oil bath at 80 °C for 3 h, followed by removal of the substrate and rinsing in clean toluene. The adsorption of the DPPH solutions before and after reaction with the plasma polymer coated surfaces were measured on a UV-vis spectrophotometer at a wavelength of 520 nm for which DPPH exhibits maximum

adsorption. Density of trapped free radicals at the surface of plasma polymer was then calculated from absorbance measurements using the Beer-Lambert law (Equation VI-1).

Equation VI-1 $$A = \varepsilon \times l \times c$$

Where l is the distance travelled by the light through the material (= path length), ε is the absorbance coefficient or the molar absorptivity of the absorber and c is the concentration of absorbing species in the material.

The extinction coefficient for DPPH was measured to equal 10527 $L.mol^{-1}.cm^{-1}$, which is similar to values previously obtained[19].

Absorbance of solutions of DPPH in toluene, DPPH in toluene heated without substrate (control experiment) and DPPH in toluene heated with the PFPA plasma polymer are then measured at a wavelength of 520 nm. From these values, the surface density of trapped free radicals in PFPA plasma polymer can be calculated using Equation VI-2.

Equation VI-2 $$d = \frac{[DPPH]_{Blank} - [DPPH]_{Substrate}}{V \times S}$$

where d : surface density of free radicals ($mol.cm^{-2}$)

$[DPPH]_{Blank}$: concentration of DPPH remaining after heating without substrate ($mol.L^{-1}$)

$[DPPH]_{Substrate}$: concentration of DPPH remaining after heating with substrate ($mol.L^{-1}$)

V : volume of DPPH solution (L)

S : surface of the substrate (cm^2)

VI.2.3. Radical polymerisation

Plasma polymer coated surfaces were introduced in a sealed glass tube containing styrene (99%, Aldrich) dissolved in toluene (99%, Fisher Scientific) at a concentration of 4 M. Multiple freeze-pump-thaw cycle were then carried out to remove any dissolved gases. Next, the tube was placed into an oil bath at a set temperature of 105°C for 3h to facilitate thermal polymerisation. Subsequently, any loosely bound polystyrene attached to the substrate surface was removed by soxhlet extraction either in tetrahydrofuran (>99%, Fisher Scientific), in toluene (99%, Fisher Scientific) or dichloromethane (>99%, Fisher) for 16 h. Corresponding control experiments with uncoated substrates were also undertaken.

VI.2.4. Analysis

A spectrophotometer (nkd-6000, Aquila Instruments Ltd.) was used for plasma polymer film thickness measurements. The obtained transmittance-reflectance curves (350-1000 nm wavelength range) were fitted to a Cauchy material model using a modified Levenberg-Marquardt algorithm[20].

Contact angle analysis on the pulsed plasma deposited films was carried out using a video capture system (ASE Products, model VCA2500XE). 2.0 μL sessile droplets of deionised water were placed onto the polymer surface and contact angle measurements taken at 20°C.

Chemical characterization by X-ray photoelectron spectroscopy (XPS) was undertaken using a VG Microtech electron spectrometer equipped with a non-monochromated Mg Kα X-ray source (1253.6 eV) and a concentric hemispherical analyzer (VG 100 AX) operating in the constant analyzer energy mode (CAE, pass energy = 20 eV for elemental analysis and 50 eV for wide scans). The XPS spectra for

the carbon envelopes were fitted using the convention established for insulating polymers, i.e. C-C bond exhibits a photopeak at a binding energy of 285.0 eV. All the Gaussian components peaks[21] were determined using a linear background and equal full-width at-half-maximum (FWHM) on a Marquardt minimization computer software. Each Gaussian component relates to different carbon bonding, the peaks are centred on the binding energy of the bond of interest as determined by Beamson and Briggs[22]. Instrument sensitivity multiplication factors were taken as C(1s): O(1s): N(1s): Si(2p): F(1s) 1.00: 0.37: 0.56: 096: 0.24.

Surface Fourier transform infrared spectroscopy (FTIR) was performed on gold substrates using an FTIR spectrometer (Perkin-Elmer, model Spectrum One) equipped with a liquid nitrogen cooled MCT detector operating at 4 cm^{-1} resolution over the 700-4000 cm^{-1} range. The instrument was fitted with a reflection-absorption spectroscopy accessory (Specac) and a KRS-5 p-polarizer with the reflection angle set to 84°. All spectra were averaged over 512 scans.

Adsorption measurements were carried out on a Perkin Elmer Lambda 900 UV/VIS/NIR spectrometer. A first, a run was done on the DPPH solution 1.5 x 10^{-4} M in toluene between 480 and 560 nm to establish the wavelength for maximum adsorption. The wavelength was set to be 520 nm.

VI.3. RESULTS

VI.3.1. Study on nature of monomer

VI.3.1.1. Plasma polymerisation

Plasma polymerisation of each of the following monomers was performed (see Scheme VI-1).

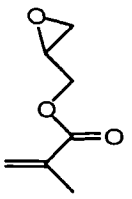

Glycidyl methacrylate

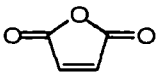

Maleic Anhydride

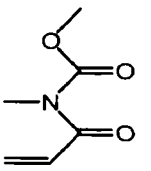

N-Acryloyl Sarcosine Methyl Ester

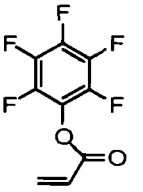

Pentafluorophenyl acrylate

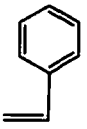

Styrene

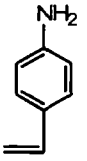

4-Vinyl Aniline

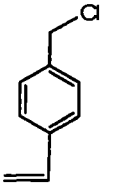

4-Vinyl Benzyl Chloride

Scheme VI-1 – Monomers plasma polymerised

Elemental analysis of the surface of each plasma polymer was done by XPS. The results are presented in Table VI-3. The good agreement between the pulsed plasma deposited films and the theoretical atomic percentages of each of the plasma polymers indicates that polymerisation occurred selectively at the alkene bond, and that functionality of each monomer remained intact during the electrical discharge process. For styrene, 4-vinyl aniline and 4-vinyl benzyl chloride, the presence of oxygen is due to oxidation of the surface after exposure to air.

Table VI-3 – XPS analysis of plasma polymer surfaces

Surfaces		Composition (at. %)				
		C	O	N	F	Cl
GMA	- theoretical	70	30			
GMA	- experimental	69.4 ± 0.5	30.6 ± 0.5			
MA	- theoretical	57.1	22.9			
MA	- experimental	61.8 ± 4.7	38.2 ± 4.7			
NASME	- theoretical	64	27	9		
NASME	- experimental	67.6 ± 2.4	24.5 ± 2.0	7.9 ± 0.4		
PFPA	- theoretical	56.2	12.5		31.3	
PFPA	- experimental	49.7 ± 2.8	12.0 ± 2.3		38.4 ± 3.2	
S	- theoretical	100				
S	- experimental	92.3 ± 3.3	7.7 ± 3.3			
4-VA	- theoretical	88.9		11.1		
4-VA	- experimental	85.4 ± 1.0	4.5 ± 1.9	10.5 ± 1.2		
4-VBC	- theoretical	90				10
4-VBC	- experimental	82.5 ± 5.7	6.3 ± 3.7			11.1 ± 4.7

For further characterisation of the plasma polymers surfaces, the carbon envelopes C (1s) of each of them and their theoretical spectra are presented in Annexe 1.

The IR spectra of each of the plasma polymers confirmed good retention of the monomer functionality within the bulk of the polymer. The characteristic absorption bands of each plasma polymer are presented in Table VI-4[23]. For all plasma polymers, the band initially present in the monomer at around 1610-1640 cm^{-1}, characteristic of the carbon-carbon double-bond, is absent, providing further proof that polymerisation occurred at the C=C bond during the discharge (see spectra in Annexe 1).

Table VI-4 – Characteristic IR absorption bands of each plasma polymer

Plasma polymer	Frequencies (cm^{-1})	Nature of the band
GMA	3060	Epoxide ring C-H stretch
	3000-2900	C-H stretch
	1728	Saturated ester C=O stretch
	1253	Epoxide ring breathing
	908	Antisymmetric epoxide ring deformation
	842	Symmetric epoxide ring deformation
MA	1849	C=O anhydride stretch
	1780	C=O anhydride stretch
	1248 -1240	Cyclic anhydride stretch
	1100 -1050	C-O-C stretch
	958-935	Cyclic unconjugated anhydride
NASME	1749	Ester carbonyl
	1653	Primary amide
	1212	Ester C-O
PFPA	1780	Ester carbonyl
	1513	Fluorinated benzene ring vibration
	1105 - 990	Benzene ring semi-circle stretch & C-F bending
S	3090	Aromatic CH stretching
	1493 - 1450	Benzene ring vibrations
4-VA	3440	Asymmetric amine stretching
	3350	Symmetric amine stretching
	3090	Aromatic CH stretching
	1615	NH_2 deformation
	1500	Para substituted aromatic ring stretching
	1415	$=CH_2$ deformation
	1300	Aromatic C-N stretching
	1170	Para substituted benzene ring stretching
	910	$=CH_2$ wagging
	850	NH_2 wagging
4-VBC	1603 - 1495	Para-substituted benzene ring stretches
	1266	CH_2-Cl wag

VI.3.1.2. Free radicals quantification and radical polymerisation

For each of the plasma polymers mentioned above, quantification of trapped free radicals and growth rate of graft polymerisation of styrene were measured. Best

retention of each of the functionalities of the monomers was ensured before proceeding to any measurements. Results are presented in Table VI-5.

Table VI-5 – Free radical quantification and graft polymerisation growth rate on different plasma polymers

Plasma polymer	Free radicals density ($x10^{-9}$ mol.cm^{-2})	Growth rate (nm.h^{-1})
GMA	11 ± 2	34 ± 2
MA	13 ± 4	10 ± 1
NASME	8 ± 3	46 ± 6
PFPA	11± 3	10 ± 1
S	13 ± 2	11 ± 2
4-VA	32 ± 6	9 ± 3
4-VBC	6 ± 1	9 ± 2

During these experiments it was observed that thickness of the initial plasma polymer did not have an influence over the results. Initial thicknesses were kept between 30 and 130 nm.

VI.3.2. Quenching of free radicals

When polymerisation of styrene is performed on GMA plasma polymer after the surface has been reacted with DPPH, the growth rate graft polymerisation of styrene only reaches 9 nm.h^{-1} compared to 29 nm.h^{-1} obtained with GMA pulsed plasma polymer (Table VI-6). This indicates that when radicals have been quenched by the radical scavenger, lower polymerisation rate are achieved.

Table VI-6 – Comparison of styrene polymerisation onto glycidyl methacrylate plasma polymer (20 µm / 20 ms – 40 W) before and after trapping of free radicals (3 h – 105°C)

Surface	Growth rate ($nm.h^{-1}$)
GMA	34 ± 4
GMA + DPPH	19 ± 1

VI.3.3. Influence of time exposure to ambient air

To evaluate the stability of the trapped free radicals and their availability, quantification of free radicals along with polymerisation rate was evaluated through the course of a week for GMA continuous wave plasma polymer (Table VI-7).

Table VI-7 - Free radicals quantification and graft polymerisation growth rate onto GMA continuous wave plasma polymer (3 W – 2 min) as a function of time

Time (days)	Free radicals density ($x10^{-9}$ $mol.cm^{-2}$)	Growth rate ($nm.h^{-1}$)
1	15 ± 2	37 ± 1
2	9 ± 2	35 ± 7
4	15 ± 2	35 ± 3
8	15 ± 2	28 ± 1

After 8 days the amount of free radicals in the plasma polymer does not seem to have varied. After 4 days the growth rate of graft polymerisation of styrene remains constant, but decreases slightly after 8 days.

VI.3.4. Influence of thickness

To verify results observed previously with the different plasma polymers with regards to thickness, graft polymerisation and free radicals quantification were performed onto continuous-wave GMA plasma polymer for various thicknesses (see Table VI-8). This

was achieved simply by increasing the duration of the plasma, all other conditions remained unchanged.

Table VI-8 – Quantification of free radicals and graft polymerisation rate on continuous wave (3W) GMA plasma polymer for various thicknesses

Thickness (nm)	Free radicals density ($x10^{-9}$ mol.cm^{-2})	Growth rate (nm.h^{-1})
18 ± 0	10 ± 4	51 ± 2
26 ± 4	8 ± 3	37 ± 1
45 ± 5	7 ± 1	37 ± 0

VI.3.5. Study on pulsing conditions

The influence of different factors such as on-time of pulsing, power and time of initial continuous wave plasma was studied with glycidyl methacrylate polymer with regards to free radicals density and graft-polymerisation rate of styrene. The influence of these factors over the amount of trapped free radicals has hardly been studied. Labelle et al. studied the influence of the off-time period on the amount of trapped free radicals in hexafluoropropylene oxide plasma polymers[24]. They found that the dangling bond concentration decreased with increasing pulse off time through interaction with a gas phase species. The influence of on-time, discharge power and initial continuous wave duration is investigated.

VI.3.5.1. Influence of on-time

The polymerisation conditions (leak rate, base pressure, monomer pressure, flow rate, power, off-time, etc...) were kept rigorously the same from one run to the other, with the exception of the on-time.

Characterisation of the different plasma polymers was followed by XPS and FTIR. The elemental analysis showed good correlation with theoretical elemental composition (Table VI-9).

Table VI-9 – Elemental composition of GMA as a function of the on-time during plasma polymerisation (P=40W)

GMA on-time (μs)	Composition (at. %)		$C_{epoxide}$ (%)
	C	O	
Theoretical	70	30	28.57
80	71.81	28.19	28.73
40	70.39	29.61	29.43
20	69.78	30.22	28.32
10	70.12	29.88	28.58
5	70.34	30.22	27.70

The carbon envelopes C(1s) of GMA pulsed plasma polymer (off-time 20 ms - P = 40 W) and 3 W continuous-wave present five types of carbon functionalities: $\underline{C}$-CH_x (285.0 eV), H_3C-$\underline{C}$-C(=O)-O (285.7 eV), O-$\underline{C}H_2$-C=O (286.7 eV), $\underline{C}_{epoxide}$ (287.2 eV), and O-$\underline{C}$=O (289.1 eV). In addition the continuous wave plasma polymer presents an additional carbon environment: $\underline{C}$=O (287.8 eV). For all pulsed plasma polymers, the peak assignments are referenced to XPS spectra obtained from conventional solution phase polymerized glycidyl methacrylate[22].

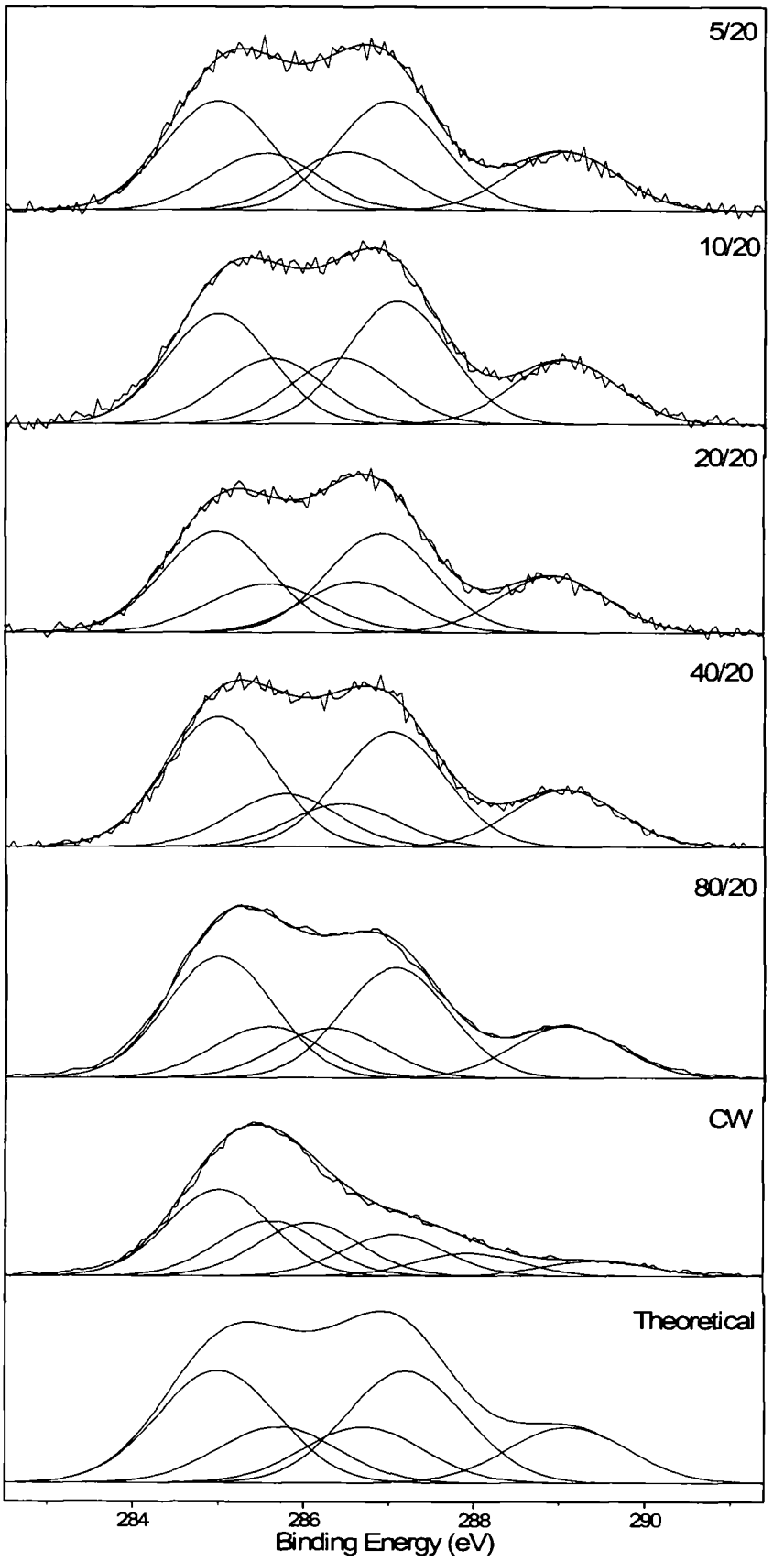

Figure VI-1 – C(1s) XPS spectra of glycidyl methacrylate plasma polymer (off-time = 20 ms – 40 W) for various on-time

The FTIR spectra of the plasma polymers, pulsed (off-time 20 ms – P = 40 w) and CW (3W) confirm good retention of the molecular structure of the starting monomer within the bulk of the coating (Figure VI-2). For glycidyl methacrylate monomer, the following band assignments were made: acrylate carbonyl stretching (1720 cm^{-1}), acrylate C=C stretching (1637 cm^{-1}), epoxide ring breathing (1253 cm^{-1}), antisymmetric epoxide ring deformation (908 cm^{-1}), and symmetric epoxide ring deformation (842 cm^{-1})[11].

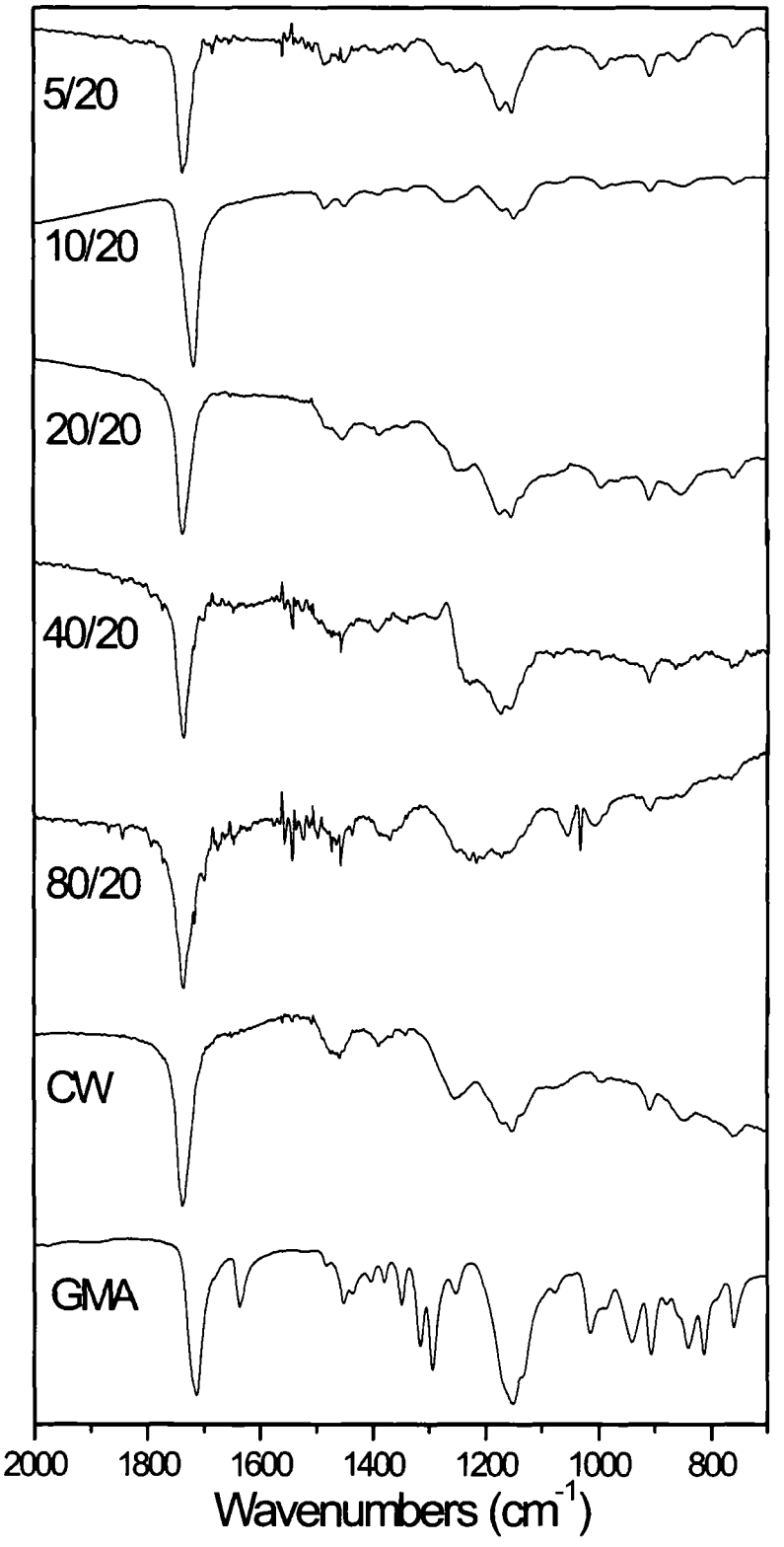

Figure VI-2 – FTIR spectra of GMA continuous (3W) and pulsed plasma polymer (off-time = 20 ms – P = 40 W)

Trapped free radicals quantification and graft polymerisation growth rate results are reported in Table VI-10.

Table VI-10 - Free radicals quantification and graft polymerisation growth rate onto GMA plasma polymer as a function of the on-time during plasma polymerisation

On-time (μs)	Free radicals density ($x10^{-9}$ mol.cm^{-2})	Growth rate (nm.h^{-1})
80	8 ± 7	34 ± 1
40	5 ± 2	34 ± 4
20	1 ± 0	25 ± 4
10	1.5 ± 0.5	23 ± 1
5	5.5 ± 0.5	26 ± 5

As the on-time decreases, the amount of free radicals measured does not vary much. The growth rate of graft polymerisation of styrene seems to decrease slightly but remains within the error margins.

VI.3.5.2. Influence of power

The plasma polymerisation conditions remain exactly the same apart from the input power. Characterisation of the different plasma polymers was followed by XPS and FTIR. The elemental analysis showed that when high power is used, the silicon substrate was not completely covered by the GMA plasma polymer (see Table VI-11). When the power used was too low, no good retention of the epoxide functionalities was seen.

Table VI-11 - Elemental composition of GMA as a function of input power during plasma polymerisation (t_{on} = 20 µs / t_{off} = 20 ms)

GMA power (W)	Composition (at. %)			$C_{epoxide}$ (%)
	C	O	Si	
Theoretical	70	30	0	28.57
80	63.31	28.45	8.24	23.51
60	70.1	27.82	2.08	18.18
40	69.62	30.38	0	33.21
20	70.92	29.08	0	33.76
10	75.65	24.35	0	13.57

The carbon envelopes C(1s) of GMA pulsed plasma polymer (t_{on} = 20 µs - t_{off} = 20 ms) for each of the input power present five types of carbon functionalities: **C**-CH_x (285.0 eV), H_3C-**C**-C(=O)-O (285.7 eV), O-**C**H_2-C=O (286.7 eV), **C**$_{epoxide}$ (287.2 eV), and O-**C**=O (289.1 eV). In addition the pulsed plasma polymer at 10 W input power presents an additional carbon environment: **C**=O (287.8 eV). For all pulsed plasma polymers, the peak assignments are referenced to XPS spectra obtained from conventional solution phase polymerized glycidyl methacrylate[22].

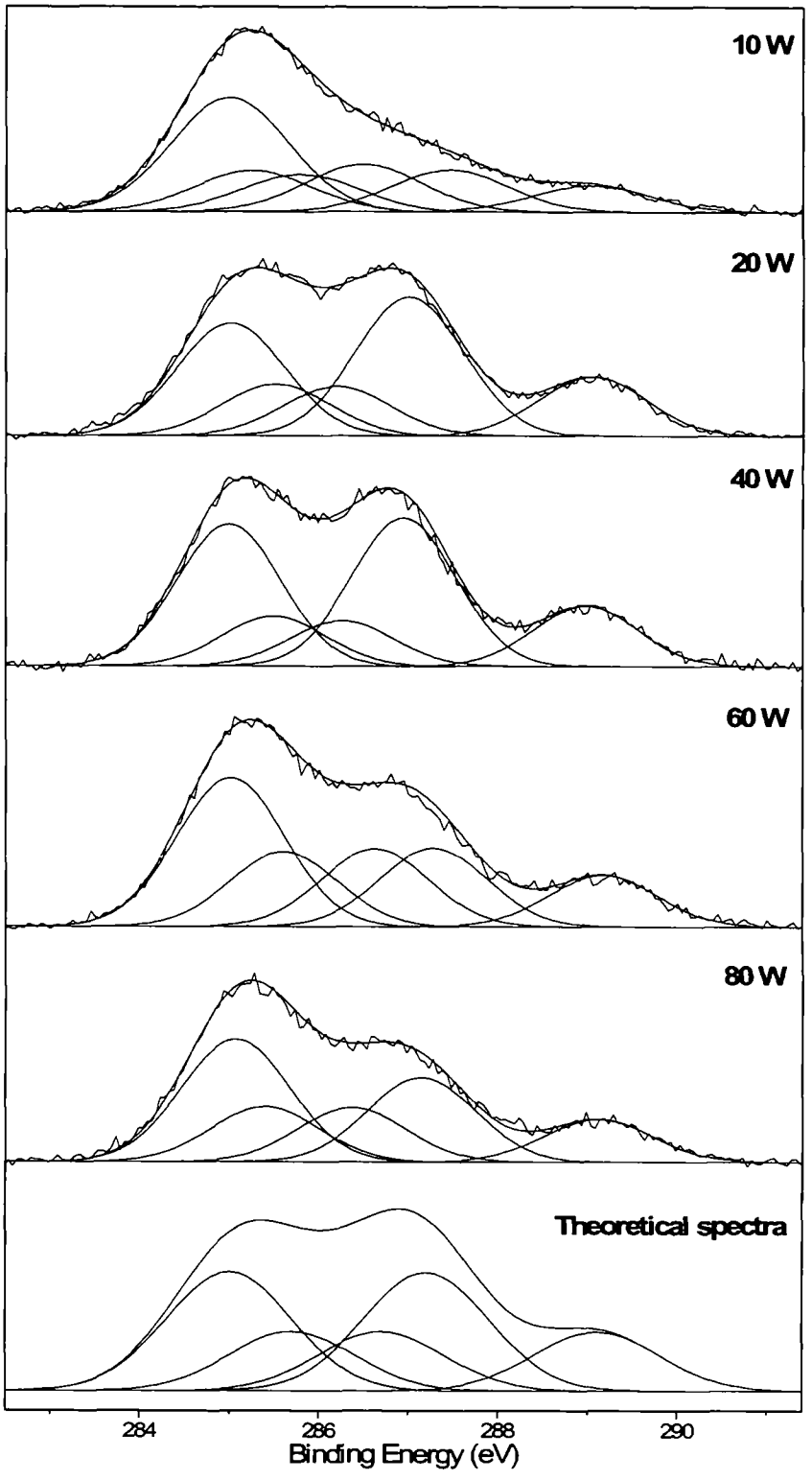

Figure VI-3 - C(1s) XPS spectra of glycidyl methacrylate plasma polymer (t_{on} = 20 µs / t_{off} = 20 ms) for various peak power

The FTIR spectra of the plasma polymers, pulsed (t_{on} = 20 µs - t_{off} = 20 ms) for each of the input power confirm good retention of the molecular structure of the starting

monomer within the bulk of the coating (Figure VI-4). For glycidyl methacrylate monomer, the following band assignments were made: acrylate carbonyl stretching (1720 cm^{-1}), acrylate C=C stretching (1637 cm^{-1}), epoxide ring breathing (1253 cm^{-1}), antisymmetric epoxide ring deformation (908 cm^{-1}), and symmetric epoxide ring deformation (842 cm^{-1})[11].

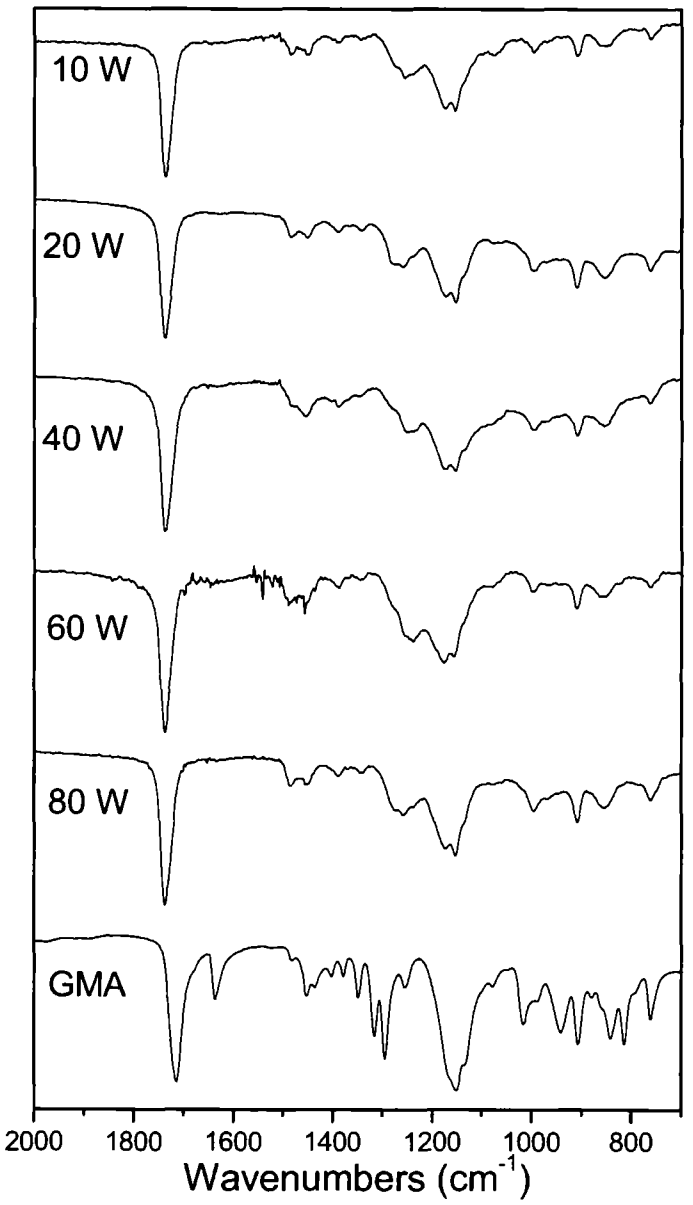

Figure VI-4 - FTIR spectra of GMA pulsed plasma polymer (t_{on} = 20 µs / t_{off} = 20 ms) for various peak power

Trapped free radicals quantification and graft polymerisation growth rate results are reported in Table VI-12.

Table VI-12 - Free radicals quantification and graft polymerisation growth rate onto GMA plasma polymer as a function of the power during pulsed plasma polymerisation (t_{on} = 20 µs / t_{off} = 20 ms – t=4 min)

Power (W)	Free radicals density ($x10^{-9}$ mol.cm^{-2})	Growth rate (nm.h^{-1})
80	9 ± 2	35 ± 0
60	8 ± 3	34 ± 6
40	9 ± 0	35 ± 3
20	9 ± 0	42 ± 3
10	6 ± 2	39 ± 4

As the peak power decreases, the amount of free radicals and the graft polymerisation growth rate of styrene do not vary.

VI.3.5.3. Influence of time of initial continuous wave

To ensure adhesion of the plasma polymer onto the silicon substrate, 50 s continuous wave at 40 W were carried out prior to pulsing. In this set of experiments, the time of the initial continuous wave is varied before pulsing of the plasma with on-time of 20 µs and off-time of 20 ms for 4 min. The amount of free radicals measured by the DPPH method along with the graft polymerisation growth rates of styrene are recorded in Table VI-13.

Table VI-13 - Free radicals quantification and graft polymerisation growth rate onto GMA plasma polymer as a function of the duration of the continuous wave during pulsed plasma polymerisation

Time CW (s)	Free radicals density ($x10^{-9}$ mol.cm^{-2})	Growth rate (nm.h^{-1})
10	9 ± 1	22 ± 2
30	17 ± 3	20 ± 2
50	18 ± 1	35 ± 0
70	16 ± 2	36 ± 1
90	15 ± 2	36 ± 1
110	11 ± 0	31 ± 0

As the duration of the continuous wave prior to pulsing increases, the free radical density remains more or less the same. However, the graft polymerisation rate of styrene increases up to a duration of 50 s, then reaches a plateau value above which the growth rate remains constant and seems to decrease slightly beyond a continuous wave of 110 s.

VI.4. DISCUSSION

VI.4.1. Study on nature of monomer

Yasuda et al. showed that all plasma polymers contained trapped free radicals[1]. Polymer grafting initiated by these radicals on such surfaces has been investigated mainly on continuous-wave plasma polymers where the nature of the radical species was unknown and no relationship could be drawn according to the nature of the plasma polymer itself.

In this study, several monomers, all of which belong to group II as defined by Yasuda et al.[3], were pulsed plasma deposited using their optimum pulsing conditions to have maximum retention of their functionalities. The influence of the nature of the functionality was evaluated with regards to the trapped free radicals density within the pulsed-plasma polymer and the growth rate of grafted styrene.

For all pulsed-plasma polymers but one, the free radical density does not appear to depend upon the nature of the functionalities present. Only 4-VA presents a higher free radical density. When more energy is delivered to a glow discharge, more radicals are created[25]. In the case of 4-VA however, the energy delivered to the discharge is less than that of S for instance and both are chemically very similar. Therefore the conditions of deposition are not sufficient to explain this fact.

In the case of 4-VBC monomer, it would have been expected to yield a plasma polymer with high amount of trapped free radicals. Indeed, the detachment of halogens during plasma polymerisation is known, mainly in the case of fluorine atoms[2], and these also contribute to the formation of free radicals. However, the amount of trapped free radicals in 4-VBC did not differ from that of non-halogen containing monomers.

In the case of PFPA plasma polymers, the lower amount of trapped free radicals can be explained despite the high amount of fluorine atoms in the structure of the monomer. Indeed, this monomer also contains oxygen, which 'poisons' the growth mechanism of cycle II (see Chapter I) therefore reducing the amount of trapped free radicals[26], counterbalancing the enhancing effect of fluorine atoms on the free radicals density.

For three of the monomers (GMA, NASME and 4-VBC), the polymerisation rate of grafted styrene appears not to be related to the amount of free radicals unlike suggested by Teare et al[16]. Indeed, the growth rate of the layer of grafted styrene onto NASME and GMA is 3 to 4-folds higher than that of all the others despite similar free radical densities. 4-VBC presents a similar growth rate to MA, PFPA, S and 4-VA even though its free radical density is three times higher. Availability of these trapped free radicals might also play a role in the polymerisation rate of the grafted styrene.

The nature of the free radicals for S, 4-VA and 4-VBC plasma polymer is very similar, only differing by the group in para-position with regards to the vinyl group. These can affect the stabilisation of the radical by the aromatic ring, however, no difference was observed in the graft-polymerisation rate. This suggests that the group in *para* has little or no influence.

When comparing the styrene-like monomers with MA, the same grafting growth rate is observed despite very different chemical structure. S, 4-VA and 4-VBC present

more hindrance at the surface because of the bulky aromatic group which might prevent graft-styrene to reach the radicals present at the surface. This suggests that styrene-like plasma polymers should yield lower grafting growth rate compared to MA, however no such difference is observed.

PFPA plasma polymer surfaces are also relatively hindered by the benzene ring fully substituted with fluorine atoms. Stabilisation of the radical in this case does not benefit from the aromatic structure within the monomer. But in that case also, similar results were obtained for the free radical density and the grafting growth rate as compared with MA, S and 4-VA.

When comparing GMA and PFPA, the nature of the polymerisable group is the same. This leads to similar surface radicals which are stabilised the same way (see Scheme VI-2). In this case the ester group appears to have an influence over the graft-polymerisation rate. This might be due to the mobility of the ester group around the acrylate function making the free radicals more available to styrene for graft polymerisation to occur. Indeed the bulky fluorinated aromatic ring is less mobile than the alkyl epoxide group and this relates directly to the fact that graft polymerisation on GMA is over 3-fold higher than that of PFPA.

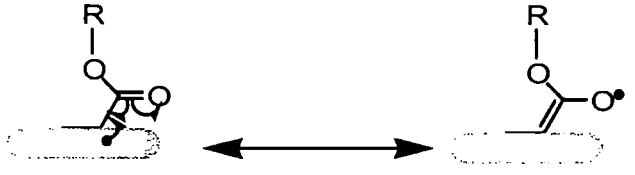

Scheme VI-2– Stabilisation of free radicals of acrylate and methacrylate monomers

In the case of NASME, the nature of the polymerisable group is slightly different from the others. Moreover, the polymerisation was carried out at elevated temperature due to the poor volatility of the monomer, which leads to higher free radicals concentration in the plasma polymer since more energy is brought to the system during

discharge. These two factors can explain why NASME present the highest polymerisation rate of all monomers tested. Moreover, the deposition rate of NASME is lower than that of the other monomers, and Yasuda et al.[27] showed that systems which yields high deposition rate contain small amount of free radicals in the polymer.

Yasuda et al.[2] found that the concentration of trapped free radicals in plasma polymers is closely related to the chemical structure of the monomer. However, the results obtained here suggest that this relationship is not straightforward. Moreover, free radical density does not appear to relate to the graft-polymerisation rate. All monomers were pulsed-plasma polymerised under different conditions of power, on-time, off-time, and this can also have an influence over the amount and the nature of the trapped-free radicals present within the plasma polymer. Also, the availability of these free radicals seems to have an influence over the rate of graft polymerisation.

In these experiments we assumed that all free radicals initiating graft polymerisation were that of the monomer's functionality since, when pulsing the plasma, we obtained very good retention of these functional groups. However, the results suggest that the nature of the free radicals along with their ability to stabilise through resonance is not sufficient to explain the free radical density at the surface or the rate of graft polymerisation. Since plasma polymers present a rough surface[1], it is possible that other kind of free radical present within the plasma polymer (e.g.: peroxides) are available to initiate grafting. Also, since the reaction is carried out in solvent some swelling is to be expected to different extent depending upon the nature of the plasma polymer. This which would allow more of these trapped free radicals to act as initiators, making the comparison more difficult between the monomers.

VI.4.2. Quenching of free radicals

Graft polymerisation onto GMA pulsed plasma polymer after free radicals scavenging using DPPH showed that graft polymerisation rate decreased by 2-fold compared to unreacted GMA pulsed plasma polymer surfaces. This confirms that graft polymerisation is initiated by free radicals. However, the growth rate after quenching does not equal 0. DPPH has been found to be a poor scavenger for oxygen active species[28]. Therefore, other types of free radicals than that of GMA are probably present in the plasma polymer which can also initiate graft-polymerisation to a lesser extent.

VI.4.3. Influence of conditions of plasma polymerisation

Plasma polymers contain high amounts of dangling bonds susceptible to react with atmospheric oxygen and / or water and are responsible for the observed aging effect of such surfaces[1]. Therefore, upon time it is expected that the amount of free radicals at the surface of plasma polymers decreases with time when exposed to ambient air. However, over the course of a week, the radical density at the surface of glycidyl methacrylate pulsed plasma polymer did not decrease. The graft polymerisation rate of styrene on such surfaces was constant for the first 4 days and seemed to decrease slightly after 8 days but not in a significant manner. This suggests that either these trapped free radicals are very stable and / or their reaction with oxygen to form peroxides does not alter their ability to initiate graft polymerisation.

The influence of the thickness of the sub-layer of GMA plasma deposited by continuous wave to ensure adhesion was investigated. The results showed that the amount of free radicals did not vary with the thickness of the deposited layer. However when the thickness was increased from 18 to 26 nm, the graft polymerisation rate decreased. During plasma polymerisation, some free radicals are also created within the

substrate[1,26]. When the plasma polymer layer is too thin, the free radicals on the substrate could initiate graft polymerisation alongside the ones trapped within the plasma polymer. Since more initiators are present, the graft polymerisation rate is increased. This hypothesis is further validated since when increasing further the thickness of the deposited plasma polymer, the rate of graft polymerisation does not increase anymore, only trapped free radicals at the surface of the plasma polymer act as initiators for the subsequent graft polymerisation of styrene.

The amount of free radicals in plasma surfaces depends upon many factors such as nature of the monomer, discharge power, flow rate and duty cycle[1,26,29]. It is expected that when the average power delivered to the system (see Chapter I) is increased the amount of trapped free radicals should also increase. However, varying the input power did not affect the amount of trapped free radicals at the surface of the plasma polymer. Also, it was observed that for some polymers, continuous wave plasma deposition gives rise to higher amount of free radicals than for the corresponding pulsed plasma deposition[3]. Therefore, for those monomers, it is expected to see the production of free radicals proportional to the duration of the discharge (i.e. on-time)[2]. Yet, increasing the on-time during pulsed plasma polymerisation did not seem to affect the amount of free radicals or the polymerisation rate of grafting of styrene. The average power delivered in these experiments varies between 8×10^{-4} and 2×10^{-4} W when the input power is decreased from 80 W to 10 W, and from 0.16 down to 10^{-2} W when the on-time is decreased from 80 to 5 μs. At these values, the differences seem to have an influence over the retention of the monomer functionalities but not on the amount of free radicals trapped towards the surface of the plasma polymer. This seems to be in direct contradiction with the findings of Teare et al.[61] who showed that for maleic anhydride a better retention of the monomer functionalities increased the availability of trapped free

radicals for subsequent grafting. However, their work concentrated on comparing continuous-wave plasma polymerisation and pulsed plasma polymerisation which presents far more differences in the plasma polymer structure than those obtained from two pulsed plasma polymerisation under different pulsing conditions.

The biggest effect observed on the trapping of free radicals seems to arise from the duration of the preliminary continuous wave plasma run to ensure adhesion on the substrate. The amount of free radicals trapped at the surface seems to remain constant as the time during which continuous wave plasma is increased, however, the polymerisation rate of grafting of styrene increases over a threshold of 50 s and remains constant over this value up to a duration of 110 s when it decreases slightly. Hence, there seems to be an equilibrium reached during this interval in which the availability of the free radicals is not altered but above and beyond which slower grafting occurs. This can be explained by the fact that when not enough energy is brought to the system, not enough radicals at the surface are created, and when too much is applied, radicals might recombine at the surface as it gets more bombarded by ionic and radical species therefore reducing their amount at the surface which translate into lower grafting polymerisation rate. Also this major effect can also be accounted for the fact that the average power delivered to the system varies greatly with the duration of the continuous wave plasma, therefore noticeable effect can be observed.

VI.5. CONCLUSIONS

These results are confined to the experimental conditions used and therefore nominal values do not apply for direct comparison. However, the general trends observed are still valid.

In this set of experiments, the nature of the monomer and the conditions used for plasma polymerisation have an influence over the amount of trapped free radicals in the pulsed plasma deposited polymer. The rate of graft-polymerisation does not appear to be directly related to the free radical density since hindrance at the surface seems to play an important role. No prediction rule could be established between the nature of the monomer, the amount of trapped free radicals and the graft polymerisation rate. Some structural effects are thought to be of importance when the trapped free radicals availability is concerned, but it can only be a rule of thumb.

When plasma polymerisation is pulsed, the input power and the duration of the on-time do not appear to have a great influence over the generation and availability of trapped free radicals. However, the method used to quantify the free radicals makes no distinction over the nature of these radicals or over which type induces graft polymerisation. Also, the differences of average power input did not vary greatly despite the wide range of conditions tested, which indicates that the generation of trapped free radicals is a stable process for that specific monomer (GMA) under the conditions tested. The only major effect observed was that of the duration of the continuous wave plasma used to ensure adhesion. In that case, average power delivered to the system varied greatly between the different periods of continuous wave tested.

VI.6. REFERENCES

1 - Yasuda, H., *Plasma polymerization*, Academic press Inc., Orlando, Florida, 1985

2 - Yasuda, H.; Hsu, T., *J. Polym. Sci.: Polym. Chem. Ed.* **1977**, 15, 81-97

3 - Yasuda, H., *J. Polym. Sci.: Macromol. Rev.* **1981**, 16, 199-293

4 - Kuzuya, M.; Kawaguchi, T.; Mizutani, S.; Okuda, T., *J. Polym. Sci., Polym. Lett.* **1985**, 23, 69-72

5 - Kuzuya, M.; Kawaguchi, T.; Nakanishi, M.; Okuda, T., *J. Chem. Soc., Faraday Trans. I* **1986**, 82, 1441-1448

6 - Kuzuya, M.; Kawaguchi, T.; Yanagihara, Y.; Nakai, S.; Okuda, T., *J. Polym. Sci., Polym. Chem.* **1986**, 24, 707-713

7 - Ji, G.; Fang, J. ; Cai, S. ; Xue, G., *Appl. Surf. Sci.* **1994**, 81, 63-68

8 - Yang, M.-R.; Chen, K.-S., *Mater. Chem. Phys.* **1997**, 50, 11-14

9 - Teare, D.O.H.; Schofield, W.C.E.; Roucoules, V.; Badyal, J.P.S., *Langmuir* **2003**, 19, 2398-2403

10 - Savage, C.R.; Timmons, R.B. *Chem. Mater.* **1991**, 3, 575-577

11 - Tarducci, C.; Kinmond, E.J.; Badyal, J.P.S. *Chem. Mater.* **2000**, 12, 1884-1889

12 - Ryan, M.E.; Hynes, A.M.; Badyal, J.P.S. *Chem. Mater.*, **1996**, 8, 37-42

13 - Teare, D.O.H.; Schofield, W.C.E.; Garrod, R.P.; Badyal, J.P.S., *J. Phys. Chem. B* **2005**, 109, 20923-20928

14 - Takenouchi, H.; Uchida. T.; Morita, S., *J. Photopolym. Sci.Technol.* **1996**, 9, 659-662

15 - Bradley, T.J.; Schofield, W.C.E.; Garrod, R.P.; Badyal, J.P.S., *Langmuir*, **2006**, 22, 7552-7555

16 - Teare, D.O.H.; Barwick, D.C.; Schofield, W.C.E.; Garrod, R.P.; Ward, L.J.; Badyal, J.P.S., *Langmuir*, **2005**, 21, 11425-11430

17 - Matheson, M.S.; Auer, E.E.; Bevilacqua, E.B.; Hart, E.J., *J. Am. Chem. Soc.* **1951**, 73, 5395-5400

18 - Johnson, D.R.; Osada, Y.; Bell, A.T.; Shen, M., *Macromol.* **1981**, 14, 118-124

19 - Yordanov, N.D.; Christova, A.G., *Fresenius J. Anal. Chem.*, **1997**, 358, 610-613

20 - Tabet, F. M.; McGahan, W. A., *Thin Solid Films* **2000**, 370, 122-127

21 - Evans, J.F.; Gibson, J.H.; Moulder, J.F.; Hammond, J.S.; Goretzki, H., *Fresenius' J. Anal. Chem.* **1984**, 319, 841-844

22 - Beamson, G.; Briggs, D. In *High-Resolution XPS of Organic Polymers: The Scienta ESCA300 Database*; John Wiley & Sons: New York, 1992

23 - Lin-Vien, D.; Colthrup, N.B.; Fateley, W.G.; Grasselli, J.G. In *The Handbook of Infrared and Raman Characteristic Frequencies of Organic Molecules*; Academic Press: New York, 1991

24 - Labelle, C.B.; Limb, S.J.; Gleason, K. K., *J. Appl. Phys.* **1997**, 82, 1784-1787

25 - Scott, T.W.; Chu, K.-C.; Venugopalan, M., *J. Polym. Sci.: Polym. Chem. Ed.* **1978**, 16, 3213-3218

26 - Grill, A. in *Cold Plasma in Materials Fabrication;* Wiley - IEEE Press: New York, 1994

27 - Yasuda, H.; Bumgarner, M.O.; Marsh, H.C.; Morosoff, N., *J. Polym. Sci.: Polym. Chem. Ed.* **1976**, 14, 195-224

28 - Ionita, P., *Chem. Pap.* **2005**, 59, 11-16

29 - Gong, X.; Dai, L.; Mau, A. W. H..; Griesser, H. J., *J. Polym. Sci.: Part A: Polym. Chem.*, **1998**, 36, 633–643

VII

CHAPTER SEVEN

Conclusions

Pulsed plasma polymerisation offers a great range of advantages over other techniques such as self-assembled monolayers and Langmuir-Blodgett films to deposit thin films at the surface of a substrate with a wide range of functionalities. This thesis concentrated on demonstrating further the applicability of such plasma polymers and also on attempting to explain some of their unique properties.

In the first experimental chapter, the pulsed plasma polymerisations of two reactive esters, N-acryloxysuccinimide and pentafluorophenyl acrylate, were achieved for the first time, allowing the creation of surfaces with very high retention of functionalities which allowed the attachment of various amine-terminated molecules such as amines, amino-acid esters, peptides, DNA stands and proteins. Whilst previously, attachment of such entities entailed several steps, plasma deposition of these reactive esters allowed attachment in a one-step process therefore increasing the amount of immobilised molecules at the surface.

In the second experimental chapter, the ability of enzymes to modify molecules immobilised at the surface of plasma polymers was demonstrated for the first time. An amino-acid ester was initially immobilised at the surface of the reactive ester plasma polymer generated according to the work carried out in the first chapter. Then it was reacted with an enzyme to cleave the ester bond. It was observed that such reactions were not always possible on self-assembled monolayer due to the high ordering of molecules at the surface. As plasma polymers present a relatively 'rough' surface in comparison with SAMs, molecules of a large diameter, such as enzymes, can reach the immobilised molecule and present their active site to undergo reaction. The mild conditions required for enzymatic reaction, along with the high selectivity of such reactions therefore proved a powerful tool to pattern surfaces with high specificity and spatial controllability.

The third chapter draws a comparison between two methods of initiation for the graft polymerisation of styrene onto plasma polymers. The first method involved the immobilisation of an azo initiators and subsequent polymerisation of styrene. The second method made use of trapped free radicals always present in plasma polymers. It was shown that the use of intermediate initiators such as azo compounds was not necessary. Indeed, trapped free radicals present in plasma polymers were able to generate polymer brushes up to 100 nm in thickness in a one-step process.

The last experimental chapter focused on establishing which factors influenced the quantity and the availability of those trapped free radicals in plasma polymers. Different monomers were pulsed plasma polymerised, and whilst the amount of free radicals did not seem to vary much from one to another, two of them (GMA and NASME) showed much higher graft polymerisation rate. The nature of the monomer could not explain these differences, and other considerations (such as steric hindrance) were significant. It was also observed that the availability and the amount of trapped free radicals within plasma polymers were stable for up to a week in open air. For a particular monomer (GMA), the duty cycle and input power were shown not to have a noticeable influence over the amount of trapped free radicals and the subsequent graft polymerisation rate. However, the duration of the continuous wave plasma used prior to pulsing to ensure adhesion seemed to be the determining factor in the rate of graft polymerisation.

VIII

ANNEXE 1

Pulsed plasma polymerisation of different monomers for trapped free radicals experiments

XPS and FTIR characterisation of the different plasma polymers employed in the experiments described in Chapter VI are presented in this annexe.

For each plasma polymer, the different carbon environments observed on the carbon envelope C (1s) obtained by XPS were compared with a theoretical spectra calculated based on elemental composition of the monomer and standard values for binding energies[1]. Some plasma polymers possessing an aromatic ring in their structure contain in their experimental spectra the π-π^* shake-up satellite at 293.5 eV indicative of the retained aromatic structure[2].

The FTIR spectra of the plasma polymers were compared to that of their corresponding monomer. The absence of the band at around 1640 cm^{-1} in each of plasma polymer confirmed that polymerisation occurred, and that good retention of the functions of the monomer was still seen within the bulk of the plasma polymer, with the exception of styrene. In most cases, the peak observed at 3300 cm^{-1} was attributed to water from ambient air as it was also observed on bare gold used for baseline.

VIII.1. GLYCIDYL METHACRYLATE

VIII.1.1. XPS

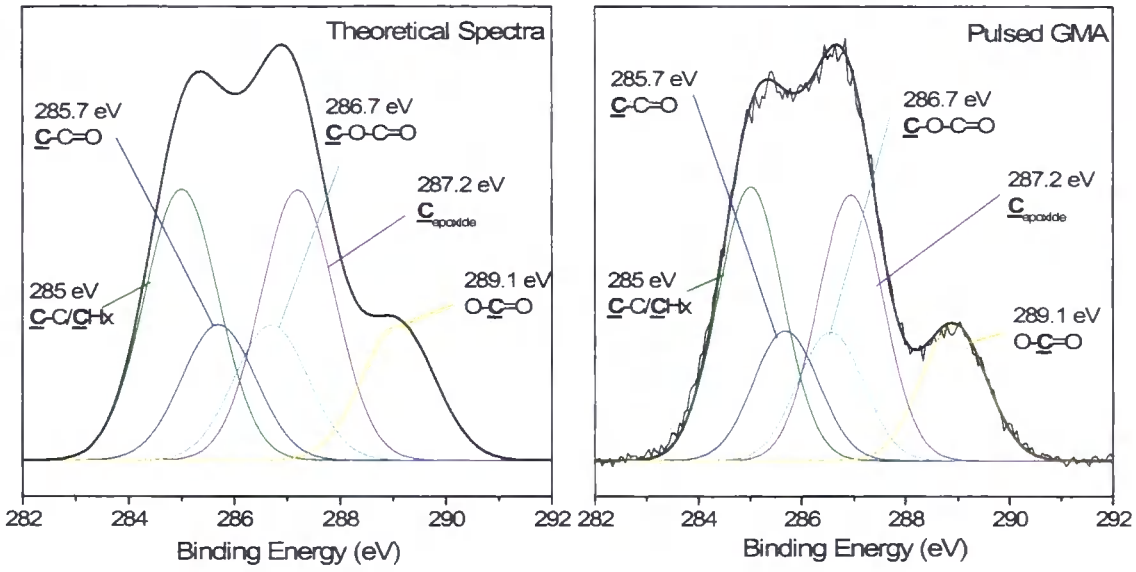

Figure VIII-1 – Theoretical and experimental C(1s) XPS spectra of glycidyl methacrylate plasma polymer (20 µm / 20 ms – 40 W)

VIII.1.2. FTIR

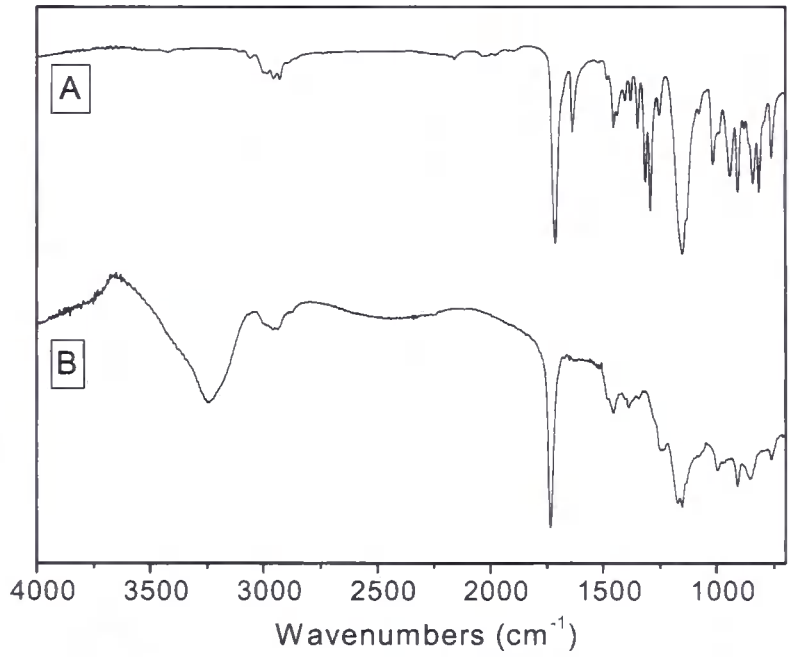

Figure VIII-2 – FTIR spectra of (A) Glycidyl methacrylate monomer and (B) GMA pulsed plasma polymer (20 µm / 20 ms – 40 W)

VIII.2. MALEIC ANHYDRIDE

VIII.2.1. XPS

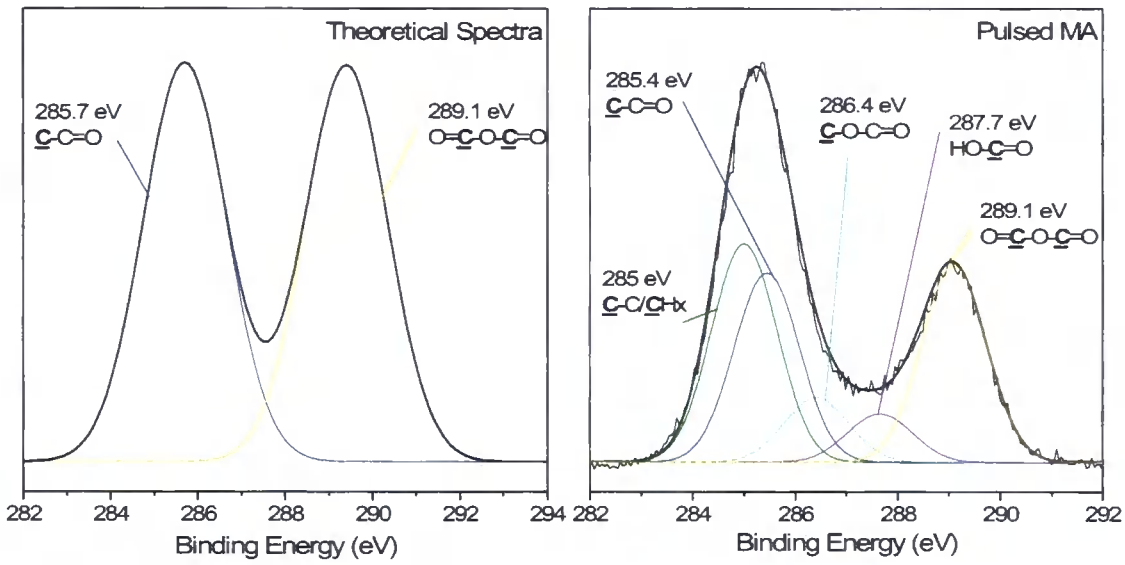

Figure VIII-3 - Theoretical and experimental C(1s) XPS spectra of maleic anhydride plasma polymer (20 µm / 1200 µs – 4 W)

VIII.2.2. FTIR

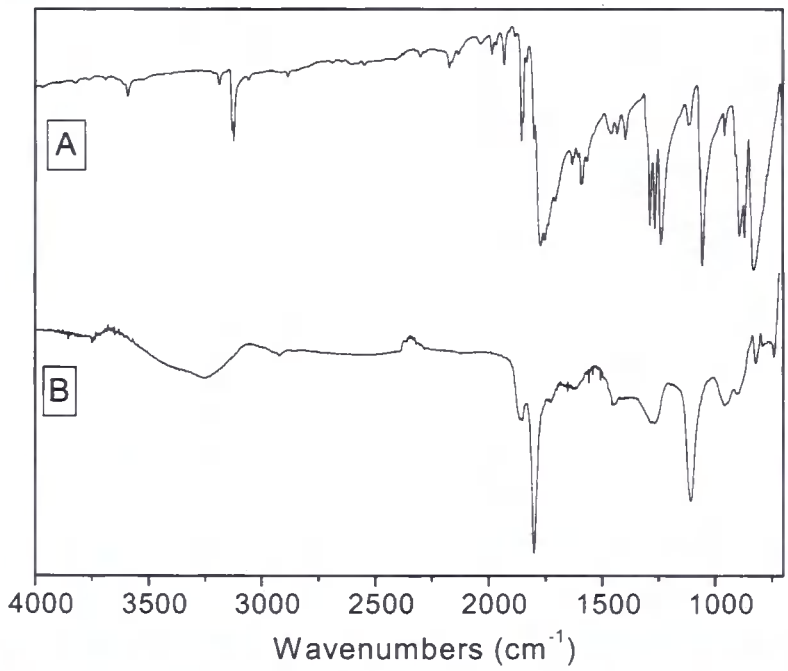

Figure VIII-4 - FTIR spectra of (A) Maleic Anhydride monomer and (B) MA pulsed plasma polymer (20 µm / 1200 µs – 4 W)

VIII.3. N-ACRYLOYL SARCOSINE METHYL ESTER

VIII.3.1. XPS

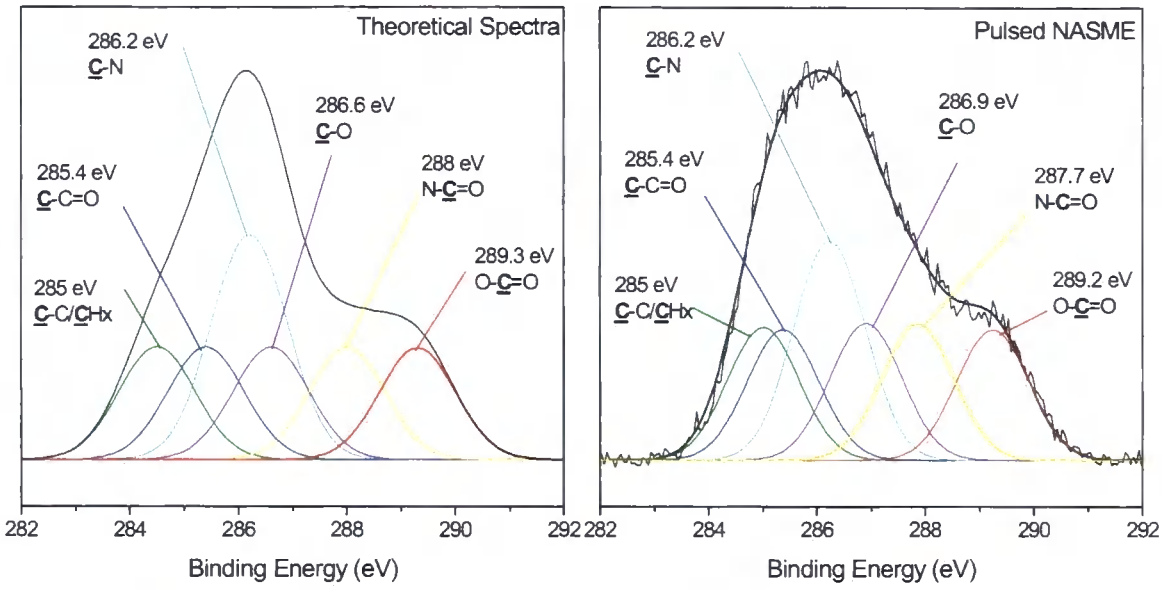

Figure VIII-5 - Theoretical and experimental C(1s) XPS spectra of N–acryloyl sarcosine methyl ester plasma polymer (20 µm / 5 ms – 30 W)

VIII.3.2. FTIR

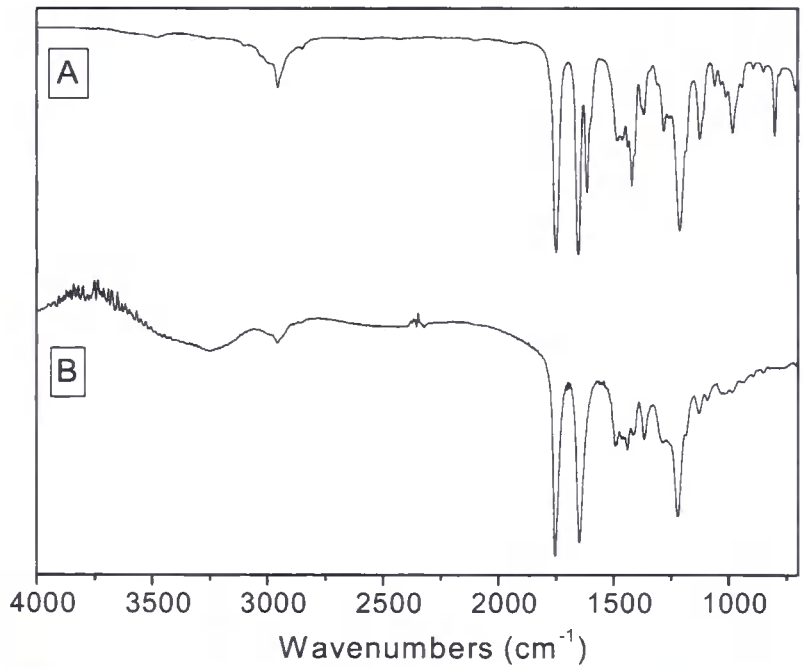

Figure VIII-6 - FTIR spectra of (A) N-acryloyl sarcosine methyl ester monomer and (B) NASME pulsed plasma polymer (20 µm / 5 ms – 30 W)

VIII.4. PENTAFLUOROPHENYL ACRYLATE

VIII.4.1. XPS

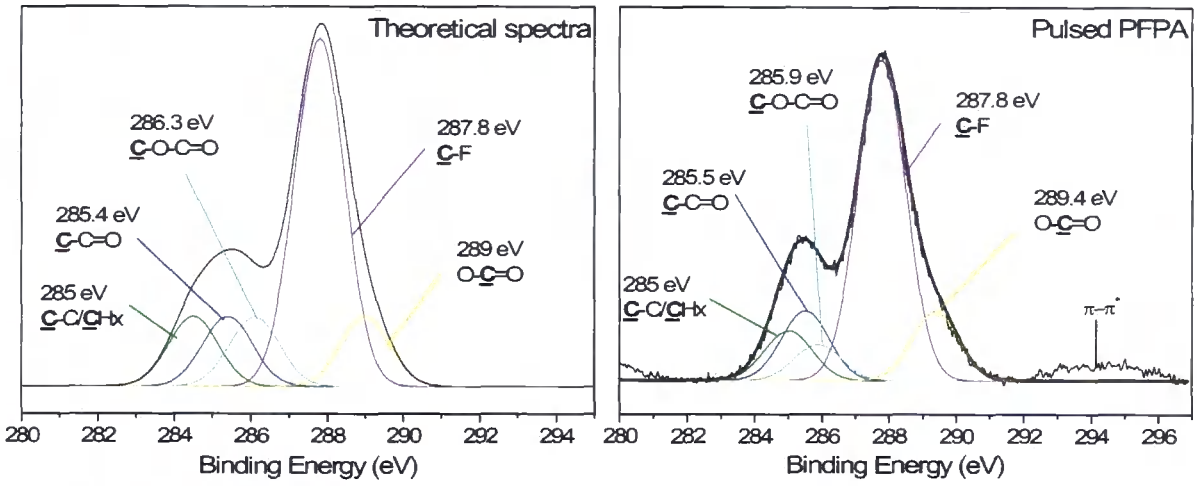

Figure VIII-7 - Theoretical and experimental C(1s) XPS spectra of pentafluorophenyl acrylate plasma polymer (10 µm / 20 ms – 30 W)

VIII.4.2. FTIR

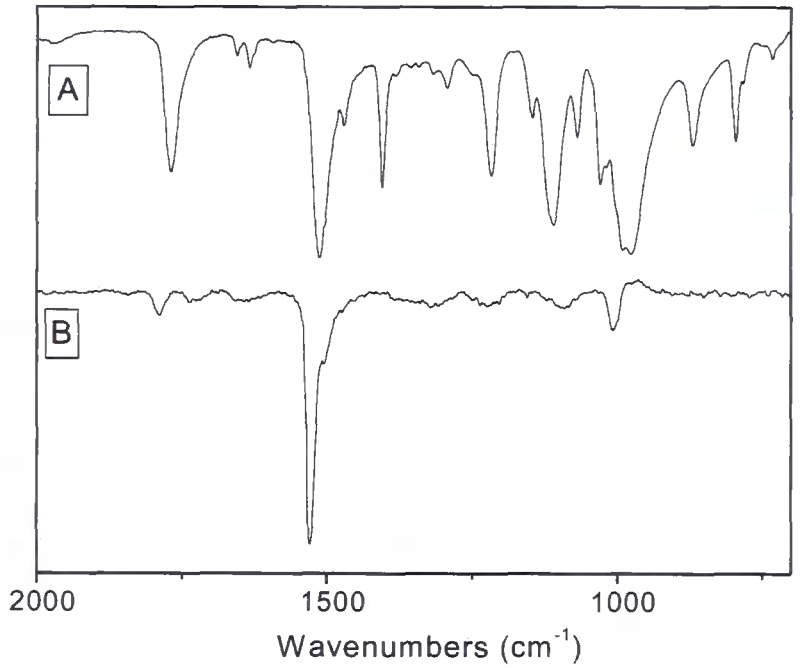

Figure VIII-8 - FTIR spectra of (A) pentafluorophenyl acrylate monomer and (B) PFPA pulsed plasma polymer (10 µm / 20 ms – 20 W)

VIII.5. STYRENE

VIII.5.1. XPS

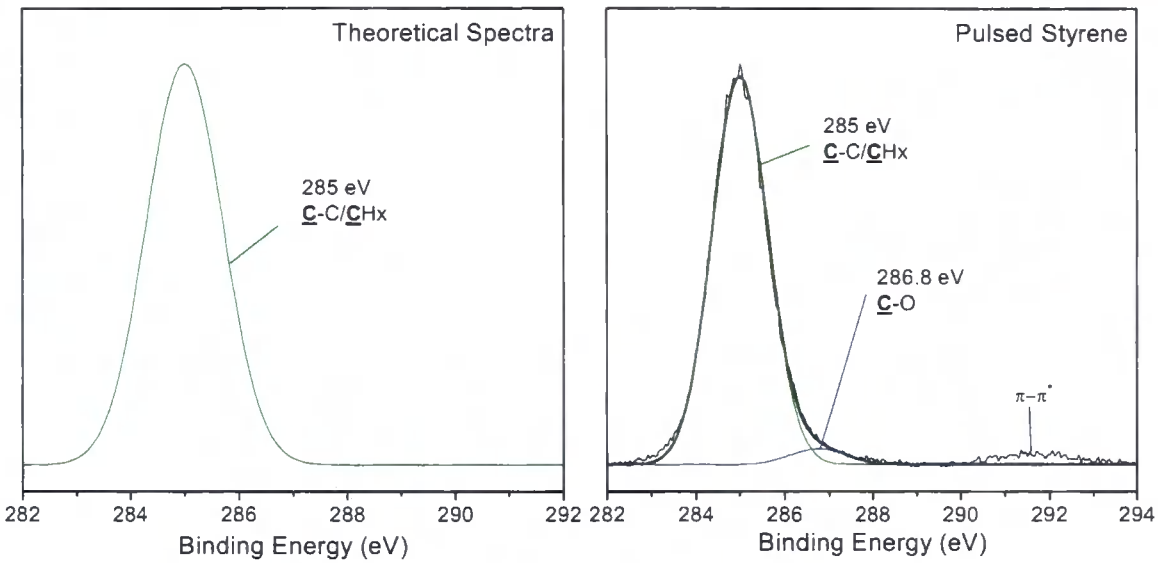

Figure VIII-9 - Theoretical and experimental C(1s) XPS spectra of styrene plasma polymer (100 µm / 4 ms – 40 W)

VIII.5.2. FTIR

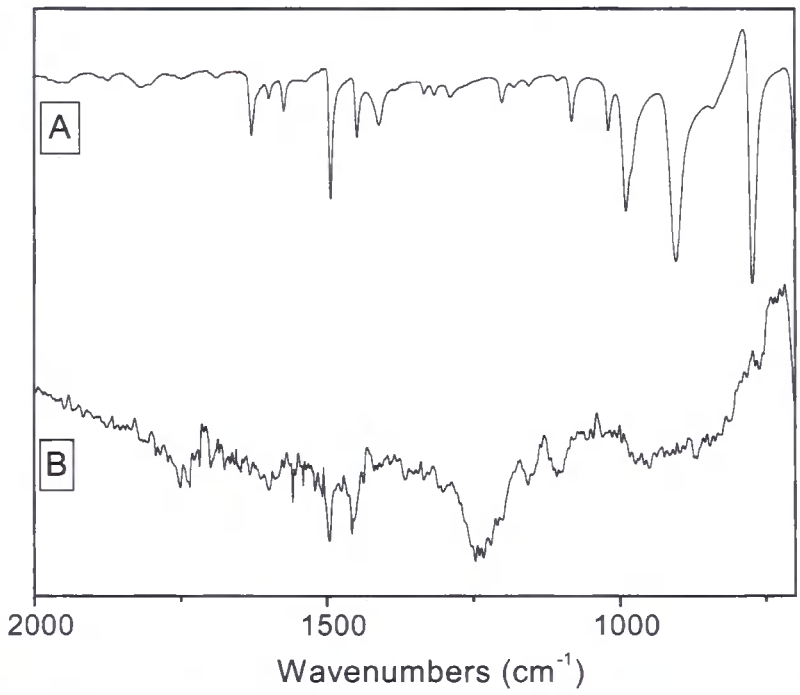

Figure VIII-10 - FTIR spectra of (A) styrene monomer and (B) S pulsed plasma polymer (100 µm / 4 ms – 40 W)

VIII.6. 4-VINYL ANILINE

VIII.6.1. XPS

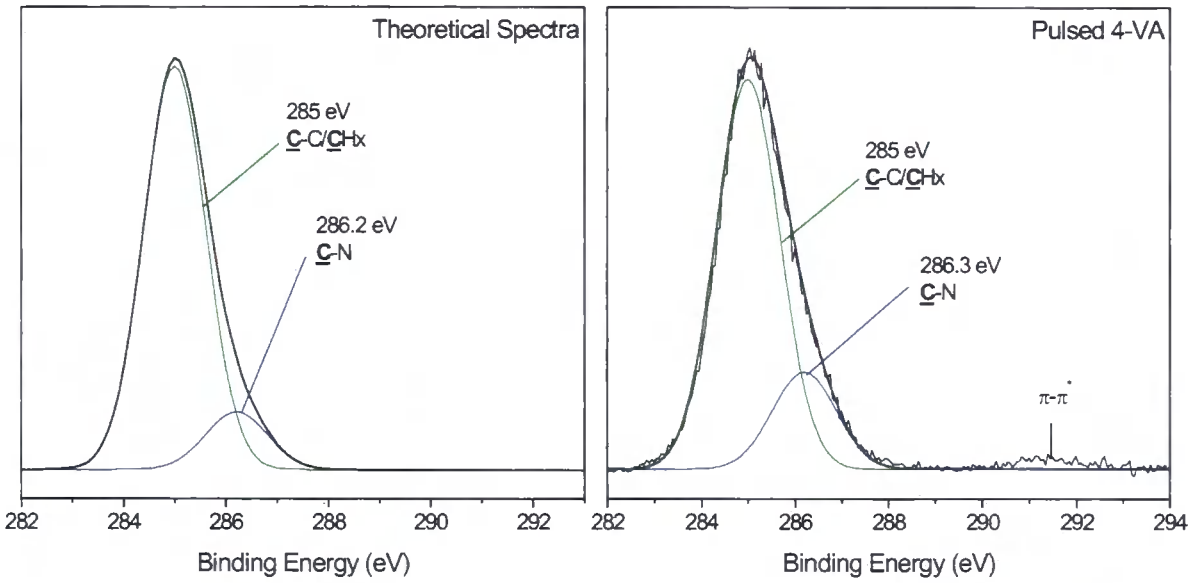

Figure VIII-11 - Theoretical and experimental C(1s) XPS spectra of 4-vinyl aniline plasma polymer (100 µm / 4 ms – 20 W)

VIII.6.2. FTIR

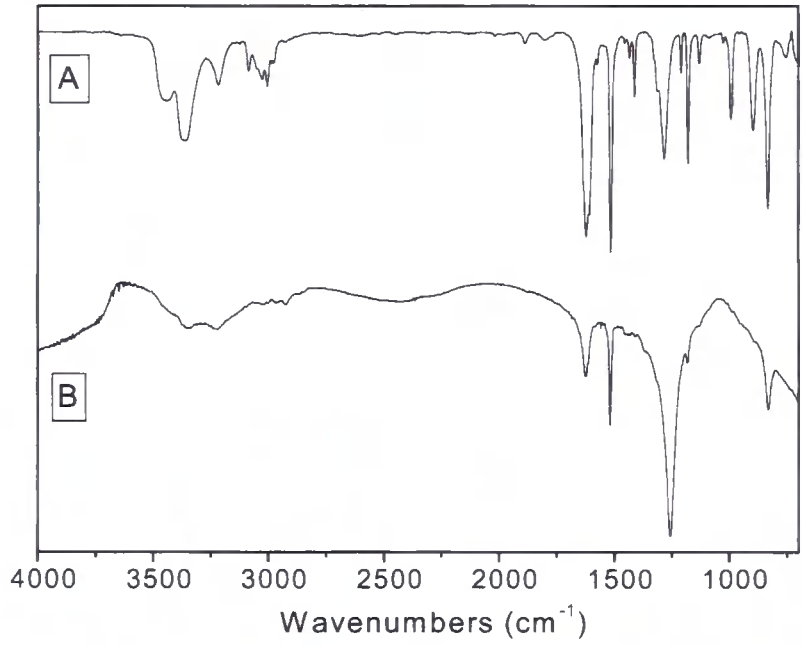

Figure VIII-12 - FTIR spectra of (A) 4-vinyl aniline monomer and (B) 4-VA pulsed plasma polymer (100 µm / 4 ms – 20 W)

VIII.7. 4-VINYL BENZYL CHLORIDE

VIII.7.1. XPS

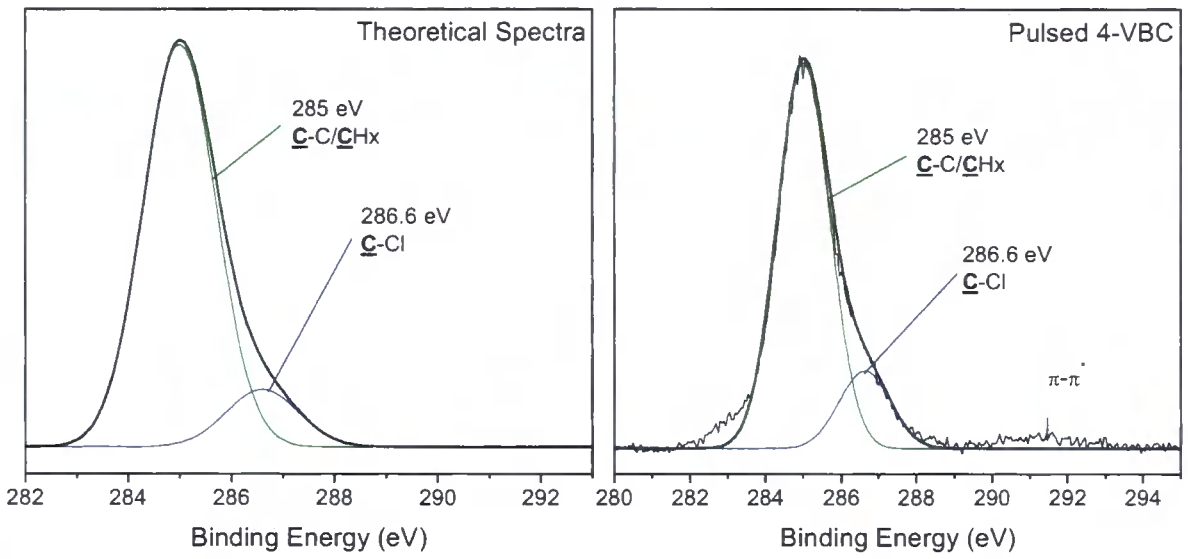

Figure VIII-13 - Theoretical and experimental C(1s) XPS spectra of 4-vinyl benzyl chloride plasma polymer (20 µm / 1200 µs – 16 W)

VIII.7.2. FTIR

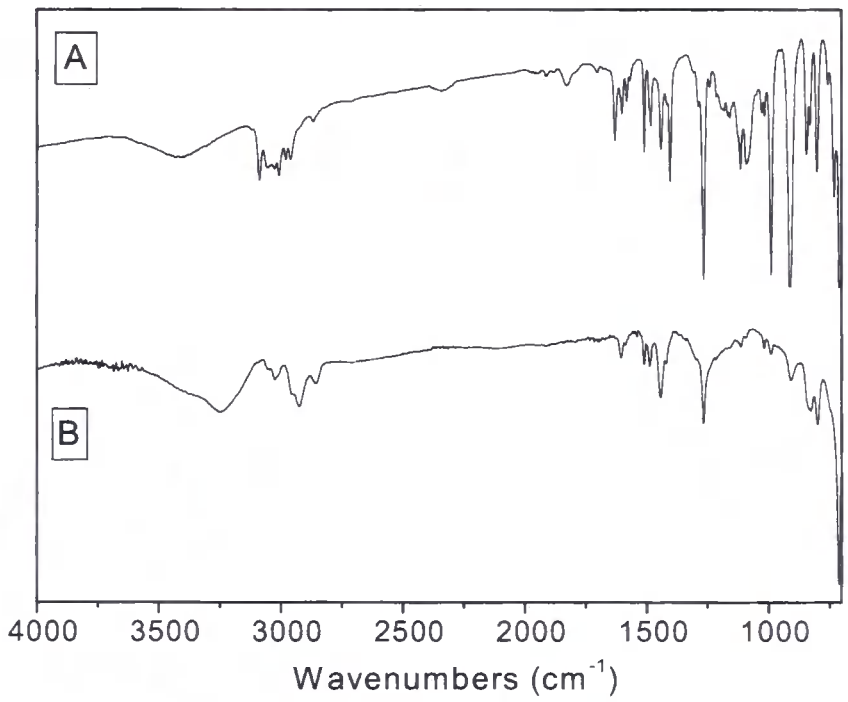

Figure VIII-14 - FTIR spectra of (A) 4-vinyl benzyl chloride monomer and (B) 4-VBC pulsed plasma polymer (20 µm / 1200 µs – 16 W)

VIII.8. REFERENCES

1 - Beamson, G.; Briggs, D. In *High-Resolution XPS of Organic Polymers: The Scienta ESCA300 Database*; John Wiley & Sons: New York, 1992

2 - Clark, D.T.; Dilks, A. *J. Polym. Sci. A* **1977**, 15, 15

IX

APPENDIX 1

List of abbreviations

4-VA – 4-vinyl aniline

4-VBC – 4-vinyl benzyl chloride

Ala – Alanine

Azobis – 2,2'-azobis-(2-amidinopropane) dihydrochloride

CHA – Concentric hemispherical analyser

CMA – Cylindrical mirror analyser

CTE – Complete thermodynamic equilibrium

CW – continuous wave

DC – Direct current

DiEA – Diethylamine

DNA – Deoxyribonucleic acid

DPPH – 2,2'-diphenyl-1-picrylhydrazyl

FTIR – Fourier transform infra-red

Gly – Glycine

GMA – Glycidyl methacrylate

His – Histidine

HPLC – High performance chromatography

IR – Infra-red

LTE – Local thermodynamic equilibrium

MA – Maleic anhydride

MIR – Multiple internal reflections

NAS – N-acryloxysuccinimide

NASME – N-acryloyl sarcosine methyl ester

PFPA – Pentafluorophenyl acrylate

PLE – Pig liver esterase

RAIRS – Reflection adsorption infra-red spectroscopy

RF – Radio frequency

RFA – Retarding field analyser

RP-HPLC – Reverse-phase high performance liquid chromatography

S – Styrene

SAM – Self-assembled monolayer

SPR – Surface plasmon resonance

TFEA – Trifluoroethylamine

UHV – Ultra-high vacuum

UV-vis – Ultra-violet-visible

VCA – Video contact angle

XPS – X-ray photoelectron spectroscopy

βA – β-alanine

βAEE.HCl – β-alanine ethyl ester hydrochloride